Instytut Nauk Geologicznych

Polskiej Akademii Nauk

Migracja i rozmieszczenie wybranych izotopów promieniotwórczych w ekosystemach jeziornych jako wskaźniki procesów sedymentacyjnych

mgr Ilona Sekudewicz

Promotor: dr hab. Michał Gąsiorowski, prof. ING PAN

Warszawa 2023

Podziękowania

Składam wyrazy wdzięczności mojemu Promotorowi, dr hab. Michałowi Gąsiorowskiemu, prof. ING PAN za wprowadzenie mnie w tematykę izotopów promieniotwórczych, cierpliwość i wyrozumiałość, wsparcie dla moich pomysłów naukowych, nieocenioną pomoc w realizowaniu badań, poświęcony czas na liczne dyskusje naukowe oraz opiekę merytoryczną w przygotowaniu niniejszej rozprawy doktorskiej.

Składam serdeczne podziękowania dr hab. Helenie Hercman, prof. ING PAN za okazane wsparcie, cenne porady oraz owocne dyskusje naukowe.

Pragnę podziękować dr Jan Rohovec oraz dr Šárka Matoušková z Instytutu Geologii Czeskiej Akademii Nauk w Pradze za okazaną życzliwość, cenne porady oraz pomoc w realizowaniu badań naukowych.

Składam serdeczne podziękowania Dyrekcji oraz wszystkim Koleżankom i Kolegom z Instytutu Nauk Geologicznych PAN, a w szczególności całemu mojemu zespołowi LUIS (Laboratorium Uranowe i Izotopów Stabilnych) za stworzenie przyjaznej atmosfery pracy, wspólnie zrealizowane projekty badawcze, okazane wsparcie, wspólnie spędzony czas oraz bezinteresowną pomoc.

Pragnę podziękować wszystkim Koleżankom i Kolegom z Instytutu Badań Polarnych i Morskich im. Alfreda Wegenera (AWI) w Bremerhaven oraz z Niemieckiego Centrum Badawczego Nauk Geologicznych (GFZ) w Poczdamie za wspólnie spędzony czas, inspirujące dyskusje naukowe oraz pomoc w realizowaniu badań naukowych.

Szczególne podziękowania składam mojej Rodzinie oraz Marcinowi za obecność i okazane zrozumienie, niezachwianą wiarę we mnie oraz wspieranie mnie we wszystkich chwilach. Chciałabym również podziękować wszystkim przyjaciołom i znajomym, którzy okazywali mi cenne wsparcie i zawsze motywowali mnie do dalszego rozwoju.

Oświadczenie

Świadoma odpowiedzialności prawnej oświadczam, że niniejsza rozprawa doktorska została napisana przeze mnie samodzielnie i nie zawiera treści uzyskanych w sposób niezgodny z obowiązującymi przepisami.

Oświadczam również, że przedstawiona rozprawa nie była wcześniej przedmiotem procedur związanych z uzyskaniem stopnia doktora w wyższej uczelni lub innej jednostce naukowej.

Oświadczam ponadto, że niniejsza wersja pracy jest identyczna z załączoną wersją elektroniczną.

22.11.2023 r.   …………………………………

Data   Podpis autora

Spis treści

Streszczenie

Głównym celem prezentowanej rozprawy doktorskiej było określenie najważniejszych mechanizmów odpowiadających za rozmieszczenie i migrację wybranych izotopów promieniotwórczych w osadach jeziornych zbiorników antropogenicznych w Polsce. Obszar badań stanowiły dwa jeziora zaporowe – Jez. Turawskie i Jez. Koronowskie oraz jedno jezioro pokopalniane – Jez. ŁK-61 dotknięte występowaniem kwaśnych wód kopalnianych (AMD – acid mine drainage). Wykazana w pracy zmienność rozmieszczenia poszczególnych izotopów w osadzie posłużyła do scharakteryzowania procesów sedymentacyjnych oraz zmian warunków środowiskowych zachodzących w ekosystemach badanych jezior w przeszłości.

W osadach jezior zaporowych zbadano powierzchniowe oraz pionowe rozmieszczenie koncentracji cezu ^{137}Cs. W jeziorze pokopalnianym analizowano pionowy rozkład zawartości ^{137}Cs oraz polonu ^{210}Po. Ponadto, ze względu na specyfikę jeziora ŁK-61, analizie poddano także rozmieszczenie zawartości metali ciężkich (Cu, Ni, Pb, Zn, itd.) w kolumnie wody oraz w profilu osadów jeziornych. W celu lepszego scharakteryzowania czynników i procesów odpowiedzialnych za rozmieszczenie radionuklidów, zbadano także pionowy rozkład koncentracji wybranych jonów i rozpuszczonego węgla organicznego (DOC) w kolumnie wody. Dodatkowo przeprowadzono analizę składu gatunkowego subfosylnych okrzemek, a także składu granulometrycznego i mineralogicznego oraz zawartości izotopu potasu ^{40}K oraz całkowitego węgla organicznego (TOC) i azotu (TN) w wybranych próbkach osadów.

Wyniki przeprowadzonych badań wykazały, że najważniejszymi czynnikami odpowiedzialnymi za powierzchniowe rozmieszczenie koncentracji ^{137}Cs w osadach dennych jezior zaporowych są rodzaj i cechy (skład granulometryczny i mineralogiczny) deponowanych osadów, charakterystyka fizyczno-limnologiczna (np. parametry morfometryczne) badanych zbiorników wodnych oraz procesy odpowiedzialne za erozję i transport osadów. Radioizotop ^{137}Cs kumuluje się w przypadku zbiorników retencyjnych głównie w osadach drobnoziarnistych (<0,063 cm) deponowanych w strefie profundalnej tych jezior, a szczególnie w pobliżu zapory wodnej. W przypadku jeziora pokopalnianego, dominującymi procesami odpowiedzialnymi za rozmieszczenie ^{137}Cs oraz ^{210}Po w osadach jeziornych są rozpuszczanie oraz wytrącanie się minerałów, a także procesy sorpcyjne zachodzące z udziałem minerałów autogenicznych i allogenicznych. Procesy te mogą być jednak zaburzane wskutek wydarzeń depozycyjnych, jak na przykład powódź. W przypadku wszystkich zbiorników antropogenicznych istotną rolę w dystrybucji wybranych radionuklidów odgrywa również dostawa zanieczyszczonych cząstek ze zlewni badanych jezior.

Słowa kluczowe: radionuklidy, zbiorniki antropogeniczne, jezioro pokopalniane, zbiorniki zaporowe, metale ciężkie, osady jeziorne, migracja radioizotopów, transport osadów

Abstract

The main goal of the presented doctoral dissertation was to determine the most important mechanisms responsible for the distribution and migration of selected radioactive isotopes in lake sediments of anthropogenic reservoirs in Poland. The research area consists of two dam lakes – Lakes Turawskie and Koronowskie and one post-mining lake – Lake ŁK-61 affected by acid mine drainage (AMD). The variability in the distribution of particular radioisotopes in the sediments demonstrated in the study was used to characterize sedimentation processes and changes in environmental conditions that occurred in the ecosystems of the studied lakes in the past.

The spatial and vertical distributions of cesium ^{137}Cs activity concentrations in the sediments of dam lakes were determined. In the post-mining lake, the vertical distribution of ^{137}Cs and polonium ^{210}Po content was analyzed. Moreover, due to the specificity of Lake ŁK-61, the distribution of heavy metals (Cu, Ni, Pb, Zn, etc.) content in the water column and in the sediment core was also examined. In order to better characterize the factors and processes responsible for the distribution of radionuclides, the vertical distributions of the concentration of selected ions and dissolved organic carbon (DOC) in the water column were also studied. Additionally, analyses of subfossil diatoms, particle-size distribution, mineralogical composition, and the content of potassium ^{40}K, total organic carbon (TOC) and nitrogen (TN) in selected sediment samples were also conducted.

The obtained results showed that the most important factors responsible for the spatial distribution of ^{137}Cs activity concentrations in the bottom sediments of dam lakes are the type and characteristics (grain size distribution and mineralogical composition) of the deposited sediments, the physical and limnological characteristics of the lakes (e.g., hydro-morphological parameters) and the processes responsible for erosion and sediment transport. Cesium ^{137}Cs accumulates in reservoirs mainly in fine-grained sediments (<0.063 cm), which are deposited in the profundal zone of these lakes, especially near the dam. In the case of a post-mining lake, the dominant processes responsible for the distribution of ^{137}Cs and ^{210}Po in the lake sediments are the dissolution and precipitation of minerals, as well as sorption processes with autogenic and allogeneic minerals. However, these processes may be disturbed by depositional events, such as floods. In all anthropogenic reservoirs, the distribution of selected radionuclides is also significantly influenced by the supply of contaminated particles from the catchments of the studied lakes.

Keywords: radionuclides, anthropogenic reservoirs, post-mining lake, dam reservoirs, heavy metals, lake sediments, radioisotope migration, sediment transport

Wstęp

Czynniki wpływające na rozmieszczenie i migrację radioizotopów, zarówno pochodzenia naturalnego (np. ołów ^{210}Pb, polon ^{210}Po) jak i antropogenicznego (np. cez ^{137}Cs) w środowisku naturalnym stanowią od lat temat licznych badań naukowych. Zrozumienie mechanizmów odpowiedzialnych za obieg radionuklidów w przyrodzie jest niezwykle istotne, zarówno pod względem ochrony radiologicznej, jak i zastosowania izotopów promieniotwórczych w naukach o Ziemi i środowisku. Szczególnie istotnymi obszarami badawczymi w tej dziedzinie są ekosystemy jeziorne, ze względu na ich znaczenie przyrodnicze (retencja wody, ochrona bioróżnorodności, etc.) oraz gospodarcze (źródło wody pitnej, ochrona przeciwpowodziowa, turystyka i rekreacja, etc.).

Osady deponowane w jeziorach stanowią ważne archiwum, z którego możemy odczytać informacje dotyczące przeszłości geologicznej, czy też klimatycznej badanego obszaru (Herschy, 2012). Mogą one ujawniać również historię zmian zachodzących w danym środowisku jeziornym, w tym zmian spowodowanych działalnością człowieka. Badanie rozmieszczenia zawartości izotopów promieniotwórczych w osadach dennych może dostarczyć wielu cennych informacji (dotyczących, m.in. wieku deponowanych osadów, tempa ich sedymentacji, itd.) umożliwiających dokładniejszą charakterystykę badanych środowisk dyspozycyjnych. Na szczególną uwagę zasługują izotopy promieniotwórcze, takie jak cez ^{137}Cs oraz ołów ^{210}Pb, które można wykorzystać jako markery chronostratygraficzne, a także jako użyteczne wskaźniki zachodzących procesów sedymentacyjnych (Appleby, 2008; Łokas i in., 2010; Swarzenski, 2014; Zapata & Nguyen, 2009; Walling & Quine, 1993; i inni).

Na rozmieszczenie radionuklidów w osadach dennych w poszczególnych środowiskach sedymentacyjnych może wpływać rodzaj i cechy powstających osadów oraz zachodzące w nich procesy sedymentacyjne, które uzależnione są od czynników środowiskowych, takich jak geometria zbiornika, energia środowiska, działalność biosfery, itd. (Appleby, 2008; Gradziński i in., 1986; Zapata & Nguyen, 2009; etc.). W przypadku ekosystemów jeziornych, procesy te są zależne w dużym stopniu od charakterystyki fizyczno-limnologicznej (typ genetyczny, cechy morfometryczne, trofizm jeziora, wielkość zlewni, obecność dopływów i odpływu, itd.) danego zbiornika wodnego (Herschy, 2012). Rodzaj oraz właściwości deponowanych osadów (ich skład granulometryczny, mineralogiczny, itd.) determinują natomiast ich zdolność do

unieruchamiania poszczególnych radioizotopów w wyniku sorpcji, co ma istotne konsekwencje dla ich rozmieszczenia w osadach jeziornych (Cornell 1993; He & Walling, 1996; Kamiński i in. 1994; Park i in., 2021; Sawhney 1972; Szarłowicz i in., 2011; i inni).

Izotopy promieniotwórcze, takie jak ^{137}Cs oraz ^{210}Pb, mogą być dostarczane do zbiorników wodnych w wyniku ich bezpośredniej depozycji z atmosfery, a także wskutek transportu zanieczyszczonych cząstek wymywanych z erodowanych gleb i osadów (Appleby, 2005; 2008; Zapata & Nguyen, 2009; itd.). Radioizotopy te ulegają relatywnie szybkiej sorpcji i akumulacji, wykazując stosunkowo ograniczoną mobilność (np. Swarzenski, 2014). Jednakże, procesy biologiczne (np. bioturbacja) czy fizyczne (np. erozja brzeżna i denna wywołana falowaniem, wahaniami poziomu wód, itd.) mogą powodować redepozycje osadów dennych, a tym samym redystrybucję zakumulowanych w nich radioizotopów (Appleby, 2005; Kansanen i in., 1991; Klaminder i in., 2012; i inni). Dodatkowo, na migrację radionuklidów mogą wpływać procesy chemiczne, jak na przykład dyfuzja w wodzie porowej (Evans i in., 1983; Comans i in., 1989; itd.). Istotny wpływ na rozmieszczenie poszczególnych radionuklidów oraz metali ciężkich w osadach jeziornych mogą mieć również wydarzenia depozycyjne, jak np. powodzie, które mogą dostarczać znaczące ilości zanieczyszczeń, a także zaburzać procesy
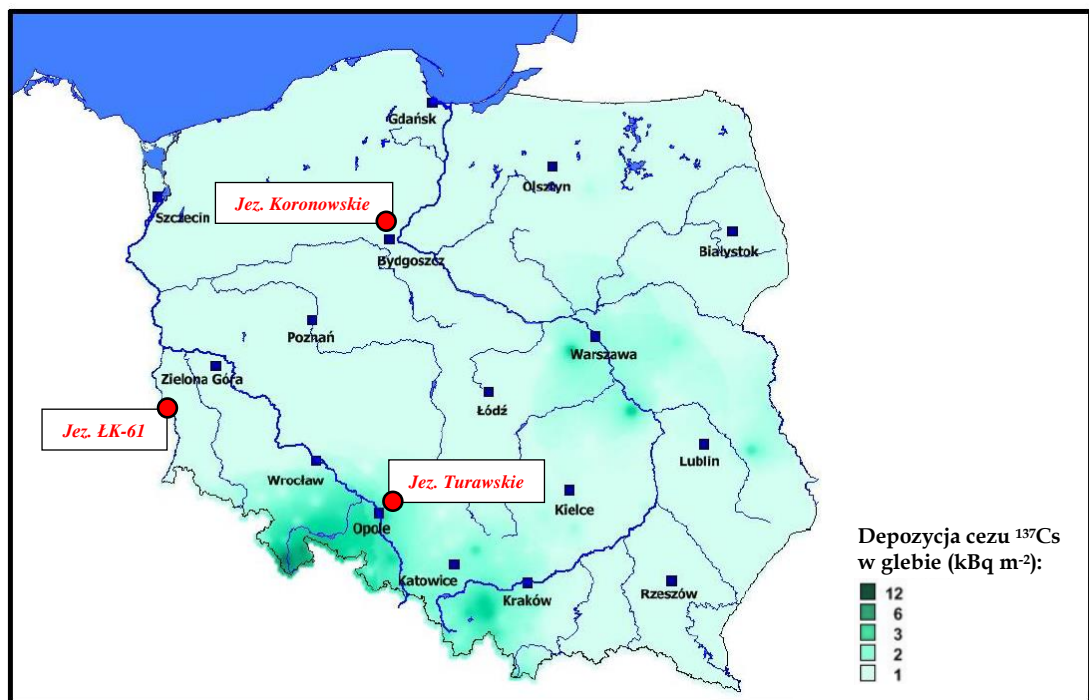
Fig. 1. *Depozycja ^{137}Cs (kBq m^{-2}) w glebie na obszarze Polski w 2020 r. (na podstawie: Isajenko i in., 2022). Lokalizację wybranych jezior stanowiących obszar badań niniejszej rozprawy doktorskiej zaznaczono kolorem czerwonym.*

sedymentacyjne odpowiedzialne za ich dystrybucję w ekosystemie jeziornym. Może mieć to szczególne znaczenie w przypadku jezior dotkniętych występowaniem kwaśnych wód kopalnianych (AMD – acid mine drainage), w których nagłe zmiany parametrów fizykochemicznych wody mogą mieć znaczący wpływ na zachowanie się pierwiastków (Cánovas i in., 2007; Herzsprung i in., 2010; Hierro i in., 2014; etc.).

Nadrzędnym celem badawczym prac prezentowanych w ramach niniejszej rozprawy doktorskiej było scharakteryzowanie mechanizmów odpowiedzialnych za rozmieszczenie wybranych radioizotopów w osadach dennych trzech zbiorników wodnych pochodzenia antropogenicznego (Fig. 1; Tabela 1). Jeziora te wybrano ze względu na fakt, że charakteryzują się one młodym wiekiem w porównaniu do większości jezior naturalnych, a tym samym bardziej niestabilnymi warunkami sedymentacji, objawiającymi się, m.in. nasiloną erozją brzeżną i denną spowodowaną falowaniem i wahaniem poziomu wód, czy też intensywnym przemieszczaniem się osadów w obrębie zbiornika wodnego. Zdecydowano się na wybór trzech zbiorników antropogenicznych (Tabela 1):

- zbiornika retencyjnego (Jez. Turawskie) położonego na obszarze znacząco zanieczyszczonym radioizotopami cezu w wyniku awarii elektrowni w Czarnobylu (tzw. *„anomalii opolskiej"*) w województwie opolskim (Wołkowicz & Strzelecki, 2002);
- zbiornika retencyjnego (Jez. Koronowskie) zlokalizowanego na obszarze stosunkowo słabo zanieczyszczonym radioizotopami cezu w województwie kujawsko-pomorskim;
- jeziora pokopalnianego (Jez. ŁK-61) położonego na obszarze stosunkowo słabo zanieczyszczonym radioizotopami cezu oraz dotkniętego występowaniem kwaśnych wód kopalnianych (AMD) w województwie lubuskim.

Tabela 1 Informacje dotyczące obszaru badań wraz z wynikami oznaczeń depozycji ^{137}Cs (kBq m^{-2}) w próbkach gleby pobranych w rejonie badanych jezior w 2020 r. (źródło: Isajenko i in., 2022).

Badane jezioro	Województwo	Czas powstania jeziora	Typ badanego jeziora	Miejsce poboru próbki gleby*	Stężenie ^{137}Cs (kBq m^{-2})*
Turawskie	Opolskie	1933–1939	zaporowe	Opole	3,72
Koronowskie	Kujawsko-Pomorskie	1953–1960	zaporowe	Bydgoszcz	0,35
ŁK-61	Lubuskie	1973	pokopalniane	Grabik	0,37

*źródło: *Isajenko i in., 2022*

Zamierzano określić w szczególności w jaki sposób charakterystyka fizyczno-limnologiczna wybranych jezior, rodzaj i cechy deponowanych osadów oraz zachodzące procesy sedymentacyjne wpływają na rozmieszczenie stężeń badanych radionuklidów w osadach wybranych zbiorników wodnych. Na podstawie badań pionowego rozkładu koncentracji wybranych radioizotopów zamierzano scharakteryzować również zmiany (związane, m.in. ze stabilizacją warunków sedymentacyjnych po powstaniu tych zbiorników wodnych, stopniowym wypełnianiem ich osadami oraz eutrofizacją (w przypadku jezior zaporowych), czy też neutralizacją oraz występowaniem zdarzeń dyspozycyjnych (np. powodzi) (w przypadku jeziora pokopalnianego)) zachodzące w wybranych jeziorach w czasie.

Motywacją do podjęcia badań był fakt, że choć prace badawcze dotyczące mechanizmów odpowiedzialnych za obieg radionuklidów, takich jak ^{137}Cs, w jeziorach zaporowych były w ostatnich latach stosunkowo często podejmowane (Funaki i in. 2019; Konoplev i in., 2022; Kurikami i in., 2014; Muñoz-Salinas i in., 2021), to tylko nieliczne z nich poruszały tę problematykę w sposób kompleksowy na terenie Polski (np. Szarłowicz i in., 2011). Przyczynkiem do podjęcia badań na obszarze Jez. Turawskiego była chęć lepszego zrozumienia czynników oraz procesów odpowiedzialnych za rozmieszczenie ^{137}Cs w osadach zbiornika retencyjnego znajdującego się na terenie tzw. *„anomalii opolskiej”*, tj. obszaru charaktertyzującego się podwyższonymi koncentracjami radioizotopów cezu zdeponowanych na skutek awarii elektrowni atomowej w Czarnobylu (Wołkowicz & Strzelecki, 2002). Problem zanieczyszczenia ^{137}Cs środowiska naturalnego w rejonie Opola był tematem wielu badań naukowych (Mietelski i in, 2010; Wołkowicz & Strzelecki, 2002; Wróbel i in, 2015; Ziembik i in, 2010; etc.). Jednakże, jedyne prace badawcze dotyczące rozmieszczenia ^{137}Cs w ekosystemie Jez. Turawskiego prowadzone były 10 lat po katastrofie w Czarnobylu przez Natkaniec (1999). Jez. Turawskie było ponadto przedmiotem badań naukowych dotyczących, m.in. zachodzących w nim procesów sedymentacyjnych, charakterystyki deponowanych osadów jeziornych, czy też morfologii dna tego zbiornika wodnego (Machowski i in., 2008; Teisseyre, 1983; Wojewoda, 2013; etc.).

Wybór Jez. Koronowskiego był uwarunkowany jego typem genetycznym, gdyż jest to także zbiornik antropogeniczny, lecz różniący się od Jez. Turawskiego czasem powstania oraz charakterystyką fizyczno-limnologiczną (Tabela 1). Jez. Koronowskie jest również jeziorem zaporowym, lecz charakteryzującym się bardziej skomplikowaną linią brzegową oraz nieregularną morfologią dna typu *„dolinnego”*, zdominowaną przez

ukształtowanie dawnego koryta rzeki Brdy (Fig. 5). Wybór tego jeziora był zdeterminowany jego położeniem na obszarze znacznie mniej zanieczyszczonym ^{137}Cs w porównaniu do tzw. *„anomalii opolskiej"* (Wołkowicz & Strzelecki, 2002). Ponadto, stopień skażenia ^{137}Cs oraz procesy odpowiedzialne za jego obieg w ekosystemie Jez. Koronowskiego nie zostały dotychczas poznane. Prace badawcze prowadzone na Zalewie Koronowskim dotyczyły, m.in. jego charakterystyki hydromorfometrycznej, czy też procesu zamulania tego jeziora (Szatten, 2016; Szatten i in., 2018; etc.). Badania rozmieszczenia koncentracji ^{137}Cs na tym obszarze dotyczyły głównie skażenia okolicznych gleb radioizotopami cezu w wyniku awarii elektrowni atomowej w Czarnobylu (np., Cieśla et al. 1994; Isajenko i in., 2022).

Ostatnim badanym zbiornikiem wodnym pochodzenia antropogenicznego, znacznie różniącym się od Jez. Turawskiego oraz Jez. Koronowskiego, było pokopalniane Jez. ŁK-61 (Tabela 1). Wybór tego zbiornika wodnego był podyktowany jego położeniem na obszarze zagrożonym powodzią (PGW WP, 2021), której wystąpienie może znacząco wpłynąć na procesy odpowiedzialne za dystrybucje radionuklidów i metali ciężkich (HMRs) w osadach dennych (Abril i in., 2018; Herzsprung i in., 2010; etc.). Jez. ŁK-61 jest dodatkowo dotknięte powstawaniem kwaśnych wód kopalnianych w wyniku utleniania pirytu występującego w lignitach, których eksploatacja na tym obszarze zakończyła się w 1973 r. (Friese, 2004; Koźma & Kupetz, 2008; Kupetz, 1997; Wisotzky, 1998; etc.). Może to znacząco wpływać na parametry fizykochemiczne wody jeziornej (np. kwaśny (<3) odczyn pH wody), co dodatkowo odróżnia to jezioro od Jez. Turawskiego i Jez. Koronowskiego.

Czynniki i procesy odpowiedzialne za rozmieszczenie radionuklidów w osadach kwaśnych jezior pokopalnianych nie zostały dotychczas szczegółowo poznane (Abril i in., 2018; Blasco i in, 2016; Mantero i in, 2020; Thomas i in., 2020, 2022). Charakterystyka procesów wpływających na obieg pierwiastków głównych i śladowych w zbiornikach wodnych na terenie Łuku Mużakowa była wielokrotnie badana (Bożęcki, 2013; Friese, 1998; 2004; Gąsiorowski i in., 2021; Lutyńska and Labus, 2015; Oszkinis-Golon i in., 2021; Pukacz i in., 201; Solski i in., 1988; etc.). W przypadku radioizotopów, analizowano pionowe rozkłady koncentracji ^{137}Cs, czy ^{210}Pb w rdzeniach jezior pokopalnianych, m.in. w celu określenia wieku deponowanych osadów (Sienkiewicz & Gąsiorowski, 2016; Sienkiewicz i in., 2023; etc.). Nie podjęto jednak dotychczas badań dotyczących mechanizmów odpowiedzialnych za dystrybucję radionuklidów w ekosystemach kwaśnych jezior występujących na tym obszarze.

1. Metodyka badań

1.1. Pobór oraz wstępna preparatyka próbek

Pomiar parametrów fizykochemicznych wody (temperatura, pH, potencjał redox (Eh), zawartość rozpuszczonego tlenu (DO), przewodność właściwa, etc.) wykonywano w trakcie prowadzonych prac terenowych *in situ* za pomocą przenośnego miernika wielokanałowego (Multi 3620 IDS SET G). Głębokość zbiorników wodnych badano za pomocą przenośnej echosondy (Echotest II).

Próbki wody pobrano za pomocą stalowego, pionowego czerpaka (poj. 5 L). Wszystkie próbki wody przefiltrowano za pomocą zestawu do filtracji próżniowej z użyciem celulozowych (CA) filtrów membranowych (wielkość porów 0,45 μm) oraz zakonserwowano poprzez dodanie 1 mL podwójnie destylowanego 35% HCl. Następnie przechowywano je w temperaturze 4 °C do czasu wykonania analiz.

Profile osadów jeziornych ze zbiorników zaporowych pobrano za pomocą rdzeniowego próbnika osadów dennych typu Kajak (Ø rury 55 mm), zaś rdzeń osadów jeziornych z Jez. ŁK-61 uzyskano za pomocą rdzeniowego próbnika osadów dennych typu UWITEC (Ø rury 90 mm). Wszystkie profile osadów jeziornych podzielono w warunkach terenowych na 1 cm warstwy, które następnie przechowywano w pojemnikach PET w temperaturze 4 °C. W podobny sposób zabezpieczono również próbki gleb, które pobierano za pomocą plastikowej szpatułki. Pomiar mokrej i suchej gęstości nasypowej oraz zawartości wody wykonano we wszystkich próbkach w Laboratorium Uranowym i Izotopów Stabilnych (LUIS) w Instytucie Nauk Geologicznych Polskiej Akademii Nauk (ING PAN).

1.2. Badania próbek wody

1.2.1. Analizy składu chemicznego

Wszystkie analizy składu chemicznego próbek wody pobranych z Jez. ŁK-61 zostały przeprowadzone w Instytucie Geologii Czeskiej Akademii Nauk (CAS). Pomiar stężenia chlorków wykonano za pomocą techniki wysokosprawnej chromatografii cieczowej (HPLC) (Knauer, Smartline pump 1050). Koncentrację rozpuszczonego węgla organicznego (DOC) zmierzono za pomocą analizatora całkowitego węgla organicznego (TOC-V CPH, Shimadzu). Analiza zawartości pierwiastków głównych (Al, Ca, Mg, S, etc.) została wykonana za pomocą optycznego spektrometru emisyjnego sprzężonego z plazmą wzbudzaną indukcyjnie (ICP-OES) (Agilent 5100). Stężenia pierwiastków

śladowych (Cu, Cr, Mn, Zn, etc.) oznaczono w niskiej (LR) oraz średniej rozdzielczości (MR) za pomocą spektrometru mas sprzężonego z plazmą wzbudzaną indukcyjnie (ICP-MS) (Element 2, ThermoFisher Scientific). Wszystkie analizy prowadzone były w tryplikatach. Dodatkowo, w celu kontroli jakości wykonywanych analiz, każdorazowo mierzono ślepe próby oraz certyfikowany materiał odniesienia (ERM CA 615; European Commission, Joint Research Centre (JRC)).

1.3. Badania próbek osadów

1.3.1. Analiza granulometryczna

Analiza składu granulometrycznego osadów dennych pobranych z Jez. Turawskiego została przeprowadzona za pomocą analizy sitowej w LUIS w ING PAN. Na podstawie uzyskanych wyników próbki osadów jeziornych zaklasyfikowano jako grubo-ziarniste (>0,063 mm) oraz drobno-ziarniste (<0,063 mm) (Cheel, 2005). Analizę rozkładu uziarnienia wybranych próbek osadów dennych pobranych z Jez. Koronowskiego oraz Jez. ŁK-61 wykonano przy użyciu laserowego analizatora wielkości cząstek (CILAS 1190) w Instytucie Geologii CAS. W tym celu próbki uprzednio przesiano przez sito (Ø 1000 μm) oraz preparowano za pomocą 32% H_2O_2, 10% KOH oraz 35% HCl w celu deflokulacji i usunięcia cząstek organicznych. Próbki sklasyfikowano na podstawie uzyskanych wyników przy użyciu pakietu R *"ggtern"* (Hamilton & Ferry, 2018) wykorzystując diagram klasyfikacyjny Sheparda (Shepard, 1954).

1.3.2. Analiza elementarna

Zawartość całkowitego węgla organicznego (TOC) oraz całkowitego azotu (TN) oznaczono we wszystkich próbkach gleb i osadów jeziornych za pomocą analizatora elementarnego (Vario CUBE) w LUIS w ING PAN. W tym celu próbki (5–6 mg) pakowano w cynowe kapsułki i spalano w temperaturze 1150 °C. Uzyskane gazy (CO_2 i N_2) separowane były na kolumnie chromatograficznej, a następnie mierzone za pomocą detektora termokonduktometrycznego. Kwas sulfanilowy (Sigma Aldrich) używany był jako wzorzec zewnętrzny w celu weryfikacji poprawność wykonywanych oznaczeń. Niepewność pomiarów wynosiła odpowiednio 0,6% dla TOC oraz 0,18% dla TN.

1.3.3. Metody radiometryczne

Pomiary aktywności radioizotopów ^{137}Cs oraz ^{40}K w próbkach gleb oraz osadów jeziornych przeprowadzono za pomocą niskotłowego spektrometru gamma (Canberra-Packard) wyposażonego w detektor germanowy (BEGe-5030) w LUIS w ING PAN. Rozdzielczość energetyczna (FWHM) detektora wynosiła około 1.28 keV dla ^{137}Cs (661.7 keV) oraz 1.72 keV dla ^{40}K (1460.8 keV). Kalibracja energetyczna detektora wykonywana była na podstawie pomiarów źródła kalibracyjnego (POLATOM). W celu wykonania kalibracji wydajnościowej detektora użyto oprogramowania ISOCS (In Situ Object Counting System).

Wysuszone oraz zhomogenizowane próbki (od 1 do 50 g w zależności od dostępności materiału) analizowano w okrągłych pojemnikach wykonanych z polietylenu. Czas pomiaru próbek wynosił średnio od 48 do 72 godz. W celu weryfikacji poprawności wykonywanych pomiarów każdorazowo analizowano również certyfikowany materiał odniesienia (IAEA-SL-2; International Atomic Energy Agency (IAEA)). Uzyskane widma spektrometryczne analizowano za pomocą programu Genie 2000. Uzyskane wyniki aktywności badanych radionuklidów korygowano każdorazowo na dzień poboru próbek zgodnie z prawem rozpadu promieniotwórczego.

W celu pomiaru aktywności ^{210}Po w próbkach przeprowadzano separację radiochemiczną tego radioizotopu na podstawie zmodyfikowanej procedury zaproponowanej przez Flynna (1968). W celu określenia chemicznej wydajności procesu odzysku ^{210}Po dodawano do próbek wzorzec $^{208+209}$Po (nr PMP 10030; AEA). Wysuszone oraz zhomogenizowane próbki (około 0,6 g) roztwarzano na płycie grzewczej przy użyciu 35% HCl oraz 65% HNO$_3$. Materia organiczna była usuwana poprzez ogrzewanie próbek wraz z 65% HNO$_3$ oraz 32% H$_2$O$_2$ (Jia i in., 2004; Matthews i in., 2007). Izotopy polonu były następnie osadzane w wyniku spontanicznej depozycji na srebrnych dyskach w 0,5 M HCl. Cytrynian sodu oraz chlorowodorek hydroksyloaminy był dodawany do roztworu, aby zapobiec depozycji konkurencyjnych jonów (np. Fe^{3+}) (Flynn, 1968; Jia i in., 2004).

Aktywność ^{208}Po, ^{209}Po and ^{210}Po mierzono za pomocą spektrometru alfa (Octete, Ortec) w LUIS w ING PAN. Czas pomiaru każdej próbki wynosił średnio około 72 godz. Kalibracja wydajnościowa detektora została przeprowadzona na podstawie pomiarów źródła kalibracyjnego (mieszaniny radioizotopów ^{238}U, ^{234}U, ^{239}Pu, ^{241}Am; nr 81364-

121; Eckert & Ziegler) z zachowaniem geometrii pomiaru. Wydajność detektorów wynosiła średnio 20%. Średni odzysk $^{208+209}$Po wynosił około 60-70%.

1.3.4. Analiza stężeń wybranych pierwiastków

Wysuszone oraz zhomogenizowane osady (około 75 mg) roztwarzano za pomocą mineralizatora mikrofalowego (MARS 6, CEM Corporation, USA) w Instytucie Badań Polarnych i Morskich im. Alfreda Wegenera (AWI). Całkowite roztwarzanie osadów przeprowadzano w pojemnikach (50 mL) wykonanych z PTFE przy użyciu 65% HNO_3, 32% HCl oraz 48% HF w laboratorium o podwyższonej czystości. Próbki po roztworzeniu odparowano stosując przystawkę do mineralizatora mikrofalowego (XVap). Próbki następnie rozpuszczono w 1,5 M HNO_3. W ten sam sposób przygotowano również ślepe próby oraz certyfikowany materiał odniesienia (NRC-MESS-4; National Research Council Canada).

Pomiar koncentracji wybranych pierwiastków (Al, Fe, S, Mg, Cu, Pb, Zn, etc.) w przygotowanych próbkach wykonano za pomocą ICP-OES (iCAP 7000 Series; Thermo Scientific) w AWI. Analizy przeprowadzono w tryplikatach. W celu kontroli jakości przeprowadzonych analiz wykonano dodatkowo pomiary wzorca wewnętrznego stworzonego z certyfikowanych roztworów kalibracyjnych (Roti®Star, CarlRoth GmbH).

1.3.5. Analizy mineralogiczne

Ilościowy skład mineralogiczny wybranych próbek osadów jeziornych pobranych z Jez. Korowskiego określono za pomocą dyfrakcji rentgenowskiej (XRD) w Laboratorium Minerałów Ilastych (ClayLab) w ING PAN. W tym celu próbki zostały utarte wraz ze standardem wewnętrznym (10 wt.% ZnO) oraz 4 mL metanolu w młynku kulowym (McCrone, Retsch). Próbki przygotowano do analizy przy użyciu metody ładowania bocznego, która minimalizuje preferowaną orientację (Środoń i in., 2001). Skład mineralogiczny próbek oznaczono za pomocą dyfraktometru rentgenowskiego ARL X'TRA (Thermo Fisher Scientific). Próbki analizowano w geometrii Bragg-Brentano z wykorzystaniem lampy Cu Kα (40 kV, 30 mA). Wzory dyfrakcyjne uzyskano w zakresie 2,5–65° 2θ z krokiem 0,02° (5 s/krok). Analizy jakościowe i ilościowe wykonano przy użyciu oprogramowania Q-min. Skład mineralogiczny opracowano poprzez dopasowanie uzyskanych dyfraktogramów próbek oraz czystych standardów (Środoń i in., 2001).

Analizy mineralogiczne wybranych próbek osadów jeziornych pobranych z Jez. Koronowskiego przeprowadzono również za pomocą skaningowej mikroskopii elektronowej (SEM) FE-SIGMA VP (Carl Zeiss Microscopy GmbH) sprzężonej z dwoma spektrometrami dyspersji energii (EDS) Quantax XFlash 6|10 (Bruker Nano GmbH) na Wydziale Geologii Uniwersytetu Warszawskiego. W tym celu próbki umieszczono na aluminiowym stoliku za pomocą przewodzącej taśmy węglowej, a następnie pokryto je warstwą spektralnie czystego węgla (o grubości 20 nm) za pomocą napylarki próżniowej Quorum 150T ES (Quorum Technologies, East Sussex). Analizy wykonywano przy aperturze 60 μm oraz napięciu przyspieszającym 20 keV.

Wszystkie analizy mineralogiczne wybranych próbek osadów jeziornych pobranych z Jez. ŁK-61 zostały wykonane w Niemieckim Centrum Badawczym Nauk Geologicznych (GFZ). Skład mineralogiczny próbek oznaczono z pomocą dyfraktometru proszkowego STOE STADI P (PANalytical XPert Pro) z wykorzystaniem lampy Ag. Dyfraktometr został wyposażony w monochromator Ge (111) oraz dwa detektory DECTRIS MYTHEN2. Dyfraktogramy rejestrowane były w zakresie 0-73° 2θ (Q = 0-13,3 Å-1). Wyniki analiz interpretowano z wykorzystaniem metody Rietvelda przy użyciu oprogramowania GSAS-II oraz bazy danych AMCSD (Toby & Von Dreele, 2013).

Analizę składu mineralogicznego wybranych próbek osadów jeziornych wykonano również za pomocą spektrometru podczerwieni (IR) Nicolet iS5 FT-IR (Thermo Fisher Scientific) wyposażonego w przystawkę iD7 oraz układ optyczny z okienkami KBr w GFZ. Dla każdej próbki uśredniono 32 widma o rozdzielczości 4 cm^{-1}. Przedstawione widma zostały zaprezentowane bez korekcji ATR. Widma referencyjne montmorylonitu, kaolinitu i ferrihydrytu mierzono przy tych samych ustawieniach co próbki, natomiast pozostałe widma referencyjne IR uzyskano z bazy danych RRUFF.

Wybrane próbki osadów jeziornych pobranych z Jez. ŁK-61 analizowano również za pomocą SEM (FEI Quanta 3D, FEG Dual Beam) sprzężonego z detektorem EDS (EDAX, Octane elect plus) w laboratorium w GFZ. Niewielką ilość każdej próbki umieszczono za pomocą taśmy węglowej na aluminiowym stoliku, którą następnie pokryto warstwą spektralnie czystego węgla (o grubości 20 nm) za pomocą napylarki próżniowej (LEICA EM ACE600). Analizy przeprowadzono przy aperturze 1000 μm oraz napięciu przyspieszającym 20 keV i prądzie 4 nA.

1.3.6. Analiza składu gatunkowego okrzemek

Skład gatunkowy okrzemek zbadano w Zespole Badań Zmian Środowiska w ING PAN. Preparaty przygotowano zgodnie ze standardową metodą opisaną przez Battarbee (1986). Materię organiczną z osadów jeziornych usunięto poprzez dodanie 30% H_2O_2. Następnie, próbki przemyto trzykrotnie wodą destylowaną oraz rozcieńczono do 20-100 mL. Preparaty trwałe wykonano przy użyciu Naphrax (R.I. = 1,75). Okrywy okrzemek zliczano za pomocą mikroskopu świetlnego (Olympus BX40) sprzężonego z obiektywem immersyjnym ×100. Identyfikację okrzemek przeprowadzono na podstawie klasyfikacji przedstawionej przez Krammera i Lange-Bertalota (1986, 1988, 1991a, 1991b), Lange-Bertalota i Metzeltina (1996), Krammera (2000) oraz Lange-Bertalota i in. (2017). Rekonstrukcję pH wody jeziornej (diatom inferred pH, DI–pH) wykonano na podstawie uzyskanych wyników za pomocą programu C2 (wersja 1.8) (Juggins, 2001). W celu wykonania modelowania zmian odczynu pH wody wykorzystano okrzemkową bazę pH utworzoną dla jezior pokopalnianych położonych na terenie Łuku Mużakowa (Sienkiewicz & Gąsiorowski, 2017).

1.3.7. Analiza danych

Analizy statystyczne przeprowadzono przy użyciu programu Past (wersja 4.03) (Hammer et al. 2001) oraz języka programowania R (R Core Team, 2021). W celu zbadania normalności rozkładu danych wykorzystano test Shapiro-Wilka. W związku z tym, że dane w większości nie charakteryzowały się rozkładem normalnym, związek między badanymi zmiennymi określono na podstawie analizy współczynników korelacji rang Spearmana (wartość p <0,05) za pomocą pakietu R *„Hmisc”* (Frank & Harrell, 2023). Analizę składowych głównych (PCA) wykonano przy użyciu pakietów R *„factoextra”, „corrplot”, „psych”, „FactoMineR”* oraz *„rgl”*. Test Kaisera-Meyera-Olkina (KMO) wykorzystano w celu oceny przydatności macierzy korelacji do przeprowadzenia analizy PCA. Współliniowość zmiennych objaśniających określono na podstawie czynnika inflacji wariancji (VIF) wykorzystując pakiety R *„car”* oraz *„olsrr”*.

Mapy rozkładów przestrzennych zawartości ^{137}Cs, [40]K, TOC oraz TN w osadach dennych Jez. Turawskiego oraz Jez. Koronowskiego wygenerowano za pomocą programu ArcGIS (wersja 10.6) (Esri Co., Ltd., Redlands, Kalifornia, USA). Mapy te opracowano z wykorzystaniem interpolacji metodą ważonych odwrotnych odległości (IDW).

Modelowania termodynamiczne stanu nasycenia roztworów wodnych przeprowadzono za pomocą oprogramowania The Geochemist's Workbench® (GWB) Community Edition (wersja 15.0) wykorzystując zmodyfikowaną bazę danych thermo-minteq firmy GWB (Bethke, 1996). Modelowanie wykonano za podstawie wyników analiz chemicznych próbek wody jeziornej pobranych z Jez. ŁK-61 oraz dostępnych danych literaturowych (Bożęcki, 2013).

2. Najważniejsze wyniki badań

2.1. Streszczenie artykułu nr 1

Sekudewicz, I., Gąsiorowski, M., 2022. Spatial and vertical distribution of ^{137}Cs activity concentrations in lake sediments of Turawa Lake (Poland). Environmental Science and Pollution Research, 29: 80882–80896 (Załącznik nr 2).

Pierwsza publikacja wchodząca w skład cyklu artykułów prezentowanych w ramach niniejszej rozprawy doktorskiej dotyczy czynników warunkujących rozmieszczenie oraz migrację ^{137}Cs w osadach dennych Jez. Turawskiego (Fig. 2). Wnioski przedstawione w niniejszej pracy opierają się na badaniach osadów powierzchniowych (0-3 cm głębokości) (45 próbek), 4 rdzeni osadów jeziornych, a także próbek gleb (5 próbek) oraz osadów dennych (3 próbki) pobranych przy ujściu dopływów (Mała Panew i Libawa) oraz odpływu (Mała Panew) badanego jeziora (Fig. 2). Profile osadów jeziornych zostały pobrane ze strefy litoralnej (TO 0.5 oraz TO 43), przejściowej (TO 19) oraz profundalnej (TO 0.0) Jez. Turawskiego.
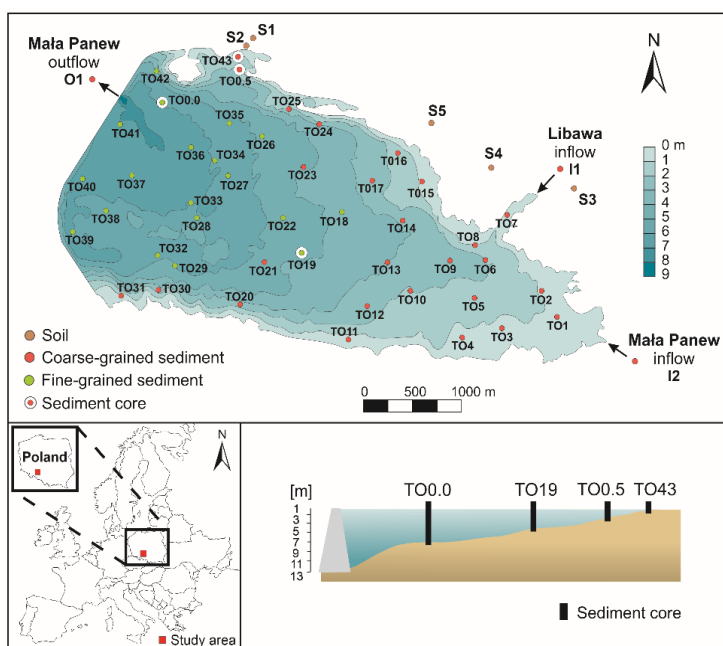
Fig. 2. Lokalizacja oraz mapa batymetryczna Jeziora Turawskiego wraz z zaznaczonymi miejscami poboru próbek (na podstawie: Dost & Mannaerts, 2005) (źródło: Sekudewicz & Gąsiorowski, 2022).

Przeprowadzone badania wykazały, że ^{137}Cs wykrywalny jest nie tylko w głębszych partiach profili osadów jeziornych (będących zapisem jego bezpośredniej depozycji z atmosfery po awarii elektrowni atomowej w Czarnobylu w 1986 r.), ale także w powierzchniowych (0-3 cm głębokości) osadach jeziornych (Fig. 3). Wskazuje to na dalszą migrację ^{137}Cs w ekosystemie Jez. Turawskiego, pomimo upływu ponad 30 lat od katastrofy w Czarnobylu. Obecnie radionuklid ten jest

najprawdopodobniej dostarczany z brzegów jeziora erodowanych w wyniku falowania oraz wahania poziomu wód, a także wskutek erozji gleb i spływu powierzchniowego z terenu zlewni (np., Teisseyre, 1983; Zapata & Nguyen, 2009). Można również przypuszczać, że izotop ten jest transportowany wraz z zanieczyszczonymi cząstkami nanoszonymi przez rzeki zasilające jezioro, szczególnie przez rzekę Libawa, która przepływa przez bardziej zanieczyszczony obszar (Fig. 3). Dowodzi tego podwyższona aktywność ^{137}Cs (59 ± 7 Bq kg^{-1}) w osadach dennych pobranych w pobliżu ujścia tej rzeki (próbka I1). Napływ materiału detrytycznego, potwierdza pośrednio podwyższony stosunek C/N (>20) charakteryzujący gruboziarniste (>0,063 cm) osady jeziorne. Wskazuje on bowiem na obecność w nich materii organicznej pochodzenia allochtonicznego (Meyers & Ishiwatari, 1995).
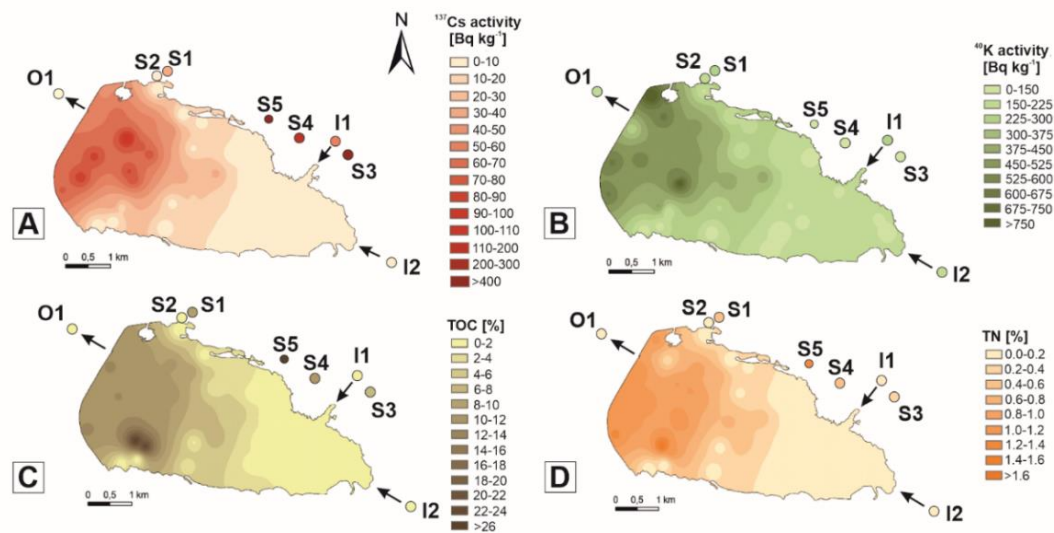

Fig. 3. *Rozkład powierzchniowy stężenia (A) cezu ^{137}Cs, (B) potasu ^{40}K, (C) całkowitego węgla organicznego (TOC) oraz (D) całkowitego azotu (TN) w osadach powierzchniowych (0-3 cm głębokości) Jeziora Turawskiego (źródło: Sekudewicz & Gąsiorowski, 2022).*

W przypadku powierzchniowych (0-3 cm głębokości) osadów jeziornych najwyższe aktywności ^{137}Cs (od 16 ± 2 Bq kg^{-1} – próbka TO 29 do 103 ± 12 Bq kg^{-1} – próbka TO 36) zaobserwowano dla osadów drobnoziarnistych (<0,063 cm) (mułów sapropelowych), które deponowane są w strefie profundalnej Jez. Turawskiego (Fig. 2; 3). Osady gruboziarniste (>0,063 cm), akumulowane w strefie litoralnej jeziora, cechują się z kolei około kilkudziesięciokrotnie niższym stężeniem tego radioizotopu (2.1 ± 0.4 Bq kg^{-1} (mediana); n = 26). Potwierdza to obserwowaną przez Natkaniec (1999) zależność pomiędzy wzrostem aktywności ^{137}Cs a malejącą wielkością uziarnienia osadów dennych. Związane jest to, m.in. z większą powierzchnią właściwą drobnych

(<0,063 cm) ziaren, obecnością minerałów ilastych charakteryzujących się dobrymi właściwościami sorpcyjnymi, a także wyższą zawartością materii organicznej (wyrażonej jako TOC oraz TN) (He & Walling, 1996; Naulier i in., 2017; Park i in., 2021; Rigol i in., 2002; etc.). Zwiększony udział minerałów ilastych w tych osadach jeziornych może potwierdzać pośrednio obserwowany w ich przypadku wzrost aktywności potasu ^{40}K (478 ± 63 Bq kg^{-1} (mediana); n = 19), który bywa stowarzyszony z minerałami zawierającymi potas, takimi jak minerały ilaste, łyszczyki, itd. (Bobos i in., 2021; Madruga i in., 2014; etc.).
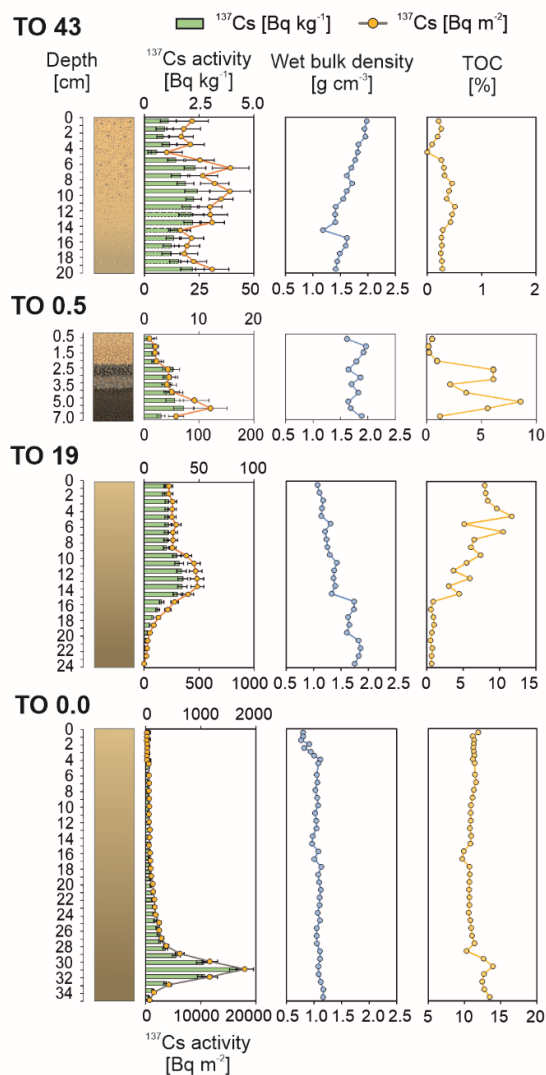
Fig. 4. *Profile pionowe stężenia cezu ^{137}Cs, gęstości nasypowej oraz całkowitego węgla organicznego (TOC) w poszczególnych rdzeniach osadów jeziornych pobranych z Jeziora Turawskiego. Miejsca poboru próbek zostały przedstawione na Fig. 2 (źródło: Sekudewicz & Gąsiorowski, 2022).*

Wyniki przeprowadzonych badań wykazały ponadto, że pionowe rozkłady aktywności ^{137}Cs, a także zawartości TOC oraz gęstości nasypowej w profilach osadów jeziornych (TO 0.5 oraz TO 43) pobranych ze strefy litoralnej Jez. Turawskiego są znacznie zaburzone (Fig. 4). Świadczy to o dynamicznych warunkach sedymentacyjnych panujących w tej części jeziora, związanych falowaniem, wahaniem

poziomu wód oraz występowaniem prądów wiatrowych i zawiesinowych zakłócających przebieg sedymentacji osadów (Teisseyre, 1983; Wojewoda, 2013). W wyniku tego może dochodzić do erozji brzegów i dna jeziora oraz redystrybucji zdeponowanych osadów, a tym samym do wymywania cząstek zawierających ^{137}Cs. Cząstki te wraz z materiałem detrytycznym (<0,063 cm) dostarczanym przez rzeki oraz w wyniku spływu powierzchniowego, deponowane są w głębszych partiach Jez. Turawskiego, gdzie panują bardziej stabilne warunki sedymentacji (Fig. 3). Potwierdza to względnie niezaburzony pionowy rozkład aktywności ^{137}Cs, a także zawartości TOC oraz gęstości nasypowej osadów obserwowany w profilu osadów jeziornych (TO 0.0) pobranym ze strefy profundalnej (Fig. 4). Ograniczony odpływ wody (przez zaporę) dodatkowo sprzyja akumulacji zanieczyszczonych cząstek, co znajduje swoje odzwierciedlenie w podwyższonej koncentracji ^{137}Cs w osadach powierzchniowych w tej części Jez. Turawskiego (Fig. 3). Skutkuje to stosunkowo dużym tempem sedymentacji $(1,0 \pm 0,1 \ \mathrm{cm \ rok^{-1}})$ osadów jeziornych w tej części zbiornika wodnego (obliczonym przy założeniu, że pik aktywności ^{137}Cs $(1670 \pm 150 \ \mathrm{Bq \ kg^{-1}})$ obserwowany na głębokości 31 cm w rdzeniu TO 0.0 jest związany bezpośrednio z opadem atmosferycznym po katastrofie w Czarnobylu) (Fig. 4). Na tej podstawie można również stwierdzić, że badane jezioro może być istotną pułapką dla zanieczyszczeń, w tym dla radioizotopów cezu.

2.2. Streszczenie artykułu nr 2

Sekudewicz, I., Matoušková, Š., Ciesielska, Z., Mulczyk, A., Gąsiorowski, M., 2022. Factors controlling ^{137}Cs distribution in bottom sediments of Koronowo Reservoir (Poland). Journal of Soils and Sediments, 22: 3189–3208 (Załącznik nr 3).

W drugim artykule naukowym stanowiącym część niniejszej rozprawy doktorskiej przedstawiono główne czynniki warunkujące dystrybucję ^{137}Cs w osadach dennych Jez. Koronowskiego. Obszar badań stanowiła część jeziora (strefa VI wg Szatten (2016)) wydzielona od ujścia rzeki Suchej (nieopodal miejscowości Wielonek) do zapory w Pieczyskach (Fig. 5). Wybór tej części Zalewu Koronowskiego motywowany był jej typowo limnicznym charakterem oraz położeniem w pobliżu zapory wodnej (Szatten, 2016). Ponadto, wzięto pod uwagę fakt, że ta część zbiornika wodnego charakteryzuje się największą powierzchnią (499,9 ha), a zgromadzone w niej wody stanowią ponad 1/3 wód retencjonowanych w całym jeziorze. Wnioski przedstawione w tej pracy oparto na badaniach powierzchniowych (0-3 cm głębokości) osadów jeziornych (20 próbek), 2 profili osadów jeziornych oraz 1 profilu glebowego. Rdzenie osadów jeziornych pobrano ze strefy profundalnej jeziora w jego północnej (P1) oraz południowej (P2) części (Fig. 5).
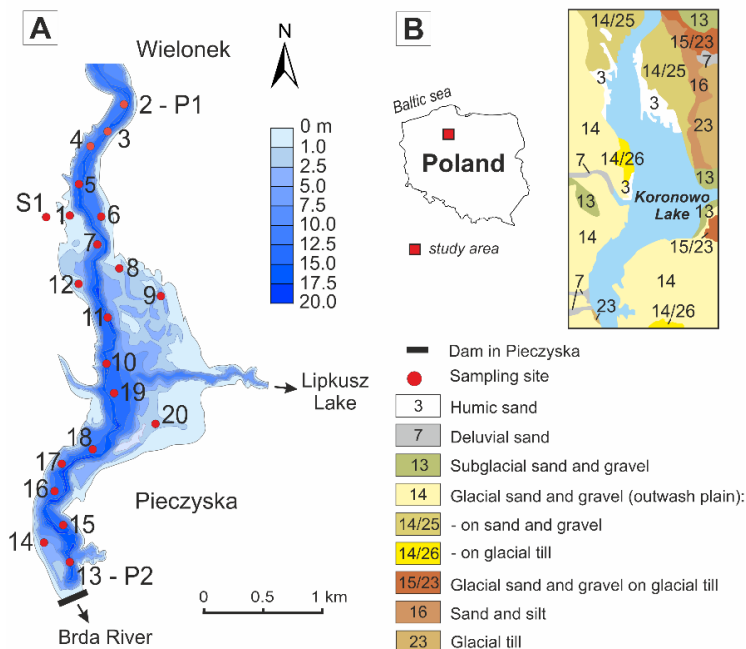
Fig. 5. *(A) Mapa batymetryczna Jeziora Koronowskiego wraz z zaznaczonymi miejscami poboru próbek oraz (B) mapa geologiczna wraz z lokalizacją badanego obszaru (na podstawie: Wieczorek & Stoiński, 2008) (źródło: Sekudewicz i in., 2022).*

Uzyskane wyniki badań wykazały, podobnie jak w przypadku Jez. Turawskiego, że ^{137}Cs wykrywalny jest w powierzchniowej (0-3 cm głębokości) warstwie kolumny

osadów jeziornych (Fig. 6). Jednakże, w tym przypadku najwyższa aktywność ^{137}Cs (30 ± 4 Bq kg^{-1} – próbka 19) zmierzona w osadach powierzchniowych (0-3 cm głębokości) była ponad trzykrotnie niższa od wartości maksymalnej zarejestrowanej w próbkach osadów dennych Jez. Turawskiego (Sekudewicz & Gąsiorowski, 2022). Obecnie ^{137}Cs jest prawdopodobnie dostarczany do Jez. Koronowskiego wraz z zanieczyszczonymi cząstkami nanoszonymi przez rzekę Brda, która jest głównym źródłem zawieszonych osadów transportowanych do tego zbiornika wodnego (Szatten i in., 2018). Nie można wykluczyć, że ^{137}Cs może być także dostarczany do Jez. Koronowskiego wraz z cząstkami wymywanymi z jego brzegów wskutek erozji spowodowanej falowaniem oraz wahaniem poziomu wód, a także ze zlewni jeziora wskutek erozji gleb oraz spływu powierzchniowego (Zapata & Nguyen, 2009).
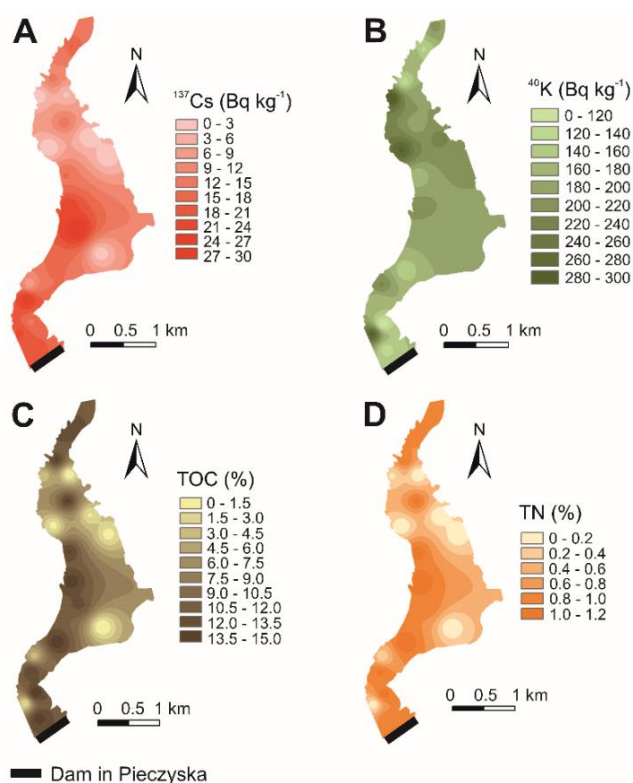
Fig. 6. Rozkład powierzchniowy stężenia (A) cezu ^{137}Cs, (B) potasu ^{40}K, (C) całkowitego węgla organicznego (TOC) oraz (D) całkowitego azotu (TN) w osadach dennych (0-3 cm głębokości) Jeziora Koronowskiego. Miejsca poboru próbek zostały przedstawione na Fig. 5 (źródło: Sekudewicz i in., 2022).

Najważniejszymi czynnikami warunkującymi powierzchniowy rozkład koncentracji ^{137}Cs w osadach dennych Zalewu Koronowskiego, podobnie jak w przypadku Jez. Turawskiego, jest jego kształt oraz morfologia dna, a także charakterystyka deponowanych osadów (przede wszystkim ich skład granulometryczny oraz mineralogiczny). W tym przypadku drobnoziarniste (<0,063 cm) osady powierzchniowe (muły jeziorne) charakteryzowały się niemal czterokrotnie wyższą aktywnością ^{137}Cs (17.7 ± 4.0 Bq kg^{-1} (średnia arytmetyczna); n = 12) w porównaniu

z gruboziarnistymi (>0,063 cm) osadami dennymi (piaskami oraz piaskami pylastymi) (5.1 ± 0.8 Bq kg^{-1} (średnia arytmetyczna); n = 8). Związane jest to, podobnie jak w przypadku Jez. Turawskiego, z obecnością drobnych ziaren (<0,063 cm) oraz podwyższoną zawartością minerałów ilastych oraz materii organicznej (wyrażonej jako TOC oraz TN) (Cornell 1993; He & Walling, 1996; Park i in., 2021; Sawhney 1972; Tachi i in., 2020; i inni).

Muły jeziorne akumulowane są wzdłuż *„dawnego biegu"* rzeki Brdy, a w szczególności w najgłębszych partiach centralnej części badanego akwenu oraz w pobliżu zapory w Pieczyskach (Fig. 6). Wynika to najprawdopodobniej z osadzania się drobnych (< 0,063 cm) cząstek zanieczyszczonych ^{137}Cs w strefie profundalnej jeziora (poniżej podstawy falowania, gdzie panują spokojniejsze warunki sedymentacyjne) w wyniku spadku prędkości przepływu rzeki oraz wskutek ograniczonego odpływu wody przez zaporę. Wyniki analiz statystycznych wykazały jednak, że korelacja pomiędzy zawartością ^{137}Cs oraz udziałem frakcji pylastej (2–63 μm) w próbkach tych osadów jest wyższa, niż w przypadku frakcji ilastej (<2 μm), co może mieć hipotetycznie związek z transportem najdrobniejszych ziaren z biegiem rzeki oraz w kierunku jeziora Lipkusz (Fig. 5) (Tanaka i in., 2015; etc.). Piaski natomiast, zubożone w ^{137}Cs oraz materię organiczną a wzbogacone w ^{40}K, deponowane są w strefie litoralnej tego zbiornika wodnego (Fig. 6). Zwiększona zawartość ^{40}K w próbkach osadów gruboziarnistych (<0,063 cm) związana jest prawdopodobnie z występowaniem w ich składzie mineralogicznym, m.in. skalenia potasowego, który może być wymywany z glin i piasków pochodzenia lodowcowego występujących w utworach zlewni jeziora (Fig. 5).

Analizy profili osadów jeziornych wykazały, że tempo sedymentacji w części południowej Jez. Koronowskiego jest szybsze (>0,8 cm rok^{-1}) niż w części północnej (0,51 cm rok^{-1}). Spowodowane jest to najprawdopodobniej ograniczonym odpływem zawieszonych cząstek przez tamę oraz występowaniem spokojniejszych warunków sedymentacyjnych) w części południowej jeziora (Szatten i in., 2018). Potwierdza to bardziej regularny rozkład pionowy gęstości nasypowej osadów w rdzeniu P2, w porównaniu do profilu osadów P1 (Fig. 7). Dowodzi tego również pionowy rozkład koncentracji ^{137}Cs w rdzeniu P1, w przypadku którego nie można wyróżnić charakterystycznego piku aktywności ^{137}Cs, tak jak w rdzeniu TO 0.0 pobranym z Jez. Turawskiego (Ivanov i in., 2021; Sekudewicz & Gąsiorowski, 2022). Ma to prawdopodobnie związek ze wzmożonym napływem zanieczyszczonych ^{137}Cs cząstek z erodowanej zlewni jeziora po zbudowaniu zapory wodnej. Hipotezę tą może

potwierdzać wzrost koncentracji ^{40}K w tej części profilu osadów jeziornych (Fig. 7) (Bobos i in., 2021; Madruga i in. 2014; Somboon i in., 2018). Wskazuje na to również malejący stosunek C/N oraz wzrost zawartości TOC i TN w rdzeniu P1, sugerujący stopniową zmianę źródła dostawy materii organicznej z allochtonicznej na autochtoniczną oraz wzrost produkcji pierwotnej w czasie (Meyers & Ishiwatari, 1995).
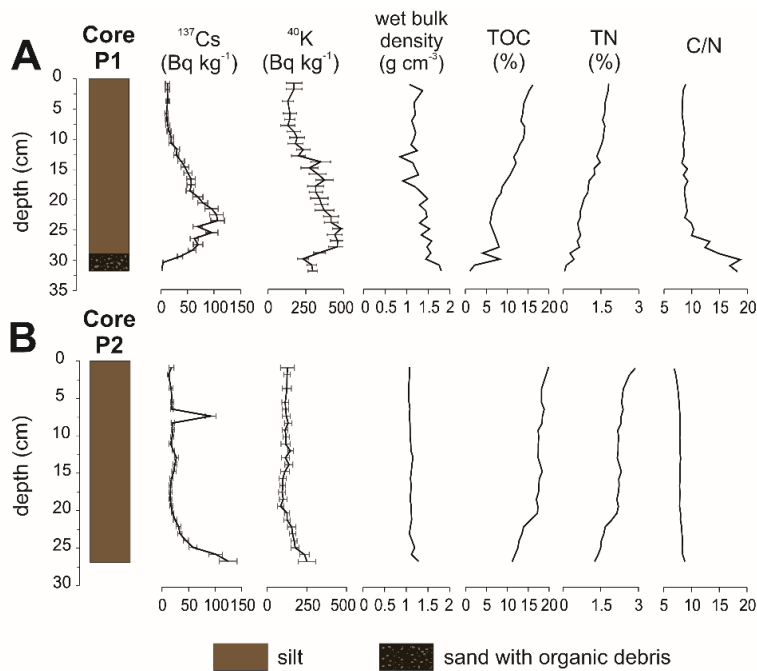


Fig. 7. Profile pionowe stężenia cezu ^{137}Cs, potasu ^{40}K, gęstości nasypowej, całkowitego węgla organicznego (TOC), całkowitego azotu (TN) oraz stosunku C/N w poszczególnych rdzeniach osadów jeziornych pobranych z Jeziora Koronowskiego. Miejsca poboru próbek zostały przedstawione na Fig. 5 (źródło: Sekudewicz i in., 2022).

2.3. Streszczenie artykułu nr 3

W trzecim artykule naukowym, wchodzącym w skład niniejszej rozprawy doktorskiej, przedstawiono najważniejsze czynniki i procesy warunkujące rozmieszczenie wybranych izotopów promieniotwórczych (ze szczególnym uwzględnieniem ^{137}Cs oraz ^{210}Po) oraz metali ciężkich (Cu, Ni, Pb, Zn, itd.) w osadach kwaśnego (pH < 3) jeziora pokopalnianego ŁK-61 (zwane także *„Hydro”* lub *„Staw Południowy”*) znajdującego się na terenie Łuku Mużakowa w zachodniej Polsce (Fig. 8). Wnioski przedstawione w niniejszej pracy opierają się na badaniach 3 próbek wody pobranej z dopływu jeziora (T 1-3), 1 profilu wody jeziornej (WA) oraz 1 profilu osadów jeziornych (C1).
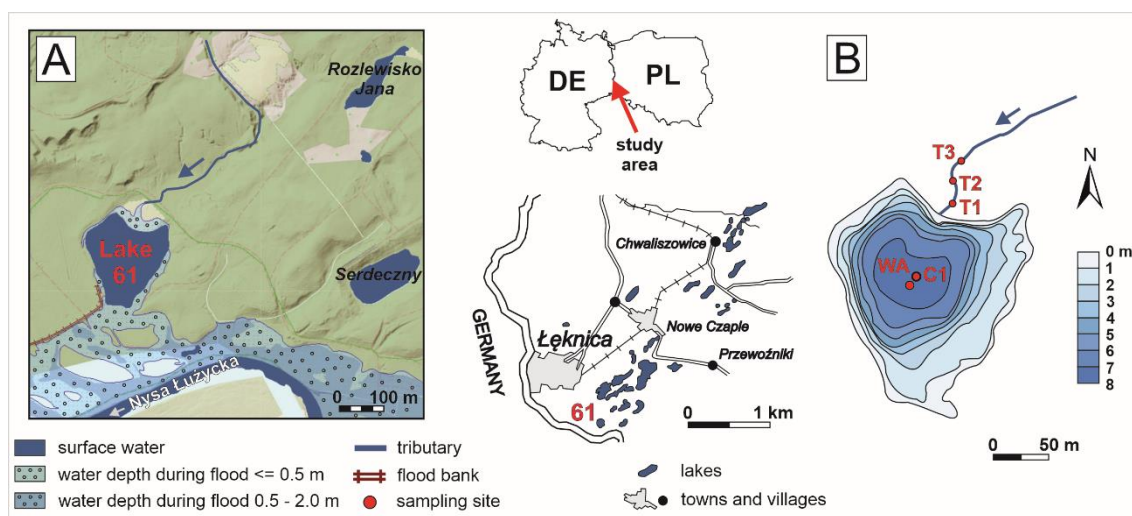
Fig. 8. *(A) Lokalizacja Jeziora ŁK-61 (na podstawie: Sienkiewicz & Gąsiorowski, 2016) wraz z mapą zagrożenia powodziowego (MZP) 10% (raz na 10 lat) (na podstawie: PGW WP, 2021) oraz (B) mapa batymetryczna badanego zbiornika wodnego (źródło: Sekudewicz i in., 2024).*

W prezentowanej pracy skoncentrowano się na badaniach pionowej zmienności stężeń wybranych metali ciężkich oraz radioizotopów (HMRs) w rdzeniu osadów jeziornych pobranego z najgłębszej części Jez. ŁK-61 (Fig. 8). Na podstawie wyników badań zaobserwowano, że ^{137}Cs jest również wykrywalny w powierzchniowej warstwie kolumny osadów, lecz charakteryzuje się on najniższą aktywnością (1.0 ± 0.3 Bq kg^{-1})

w porównaniu z osadami powierzchniowymi (0-3 cm głębokości) pobranymi ze strefy profundalnej Jez. Turawskiego i Jez. Koronowkiego (Fig. 9) (Sekudewicz & Gąsiorowski, 2022; Sekudewicz i in., 2022). Podobnie jak w przypadku wspomnianych jezior zaporowych, ^{137}Cs prawdopodobnie jest obecnie dostarczany do Jez. ŁK-61 wraz z zanieczyszczonymi cząstkami nanoszonymi przez dopływający strumień oraz ze zlewni jeziora w wyniku spływu powierzchniowego (Zapata & Nguyen, 2009; etc.). Ołów ^{210}Pb oraz jego izotop potomny – polon ^{210}Po, mogą być transportowane do Jez. ŁK-61 w podobny sposób jak ^{137}Cs, oprócz bezpośredniej depozycji allogenicznego (z ang. *„unsupported"*) ^{210}Pb z atmosfery (Appleby, 2005; Swarzenski, 2014; etc). Metale ciężkie (Cu, Ni, Zn, zn, itd.) mogą natomiast pochodzić zarówno z utleniania pirytu występującego w lignitach, jak i ze zlewni jeziora (Geller i in., 2013; Wisotzky, 1998; etc.). Hipotezę tą potwierdzają wyniki analiz składu chemicznego próbek wody pobranych z dopływu jeziora, które wykazały, że stanowi on ważne źródło jonów, a prawdopodobnie także cząstek stałych.

Na podstawie przeprowadzonych badań wykazano, że najważniejszymi procesami wpływającymi na dystrybucję HMRs w osadach jeziornych Jez. ŁK-61 są: 1) rozpuszczanie się poszczególnych minerałów, 2) strącanie się/współstrącanie się rozpuszczonych pierwiastków wraz z krystalizującymi minerałami wtórnymi (jak ferrihydryt, czy kaolinit), a także 3) ich adsorpcja/absorpcja na minerałach autogenicznych oraz allogenicznych (Cánovas i in., 2007; Carvalho i in., 2017; Cook i in., 2018; Hierro i in., 2014; Park i in., 2021; Sawhney, 1972; Shi i in., 2021; Walling & Quine, 1993; etc.).

Zaburzenia w profilach pionowych stężeń HMRs w kolumnie osadów jeziornych (objawiające się znacznym wzrostem zawartości tych pierwiastków pomiędzy 7 a 12 cm głębokości rdzenia) wskazują, że wymienione procesy zostały najprawdopodobniej zakłócone w przeszłości (Fig. 9, 10). Prawdopodobną przyczyną tego zjawiska było wezbranie w zlewni Nysy Łużyckiej w dniach 7 – 10 sierpnia 2010 r. (MKOO, 2010). Powódź ta spowodowała najprawdopodobniej wlanie się wód rzeki do badanego zbiornika, a to doprowadziło z kolei do zmiany właściwości fizykochemicznych (wzrost pH, spadek konduktywności, itd.) oraz składu chemicznego wody jeziornej, na co mogą wskazywać wyniki pomiarów wykonane w tamtym czasie przez Bożęckiego (2013). Znaczny wzrost pH (do około $7 \pm 0,5$) wody jeziornej w przeszłości został potwierdzony poprzez rekonstrukcję pH wykonaną na podstawie analizy składu

gatunkowego okrzemek w próbkach pochodzących z głębokości 8 – 10 cm profilu osadów jeziornych.
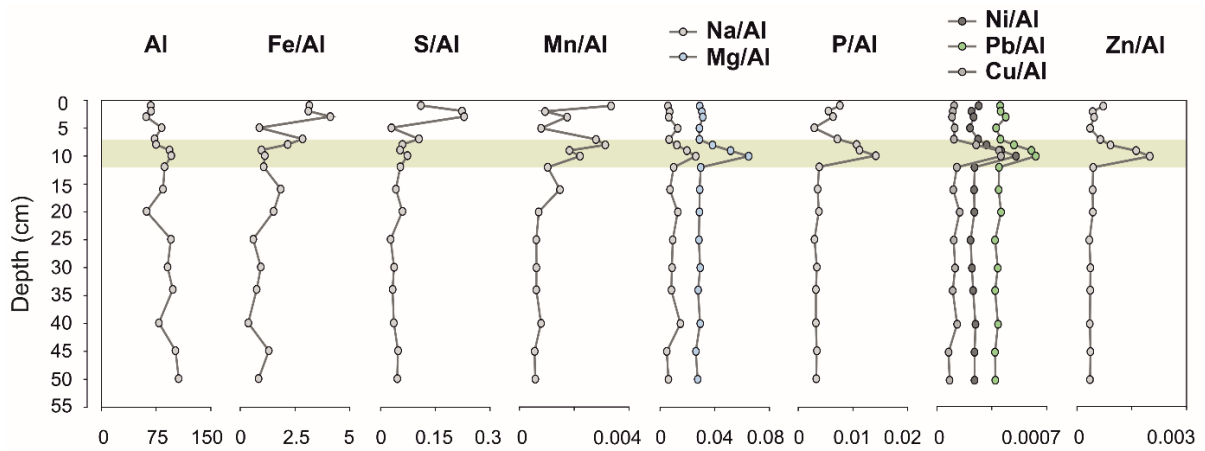
Fig. 10. *Profile pionowe stężenia glinu (Al) oraz znormalizowanych do Al zawartości wybranych pierwiastków (Fe, S, Mn, Na, Mg, P, Ni, Pb, Cu, oraz Zn) w rdzeniu osadów jeziornych (C1) pobranego z Jeziora ŁK-61 (źródło: Sekudewicz i in., 2024).*
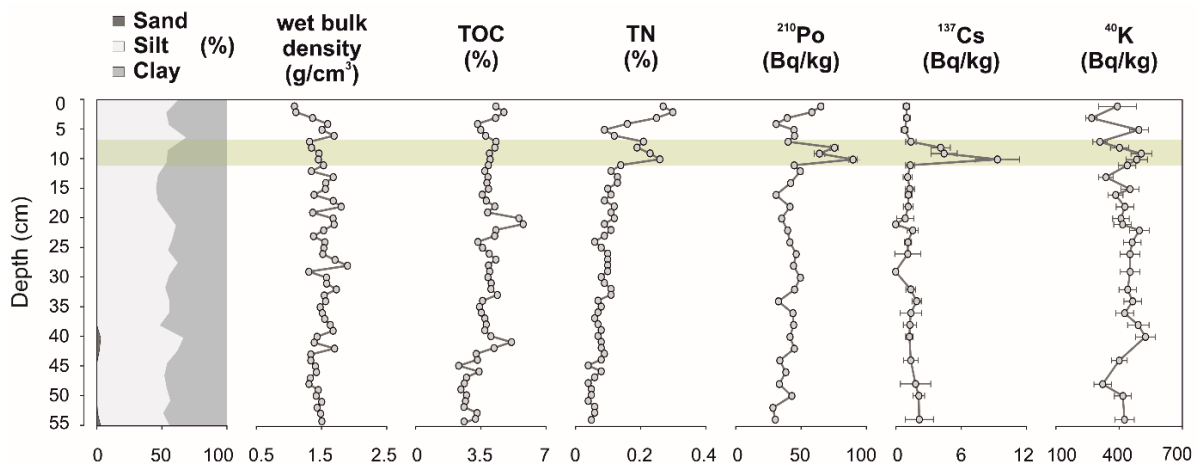
Fig. 9. *Profile pionowe zwartości poszczególnych frakcji uziarnienia (piasku, pyłu i mułu), gęstości nasypowej, stężenia całkowitego węgla organicznego (TOC), całkowitego azotu (TN), polonu ^{210}Po, cezu ^{137}Cs oraz potasu ^{40}K w rdzeniu osadów jeziornych (C1) pobranego z Jeziora ŁK-61 (źródło: Sekudewicz i in., 2024).*

Nagła zmiana właściwości fizykochemicznych wody jeziornej mogła spowodować wytrącanie się nowych faz mineralnych (np. schwertmannitu) wraz z rozpuszczonymi pierwiastkami, które były następnie deponowane na dnie zbiornika, tworząc warstwę wzbogaconą w HMRs (Alpers i in., 1994; Azzali i in., 2014; Cánovas i in., 2007; Hierro i in., 2014; etc.). Hipotezę tą potwierdzają modelowania geochemiczne oraz analizy mineralogiczne wybranych próbek osadów jeziornych. Wzrost zawartości HMRs w tej części rdzenia można dodatkowo tłumaczyć dostawą cząstek wraz z wodami

powodziowymi, które sorbowały rozpuszczone pierwiastki (Mayes i in., 2021). Wzrost odczynu pH wody jeziornej mógł z kolei sprzyjać sorpcji zanieczyszczeń przez minerały ilaste, takie jak kaolinit, który wykazuje lepsze właściwości sorpcyjne w wyższych wartościach pH (Jiang i in., 2010). Ponadto, nie można wykluczyć, że w wyniku powodzi zostały dostarczone znaczne ilości rozpuszczonych substancji oraz cząstek zanieczyszczonych HMRs, które zostały następnie zakumulowane na dnie badanego zbiornika wodnego (Herzsprung i in., 2010). Sugerowany napływ materiału detrytycznego do Jez. ŁK-61 może potwierdzać wzrost aktywności ^{137}Cs w tej części (7 – 12 cm) rdzenia, ponieważ izotop ten może być istotnym wskaźnikiem erozji i redystrybucji gleby, a także może służyć jako marker chronostratygraficzny, np. na terenach zalewowych (Łokas i in., 2010; Walling & He, 1997; Walling & Quine, 1993; Zapata & Nguyen, 2009; etc.). Dodatkowo, hipotezę tą potwierdza podwyższony stosunek C/N (>20) w tych próbkach osadów jeziornych, wskazujący na obecność materii organicznej pochodzenia allochtonicznego (Meyers & Ishiwatari, 1995).

Biorąc pod uwagę, że roczny transport ^{210}Po (245 kBq rok^{-1}) w Nysie Łużyckiej jest stosunkowo wysoki, można przypuszczać, że obserwowany wzrost aktywności ^{210}Po pomiędzy 7 – 12 cm głębokości rdzenia może być również wynikiem wezbrania w zlewni Nysy Łużyckiej (Skwarzec i in., 2012). Źródłem ^{210}Po zakumulowanego w tej warstwie osadów mogły być również nawozy fosforowe, które znane są jako główne źródła antropogeniczne ^{210}Pb oraz ^{210}Po (Cook i in., 2018; Barbero i in., 2014; Carvalho i in., 2017). Hipotezę tą może potwierdzać wzrost zawartości NO^{3-} oraz PO_4^{3-} w wodzie jeziornej w sierpniu 2010 r. zarejestrowany przez Bożęckiego (2013). Co więcej, wzrost ten prawdopodobnie można powiązać z podwyższoną zawartością TN oraz P pomiędzy 7 a 12 cm głębokości rdzenia (Fig. 9, 10). Podejrzewa się również, że dostawa składników odżywczych mogła spowodować zwiększoną produktywność pierwotną oraz wpłynąć na większą różnorodność gatunkową glonów (na co wskazują badania subfosylnych okrzemek). Nie wykluczone jest, że zjawisko to mogło również odegrać istotną rolę w sorpcji rozpuszczonych HMRs oraz ich późniejszej akumulacji w osadach dennych Jez. ŁK-61 (Kleeberg & Grüneberg, 2005; Paulsson & Widerlund, 2021).

3. Podsumowanie

Wyniki badań przedstawione w niniejszej rozprawie doktorskiej pozwoliły na określenie najważniejszych mechanizmów odpowiedzialnych za rozmieszczenie wybranych radionuklidów w osadach dwóch jezior zaporowych – Jez. Turawskiego i Jez. Koronowskiego oraz jeziora pokopalnianego – Jez. ŁK-61 dotkniętego występowaniem kwaśnych wód kopalnianych (AMD).

Przeprowadzone badania wykazały przede wszystkim, że:

- Dominującymi czynnikami warunkującymi rozkład zawartości ^{137}Cs w osadach powierzchniowych zbiorników zaporowych są rodzaj oraz cechy deponowanego osadu, przy czym na ich powstawanie i rozmieszczenie wpływają zachodzące procesy sedymentacyjne oraz inne czynniki środowiskowe (np. geometria zbiornika).

- Osady drobnoziarniste (<0,063 cm) deponowane w strefie profundalnej badanych jezior charakteryzują się wyższą zawartością ^{137}Cs, w porównaniu do osadów gruboziarnistych (>0,063 cm) akumulowanych w strefie litoralnej. Związane jest to, m.in z większą powierzchnią właściwą drobnych ziaren oraz zwiększoną zawartością minerałów ilastych (charakteryzujących się dobrymi właściwościami sorpcyjnymi) w osadach drobnoziarnistych.

- Dominującymi procesami odpowiedzialnymi za rozmieszczenie izotopów ^{137}Cs, ^{210}Po oraz metali ciężkich (Cu, Pb, Ni, Zn, itd.) w osadach kwaśnego (pH <3) jeziora pokopalnianego (Jez. ŁK-61) są strącanie/współstrącanie się HMRs z minerałami wtórnymi oraz ich sorpcja na minerałach autogenicznych oraz allogenicznych, które to procesy są znacząco uzależnione od parametrów fizykochemicznych wody jeziornej.

- Ważnym czynnikiem wpływającym na zawartość oraz rozmieszczenie badanych radionuklidów w osadach jeziornych wybranych zbiorników antropogenicznych jest obecność dopływów, które są prawdopodobnie istotnym źródłem zanieczyszczonych cząstek.

- Ograniczony odpływ wody z jeziora również znacząco wpływa na akumulację i rozmieszczenie radioizotopów, co zaobserwowano szczególnie w przypadku zbiorników retencyjnych, w których nagromadzenie ^{137}Cs następuje w dużej mierze w pobliżu zapory wodnej (ze względu na ograniczony odpływ wody i zawiesiny). Wskazuje to również na fakt, że jeziora te mogą stanowić dobrą pułapkę dla zanieczyszczeń, takich jak radioizotopy cezu.

• Analizy pionowego rozkładu koncentracji wybranych radioizotopów w profilach osadów jeziornych wykazały, że na ich podstawie możemy śledzić zmiany zachodzące w badanych jeziorach w przeszłości. Odchylenia od modelowego rozkładu koncentracji ^{137}Cs w rdzeniu osadów jeziornych pobranym z północnej części basenu Jez. Koronowskiego wskazały na wzmożoną erozję osadów w zlewni jeziora oraz napływ zanieczyszczonych ^{137}Cs cząstek tuż po zbudowaniu zapory wodnej oraz stopniową stabilizację panujących warunków w jeziorze w czasie.

• W przypadku Jez. ŁK-61 zaobserwowano, że procesy odpowiedzialne za dystrybucję radioizotopów i metali ciężkich (HMRs) w tym zbiorniku wodnym mogą być zaburzane przez wydarzenia depozycyjne, co miało miejsce prawdopodobnie w wyniku wezbrania w zlewni Nysy Łużyckiej w sierpniu 2010 r. Zaburzenia obserwowane w pionowym rozmieszczeniu zawartości HMRs w profilu osadów jeziornych pobranym z Jez. ŁK-61 uniemożliwiły dokładne określenie wieku zdeponowanych osadów, jednak wskazały, że izotopy ^{137}Cs oraz ^{210}Po mogą służyć jako istotne markery chronostratygraficzne wydarzeń depozycyjnych, takich jak powódź.

4. Bibliografia

Abril, J.M., San Miguel, E.G., Ruiz-Canovas, C., Casas-Ruiz, M., Bolívar, J.P., 2018. From floodplain to aquatic sediments: Radiogeochronological fingerprints in a sediment core from the mining impacted Sancho reservoir (SW Spain). Sci. Total Environ., 631–632, 866–878.

Acero, P., Ayora, C., Torrent´o, C., Nieto, J.M., 2006. The behavior of trace elements

Alpers, C.N., Blowes, D., Nordstrom, D.K., Jambor, J.L., 1994. Secondary minerals and acid mine-water chemistry. Mineral. Assoc. Canada Short Course 247–270.

Ambrożewski Z. J., 2011. 50 lat zbiornika i elektrowni wodnej Koronowo. Gospodarka Wodna, 12, 512–519.

Appleby, P.G., 2005. Chronostratigraphic techniques in recent sediments. W: Tracking Environmental Change Using Lake Sediments. Kluwer Academic Publishers, 171–203.

Appleby, P.G., 2008. Three decades of dating recent sediments by fallout radionuclides: A review. Holocene. https://doi.org/10.1177/0959683607085598

Azzali, E., Marescotti, P., Frau, F., Dinelli, E., Carbone, C., Capitani, G., Lucchetti, G., 2014. Mineralogical and chemical variations of ochreous precipitates from acid sulphate waters (asw) at the Ros¸ia Montan˘a gold mine (Romania). Environ. Earth Sci. 72, 3567–3584.

Barbero, L., Gazquez, M.J., Bolívar, J.P., Casas-Ruiz, M., Hierro, A., Baskaran, M., Ketterer, M.E., 2014. Mobility of Po and U-isotopes under acid mine drainage conditions: an experimental approach with samples from Río Tinto area (SW Spain). J. Environ. Radioact. 138, 384–389.

Bartczak, E., Gancarz, A., 1998. Szczegółowa Mapa Geologiczna Polski 1:50 000. Seria: 645 – Łęknica (M-33-18-A), 646 – Trzebiel (M-33-18-B). Polski Instytut Geologiczny (PIG).

Battarbee, R. W., 1986. Diatom analysis. W: Berglund, B.E. (ed.), Handbook of Holocene Palaeoecology and Palaeohydrology. John Willey and Sons, 527–570.

Bethke, C.M., 1996. Geochemical Reaction Modeling. Oxford University Press.

Blasco, M., Gazquez, M.J., Perez-Moreno, S.M., Grande, J.A., Valente, T., Santisteban, M., de la Torre, M.L., Bolívar, J.P., 2016. Polonium behaviour in reservoirs potentially affected by acid mine drainage (AMD) in the Iberian Pyrite Belt (SW of Spain). J. Environ. Radioact. 152, 60–69.

Bobos, I., Madruga, M.J., Reis, M., Esteves, J., Guimarães, V., 2021. Clay mineralogy insights and assessment of the natural (^{228}Ra, ^{226}Ra, ^{210}Pb, ^{40}K) and anthropogenic (^{137}Cs) radionuclides dispersion in the estuarine and lagoon systems along the Atlantic coast of Portugal. Catena, 206: 105532.

Bożęcki, P., 2013. Studium osadów tworzących się w obszarze eksploatacji węgla brunatnego w rejonie Łęknicy (Łuk Mużakowa) (rozprawa doktorska). Akademia Górniczo-Hutnicza im. Stanisława Staszica (rozprawa doktorska), Kraków.

Cánovas, C.R., Olías, M., Nieto, J.M., Sarmiento, A.M., Ceron, J.C., 2007. Hydrogeochemical characteristics of the Tinto and Odiel Rivers (SW Spain). Factors controlling metal contents. Sci. Total Environ. 373, 363–382.

Carvalho, F., Fernandes, S., Fesenko, S., Holm, E., Howard, B., Martin, P., Phaneuf, M., Porcellid, D., Prohl, G., Twining, J., 2017. The Environmental Behaviour of Polonium. In: Technical Reports Series No. 484. International Atomic Energy Agency, Vienna.

Cieśla, W., Malczyk, P., Kędzia, W., Majle, T., Pachocki, K., 1994. [137]Cs i [134]Cs w glebach województwa bydgoskiego. Zesz Probl Postępów Nauk Rol, 414: 11–20.

Ciszewski, D., Czajka, A., Błażej, S., 2008. Rapid migration of heavy metals and ^{137}Cs in alluvial sediments, Upper Odra River valley, Poland. Environ. Geol., 55, 1577–1586.

Comans, R.N.J., Middelburg, J.J., Zonderhuis, J., Woittiez, J.R.W., De Lange, G.J., Lange, G.J., Das, H.A., Van der Weijden, C.H., 1989. Mobilization of radiocaesium in pore water of lake sediments. Nature, 339: 367–369.

Cook, N., Ehrig, K., Rollog, M., Ciobanu, C., Lane, D., Schmandt, D., Owen, N., Hamilton, T., Grano, S., 2018. [210]Pb and [210]Po in Geological and Related Anthropogenic Materials: Implications for Their Mineralogical Distribution in Base Metal Ores. Minerals 8, 211.

Cornell, R.M., 1993. Adsorption of cesium on minerals: a review. J Radioanal Nucl Chem Artic, 171: 483–500.

Cheel, R.J., 2005. Grain texture. W: Cheel, R.J. (ed) Introduction to clastic sedimentology. Brock University Middleton, Ontario, 8–46.

Dost, R.J.J., Mannaerts, C.M.M., 2005. Generation of lake bathymetry using SONAR, satellite imagery and GIS. W: ESRI 2008: Proceedings of the 2008 ESRI International User Conference Enschede, The Netherlands.

Evans, D.W., Alberts, J.J., Clark, R.A., 1983. Reversible ion-exchange fixation of cesium-137 leading to mobilization from reservoir sediments. Geochim Cosmochim Acta 47:1041–1049

Flynn, W.W., 1968. The determination of low levels of polonium-210 in environmental materials. Anal Chim Acta, 43: 221–227.

Frank, M., Harrell, E., 2023. Package "Hmisc" Title Harrell Miscellaneous.

Friese, K., 2004. Depth distribution of heavy metals in lake sediments from lignite mine pit lakes of Lusatia (Germany). Stud Quat, 21, 197–205.

Friese, K., Hupfer, M., Schultze, M., 1998. Chemical characteristics of water and sediment in acid mining lakes of the Lusatian Lignite District. In: Geller, W., Klapper, H., Salomons, W. (Eds.), Acidic Mining Lakes, Environmental Science. Springer, Berlin, Heidelberg, pp. 25–45.

Funaki, H., Yoshimura, K., Sakuma, K., Iri, S., Oda, Y., 2019. Evaluation of particulate ^{137}Cs discharge from a mountainous forested catchment using reservoir sediments and sinking particles. J Environ Radioact, 210: 105814.

Gąsiorowski, M., Stienss, J., Sienkiewicz, E., Sekudewicz, I., 2021. Geochemical Variability of Surface Sediment in Post-Mining Lakes Located in the Muskau Arch (Poland) and Its Relation to Water Chemistry. Water Air Soil Pollut, 232, 1–12.

Geller, W., Schultze, M., Kleinmann, R., Wolkersdorfer, C., 2013. Acidic pit lakes: The legacy of coal and metal surface mines. Environ. Sci. Eng. Springer.

Gradziński, R., Kostecka, A., Radomski, A. Unrug, R., 1986. Zarys Sedymentologii. Wydawnictwa Geologiczne, Warszawa.

Hamilton, N.E., Ferry, M., 2018. ggtern: ternary diagrams using ggplot2. J Stat Softw Code Snippets, 87(3): 1–17.

Hammer, Ø., Harper, D.A.T., Ryan, P.D., 2001. PAST: paleontological statistics software package for education and data analysis. Palaeontol Electron, 4: 9.

He, Q., Walling, D.E., 1996. Interpreting particle size effects in the adsorption of ^{137}Cs and unsupported ^{210}Pb by mineral soils and sediments. J Environ Radioact, 30(2): 117–137.

Herschy, R.W. 2012. Lake Sediments. In: Bengtsson, L., Herschy, R.W., Fairbridge, R.W. (eds) Encyclopedia of Lakes and Reservoirs. Encyclopedia of Earth Sciences Series. Springer, Dordrecht.

Herzsprung, P., Schultze, M., Hupfer, M., Boehrer, B., Tümpling, W. v., Duffek, A., Van der Veen, A., Friese, K., 2010. Flood effects on phosphorus immobilisation in a river water filled pit lake-Case study Lake Goitsche (Germany). Limnologica 40, 182–190.

Hierro, A., Olías, M., Ketterer, M.E., Vaca, F., Borrego, J., C´anovas, C.R., Bolivar, J.P., 2014. Geochemical behavior of metals and metalloids in an estuary affected by acid mine drainage (AMD). Environ. Sci. Pollut. Res. 21, 2611–2627.

Isajenko, K., Piotrowska, B., Stawarz, O., Wojtkowski, K., 2022. Monitoring promieniowania jonizującego realizowany w ramach państwowego monitoringu środowiska w latach 2020-2022. Centralne Laboratorium Ochrony Radiologicznej, Zakład Dozymetrii, Warszawa.

Ivanov, M.M., Konoplev, A.V., Walling, D.E., i in., 2021. Using reservoir sediment deposits to determine the longer-term fate of chernobyl derived ^{137}Cs fallout in the fluvial system. Environ Pollut, 274.

Jia, G., Torri, G., Petruzzi, M., 2004. Distribution coefficients of polonium between 5% TOPO in toluene and aqueous hydrochloric and nitric acids. Appl. Radiat. Isot., 61, 279–282.

Jiang, M. Qin, Jin, X. Ying, Lu, X.Q., Chen, Z. Liang, 2010. Adsorption of Pb(II), Cd(II), Ni(II) and Cu(II) onto natural kaolinite clay. Desalination 252, 33–39.

Juggins, S., 2001. Software for ecological and palaeoecological data analysis and visualization. User guide Version, 1.5, 1–73.

Kaminski, S., Richter, T., Walser, M., Lindner, G., 1994. Redissolution of cesium radionuclides from sediments of freshwater lakes due to biological degradation of organic matter. Radiochim Acta, 66(67): 433–436.

Kansanen, P.H., Jaakkola, T., Kulmala, S., Suutarinen, R., 1991. Sedimentation and distribution of gamma emitting radionuclides in bottom sediments of southern Lake Piijanne, Finland, after the Chernobyl accident. Hydrobiologia, 222: 121–140.

Klaminder, J., Appleby, P., Crook, P., Renberg, I., 2012. Post-deposition diffusion of 137Cs in lake sediment: Implications for radiocaesium dating. Sedimentology, 59, 2259–2267.

Kleeberg, A., Grüneberg, B., 2005. Phosphorus mobility in sediments of acid mining lakes, Lusatia, Germany. Ecol. Eng. 24, 89–100.

Konoplev, A., Wakiyama, Y., Wada, T., i in., 2022. Reconstruction of time changes in radiocesium concentrations in the river of the Fukushima Dai-ichi NPP contaminated area based on its depth distribution in dam reservoir's bottom sediments. Environ Res, 206: 112307.

Koźma J., 2009. Rezerwat geologiczno-krajobrazowy Kopalnia Babina w Łęknicy, W: Kupetz A., Kupetz M., Der Muskauer Faltenbogen. Wyd. Verlag Dr Freidrich Pfeil, München.

Koźma, J., Kupetz, M., 2008. The transboundary Geopark Muskau Arch (Geopark Łuk Mużakowa, Geopark Muskauer Faltenbogen). Przegląd Geol., 56, 692–698.

Krammer, K., 2000. Diatoms of Europe. Vol. 1: The Genus Pinnularia. A.R.G. Gantner Verlag. Kommanditgesellschaft, Königstein, 1-703.

Krammer, K., Lange-Bertalot, H., 1986. Süßwasserflora von Mitteleuropa. Bacillariophyceae. I. Teil: Naviculaceae. Gustav Fisher Verlag, Stuttgart.

Krammer, K., Lange-Bertalot, H., 1988. Süßwasserflora von Mitteleuropa. Bacillariophyceae. 2. Teil: Bacillariaceae, Epithemiaceae, Surirellaceae. Gustav Fisher Verlag, Stuttgart.

Krammer, K., Lange-Bertalot, H., 1991a. Süßwasserflora von Mitteleuropa. Bacillariophyceae. 3. Teil: Centrales, Fragilariaceae, Eunotiaceae. Gustav Fisher Verlag, Stuttgart.

Krammer, K., Lange-Bertalot, H., 1991b. Süßwasserflora von Mitteleuropa. Bacillariophyceae. 4. Teil: Achnanthaceae, Kritische Ergänzungen zu Navicula (Lineolatae) und Gomphonema, Gesamtliteraturverzeichnis Teil, 1–4. Gustav Fisher Verlag, Stuttgart.

Kupetz, M., 1997. Geologischer Bau und Genese der Stauchendmorane Muskauer Faltenbogen. Brandenburgische Geowiss. Beitr. 4, 2.

Kurikami, H., Kitamura, A., Thomas Yokuda, S., Onishi, Y., 2014. Sediment and 137Cs behaviors in the Ogaki Dam Reservoir during a heavy rainfall event. J Environ Radioact, 137:10–17.

Laceby, J.P., Huon, S., Onda, Y., I in., 2016. Do forests represent a long term source of contaminated particulate matter in the Fukushima Prefecture? J. Environ. Manage., 183(3): 742–753.

Lange-Bertalot, H., Hofmann, G., Werum, M. and Cantonati, M., 2017. Freshwater Benthic Diatoms of Central Europe: Over 800 Common Species Used in Ecological Assessment. English edition with updated taxonomy and added species. Koeltz Botanical Books, Schmitten-Oberreifenberg, 942.

Lange-Bertalot, H., Metzeltin, D., 1996. Indicators of oligotrophy. 800 taxa representative of three ecologically distinct lake types: carbonate buffered, oligodystrophic, weakly buffered soft water. W: Lange-Bertalot, H., (ed.), Iconographia Diatomologica, Annotated Diatom Micrographs 2, Koeltz Scientic Books, Köningstein.

Łokas, E., Wachniew, P., Ciszewski, D., Owczarek, P., Chau, N.D., 2010. Simultaneous use of trace metals, ^{210}Pb and ^{137}Cs in floodplain sediments of a lowland river as indicators of anthropogenic impacts. Water. Air. Soil Pollut., 207, 57–71.

Lutyńska, S., Labus, K., 2015. Identification of processes controlling chemical composition of pit lakes waters located in the eastern part of Muskau Arch (Polish- German borderland). Arch. Environ. Prot. 41, 60–69.

Machowski, R., Ruman, M., Rzętała, M.A., Rzętała, M., 2008. Morfologia dna i strefy litoralnej Zbiornika Turawskiego. Kształtowanie środowiska geograficznego i ochrona przyrody na obszarach uprzemysłowionych i zurbanizowanych, 39: 45–57.

Madruga, M.J., Silva, L., Gomes, A.R., Libânio, A., Reis, M., 2014. The influence of particle size on radionuclide activity concentrations in Tejo River sediments. J Environ Radioact, 132: 65–72.

Mantero, J., Thomas, R., Holm, E., R¨a¨af, C., Vioque, I., Ruiz-Canovas, C., García-Tenorio, R., Forssell-Aronsson, E., Isaksson, M., 2020. Pit lakes from southern Sweden: natural radioactivity and elementary characterization. Sci. Rep. 10, 1–17.

Matthews, K.M., Kim, C.K., Martin, P., 2007. Determination of ^{210}Po in environmental materials: a review of analytical methodology. Appl Radiat Isot, 65: 267–279.

Mayes, W.M., Perks, M.T., Large, A.R.G., Davis, J.E., Gandy, C.J., Orme, P.A.H., Jarvis, A.P., 2021. Effect of an extreme flood event on solute transport and resilience of a mine water treatment system in a mineralised catchment. Sci. Total Environ., 750.

Meyers, P.A., Ishiwatari, R., 1995. Organic matter accumulation records in lake sediments. W: Lerman, A., Imboden, D.M., Gat, J.R. (eds.) Physics and Chemistry of Lakes. Springer, Berlin, 279–328.

Mietelski, J.W., Dubchak, S., Błażej, S., Anielska, T., Turnau, K., 2010. ^{137}Cs and ^{40}K in fruiting bodies of different fungal species collected in a single forest in southern Poland. J Environ Radioact, 101(9): 706–711.

MKOO (Międzynarodowa Komisja Ochrony Odry przed Zanieczyszczeniem), 2010. Wezbranie w zlewni Nysy Łużyckiej 7–10 sierpnia 2010 r. Wrocław, Drezno, Praga. http://www.mkoo.pl/download.php?fid=4043&lang=PL

Muñoz-Salinas, E., Castillo, M., Romero, F., Correa-Metrio, A., 2021. Understanding sedimentation at the El Molinito reservoir (NW Mexico) before and after dam construction using physical sediment analyses. J. South Am. Earth Sci. 111, 103401.

Natkaniec, J., 1999. Akumulacja antropogenicznych pierwiastków promieniotwórczych w glebach okolic Nysy i Opola oraz osadach zbiornika Turawa. Zesz Nauk AR Krak Inż Środ, 19(355): 57–70.

Naulier, M., Eyrolle-Boyer, F., Boyer, P., i in., 2017. Particulate organic matter in rivers of Fukushima: an unexpected carrier phase for radiocesiums. Sci Total Environ, 579: 1560– 1571.

Oszkinis-Golon, M., Frankowski, M., Pukacz, A., 2021. Macrophyte diversity as a response to extreme conditions in the post-mining lakes of the muskau arch (West Poland). Water (Switzerland) 13, 2909. https://doi.org/10.3390/W13202909/S1.

Park, C.W., Kim, S.M., Kim, I., i in., 2021. Sorption behavior of cesium on silt and clay soil fractions. J Environ Radioact, 233: 106592.

Paulsson, O., Widerlund, A., 2021. Algal nutrient limitation and metal uptake experiment in the Åkerberg pit lake, northern Sweden. Appl. Geochem., 125.

PGW WP (Państwowe Gospodarstwo Wodne Wody Polskie), 2021. MZP (Mapy zagrożenia powodziowego). https://wody.isok.gov.pl/imap_kzgw/?gpmap=gpMZP

Pukacz, A., Oszkinis-Golon, M., Frankowski, M., 2018. The physico-chemical diversity of pit lakes of the Muskau arch (Western Poland) in the context of their evolution and genesis. Limnol. Rev. 18, 115–126.

R Core Team, 2021. R: A language and environment for statistical computing. R Foundation for Statistical Computing, Vienna, Austria. R version 4.0.4.

Rigol, A., Vidal, M., Rauret, G., 2002. An overview of the effect of organic matter on soil-radiocaesium interaction: implications in root uptake. J Environ Radioact, 58: 191–216.

Sawhney, B.L., 1972. Selective sorption and fixation of cations by clay minerals. A Rev Clays Clay Miner, 20: 93–100.

Sekudewicz, I., Gąsiorowski, M., 2022. Spatial and vertical distribution of ^{137}Cs activity concentrations in lake sediments of Turawa Lake (Poland). Environmental Science and Pollution Research, 29: 80882–80896.

Sekudewicz, I., Matoušková, Š., Ciesielska, Z., Mulczyk, A., Gąsiorowski, M., 2022. Factors controlling ^{137}Cs distribution in bottom sediments of Koronowo Reservoir (Poland). J. Soils Sediments, 22, 3189–3208.

Sekudewicz, I., Syczewski, M., Rohovec, J., Matoušková, Š., Kowalewska, U., Blukis, R., Geibert, W., Stimac, I., Gąsiorowski, M., 2024. Geochemical behavior of heavy metals and radionuclides in a pit lake affected by acid mine drainage (AMD) in the Muskau Arch (Poland). Sci. Total Environ. 908, 168245.

Shepard, F.P., 1954. Nomenclature based on sand-silt-clay ratios. J Sed Pet, 24: 151–158.

Sienkiewicz, E., Gasiorowski, M., 2016. The evolution of a mining lake - From acidity to natural neutralization. Sci. Total Environ., 557–558, 343–354.

Sienkiewicz, E., Gąsiorowski, M., 2017. The diatom-inferred pH reconstructions for a naturally neutralized pit lake in south-west Poland using the Mining and the Combine pH training sets. Sci. Total Environ., 605–606, 75–87.

Sienkiewicz, E., Gąsiorowski, M., Sekudewicz, I., Kowalewska, U., Matoušková, Š., 2023. Responses of diatom composition and teratological forms to environmental pollution in a post-mining lake (SW Poland). Environ. Sci. Pollut. Res. Int. https://doi.org/10.1007/S11356-023-30113-7

Solski, A., Jędrczak, A., Matejczuk, W., 1988. Skład chemiczny wód zbiorników pojezierza antropogenicznego w rejonie Tuplice-Łęknica. Zeszyty Naukowe Uniwersytetu Zielonogórskiego, 84, 65–76.

Somboon, S., Kavasi, N., Sahoo, S.K., i in., 2018. Radiocesium and ^{40}K distribution of river sediments and floodplain deposits in the Fukushima exclusion zone. J Environ Radioact, 195:40–53.

Środoń, J., Drits, V.A., McCarty, D.K., Hsieh, J.C., Eberl, D.D., 2001. Quantitative X-ray diffraction analysis of clay-bearing rocks from random preparations. Clays Clay Miner, 49(6): 514–528.

Swarzenski, P.W., 2014. [210]Pb Dating, W: Encyclopedia of Scientific Dating Methods. Springer Netherlands, Dordrecht, 1–11.

Szarłowicz, K., Reczyński, W., Gołaś, J., Kościelniak, P., Skiba, M., Kubica, B., 2011. Sorption of ^{137}Cs and Pb on sediment samples from a drinking water reservoir. Polish J. Environ. Stud. 20, 1305–1312.

Szatten, D., 2016. Propozycja nowego podziału hydromorfometrycznego Zbiornika Koronowskiego. Geograph Tour, 4: 79–84.

Szatten, D., Habel, M., Pellegrini, L., Maerker, M., 2018. Assessment of siltation processes of the Koronowski Reservoir in the northern Polish lowland based on bathymetry and empirical formulas. Water, 10(11): 1681.

Tachi, Y., Sato, T., Takeda, C., i in., 2020. Key factors controlling radiocesium sorption and fixation in river sediments around the Fukushima Daiichi Nuclear Power Plant. Part 2: Sorption and fixation behaviors and their relationship to sediment properties. Sci Total Environ, 724: 138097.

Tanaka, K., Iwatani, H., Sakaguchi, A., Fan, Q., Takahashi, Y., 2015. Size-dependent distribution of radiocesium in riverbed sediments and its relevance to the migration of radiocesium in river systems after the Fukushima Daiichi Nuclear Power Plant accident. J. Environ. Radioact. 139, 390–397.

Thomas, R., Mantero, J., P´erez-Moreno, S.M., Ruiz-Canovas, C., Vioque, I., Isaksson, M., Forssell-Aronsson, E., Holm, E., García-Tenorio, R., 2020. [226]Ra, [210]Po and lead isotopes in a pit lake water profile in Sweden. J. Environ. Radioact., 223–224.

Thomas, R.I., Mantero, J.I., Ruiz Ca Novas, C.I., Holm, E., García-Tenorio, R., Forssell-AronssonID, E., IsakssonID, M., 2022. Natural Radioactivity and Element Characterization in Pit Lakes in Northern Sweden. https://doi.org/10.1371/journal.pone.0266002

Toby, B.H., Von Dreele, R.B., 2013. GSAS-II: The genesis of a modern open-source all purpose crystallography software package. J. Appl. Crystallogr., 46, 544–549.

Walling, D E, Quine, T.A., 1993. Use of caesium-137 as a tracer of erosion and sedimentation: Handbook for the application of the caesium-137 technique. UK Overseas Dev. Adm. Res. Scheme R 4579.

Walling, D.E., He, Q., 1997. Use of fallout ^{137}Cs in investigations of overbank sediment deposition on river floodplains. Catena, 29, 263–282.

Wieczorek, D., Stoiński, A., 2008. Szczegółowa mapa geologiczna Polski 1:50 000. Seria: 241 – Gostycyn (N-33-96-D). Polski Instytut Geologiczny (PIG).

Wiśniewska, M., Paczuska, B., 2015. Oceanological and Hydrobiological Studies Long-term changes in the dynamics and structure of cyanobacteria in Koronowo Reservoir. Oceanol Hydrobiol Stud, 44(1): 127–138.

Wisotzky, F., 1998. Chemical Reactions in Aquifers Influenced by Sulfide Oxidation and in Sulfide Oxidation Zones. Acidic Min. Lakes, 223–236.

Wojewoda, J., 2013. Mierzeje Jeziora Turawskiego – studium sedymentologiczne. Abstrakt konferencyjny – POKOS 5'2013, 90–92

Wołkowicz, S., Strzelecki, R., 2002. Geochemia poczarnobylskiego cezu w glebach i roślinach anomalii opolskiej. Przegl Geol, 50(10): 941–944.

Wróbel, Ł., Dołhańczuk-Śródka, A., Kłos, A., Ziembik, Z., 2015. The activity concentration of post-Chernobyl ^{137}Cs in the area of the Opole Anomaly (southern Poland). Environ Monit Assess, 187(1): 4084.

Zapata, F., Nguyen, M.L., 2009. Soil erosion and sedimentation studies using environmental radionuclides. Radioact Environ, 16: 295–322.

Ziembik, Z,, Dołhańczuk-Śródka, A., Komosa, A., Orzeł, J., Wacławek, M., 2010. Assessment of ^{137}Cs and [239, 240]Pu distribution in forest soils of the Opole anomaly. Water Air Soil Pollut, 206(1): 307–320.

5. Spis załączników

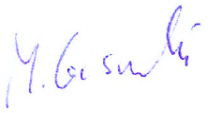**5.1.** Załącznik nr 1. Spis artykułów wchodzących w skład rozprawy doktorskiej

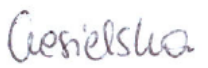**5.2.** Załącznik nr 2. Artykuł nr 1 – Sekudewicz & Gąsiorowski, 2022
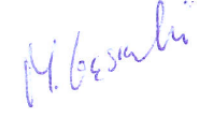
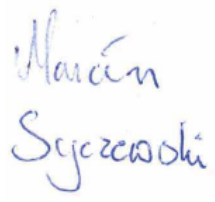**5.3.** Załącznik nr 3. Artykuł nr 2 – Sekudewicz i in., 2022

5.4. Załącznik nr 4. Artykuł nr 3 – Sekudewicz i in., 2024

Spis artykułów wchodzących w skład rozprawy doktorskiej

Prezentowana rozprawa doktorska składa się z cyklu trzech artykułów naukowych, które zostały opublikowane w recenzowanych czasopismach międzynarodowych:

Artykuł nr 1			
Sekudewicz, I., Gąsiorowski, M., 2022. Spatial and vertical distribution of ^{137}Cs activity concentrations in lake sediments of Turawa Lake (Poland). Environmental Science and Pollution Research, 29: 80882–80896. DOI: 10.1007/S11356-022-21417-1			
Impact Factor: 5.8		*MNiSW: 100 pkt*	
Imię i nazwisko współautora:	**Zakres prac:**	**Udział (%):**	**Podpis:**
Ilona Sekudewicz	• Opracowanie szczegółowej koncepcji badań oraz artykułu naukowego. • Udział w pracach terenowych. • Przygotowanie próbek do analiz oraz wykonanie badań laboratoryjnych (pomiar zawartości wody oraz gęstości nasypowej gleb i osadów jeziornych, analiza aktywności ^{137}Cs oraz ^{40}K w pobranych próbkach). • Określenie składu granulometrycznego osadów jeziornych za pomocą analizy sitowej. • Analiza statystyczna i interpretacja uzyskanych wyników badań. • Przygotowanie artykułu do publikacji (opracowanie figur, współautorstwo wszystkich rozdziałów manuskryptu). • Przesłanie manuskryptu do redakcji czasopisma, udzielenie odpowiedzi recenzentom oraz wykonanie ostatecznych poprawek redakcyjnych (autor korespondencyjny).	75%	*J. Sekudewicz*
Michał Gąsiorowski	• Pomoc w opracowaniu koncepcji badań oraz artykułu naukowego. • Udział w pracach terenowych oraz nadzór merytoryczny nad wykonywanymi badaniami laboratoryjnymi. • Pomoc w wykonaniu analiz statystycznych oraz w interpretacji uzyskanych wyników badań. • Współautorstwo rozdziałów artykułu: *Results* oraz *Discussion*. • Pomoc w opracowaniu figury lokalizacyjnej oraz nadzór merytoryczny na każdym etapie przygotowania manuskryptu. • Zapewnienie finansowania przeprowadzonych badań oraz korekty językowej manuskryptu.	25%	*M. Gąsior...*

Artykuł nr 2

Sekudewicz, I., Matoušková, Š., Ciesielska, Z., Mulczyk, A., Gąsiorowski, M**.,** 2022. Factors controlling ^{137}Cs distribution in bottom sediments of Koronowo Reservoir (Poland). Journal of Soils and Sediments, 22: 3189–3208. DOI: 10.1007/s11368-022-03326-5

Imię i nazwisko współautora:	Zakres prac:	Udział (%):	Podpis:
Ilona Sekudewicz	• Opracowanie szczegółowej koncepcji badań oraz artykułu naukowego. • Udział w pracach terenowych. • Przygotowanie próbek do analiz oraz wykonanie badań laboratoryjnych (pomiar zawartości wody oraz gęstości nasypowej gleb i osadów jeziornych, analiza aktywności ^{137}Cs oraz ^{40}K w pobranych próbkach). • Analiza statystyczna i interpretacja uzyskanych wyników badań. • Przygotowanie artykułu do publikacji (opracowanie figur, współautorstwo wszystkich rozdziałów manuskryptu). • Kierowanie projektem dla młodych naukowców ING PAN, w ramach którego finansowane były przeprowadzone badania. • Przesłanie manuskryptu do redakcji czasopisma, udzielenie odpowiedzi recenzentom oraz wykonanie ostatecznych poprawek redakcyjnych (autor korespondencyjny).	70%	*J. Sekudewicz*
Šárka Matoušková	• Wykonanie analizy składu granulometrycznego wybranych próbek osadów jeziornych za pomocą laserowego analizatora wielkości cząstek.	5%	*Matouškm*
Zuzanna Ciesielska	• Wykonanie analizy składu mineralogicznego wybranych próbek osadów jeziornych za pomocą XRD oraz opracowanie uzyskanych wyników.	5%	*Ciesielska*
Anna Mulczyk	• Wykonanie analizy elementarnej (CHNS) próbek gleb oraz osadów jeziornych za pomocą analizatora elementarnego Vario CUBE.	5%	*A.Mulczyk*
Michał Gąsiorowski	• Pomoc w opracowaniu koncepcji badań oraz artykułu naukowego. • Udział w pracach terenowych oraz nadzór merytoryczny nad wykonywanymi badaniami laboratoryjnymi. • Pomoc w wykonaniu analiz statystycznych oraz w interpretacji uzyskanych wyników badań. • Współautorstwo rozdziałów artykułu: *Results* oraz *Discussion*. • Nadzór merytoryczny oraz pomoc na każdym etapie przygotowania manuskryptu.	15%	*M.Gąsiorowski*

Artykuł nr 3			
Sekudewicz, I., Syczewski, M., Rohovec, J., Matoušková, Š., Kowalewska, U., Blukis, R., Geibert, W., Stimac, I., Gąsiorowski, M., 2024. Geochemical behavior of heavy metals and radionuclides in a pit lake affected by acid mine drainage (AMD) in the Muskau Arch (Poland). Sci. Total Environ. 908, 168245. DOI: 10.1016/j.scitotenv.2023.168245			
Impact Factor: 9.8		*MNiSW: 200 pkt*	
Imię i nazwisko współautora:	**Zakres prac:**	**Udział (%):**	**Podpis:**
Ilona Sekudewicz	•Opracowanie szczegółowej koncepcji badań oraz artykułu naukowego. •Udział w pracach terenowych. •Przygotowanie próbek do analiz oraz wykonanie badań laboratoryjnych (analiza zawartości wody oraz gęstości nasypowej osadów jeziornych, pomiar aktywności ^{210}Po, ^{137}Cs oraz ^{40}K, analiza stężeń wybranych pierwiastków w próbkach osadów jeziornych za pomocą ICP-OES). •Analiza statystyczna, modelowanie geochemiczne wód jeziornych oraz interpretacja uzyskanych wyników. •Przygotowanie artykułu do publikacji (opracowanie figur, współautorstwo wszystkich rozdziałów manuskryptu). •Przesłanie manuskryptu do redakcji czasopisma, udzielenie odpowiedzi recenzentom oraz wykonanie ostatecznych poprawek redakcyjnych (autor korespondencyjny).	60%	*J. Sekudewicz*
Marcin Syczewski	•Wykonanie analizy składu mineralogicznego wybranych próbek osadów jeziornych za pomocą SEM-EDS. •Opisanie uzyskanych wyników uzyskanych za pomocą SEM-EDS oraz opracowanie figur nr 8 i 9. •Pomoc merytoryczna w wykonaniu modelowania geochemicznego oraz w interpretacji uzyskanych wyników.	7%	*Marcin Syczewski*
Jan Rohovec	•Analiza stężeń pierwiastków głównych w próbkach wody jeziornej za pomocą ICP-OES. •Pomiar koncentracji rozpuszczonego węgla organicznego (DOC) w próbkach wody jeziornej. • Analiza stężeń wybranych jonów w próbkach wody jeziornej za pomocą chromatografu cieczowego (HPLC).	5%	*Rohovec*

Šárka Matoušková	•Pomoc w pracach terenowych. •Pomiar koncentracji pierwiastków śladowych w próbkach wody jeziornej za pomocą ICP-MS. •Analiza składu granulometrycznego wybranych próbek osadów jeziornych za pomocą laserowego analizatora wielkości cząstek.	3%	
Urszula Kowalewska	•Analiza składu gatunkowego okrzemek w próbkach osadów jeziornych. •Rekonstrukcja pH wody na podstawie analizy okrzemek oraz opisanie uzyskanych wyników.	5%	
Roberts Blukis	•Wykonanie analizy składu mineralogicznego wybranych próbek osadów jeziornych za pomocą IR oraz XRD. •Opisanie uzyskanych wyników za pomocą IR i XRD oraz opracowanie figur nr 6 i 7.	5%	
Walter Geibert	•Pomoc w opracowaniu wyników analizy składu pierwiastkowego wybranych próbek osadów jeziornych za pomocą ICP-OES. • Wsparcie merytoryczne w interpretacji uzyskanych wyników badań.	3%	10.11.23
Ingrid Stimac	•Pomoc w przeprowadzeniu pomiarów stężeń pierwiastków w wybranych próbkach osadów jeziornych za pomocą ICP-OES. •Pomoc w opracowaniu wyników analiz wykonanych za pomocą ICP-OES.	2%	10.11.23
Michał Gąsiorowski	•Pomoc w opracowaniu koncepcji badań oraz artykułu naukowego. •Udział w pracach terenowych oraz nadzór merytoryczny nad wykonywanymi badaniami laboratoryjnymi. •Pomoc w opracowaniu figury lokalizacyjnej oraz w interpretacji uzyskanych wyników. •Nadzór merytoryczny na każdym etapie przygotowania manuskryptu. •Pomoc w wykonaniu końcowych poprawek redakcyjnych.	10%	

RESEARCH ARTICLE

Spatial and vertical distribution of ^{137}Cs activity concentrations in lake sediments of Turawa Lake (Poland)

Ilona Sekudewicz[1] · Michał Gąsiorowski[1]

Abstract

The main objective of this research was to study the spatial and vertical distribution of ^{137}Cs activity concentrations in the bottom sediments of Turawa Lake 32 years after the Chernobyl fallout to investigate possible factors responsible for the post-fallout migration and accumulation of ^{137}Cs in the selected reservoir. The results demonstrated a strong relationship between the increasing ^{137}Cs and ^{40}K activity concentrations and the decreasing grain size of sediments. Significant amounts of ^{137}Cs were detected in the bottom sediments deposited in the deeper parts of the reservoir (especially near the dam). Therefore, this research showed that Turawa Lake can be an important trap for sediments polluted with ^{137}Cs. Moreover, disturbed vertical distribution of ^{137}Cs activity concentrations in the sediment columns collected from the littoral zone of this lake was observed, which is probably related to the bottom erosion intensified by wind-wave action, bioturbations, and water-level fluctuations. In the profundal zone, the vertical distribution of ^{137}Cs activity concentrations was undisturbed, which indicates stable sedimentation conditions in this part of Turawa Lake.

Introduction

The Chernobyl nuclear power plant (ChNPP) accident in 1986 caused contamination with radioactive isotopes (e.g. ^{131}I, ^{134}Cs, and ^{137}Cs) throughout a large area of Europe. The emitted radioisotopes accumulated then in various components of the environment. Some of these radionuclides, for example, radiocesium ^{137}Cs, remain detectable in nature due to their relatively long half-lives (30.17 years for ^{137}Cs). Due to this property, radiocesium pollution can have serious and long-term effects on the environment. However, knowing the half-life of ^{137}Cs has allowed researchers to use it as a marker to study radionuclide transfer in catchment-lake systems (e.g., Edgington et al. 1991; Ries et al. 2019), soil erosion, sedimentation processes (e.g., Zapata and Nguyen 2010; Muñoz-Salinas et al. 2021), and to date lake sediments

(e.g., Klaminder et al. 2012; Putyrskaya et al. 2020; Lan et al. 2020).

The occurrence of ^{137}Cs in the lacustrine ecosystem has been related to its delivery by direct atmospheric fallout, riverine transport, and surface runoff from the surrounding drainage areas (e.g., Smith and Beresford 2005; Anselmetti et al. 2007; Pulley et al. 2018; Sakuma et al. 2018). The delivered cesium radioisotopes have been rapidly immobilized in lake sediments in a manner similar to that in the organic surface layer (e.g., plant litter) in watershed soils (Carlsson 1978; Eyrolle-Boyer et al. 2016; Naulier et al. 2017; Santschi et al. 1990). This is due to dissolved radiocesium being likely removed from the water column by deposition with suspended particles, which is related to its strong ability to be sorbed by clay fraction (Kaminski et al. 1994; He and Walling 1996; Santschi et al. 1990). Therefore, radiocesium (in the case of undisturbed deposition) should be immobilized at a specified depth in the sediment profile (depending on the sedimentation rate) and form a characteristic peak of elevated activity concentration associated with a particular radioactive fallout (e.g., Appleby 2005; Klaminder et al. 2012). Moreover, some amounts of ^{137}Cs can also be derived to the lake in the long term, due to soil

✉ Ilona Sekudewicz
  i.sekudewicz@twarda.pan.pl

[1] Institute of Geological Sciences, Polish Academy of Sciences, Twarda St. 51/55, 00818 Warsaw, Poland

erosion and ^{137}Cs wash-off or decomposition of organic matter that has integrated radiocesium at initial deposition (e.g., Eyrolle-Boyer et al. 2016; Golosov et al. 2021; Naulier et al. 2017; Wakiyama et al. 2019).

The amount of accumulated ^{137}Cs in lake sediments is associated with many factors, for example, the initial amount of deposited radiocesium, catchment area, hydraulic retention time, limnological properties, and sediment characteristics (e.g., sediment particle size and content of clay minerals) (Kaminski et al. 1994; He and Walling 1996; Szarłowicz et al. 2011; Yoshimura et al. 2014; Funaki et al. 2019; Huon et al. 2018). An example of lakes known as good traps for polluted sediments, for example, with cesium radioisotopes, are dam lakes (e.g., Huon et al. 2018; Majerová et al. 2018; Mclean et al. 1990). Such lakes may also pose a potential threat if the accumulated sediments were re-released into river systems (e.g., Bábek et al. 2020; Ivanov et al. 2021). On the other hand, Ivanov et al. (2021) demonstrated that the sediments of the reservoirs can be also essential sources of information on the post-fallout migration and accumulation of Chernobyl-derived [137]Cs.

Radiocesium can be remobilized from lake sediments by, for example, bioturbation, diffusion in pore water, vertical mixing by wind-wave disturbances, slumping on slopes, and re-deposited in deep parts of the lake (e.g., Evans et al. 1983; Hilton et al. 1986; Comans et al. 1989; Kansanen et al. 1991; Kapała et al. 2008; Tsuji et al. 2019; Wang et al. 2020). For instance, the resuspension of lake sediments from the littoral zone (which was probably related to deep currents and slumping of sediments on slopes), and their accumulation in the profundal zone resulted in an increase in ^{137}Cs activity concentration in the bottom sediments of Piijanne Lake in Finland (Kansanen et al. 1991). Similar conclusions were obtained based on the research conducted on lakes in the Masuria region in northeastern Poland (Kapała et al. 2008). In turn, after the Fukushima Daiichi nuclear power plant accident, the increased ^{137}Cs activity concentrations in the surface lake sediments of Nishiura Lake in Japan was related to the vertical mixing of sediments (affected by wind-wave disturbances and bioturbation) and the focusing of fine-grained radiocesium-bearing particles in the deep parts of this reservoir (Tsuji et al. 2019).

The main aim of this research was to study the variations in ^{137}Cs activity concentrations in the bottom sediments of Turawa Lake in order to investigate the main factors responsible for the post-fallout redistribution of ^{137}Cs after the ChNPP in a selected study area. Another objective was to investigate the possible sources of ^{137}Cs causing its presence in the surface layer of the sediment column in Turawa Lake despite 32 years passing since the Chernobyl fallout. To accomplish these goals, we investigated the spatial and vertical distributions of ^{137}Cs activity concentrations in the lake sediments of Turawa Lake. To determine the potential

factors responsible for the distribution of ^{137}Cs in the bottom sediments of the studied lake, we considered its limnological properties (type of the lake and bottom morphology), sedimentation processes, the presence of tributaries, and sediments characteristics (grain size and type of deposited sediments). The concentration of [40]K activity, an additional source of information (e.g., as an indicator of detrital layers) that may improve the understanding of the possible mechanism of ^{137}Cs distribution in lake sediments, was also examined (Putyrskaya et al. 2020; Somboon et al. 2018). In addition, the content of total organic carbon (TOC) and total nitrogen (TN) in the collected sediment samples was measured to determine the potential relationship between ^{137}Cs and organic matter deposited in this lake (Fujii et al. 2018; Meyers and Ishiwatari 1995; Naulier et al. 2017), and the C/N ratio was calculated to track the origin of the organic matter (Contreras et al. 2018; Huon et al. 2018).

Materials and methods

Study site

Turawa Lake is a dam lake located in the Mała Panew Valley (a part of the Silesian Lowland) in southwestern Poland (Fig. 1). The dam was built between 1933 and 1939. The surface area, mean depth, and capacity of the lake were 20.7 km^2, 4–5 m, and 106 million m^3, respectively (Gurwin 2010). The lake is supplied mainly by the Mała Panew River and the Libawa River (a smaller tributary). Turawa Lake was created on glaciofluvial sediments (the North-Polish Glaciation, Weichselian), alluvial sands, and clays (Holocene). Sapropelic mud has been depositing in the deeper part of the lake (in the southwest), and sands dominate in the shallow part (in the northeast) (Teisseyre 1983; Gurwin et al. 2005). The sedimentation processes occurring in Turawa Lake are controlled by the shape and small depth of the basin, fluctuations in water levels, and dominant western winds. The wave base is located below a depth of 5.5 m, which results in the resuspension of sediments in shallow sites and intensified coastal erosion. In addition, tributaries (especially the Mała Panew River) have a significant impact on sediment deposition in Turawa Lake because of the intensive delivery of detrital material (Teisseyre 1983).

The study area is located in the Opole region, also known as the Opole Anomaly, due to the high concentrations of ^{137}Cs activity detected in the upper soil layers (Strzelecki et al. 1993; Jagielak et al. 1998). This area was heavily polluted by the Chernobyl fallout in May 1986 because of atmospheric conditions (air circulation, rainfall, and dry deposition). Studies on the behavior of cesium radioisotopes in the terrestrial environment in the Opole region have been conducted (e.g., Wołkowicz and Strzelecki 2002;

Fig. 1 Bathymetric map of Turawa Lake and sampling locations (Dost and Mannaerts 2005; modified)
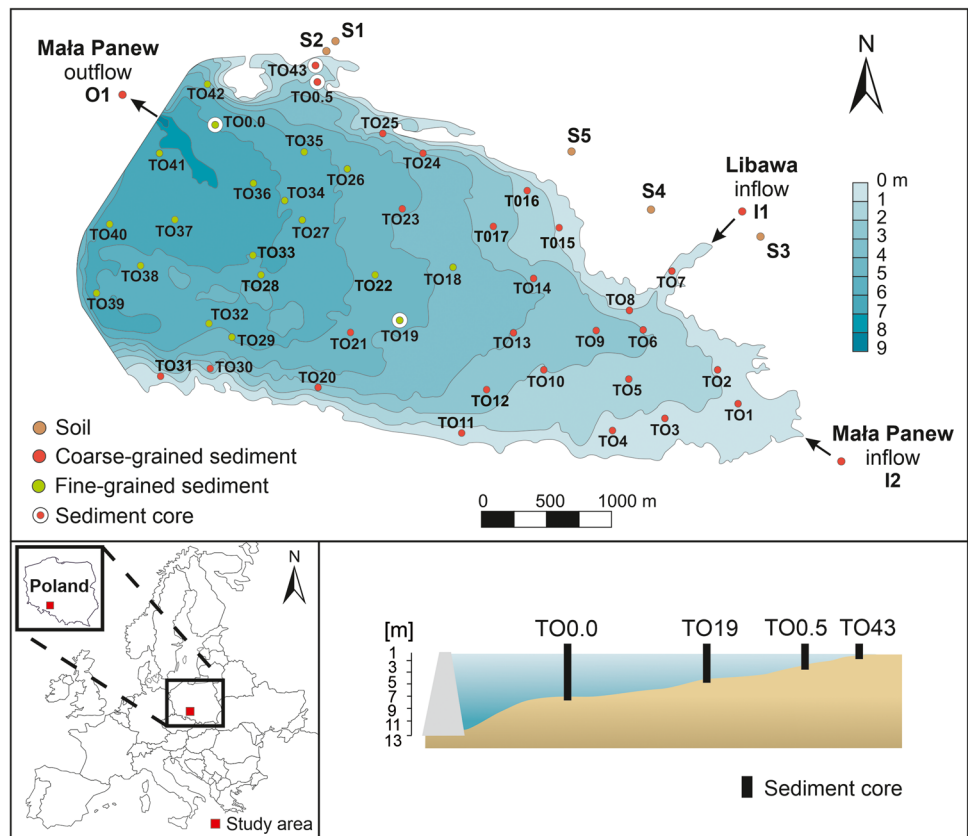
Mietelski et al. 2010; Ziembik et al. 2010; Wróbel et al. 2015). The research showed that 27 years after the Chernobyl accident, the average ^{137}Cs activity concentration in the surface layer of soil (measured in situ by portable spectrometer) in the Opole region was 14.3 kBq m^{-2}, and the maximum was as high as 125 kBq m^{-2} (Wróbel et al. 2015). However, research on the distribution and migration of ^{137}Cs activity in the lacustrine ecosystem in this area has not been sufficiently developed.

One study that included measurements of ^{137}Cs activity concentrations in the catchment soils and lake sediments was conducted in Turawa Lake 10 years after the Chernobyl accident (Natkaniec 1999). The study showed that the concentration of ^{137}Cs activity in two bottom sediment samples (0–3 cm depth) in Turawa Lake was 30 ± 1 and 70 ± 2 Bq kg^{-1}. The concentration of ^{40}K activity in the same samples was 220 ± 10 and 310 ± 16 Bq kg^{-1}. A positive correlation between decreasing grain size and increasing ^{137}Cs activity concentration in these sediments was also found. Turawa Lake was also the subject of another research that precisely described the characteristics of the lake sediments, bottom morphology, and occurring sedimentation processes (e.g., Teisseyre 1983; Latala and Wierzba 2007; Machowski et al. 2008; Wojewoda 2013). However, the detailed spatial and vertical distributions of ^{137}Cs activity concentrations in the lake sediments of this reservoir have not been analyzed.

Sampling and measurements

Sample collection

We collected 45 surface lake sediment samples in nine transects, two sediment columns from the profundal zone (at sampling sites TO 0.0 and TO 19), and one sediment column from the littoral zone (at sampling site TO 0.5) from Turawa Lake during two sampling campaigns in 2018 (Fig. 1). Additionally, five soil samples (at sampling sites S 1–5), two stream sediment samples from the inflows (the Libawa [I 1] and Mała Panew [I 2] Rivers), one stream sediment sample from the outflow (the Mała Panew River [O 1]), and one sediment column from the littoral zone (at sampling site TO 43) were collected in 2020. All surface sediment samples constituted the uppermost 3-cm-thick portion of the sediment column. The lengths of the collected sediment cores were 35 cm (TO 0.0), 24 cm (TO 19), 7 cm (TO 0.5), and 20 cm (TO 43). Samples were collected using a Kayak-type gravity corer (55 mm in internal diameter). The collected lake sediment profiles were divided in the field into 0.5- or 1-cm-thick slices. The sediments were packed in plastic string bags and stored in a refrigerator. Next, the samples were weighed, dried (48 h at 60 °C), homogenized, and prepared for analyses in the Uranium-Series Laboratory at the Institute of Geological Sciences of the Polish Academy of Sciences.

Sediment analyses

Concentrations of ^{137}Cs and ^{40}K activity in all sediment samples were determined by low-background gamma spectrometry (Canberra-Packard) with a broad energy germanium (BE-5030) detector (FWHM = 1.28 keV at 661.7 keV [for ^{137}Cs] and 1.72 keV at 1460.8 keV [for ^{40}K]). Samples (dry mass from 2 to 50 g) were analyzed in a dry state in a round, polyethylene cup (flat cylinder geometry). The energy calibration was performed based on the radioactive source of ^{241}Am (59.5 keV), ^{137}Cs (661.7 keV), ^{60}Co (1173.2 and 1332.5 keV), and ^{40}K (1460.8 keV). The spectra were analyzed using Genie 2000 software. The average counting time ranged from 48 to 72 h. The uncertainty of ^{137}Cs and ^{40}K activity measurements varied from 10 to 15%. The minimum detectable activity (MDA) for ^{137}Cs and ^{40}K was 0.22 Bq kg^{-1} and 2.42 Bq kg^{-1}, respectively. The obtained ^{137}Cs and ^{40}K activity concentrations for all samples were standardized to the date of the first sampling campaign (September 10, 2018).

Macroscopic lithological analyses of all sediment samples were performed. The sediment samples were divided based on sieve analysis into fine-grained (< 0.063 mm) and coarse-grained (> 0.063 mm) sediments (Cheel 2005). Subsequently, the measurements of TOC and TN content were conducted using a Vario CUBE elemental analyzer. Sulfanilic acid ($NH_2C_6H_4SO_3H$) was used as a standard for analysis. Next, 5–6 mg of analyzed sediment was transferred into tin capsules and burned at 1150 °C. Subsequently, the obtained CO_2 and N_2 gases were separated in a chromatographic column and measured using a thermal conductivity detector. The uncertainties of the TOC and TN measurements were 0.6% and 0.18%, respectively.

Data analyses

The results of the measurements of ^{137}Cs and ^{40}K activity concentrations and the content of TOC and TN were used to describe the spatial and vertical distribution of these parameters in the bottom sediments of Turawa Lake. Data points were used to generate maps by the inverse distance weighting (IDW) interpolation method with the geographic information system software ArcGIS ver. 10.6 (Esri Co., Ltd., Redlands, CA, USA). Statistical analyses were conducted using Past 4.03 (Hammer et al. 2001) and R 4.1.1 software (R Development Core Team 2012). The dataset was tested for normal distribution by using the Shapiro–Wilk test. The multi-collinearity of the variables was tested by calculating the variance inflation factor (VIF). Principal component analysis (PCA) was conducted to investigate the relationship between the concentration of ^{137}Cs activity and the measured parameters. Only the variables that had a VIF < 10 were included in the PCA. Next, the data were centered,

scaled, and tested to examine their suitability by using the Kaiser–Meyer–Olkin test.

Results

^{137}Cs activity concentrations and organic matter content in soils and stream sediments

The obtained results showed that the surface layer of the soil in the area of Turawa Lake is highly contaminated with radiocesium (^{137}Cs content ranged from 3.88 ± 0.6 to 672 ± 81 Bg kg^{-1}). The highest concentrations of ^{137}Cs activity were observed in the organic surface layer (0–3 cm depth) of the soil collected at sampling site S3 (398 ± 48 Bq kg^{-1}) in the forest near the Libawa River; at sampling site S4 (128 ± 16 Bq kg^{-1}) on the grassland; and at sampling site S5 (672 ± 81 Bq kg^{-1}) in the forest on the northern shore of the lake (Fig. 2). Soil samples, collected at sampling sites S3, S4, and S5 were characterized by a different content of TOC: 6.7%, 8.4%, and 32.8%, respectively. The stream sediments (0–3 cm depth) of the Libawa River (sampling site I1) also had a relatively high concentration of ^{137}Cs activity (59 ± 7 Bq kg^{-1}). By contrast, stream sediments (0–3 cm depth) collected from the Mała Panew River (sampling site I2) were characterized by a relatively low concentration of ^{137}Cs activity (0.6 ± 0.3 Bq kg^{-1}). The stream sediments (0–3 cm depth) deposited at the outflow of the Mała Panew River (sampling site O1) contained more ^{137}Cs (7.1 ± 0.9 Bq kg^{-1}) than at its outlet to the lake (Fig. 2).

Spatial distribution of radionuclides and organic matter in surface lake sediments

The macroscopic lithological analyses showed an expected (Teisseyre 1983) relationship between the depth of the lake and the type of deposited bottom sediments. Surface lake sediments collected from deeper parts of the reservoir (mainly near the dam) were mostly fine-grained (< 0.063 mm) sapropel muds (Fig. 1). In turn, samples collected from shallow parts of the basin (near the Mała Panew and Libawa River inflows and close to the lakeshore) were mostly fine- to coarse-grained (> 0.063 mm) sands. The measured parameters of the collected surface lake sediments were characterized by a bimodal distribution caused by the presence of two types of bottom sediments in Turawa Lake (Fig. 3). The selected parameters, examined in particular groups of bottom sediments (fine- and coarse-grained), were mainly non-normally distributed. The exceptions were the distributions of ^{137}Cs and ^{40}K activity concentrations in fine-grained sediment samples and the distributions of wet bulk density and water content in coarse-grained sediment samples, which were characterized by a normal distribution.
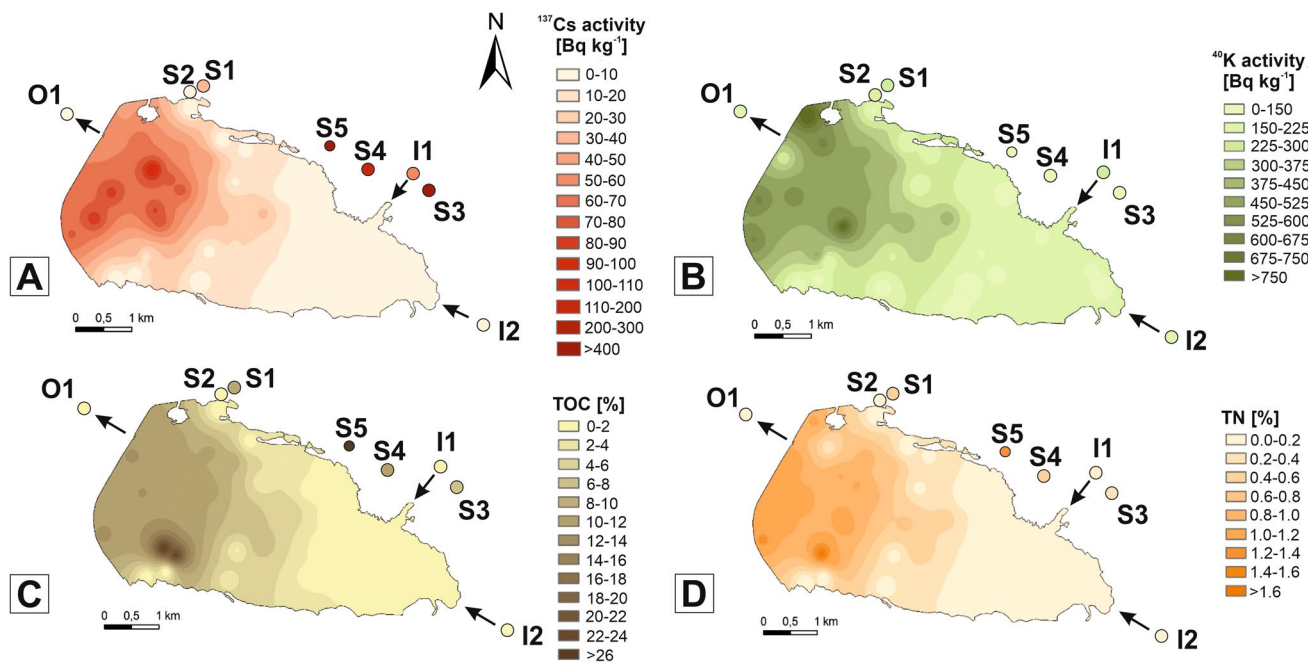
Fig. 2 Spatial distribution of **a** ^{137}Cs and **b** ^{40}K activity concentrations and the content of **c** total organic carbon (TOC) and **d** total nitrogen (TN) in surface lake sediments (0–3 cm depth) of Turawa Lake
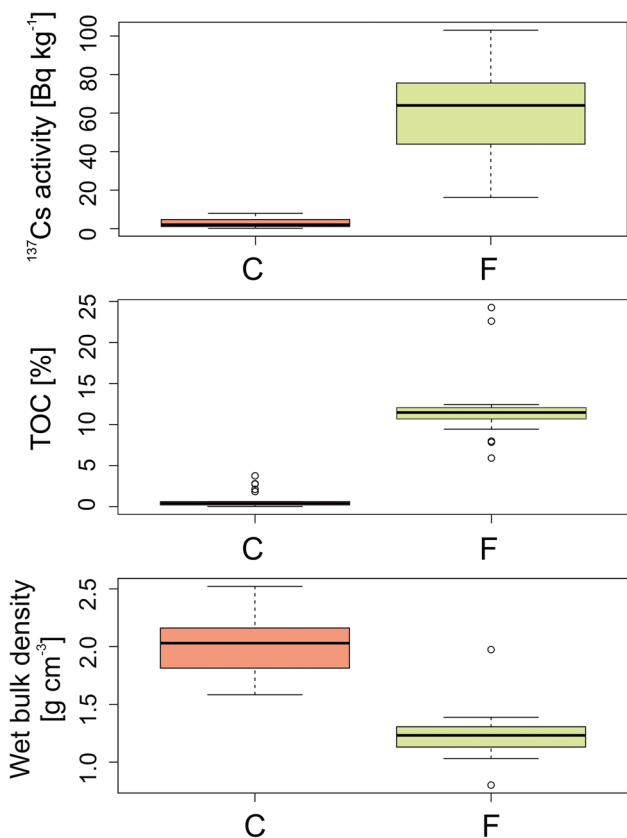
Fig. 3 Box-plots showing ^{137}Cs activity concentrations, total organic carbon (TOC) content, and wet bulk density of coarse-grained (C) and fine-grained (F) surface lake sediments of Turawa Lake

The obtained values of selected parameters differed significantly by the type of sediment (Fig. 3). The water content in coarse-grained sediments ranged from 15 to 48 wt.%, and in fine-grained sediments, it varied between 68 and 96 wt.%. The wet bulk density of coarse-grained surface sediments varied significantly (from 1.6 to 2.5 g cm^{-3}), while in the case of fine-grained surface sediments was more homogeneous and equal to approx. 1.2 g cm^{-3} (median; $n = 19$). The concentrations of ^{137}Cs activity in the collected samples varied from < MDA (0.22 Bq kg^{-1}) to 103 ± 12 Bq kg^{-1} (from < 16.2 to 3740 ± 420 Bq m^{-2}). The concentrations of ^{40}K activity in these samples ranged from 90 ± 9 to 820 ± 98 Bq kg^{-1} (from 4440 ± 450 to $29{,}800 \pm 3540$ Bq m^{-2}). The elevated concentrations of ^{137}Cs and ^{40}K activity were observed in the case of fine-grained surface lake sediments collected from deeper parts of the studied reservoir (Figs. 1 and 2). The average content of ^{137}Cs in muds was 64 ± 9 Bq kg^{-1} (median; $n = 19$), and in sands, 2.1 ± 0.4 Bq kg^{-1} (median; $n = 26$) (Fig. 3). Similarly, the concentrations of ^{40}K activity were higher (478 ± 63 Bq kg^{-1}) (median; $n = 19$) in fine-grained sediments than in coarse-grained sediments (149 ± 13 Bq kg^{-1}) (median; $n = 26$). The calculated significant difference (ANOSIM $p = 0.0001$) between these two types of sediments, in the case of ^{137}Cs and ^{40}K activity measurements, was 0.87 and 0.80, respectively.

The spatial distribution of the content of TOC and TN in the surface lake sediments of Turawa Lake is presented in Fig. 2. On the basis of the obtained results, the relationship

between the content of organic matter (expressed as TOC and TN percentages) and the types of collected surface lake sediments was also observed (Figs. 3 and 4). The fine-grained surface lake sediments were characterized by a much higher content of TOC (12%) and TN (1%) (median, $n = 19$) than the coarse-grained surface lake sediments (containing TOC and TN of approximately < 0.6% and < 1%, respectively). The significant difference (ANOSIM $p = 0.0001$) between the elemental compositions investigated for these two types of bottom sediments was 0.89 (TOC) and 0.98 (TN). The C/N ratio calculated for muds was approx. 11, and that for sands was greater than 20.

The correlation between the content of ^{137}Cs and TOC in the surface lake sediments of Turawa Lake is shown in Fig. 4. The presented plot shows that fine-grained surface lake sediments contain much more ^{137}Cs and organic matter than coarse-grained surface lake sediments. The fine-gr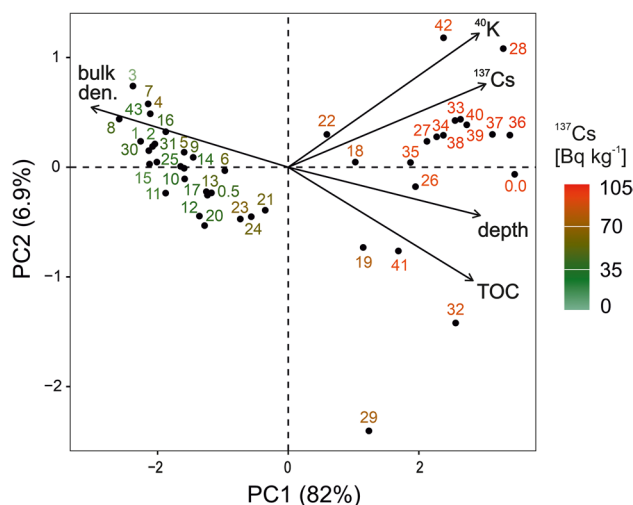ained surface lake sediments collected from the area between the shallows and the southern shore of the lake (sampling sites TO 29 and 32) were characterized by an increased TOC content (Figs. 1 and 5). A slightly less content of TOC and ^{137}Cs was detected in fine-grained surface lake sediments collected from sampling sites TO 18, 19, and 22, which are located in the transition zone between the muds and the

Fig. 5 Principal component analysis (PCA) results from the examined variables in the surface (0–3 cm depth) lake sediments of Turawa Lake: ^{40}K — potassium-40 activity concentrations (Bq kg^{-1}), ^{137}Cs — cesium-137 activity contractions (Bq kg^{-1}), TOC — total organic carbon content (%), bulk. den. — wet bulk density (g cm^{-3}), and depth — depth of the lake (m) at sampling sites. Concentration of ^{137}Cs activity in particular sediment samples is marked with a gradient color. Sampling sites are shown in Fig. 1

Fig. 4 Correlation between ^{137}Cs activity concentrations and the content of total organic carbon (TOC) in coarse-grained (marked in green) and fine-grained (marked in red) surface lake sediments (0–3 cm depth) of Turawa Lake. Sampling sites are shown in Fig. 1

sands. Coarse-grained surface lake sediments deposited near the southern shore of the lake (sampling sites TO 11 and TO 20) contain more TOC, while coarse-grained surface lake sediments collected from deeper parts of the lake (sampling sites TO 21, 23, and 24) contain both more ^{137}Cs and TOC (Figs. 1 and 5). The increased concentrations of ^{137}Cs activity in the sands were also observed in the samples collected from sampling sites TO 4, 5, 6, and 7, which are situated near the Libawa River's estuary.

Spearman's rank correlation showed that the concentration of ^{137}Cs activity is significantly correlated with the depth of the lake, the content of ^{40}K, water, organic matter (expressed as TOC and TN), and the wet bulk density of the collected surface lake sediments of Turawa Lake (Table 1). The wet bulk density of surface lake sediments is negatively correlated with all measured parameters. The concentration of ^{40}K activity and the depth of the lake are the factors most strongly correlated with the concentration of ^{137}Cs activity in the collected sediment samples (correlation coefficient = 0.83; p value > 0.001).

The PCA was used to investigate the most important factors that determine the spatial distribution of ^{137}Cs activity concentrations in the bottom sediments of Turawa Lake (Fig. 5). Only variables with VIF < 10 were included in the analysis. The obtained results demonstrated that the first two PC axes explain 82% and 6.9% of the total variance in the studied dataset, respectively. Component 1 (PC1) is associated with all considered variables, especially with the concentration of ^{137}Cs activity, depth of the lake, and wet bulk

Table 1 Spearman's rank correlation among parameters measured in the surface (0–3 cm depth) lake sediments of Turawa Lake (*p* value > 0.001)

	^{137}Cs	^{40}K	TN	TOC	w. bulk	w.c
^{137}Cs						
^{40}K	0.83					
TN	0.79	0.77				
TOC	0.77	0.70	0.97			
w. bulk	−0.79	−0.71	−0.84	−0.81		
w.c	0.79	0.80	0.90	0.88	−0.85	
Depth	0.83	0.75	0.83	0.83	−0.83	0.85

^{137}Cs activity concentration [Bq kg^{-1}]; ^{40}K activity concentration [Bq kg^{-1}]; *TN* total nitrogen [%]; *TOC* total organic carbon [%]; *w. bulk.* wet bulk density [g cm^{-3}]; *w.c.* water content [%]; lake's depth at a sampling point [m]

density of the surface lake sediments. Component 2 (PC2) is mainly associated with the ^{40}K activity concentration and the TOC content in the collected sediments. The presented biplot shows that the samples with an increased concentration of ^{137}Cs activity are mainly fine-grained surface lake sediments (characterized by a low value of wet bulk density) with an increased ^{40}K content. It also indicates that differences in the depth of the reservoir significantly affect the type of deposited sediments, and thus the content of ^{137}Cs, as well as ^{40}K and TOC. The obtained data show that an elevated content of TOC in the surface lake sediments indicates an increase in the concentration of ^{137}Cs activity; however, it may also strongly depend on local changes in the reservoir, namely, the occurrence of shallower sites and the associated increasing primary production and deposition of organic matter (sampling sites TO 29 and TO 32) (Fig. 1; 5).

## Vertical distribution of radionuclides and organic matter in sediment cores

The vertical distributions of ^{137}Cs activity concentration, TOC content, and wet bulk density of lake sediments in the collected sediment cores are shown in Fig. 6. Core TO 43, collected from the shallowest part of the reservoir (1 m depth of the lake), consisted mainly of coarse-grained (upper part of the core) and fine-grained (lower part of the core) sands (Figs. 1 and 6). The wet bulk density of the sediments in this core ranged from 1.2 to 2 g cm^{-3}, and the TOC content was less than 1% along its entire length. Core TO 0.5, also collected from the littoral zone (2 m depth of the lake), was composed of yellow–brown sands (core depth 0–2 cm) and black sands with organic matter particles (core depth 2–7 cm). The wet bulk density of the sediments in this core varied between 1.6 and 2 g cm^{-3}. Core TO 19, collected from the transition zone between the littoral and profundal (4 m water depth), was composed of muds along the entire its length (Figs. 1 and 6). The wet bulk density of the sediments increased with depth (from 1.0 to 1.8 g cm^{-3}). The content of TOC in the sediments was irregular along the

entire length of the core and decreased with the depth to less than 1% (from 16 cm of the core depth). Core TO 0.0 was collected from the profundal zone (6 m depth of the lake) and also consisted mainly of muds. The wet bulk density of these sediments was relatively constant (approx. 1.0 g cm^{-3}) along the entire length of this core. The content of TOC (equal to approx. 11%) was also regularly distributed in the sediments of this core, except for the sediments occurring above 30 cm depth, where it increased above 13%. The C/N ratio in the upper part of core TO 19 ranged from 13 to 18, and in the lower part of the core (from 16 cm depth), it increased above 20. In the case of core TO 0.0, the C/N ratio increased gradually from 11 to 17 with the depth of the sediment column. Calculating the C/N ratio for most of the bottom sediments of cores TO 0.5 and TO 43 was not possible, because the TN values in these sediment samples were below the detection limit. Only for selected samples was it possible to calculate the C/N, which was mostly above 30.

The content of ^{137}Cs in core TO 43 was relatively low along the entire length of the sediment column and was approx. 1.5 ± 0.4 Bq kg^{-1} (median; $n = 20$). The vertical distribution of ^{137}Cs activity concentrations in core TO 0.5 was irregular. The elevated concentrations of ^{137}Cs activity were observed between 2.5 cm (5.3 ± 1.2 Bq kg^{-1}) and 6 cm (7.2 ± 1.8 Bq kg^{-1}) depth of this core. The sediment columns collected from the deeper parts of Turawa Lake (TO 19 and TO 0.0) were characterized by a much higher content of ^{137}Cs compared to the cores collected from the shallower part of this lake (Figs. 1 and 6). A significant increase in the concentration of ^{137}Cs activity in core TO 19 was observed between 10 and 16 cm of the depth of this sediment column (up to 35.3 ± 4.5 Bq kg^{-1} at a depth of 13 cm). Assuming that the peak of ^{137}Cs activity concentration at a depth of approx. 13 cm of this core is originated from the Chernobyl fallout, the sedimentation rate of lake sediments at this sampling site can be estimated at 0.41 ± 0.06 cm year^{-1}. The peak of ^{137}Cs activity concentration in core TO 0.0 was 1670 ± 150 Bq kg^{-1} and

Fig. 6 Vertical distribution of ^{137}Cs activity concentrations, wet bulk density, and total organic carbon (TOC) content in lake sediments in cores: TO 43, TO 0.5, TO 19, and TO 0.0. Sampling sites are shown in Fig. 1
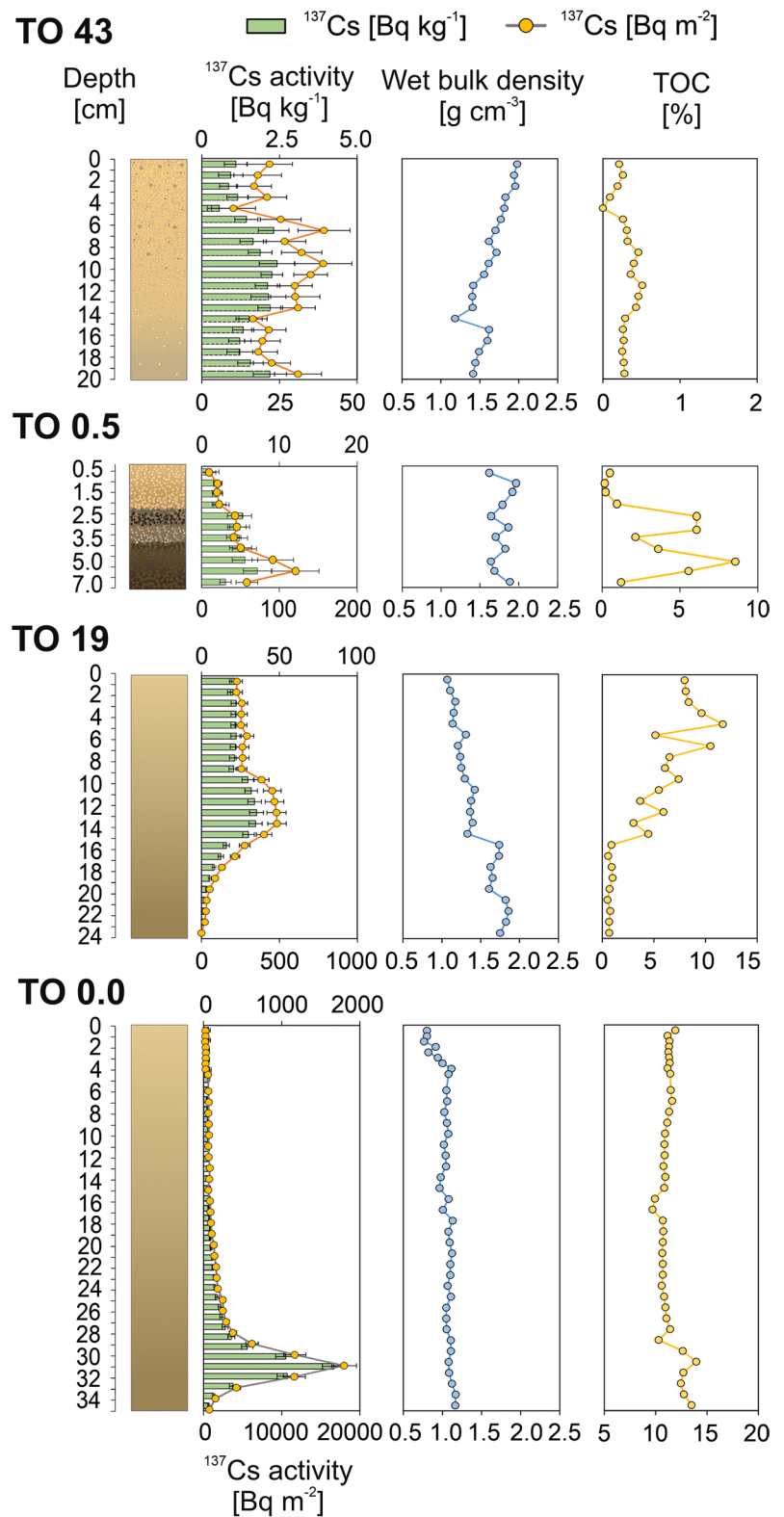
was found 31 cm below the sediment surface. Assuming that this peak also originates from the Chernobyl fallout, the sedimentation rate of lake sediments at this sampling site can be 1.0 ± 0.1 cm year^{-1}.

Discussion

Results: overview and comparison

The conducted research has shown that the highest ^{137}Cs activity concentration (2.08 ± 0.3 kBq m^{-2} at sampling site S5) in the surface layer of soil collected from the forest located on the north of Turawa Lake is much lower than the maximum surface activity concentration (67.5 kBq m^{-2}) detected almost 27 years after the Chernobyl accident in the soils in this region (Wróbel et al. 2015). However, the measurements of the surface activity concentration of ^{137}Cs presented by Wróbel et al. (2015) were performed with a portable scintillation spectrometer, which makes it difficult to compare these results. Nevertheless, we can assume that this difference may be related to the unequal distribution of ^{137}Cs in the terrestrial and aquatic ecosystems of the Opole region. Thus, the soils investigated in this study might have been collected from a less contaminated site than theirs. Another reason for this difference may be that only the top of the sediment profile (0–3 cm depth) was measured in this study, and significant amounts of ^{137}Cs could have accumulated in the deeper parts of the soil profile as a result of, for example, vertical migration of radiocesium (Dorr and Munnich 1989; Konoplev et al. 2018; Mishra et al. 2016).

The obtained results also showed that ^{137}Cs remains detectable in the surface layer of the sediment column of Turawa Lake more than 32 years after the ChNPP and that its activity concentrations in the fine-grained surface lake sediments are relatively high (median $= 64 \pm 9$ Bq kg^{-1}; $n = 19$). Notably, the maximum detected ^{137}Cs activity concentration (103 ± 12 Bq kg^{-1}) in the surface lake sediments of Turawa Lake is higher by approx. 45 Bq kg^{-1} than in another reservoir, Dobczyce Lake, in southern Poland (Szarłowicz et al. 2011). This difference may be related to the location of these lakes in areas with different levels of pollution with cesium radioisotopes after the Chernobyl fallout (Jagielak et al. 1998). On the other hand, in the Masuria region (northeastern Poland), which was not as highly polluted as the Opole area, much higher ^{137}Cs activity in the surface layer of sediment columns in some lakes was found than in our case (Kapała et al. 2008). For example, the specific activity of ^{137}Cs in the surface lake sediment collected in 2005 from the profundal zone of Garbas Lake was 515 Bq kg^{-1}. However, the most distinct difference can be observed between the ^{137}Cs content detected in the surface lake sediments of Turawa Lake and some of Finnish lakes, where, for example, the concentration of ^{137}Cs activity measured in 2003 in the bottom sediments (0–2 cm depth) of Vehkajärvi Lake was approx. 20 kBq kg^{-1} (Ilus and Saxen 2005). These substantial differences are due to the irregular distribution of pollution from the Chernobyl fallout in Europe and the latter circulation of cesium radioisotopes in lake catchments and ecosystems.

Our research has also shown that the concentrations of ^{137}Cs activity in the coarse-grained surface lake sediments in Turawa Lake (sampling sites marked in red in Fig. 1) are lower than those obtained in this area 10 years after the ChNPP accident (Natkaniec 1999). The concentrations of ^{137}Cs activity in two surface (depth 0–3 cm) lake sediment samples collected in 1996 from the littoral zone were 30 ± 1 and 70 ± 2 Bq kg^{-1}, which is slightly higher than in our case (the maximum content of ^{137}Cs in the surface lake sediments collected from the littoral zone in this study was up to 7.94 ± 1.07 Bq kg^{-1}). In addition, the concentration of ^{137}Cs activity in the sands collected in 1996 from the beach on the northern bank of Turawa Lake was 2700 ± 80 Bq m^{-2} (Natkaniec 1999), and in our study, the highest content of ^{137}Cs in sands deposited close to this location (sampling site TO 0.5) was more than 25 times lower (102 ± 26 Bq m^{-2}). On this basis, we can conclude that the concentration of ^{137}Cs activity in this area has decreased significantly since 1996. These differences, however, cannot be simply explained by the disintegration of ^{137}Cs related to its half-life. A reason for this phenomenon might be the sedimentation of "fresh" sediments with low ^{137}Cs content. Moreover, post-depositional downcore migration of ^{137}Cs in the sediment column should be considered as another mechanism of sediment surface depletion in radioisotopes. However, verifying this hypothesis is difficult because of the limited length of the collected cores and the significantly disturbed vertical distribution of ^{137}Cs activity concentrations in the bottom sediments from the littoral zone of Turawa Lake (Fig. 6).

Notably, the highest content of ^{137}Cs measured in surface lake sediment sample (TO36) in this study was 103 ± 12 Bq kg^{-1}, which is more than 30 Bq kg^{-1} higher than the maximum value of ^{137}Cs activity concentration (70 ± 2 Bq kg^{-1}) in the surface lake sediments reported by Natkaniec (1999). Nevertheless, surface lake sediments with a significantly elevated content of ^{137}Cs in this study were collected from the profundal zone of Turawa Lake; thus, comparing these values with coarse-grained lake sediments collected from the littoral zone (all available data) might not be informative. Moreover, the highest content of ^{137}Cs (1670 ± 150 Bq kg^{-1}) detected in the bottom sediments among all the cores collected in this study was significantly higher than in the surface lake sediment samples and was found at a depth of approx. 31 cm below the surface of the sediment core (TO 0.0) collected near the dam (Figs. 1 and 6). The peak of ^{137}Cs activity concentration in this case is much lower than that in the sediment columns collected, for example, from Lakes Konnevesi or Vehkajärvi in Finland (Ilus and Saxen 2005).

Moreover, assuming that the peak of ^{137}Cs activity concentration in sediment core TO 0.0 represents the Chernobyl fallout to the lake surface, and its shape is the effect of the subsequent dispersion of deposited ^{137}Cs upward and downward within the sediment core (Ivanov et al. 2021), the sedimentation rate for this site was calculated at 1.0 ± 0.1 cm year^{-1}. In comparison, the presented value is higher than that for natural close lakes in Poland (Gąsiorowski 2008) but similar to that for oxbows (Gąsiorowski and Hercman 2005) and other dam lakes (e.g., Anselmetti et al. 2007; Diemer et al. 2011). In addition to the supplying of the particles by tributaries and limited outflow from the lake, the location of the peak of ^{137}Cs activity concentration at such depth may be caused by intensified primary production related to the trophic state (eutrophic) of Turawa Lake. Such a relationship could have been observed, for example, in the case of Siikajärvi Lake (oligotrophic) and Pyhäjärvi Lake (eutrophic), where the peak of ^{137}Cs content was observed at the 0–2 cm and 6–7 cm depth of the sediment profile 14 and 17 years after the Chernobyl fallout, respectively (Ilus and Saxen 2005).

Origin of ^{137}Cs in lake sediments

The most important source of ^{137}Cs deposited in the lake sediments of Turawa Lake was the Chernobyl fallout, as in the case of other lakes located in the contaminated area by this accident (e.g., Erlinger et al. 2008; Ivanov et al. 2021; Pulley et al. 2018). Hence, we can assume that the characteristic peaks of the elevated content of ^{137}Cs in the undisturbed sediment columns (e.g., cores TO 0.0 and 19) collected from the profundal zone of Turawa Lake are derived directly from the initial deposition (Fig. 6). The obtained results also showed that ^{137}Cs remains present in the surface layer of the bottom sediments of Turawa Lake 32 years after the ChNPP accident. Theoretically, in this type of lake (eutrophic, with circumneutral water pH and high sedimentation rate), ^{137}Cs should have been removed from the water column relatively fast after the fallout and should be immobile in lake sediments at a particular depth (depending on the sedimentation rate) (e.g., Santschi et al. 1986; Klaminder et al. 2012). Notably, the vertical distribution of ^{137}Cs activity concentrations in cores TO 0.0 and TO 19 may confirm this hypothesis: this isotope remains detectable in the surface layers of the sediment columns (Figs. 2 and 6). The potential reason for this phenomenon might be (1) the post-fallout redistribution of this isotope caused by surface runoff and sediment transport processes through tributaries, or (2) the resuspension of already deposited ^{137}Cs in lake sediments by coastal and bottom erosion, and bioturbations (e.g., Hilton et al. 1986; Santschi et al. 1986; Smith and Beresford 2005; Pulley et al. 2018; Sakuma et al. 2018).

The Mała Panew River supplies coarse-grained sediments characterized by relatively low ^{137}Cs activity concentration (i.e., < 1 Bg kg^{-1} at sampling sites TO1 and I2). In a similar dam reservoir (Dobczyce Lake), a low concentration of ^{137}Cs activity was also measured in coarse-grained sediments deposited by the Raba River (Szarłowicz et al. 2011). Consequently, an assumption might be that rivers have a negligible influence on delivering ^{137}Cs to these lakes, as in Nishiura Lake, where the majority of cesium radioisotopes were deposited directly by the fallout after the Fukushima Daiichi nuclear power plant accident (Tsuji et al. 2019). On the other hand, the surface lake sediments deposited near the Libawa River's inlet are characterized by an increased concentration of ^{137}Cs activity (e.g., 5.1 ± 0.8 Bq kg^{-1} at sampling site TO7). This indicates that the Libawa River may deliver larger amounts of ^{137}Cs to the lake. This difference may be because the Libawa River flows through a forested area enriched in ^{137}Cs (e.g., 398 ± 48 Bq kg^{-1} at sampling site S3), which is probably transported to the river, as evidenced by increased concentrations of ^{137}Cs activity in the stream sediments collected from this tributary (e.g., 59.3 ± 7.2 Bq kg^{-1} at sampling site I1). The source of radiocesium, in this case, may be contaminated organic matter (e.g., forest litter), which releases ^{137}Cs into the river water during its decomposition (Koarashi et al. 2016; Laceby et al. 2016; Sakuma et al. 2018; Wakiyama et al. 2019). However, improving the understanding of the relationship between the decomposition of organic matter and ^{137}Cs leaching into water requires further research, as emphasized by, e.g., Wakiyama et al. (2019). Moreover, both tributaries may deliver significant amounts of muds enriched with ^{137}Cs transported through the stream flow and deposited in the deeper parts of the lake (Teisseyre 1983). However, because of the lack of data on the content of this isotope in the suspended particles, we could not confirm this hypothesis.

Another source of ^{137}Cs could be lakeshore sediments of Turawa Lake, which are eroded by wind-wave action and water-level fluctuation (Teisseyre 1983). This is because Turawa Lake is a vast, shallow lake with intense wave action, and the operation of a hydroelectric power plant may change the water level. Support for this thesis is that our research has shown that the sediments at the lakeshore contain a certain amount of ^{137}Cs (e.g., 3.9 ± 0.6 Bq kg^{-1} at sampling site S2), which can be delivered to the reservoir along with the washed-out particles. The inflow of detrital material from land to the lake may be confirmed by the presence of coarse-grained bottom sediments characterized by an increased C/N ratio (up to 34), indicating the influx of terrestrial organic matter (Contreras et al. 2018; Meyers and Ishiwatari 1995). A similar explanation can be applied in the case of sediment columns collected from the littoral zone of the lake (cores TO 0.5 and 43), for which it is difficult to assess whether the peaks of the ^{137}Cs activity concentrations originated directly

from the Chernobyl fallout. The elevated C/N ratio (over 30) in the bottom sediments of these cores suggests that the organic matter in this case originated mainly from terrestrial sources (Contreras et al. 2018; Meyers and Ishiwatari 1995). Thus, we can assume that the ^{137}Cs in these sediment profiles is probably from secondary sources and was washed together with terrestrial plant debris and deposited in the littoral zone, and that directly Chernobyl-derived radiocesium should be observed in the deeper part of the core or has been eroded and redeposited into deeper parts of the lake.

Another reason for the presence of ^{137}Cs in the surface layer of the bottom sediments of Turawa Lake can be the resuspension of already deposited sediments. In this case, due to the shallow depth of the lake, the bottom erosion might be intensified by bioturbations, water-level fluctuations, and wind-wave disturbances in the littoral zone. Then, sediments can be transported by deep currents and slumping of lake sediments on steep slopes into deeper sites, such as in Lakes Garbas or Pijanne (Kansanen et al. 1991; Kapała et al. 2008; Tsuji et al. 2019). This assumption might be confirmed by the irregular distribution of ^{137}Cs activity concentrations and the variable type of sediments in cores TO 0.5 and TO 43, which may indicate the variability of sedimentation processes in the shallow part of the lake (Figs. 2 and 6). By contrast, the vertical distribution of ^{137}Cs activity concentrations in cores TO 0.0 and TO 19 suggests stable sedimentation conditions in the profundal zone because this isotope remains immobilized at the particular depth of the sediment columns.

Factors determining post-fallout redistribution of ^{137}Cs in lake sediments

Dam lakes, such as Turawa Lake, are characterized by specific features that determine the distribution of deposited sediments and therefore ^{137}Cs. One of the most important features is the relatively high trap efficiency and limited outflow, which results in a relatively high deposition rate (Majerová et al. 2018; Sedláček et al. 2016). They also determine the lithological diversity and grain size variation, which is reflected in the accumulation of coarse-grained particles close to the inflow and the prevalent of fine-grained sediments near the dam (Huon et al. 2018). This tendency is also observed in the case of Turawa Lake, also strongly influenced by the bottom morphology and the presence of tributaries. The obtained results show that the increased concentration of ^{137}Cs activity is strongly associated with the fine-grained (< 0.063 mm) lake sediments in the deeper parts of the reservoir (Figs. 2 and 4). On this basis, a conclusion is that two of the most important factors determining the distribution of ^{137}Cs in the bottom sediments of Turawa Lake are the type and grain size of the deposited sediments (Figs. 2 and 6). This phenomenon is due to the larger specific

surface area of finer particles and the good sorption properties of clay minerals, which likely occur in fine sediment fractions (e.g., He and Walling 1996; Park et al. 2021; Tachi et al. 2020). Similar conclusions have been obtained in the cases of, for example, Ogaki Dam Reservoir (Funaki et al. 2019), Mano Dam Reservoir (Huon et al. 2018), and Hibara Lake (Basuki et al. 2018). By contrast, in the case of coarse-grained sediments, characterized by low sorption properties due to, e.g., the lack of clay minerals, lower concentrations of ^{137}Cs activity were observed (Figs. 1 and 2). Moreover, potassium ^{40}K (commonly used as an indicator of detrital layers) was not recorded in sands potentially containing K-feldspars but was associated with the fine-grained bottom sediments (Table 1; Fig. 5) (e.g., Putyrskaya et al. 2020). This appearance probably occurred because sandy material transported by tributaries and by offshore erosion to Turawa Lake is well-washed fluvioglacial sands consisting mainly of quartz grains. On the other hand, the enrichment of ^{40}K in fine-grained lake sediments may result from its concentration within clay minerals, which indirectly may explain its significant positive correlation with ^{137}Cs (Table 1; Fig. 5) (Madruga et al. 2014; Tsabaris et al. 2007).

The limnological properties (e.g., trophic index) of Turawa Lake and occurring deposition processes also affect the content of organic matter, which increases with the depth of this reservoir and the decreasing bulk density of the surface lake sediments (Figs. 2 and 6). The obtained results also showed a significant positive correlation between the content of TOC and TN and the concentration of ^{137}Cs activity in the collected bottom sediments of the studied lake (Table 1, Fig. 4). On this basis, we can hypothesize that organic matter could be another important carrier of ^{137}Cs in Turawa Lake. However, organic compounds are unlikely to adsorb radiocesium; therefore, this relationship remains unclear (Fujii et al. 2018; Naulier et al. 2017; Rigol et al. 2002). We can assume that this correlation is because organic litter, delivered to the lake as organic debris or their decomposition products, may have integrated some amounts of radiocesium shortly after the radioactive fallout (Koarashi et al. 2016; Naulier et al. 2017; Wakiyama et al. 2019). However, the calculated C/N ratio (approx.11) indicates the autochthonous (plankton) origin of the organic matter deposited within the surface lake sediments enriched with ^{137}Cs (Contreras et al. 2018; Meyers and Ishiwatari 1995). This finding may, therefore, suggest that the observed correlation between organic matter and ^{137}Cs may be most likely due to radiocesium deposition in organic-rich sediments (Fujii et al. 2018).

The conducted research also showed that the sediment transport process also significantly affects the post-fallout redistribution of ^{137}Cs activity concentrations in the bottom sediments of Turawa Lake. This may be evidenced, for example, by the declined concentrations of ^{137}Cs activity in the surface lake sediments in the littoral zone of

Turawa Lake by the transport of newly suspended fine-grained particles with ^{137}Cs to the deeper parts of the lake. These radiocesium-bearing particles then likely settle in the profundal zone of the lake, where sedimentation conditions are more stable than in the littoral zone, what can be evidenced by the undisturbed vertical distributions of ^{137}Cs activity concentrations in the sediment cores TO 0.0 and TO 19. This "sediment focusing" process might be observed based on the relationship between the ^{137}Cs distribution in the bottom sediments and the bathymetry of Turawa Lake (Figs. 2 and 6). A similar relationship was observed in the case of another dam reservoir (Dobczyce Lake) in Poland, where elevated concentrations of ^{137}Cs activity were found in Wolnica (the deepest part of the reservoir), and the lowest concentrations were found in the Myślenice Gulf (the shallowest part). In our case, we also observed that some of the suspended particles are probably removed with ^{137}Cs from the lake along with its outflow (the Mała Panew River), which is indicated by increased ^{137}Cs activity concentrations in the surface stream sediments collected from the river behind the dam (e.g., 7.04 ± 0.94 Bq kg^{-1} at sampling site O1). However, as aforementioned, most of radiocesium-bearing particles are accumulated in the bottom sediments in the profundal zone, which makes Turawa Lake an important trap for sediments polluted with ^{137}Cs (e.g., Huon et al. 2018; Ivanov et al. 2021; Sedláček et al. 2016). Additionally, this phenomenon may pose a great risk in the event of a possible re-mobilization of significant amounts of accumulated ^{137}Cs from lake sediments and their introduction into the fluvial system (Ivanov et al. 2021).

Another factor that may significantly determine the distribution of ^{137}Cs in the surface lake sediments of Turawa Lake is bottom erosion. As aforementioned, evidence for this process is the significantly decreased content of ^{137}Cs in coarse-grained surface lake sediments deposited in the littoral zone, which probably result from the resuspension of the deposited radiocesium-bearing particles and their transport to the deeper parts of the basin, as in the case of Nishiura Lake (Tsuji et al. 2019). The washing out of this isotope is probably caused by the intensified bottom erosion in Turawa Lake, which is related to the shallow depth of this reservoir (Teisseyre 1983). Moreover, the position of the peak of ^{137}Cs content in sediments in core TO 19 (at 13 cm depth) can indicate that in this sampling site, there is a much lower mean sedimentation rate (0.41 ± 0.06 cm year^{-1}) than, for example, in sampling site TO 0.0. An explanation for this difference might be that this sampling site is located in a shallow part of the basin; therefore, the sediment deposition at this point may be affected by the more intensive bottom erosion (also related to wind-wave action) and the subsequent transport of sediments into the deeper parts of the reservoir.

Conclusions

This study showed that ^{137}Cs originating from the ChNPP is not only bound in the sediment horizon deposited shortly after the radioactive fallout but also detectable in the surface layer of the sediment column of Turawa Lake as a result of its post-fallout redisposition. Today, ^{137}Cs is delivered to Turawa Lake mainly from the shore (by coastal erosion) and with the sediments deposited by tributaries. The conducted research also indicated that relatively large amounts of ^{137}Cs are likely to be transported to the lake by a smaller tributary (the Libawa River), the catchment of which is located in a significantly polluted area.

The main factors responsible for the spatial distribution of ^{137}Cs activity concentrations in the bottom sediments of Turawa Lake are the type of deposited sediments (grain size and organic matter content), characteristics of the reservoir (bottom morphology and limited outflow), and sedimentation processes (bottom erosion caused by wind-wave action, bioturbations and water-level fluctuations). Based on the obtained results, the "focusing process" of ^{137}Cs in the bottom sediments in the profundal zone (near the dam) was observed. In this part of the reservoir, mainly fine-grained lake sediments with significantly increased concentrations of ^{137}Cs activity are deposited. This relationship is probably related to the good sorption properties of fine-grained sediments characterized by an increased content of clay minerals. However, to improve the understanding of the sorption processes of ^{137}Cs in the lake sediments of Turawa Lake, further research could conduct a mineralogical analysis of the collected sediments.

This research also showed that the study of the vertical distribution of ^{137}Cs activity concentrations in the bottom sediments can provide valuable information on the processes responsible for the distribution of ^{137}Cs in the lake. We observed that the vertical distribution of ^{137}Cs content in the lake sediments of the cores collected from the littoral zone of Turawa Lake is significantly disturbed, which is related to the intensified bottom erosion due to probable bioturbations, wind-wave action, and water-level fluctuations in the studied reservoir. Thus, the vertical distribution of ^{137}Cs activity concentrations in the bottom sediments in the profundal zone is undisturbed. An explanation for this may be the relatively stable sedimentation conditions in this part of the lake.

Declarations

References

R Development Core Team (2012) R: a language and environment for statistical computing. R Foundation for Statistical Computing, Vienna, Austria

Anselmetti FS, Bühler R, Finger D, Girardclos S, Lancini A, Rellstab C, Sturm M (2007) Effects of Alpine hydropower dams on particle transport and lacustrine sedimentation. Aquat Sci 69:179–198

Appleby PG (2005) Chronostratigraphic techniques in recent sediments. In: Tracking Environmental Change Using Lake Sediments. Kluwer Academic Publishers, pp 171–203

Bábek O, Kielar O, Lenďáková Z et al (2020) Reservoir deltas and their role in pollutant distribution in valley-type dam reservoirs: Les Království Dam, Elbe River, Czech Republic. Catena 184:104251. https://doi.org/10.1016/j.catena.2019.104251

Basuki T, Miyashita S, Tsujimoto M, Nakashima S (2018) Deposition density of ^{134}Cs and ^{137}Cs and particle size distribution of soil and sediment profile in Hibara Lake area, Fukushima: an investigation of ^{134}Cs and ^{137}Cs indirect deposition into lake from surrounding area. J Radioanal Nucl Chem 316:1039–1046

Carlsson S (1978) A model for the movement and loss of ^{137}Cs in a small watershed. Health Phys 34:33–37

Cheel RJ (2005) Grain texture. In: Cheel RJ (ed) Introduction to clastic sedimentology. Brock University Middleton, Ontario, pp 8–46

Comans RNJ, Middelburg JJ, Zonderhuis J, Woittiez JRW, De Lange GJ, Lange GJ, Das HA, Van der Weijden CH (1989) Mobilization of radiocaesium in pore water of lake sediments. Nature 339:367–369

Contreras S, Werne JP, Araneda A et al (2018) Organic matter geochemical signatures (TOC, TN, C/N ratio, δ13C and δ15N) of surface sediment from lakes distributed along a climatological gradient on the western side of the southern Andes. Sci Total Environ 630:878–888. https://doi.org/10.1016/J.SCITOTENV.2018.02.225

Diemer J, Allan G, Eckardt I, Kroening D, Vinson D (2011) Sedimentation in a Piedmont reservoir: evidence from Brown's Cove, Lake Wylie, North Carolina. Environ Eng Geosci 17(2):123–142

Dorr H, Munnich KO (1989) Downward movement of soil organic matter and its influence on trace-element transport (^{210}Pb, ^{137}Cs) in the soil. Radiocarbon 31:655–663. https://doi.org/10.1017/S003382220001225X

Dost RJJ, Mannaerts CMM (2005) Generation of lake bathymetry using SONAR, satellite imagery and GIS. In: ESRI 2008: Proceedings of the 2008 ESRI International User Conference Enschede, The Netherlands

Edgington DN, Val Klump J, Robbins JA, Kusner YS, Pampura VD, Sandimirov IV (1991) Sedimentation rates, residence times and radionuclide inventories in Lake Baikal from ^{137}Cs and ^{210}Pb in sediment cores. Nature 350:601–604

Erlinger C, Lettner H, Hubmer A et al (2008) Determining the Chernobyl impact on sediments of a pre-Alpine lake with a very comprehensive set of data. J Environ Radioact 99:1294–1301. https://doi.org/10.1016/J.JENVRAD.2008.03.012

Evans DW, Alberts JJ, Clark RA (1983) Reversible ion-exchange fixation of cesium-137 leading to mobilization from reservoir sediments. Geochim Cosmochim Acta 47:1041–1049

Eyrolle-Boyer F, Boyer P, Garcia-Sanchez L et al (2016) Behaviour of radiocaesium in coastal rivers of the Fukushima Prefecture (Japan) during conditions of low flow and low turbidity – Insight on the possible role of small particles and detrital organic compounds. J Environ Radioact 151(Pt 1):328–340. https://doi.org/10.1016/J.JENVRAD.2015.10.028

Fujii M, Ono K, Yoshimura C, Miyamoto M (2018) The role of autochthonous organic matter in radioactive cesium accumulation to riverine fine sediments. Water Res 137:18–27. https://doi.org/10.1016/J.WATRES.2018.02.063

Funaki H, Yoshimura K, Sakuma K, Iri S, Oda Y (2019) Evaluation of particulate ^{137}Cs discharge from a mountainous forested catchment using reservoir sediments and sinking particles. J Environ Radioact 210:105814

Gąsiorowski M (2008) Deposition rate of lake sediments under different alternative stable states. Geochronometria 32:29–35

Gąsiorowski M, Hercman H (2005) Recent changes of sedimentation rate in three Vistula oxbow lakes determined by ^{210}Pb dating. Geochronometria 24:33–39

Golosov VN, Ivanov MM, Tsyplenkov AS et al (2021) Erosion as a factor of transformation of soil radioactive contamination in the basin of the Shchekino Reservoir (Tula Region). Eurasian Soil Sci 54:291–303. https://doi.org/10.1134/S106422932102006X

Gurwin J (2010) Groundwater hazard regarding environmental impact assessment of renaturalisation of the Turawa reservoir (in Polish). Biul Państw Inst Geol 440:65–76

Gurwin J, Kryza H, Kryza J, Poprawski L (2005) Groundwater recognizing in the region of Turawa Lake for needs of ecological state assessment (in Polish). Współczesne Probl Hydrogeol 12:241–253

Hammer Ø, Harper DAT, Ryan PD (2001) PAST: paleontological statistics software package for education and data analysis. Palaeontol Electron 4:9

He Q, Walling DE (1996) Interpreting particle size effects in the adsorption of ^{137}Cs and unsupported ^{210}Pb by mineral soils and sediments. J Environ Radioact 30(2):117–137

Hilton J, Lishman JP, Allen PV (1986) The dominant processes of sediment distribution and focusing in a small, eutrophic, monomictic lake. Limnol Oceanogr 31(1):125–133

Huon S, Hayashi S, Laceby JP, Tsuji H, Onda Y, Evrard O (2018) Source dynamics of radiocesium-contaminated particulate matter deposited in an agricultural water reservoir after the Fukushima nuclear accident. Sci Total Environ 612:1079–1090

Ilus E, Saxen R (2005) Accumulation of Chernobyl-derived ^{137}Cs in bottom sediments of some Finnish lakes. J Environ Radioact 82:199–221

Ivanov MM et al (2021) Using reservoir sediment deposits to determine the longer-term fate of chernobyl-derived ^{137}Cs fallout in the fluvial system. Environ Pollut 274:116588

Jagielak J, Biernacka M, Henschke J, Sosińska A (1998) Radiological Atlas of Poland (in Polish). Biblioteka Monitoringu Środowiska PIOŚ, Warsaw

Kaminski S, Richter T, Walser M, Lindner G (1994) Redissolution of cesium radionuclides from sediments of freshwater lakes due to biological degradation of organic matter. Radiochim Acta 66(67):433–436

Kansanen PH, Jaakkola T, Kulmala S, Suutarinen R (1991) Sedimentation and distribution of gamma emitting radionuclides in bottom sediments of southern Lake Piijanne, Finland, after the Chernobyl accident. Hydrobiologia 222:121–140

Kapała J, Karpińska M, Mnich Z, Szpak A, Milewski R, Citko D (2008) The changes in the contents of ^{137}Cs in bottom sediments of some Masurian lakes during 10–15 y observation (Poland). Radiat Prot Dosimetry 130(2):178–185

Klaminder J, Appleby P, Crook P, Renberg I (2012) Post-deposition diffusion of ^{137}Cs in lake sediment: Implications for radiocaesium dating. Sedimentology 59(7):2259–2267

Koarashi J, Nishimura S, Nakanishi T et al (2016) Post-deposition early-phase migration and retention behavior of radiocesium in a litter–mineral soil system in a Japanese deciduous forest affected by the Fukushima nuclear accident. Chemosphere 165:335–341. https://doi.org/10.1016/J.CHEMOSPHERE.2016.09.043

Konoplev et al (2018) Natural attenuation of Fukushima-derived radiocesium in soils due to its vertical and lateral migration. J Environ Radioact 186:23–33

Laceby JP, Huon S, Onda Y et al (2016) Do forests represent a long-term source of contaminated particulate matter in the Fukushima Prefecture? https://doi.org/10.1016/j.jenvman.2016.09.020

Lan J, Wang T, Chawchai S, Cheng P, Zhou K, Yu K, Yan D, Wang Y, Zang J, Liu Y, Tan L, Ai L, Xu H (2020) Time marker of ^{137}Cs fallout maximum in lake sediments of Northwest China. Quatern Sci Rev 241:106413

Latala A, Wierzba S (2007) Biodegradation of bottom sediments of Turawa Lake. Pol J Chem Technol 9(2):73–77

Machowski R, Ruman M, Rzętała MA, Rzętała M (2008) Morphology of the bottom and the littoral zone of Turawa reservoir (in Polish). Kształtowanie środowiska geograficznego i ochrona przyrody na obszarach uprzemysłowionych i zurbanizowanych 39:45–55

Madruga MJ, Silva L, Gomes AR et al (2014) The influence of particle size on radionuclide activity concentrations in Tejo River sediments. J Environ Radioact 132:65–72. https://doi.org/10.1016/J.JENVRAD.2014.01.019

Majerová L, Bábek O, Navrátil T et al (2018) Dam reservoirs as an efficient trap for historical pollution: the passage of Hg and Pb through the Ohře River, Czech Republic. Environ Earth Sci 77. https://doi.org/10.1007/s12665-018-7761-3

Mclean RI, Summers JK, Mclean RL (1990) Evaluation of transport and storage of 6°Co, 134Cs, 137Cs and 65Zn by river sediments in the lower Susquehanna River. Environ Pollut 63:137–153

Meyers PA, Ishiwatari R (1995) Organic matter accumulation records in lake sediments. In: Lerman A, Imboden DM, Gat JR (eds) Physics and Chemistry of Lakes. Springer, Berlin, pp 279–328

Mietelski JW, Dubchak S, Błażej S, Anielska T, Turnau K (2010) ^{137}Cs and ^{40}K in fruiting bodies of different fungal species collected in a single forest in southern Poland. J Environ Radioact 101(9):706–711

Mishra S, Sahoo SK, Bossew P et al (2016) Vertical migration of radio-caesium derived from the Fukushima Dai-ichi Nuclear Power Plant accident in undisturbed soils of grassland and forest. J Geochem Explor 169:163–186. https://doi.org/10.1016/J.GEXPLO.2016.07.023

Muñoz-Salinas E, Castillo M, Romero F, Correa-Metrio A (2021) Understanding sedimentation at the El Molinito reservoir (NW Mexico) before and after dam construction using physical sediment analyses. J S Am Earth Sci 111:103401

Natkaniec J (1999) Accumulation of anthropogenic radioactive elements in soils near Nysa and Opole and sediments of Turawa reservoir (in Polish). Zesz Nauk AR Krak Inż Środ 19(355):57–70

Naulier M, Eyrolle-Boyer F, Boyer P et al (2017) Particulate organic matter in rivers of Fukushima: an unexpected carrier phase for radiocesiums. Sci Total Environ 579:1560–1571. https://doi.org/10.1016/J.SCITOTENV.2016.11.165

Park CW, Kim SM, Kim I et al (2021) Sorption behavior of cesium on silt and clay soil fractions. J Environ Radioact 233:106592. https://doi.org/10.1016/J.JENVRAD.2021.106592

Pulley S, Foster IDL, Collins AL, Zhang Y, Evans J (2018) An analysis of potential controls on long-term ^{137}Cs accumulation in the sediments of UK lakes. J Paleolimnol 60:1–30

Putyrskaya V, Klemt E, Röllin S, Corcho-Alvarado JA, Sahli H (2020) Dating of recent sediments from Lago Maggiore and Lago di Lugano (Switzerland/Italy) using ^{137}Cs and ^{210}Pb. J Environ Radioact 212:106135

Ries T, Putyrskaya V, Klemt E (2019) Long-term distribution and migration of ^{137}Cs in a small lake ecosystem with organic-rich catchment: a case study of Lake Vorsee (Southern Germany). J Environ Radioact 198:89–103

Rigol A, Vidal M, Rauret G (2002) An overview of the effect of organic matter on soil-radiocaesium interaction: implications in root uptake. J Environ Radioact 58:191–216. https://doi.org/10.1016/S0265-931X(01)00066-2

Sakuma K, Malins A, Funaki H, Kurikami H, Niizato T, Nakanishi T, Mori K, Tada K, Kobayashi T, Kitamura A, Hosomi M (2018) Evaluation of sediment and ^{137}Cs redistribution in the Oginosawa River catchment near the Fukushima Dai-ichi Nuclear Power Plant using integrated watershed modeling. J Environ Radioact 182:44–51

Santschi PH, Bollhalder S, Zingg S, Lueck A, Farrenkothen K (1990) The self-cleaning capacity of surface waters after radioactive fall-out evidence from European waters after Chernobyl, 1986–1988. Environ Sci Technol 24(4):519–527

Santschi PH, Nyffeler UP, Anderson RF, Schiff SL, O'Hara P, Hesslein RH (1986) Response of radioactive trace metals to acid-base titrations in controlled experimental ecosystems: evaluation of transport parameters for application to whole-lake radiotracer experiments. Can J Fish Aquat Sci 43:60–77

Sedláček J, Bábek O, Kielar O (2016) Sediment accumulation rates and high-resolution stratigraphy of recent fluvial suspension deposits in various fluvial settings, Morava River catchment area, Czech Republic. Geomorphology 254:73–87

Smith JT, Beresford NA (2005) Chernobyl – catastrophe and consequences. Springer

Somboon S, Kavasi N, Sahoo SK et al (2018) Radiocesium and 40K distribution of river sediments and floodplain deposits in the Fukushima exclusion zone. J Environ Radioact 195:40–53. https://doi.org/10.1016/j.jenvrad.2018.09.003

Strzelecki R, Wołkowicz S, Szewczyk J, Lewandowski P (1993) Map of cesium concentration in Poland, radiological map of Poland (I) (in Polish). Polish Geological Institute, Warsaw

Szarłowicz K, Reczyński W, Gołaś J, Kościelniak P, Skiba M, Kubica B (2011) Sorption of ^{137}Cs and ^{210}Pb on sediment samples from a drinking water reservoir. Pol J Environ Stud 20(5):1305–1312

Tachi Y, Sato T, Takeda C et al (2020) Key factors controlling radiocesium sorption and fixation in river sediments around the Fukushima Daiichi Nuclear Power Plant. Part 2: Sorption and fixation behaviors and their relationship to sediment properties. Sci Total Environ 724:138097. https://doi.org/10.1016/J.SCITOTENV.2020.138097

Teisseyre AK (1983) Bottoms of Turawa Lake in the light of geological research (in Polish). Geol Sudet 18(1):21–60

Tsabaris C, Eleftheriou G, Kapsimalis V et al (2007) Radioactivity levels of recent sediments in the Butrint Lagoon and the adjacent coast of Albania. Appl Radiat Isot 65:445–453. https://doi.org/10.1016/J.APRADISO.2006.11.006

Tsuji H, Tanaka A, Komatsu K, Kohzu A, Matsuzaki SS, Hayashi S (2019) Vertical/spatial movement and accumulation of ^{137}Cs in a shallow lake in the initial phase after the Fukushima Daiichi nuclear power plant accident. Appl Radiat Isot 147:59–69

Wakiyama Y, Onda Y, Yoshimura K et al (2019) Land use types control solid wash-off rate and entrainment coefficient of Fukushima-derived ^{137}Cs, and their time dependence. J Environ Radioact 210:105990. https://doi.org/10.1016/J.JENVRAD.2019.105990

Wang Q, Sha Z, Wang J, Zhong Q, Fang P, Ma Y, Du J (2020) Vertical distribution of radionuclides in Lake Qinghai, Qinghai-Tibet Plateau, and its environmental implications. Chemosphere 259(8):127489

Wojewoda J (2013) The sand spit in Turawa Lake - sedimentological study (in Polish). Conference abstract, POKOS 5'2013, 90–92

Wołkowicz S, Strzelecki R (2002) Geochemistry of post-Chernobyl cesium in soils and plants in Opole region (in Polish). Przegl Geol 50(10):941–944

Wróbel Ł, Dołhańczuk-Śródka A, Kłos A, Ziembik Z (2015) The activity concentration of post-Chernobyl ^{137}Cs in the area of the Opole Anomaly (southern Poland). Environ Monit Assess 187(1):4084

Yoshimura K, Onda Y, Fukushima T (2014) Sediment particle size and initial radiocesium accumulation in ponds following the Fukushima DNPP accident. Sci Rep 4(4514):1–6

Zapata F, Nguyen ML (2010) Soil erosion and sedimentation studies using environmental radionuclides. Radioact Environ 16:295–322

Ziembik Z, Dołhańczuk-Śródka A, Komosa A, Orzeł J, Wacławek M (2010) Assessment of ^{137}Cs and $^{239, 240}$Pu distribution in forest soils of the Opole anomaly. Water Air Soil Pollut 206(1):307–320

Publisher's Note Springer Nature remains neutral with regard to jurisdictional claims in published maps and institutional affiliations.

Factors controlling ^{137}Cs distribution in bottom sediments of Koronowo Reservoir (Poland)

Ilona Sekudewicz[1] · Šárka Matoušková[2] · Zuzanna Ciesielska[3] · Anna Mulczyk[1] · Michał Gąsiorowski[1]

Abstract

Purpose The main aim of this study was to investigate factors influencing the long-term distribution of ^{137}Cs activity concentrations in the bottom sediments of the dam lake, Koronowo Reservoir, 32 years after the Chernobyl nuclear power plant accident. For this purpose, selected properties of the collected sediment samples, such as grain size, mineralogical composition, and organic matter (OM) content, were investigated.

Materials and methods The samples of lake sediments were collected with a Kayak-type gravity corer. The spatial and vertical distributions of ^{137}Cs and ^{40}K activity concentrations in the bottom sediments were investigated based on gamma spectrometry measurements. The particle size distribution of surface lake sediments was determined using a laser particle size analyzer. SEM and XRD were used for the mineralogical analysis of the collected sediment samples. Additionally, the content of organic matter was examined in all samples using an elemental analyzer.

Results The ^{137}Cs content was significantly elevated in the case of fine-grained ($<63\ \mu m$) surface lake sediments (classified as silts, which are deposited in the profundal zone of Koronowo Lake) and ranged from 12.5 ± 4.1 to 29.2 ± 4.0 Bq kg^{-1}. It was found that the increased concentration of ^{137}Cs activity is more closely related to the content of the silt fraction (2–$63\ \mu m$) than to the clay fraction ($<2\ \mu m$) in the collected surface lake sediments. The content of clay minerals also showed a significant positive correlation with ^{137}Cs activity concentration in the surface lake sediments of Koronowo Lake. A similar relationship was noticed for the OM content, but it may be suspected that it is the result of radiocesium-bearing particle accumulation in OM-rich sediments.

Conclusion The most important factor influencing the spatial distribution of ^{137}Cs activity concentrations in the surface lake sediments of Koronowo Lake, apart from the bottom morphology and grain size of sediments, is the content of clay minerals. Moreover, the increased detrital inflow to the lake after the construction of the dam could have probably affected the vertical distribution of ^{137}Cs activity concentrations in the bottom sediments, as evidenced by, e.g., the measurements of ^{40}K activity concentration.

✉ Ilona Sekudewicz
  i.sekudewicz@twarda.pan.pl

1   Institute of Geological Sciences, Polish Academy of Sciences, ul. Twarda 51/55, 00-818 Warszawa, Poland

2   Institute of Geology, Czech Academy of Sciences, Rozvojová 269, 165 00 Prague, Czech Republic

3   Institute of Geological Sciences, Polish Academy of Sciences, ul. Senacka 1, 30-063 Kraków, Poland

1 Introduction

Radiocesium ^{137}Cs has been released into the environment as a result of nuclear weapon tests and nuclear power plant accidents, e.g., in Chernobyl and Fukushima (e.g., Ashraf et al. 2014; Beresford et al. 2016; Evrard et al. 2020). Due to its high affinity for fine particles, this isotope is immobilized readily in soils and sediments (He and Walling 1996; Zachara et al. 2002; Park et al. 2021). As a result, ^{137}Cs can be used as a time marker for sediment dating or as an indicator of soil erosion (e.g., Appleby 2008; Zapata and Nguyen

2009; Putyrskaya et al. 2020). The deposited ^{137}Cs has also been redistributed within and beyond contaminated areas by surface process such as fluvial transport (e.g., Tanaka et al. 2015; Ivanov et al. 2021). Diaz-Asencio et al. (2017) emphasized that intensified erosion of a catchment area increases the load of particles and thus the influx of pollutants into the fluvial system. Moreover, anthropogenic changes in river morphology (related to, e.g., dam construction) may affect the storage of sediments contaminated with ^{137}Cs (Kurikami et al. 2014; Díaz-Asencio et al. 2017; Funaki et al. 2019; Sekudewicz and Gąsiorowski 2022). As a consequence, the reservoirs may trap significant amounts of radiocesium-bearing particles, which can also pose a serious environmental risk if this radionuclide is rereleased into the fluvial system (Ivanov et al. 2021). On the other hand, bottom sediments can provide a valuable source of information concerning the long-term redistribution of ^{137}Cs (Konoplev et al. 2019). On this basis, changes in, e.g., the level of contamination of transported particles by ^{137}Cs or the sediment load can be reconstructed.

The distribution of ^{137}Cs in lake sediments is significantly related to the characteristics of the lake and its catchment area, and sediment properties such as particle size, mineralogical composition and organic matter (OM) content (He and Walling 1996; Fan et al. 2014; Tanaka et al. 2015; Tachi et al. 2020a, b; Park et al. 2021; etc.). One of the most important factors that may affect the accumulation and distribution of ^{137}Cs in freshwater ecosystems are transport processes and related sorting of sediment particles (e.g., Tanaka et al. 2015; Huon et al. 2018). It has been widely observed that the concentration of ^{137}Cs activity generally increases while the particle size decreases (He and Walling 1996; Fan et al. 2014; and others). This increase is because the fine-sized (< 63 μm) particle fraction is characterized, e.g., by a large specific surface area and an increased content of clay minerals, which affects the binding of ^{137}Cs and makes it an important carrier of this radionuclide (He and Walling 1996; Spezzano 2005; Funaki et al. 2019; Mouri 2020). Therefore, studying the particle transport processes and the properties of sediments may be the key to understanding the behavior of radiocesium in freshwater ecosystems (Fan et al. 2014). However, it should also be noted that the relation between the distribution of radiocesium and the grain size of sediment particles still remains unclear (Hagiwara et al. 2020). It was observed, for example, that the silt-size (2–63 μm) particle fraction of bottom sediments at the midstream Kuchibuto, Kuroiwa, and Fushiguro sites contains more ^{137}Cs than the clay-size (< 2 μm) particle fraction (Tanaka et al. 2015).

Another important factor that could influence the accumulation of ^{137}Cs in lake sediments is their mineralogical composition (Ashraf et al. 2014; Tanaka et al. 2015; Huon et al. 2018; Hagiwara et al. 2020). This influence is due to the sorption and fixation of Cs is particularly determined by the type and amount of phyllosilicate minerals (Sawhney 1972; Zachara et al. 2002; Tachi et al. 2020a; Park et al. 2021). Depending on their different physicochemical properties, such as chemical composition, expandability, cation exchange capacity (CEC), and layer charge, they are able to bind Cs to varying degrees (Cornell 1993; Mukai et al. 2016; Park et al. 2021). Moreover, in the case of clay minerals, the sorption of Cs is highly controlled by the specific sorption at frayed edge sites (FES) and the exchangeable sorption at regular exchange sites (RES) (Sawhney 1972; Cornell 1993; Zachara et al. 2002; Tachi et al. 2020b). The mineralogical composition of lake sediments can be additionally used to trace the origin of particles contaminated with ^{137}Cs (Hagiwara et al. 2020). It may indicate, for example, whether the accumulated particles originate from eroded surrounding rocks or were produced within the reservoir (Díaz-Asencio et al. 2017). It was also found that ^{40}K can be used as an indicator of detrital layers in sediment records (Putyrskaya et al. 2020). The validity of the use of ^{40}K in the study of sediment distribution was also emphasized by Somboon et al. (2018), who indicated that such analyses can readily help to reveal differences in the mineral composition of sediment samples.

Understanding the role of OM in the distribution of ^{137}Cs is also very important, as it can affect the mobility and bioavailability of radiocesium in freshwater ecosystems (Kaminski et al. 1994; Staunton et al. 2002; Fujii et al. 2018). On the other hand, the adsorption of radiocesium by OM is rather negligible; therefore, the mechanism of ^{137}Cs accumulation in OM-enriched sediments still remains unclear (Fujii et al. 2018). Moreover, it is known that the presence of OM might even inhibit the sorption of Cs$^+$ on clay minerals by blocking access to FESs (Rigol et al. 2002; Fan et al. 2014; Suga et al. 2014). Therefore, the accumulation of ^{137}Cs can be more closely related to a combination of factors determining its immobilization, such as the grain size of sediment particles, their mineral composition, and OM content (Kim et al. 2007; Fujii et al. 2018; Tachi et al. 2020b). In addition, the composition of OM can be used as an indicator of anthropogenic impacts or environmental changes (Meyers and Ishiwatari 1993; Contreras et al. 2018). For instance, it may indicate the origin of organic particles, as it is known that the C/N ratio for nonvascular aquatic plants is typically between 4 and 10, while for vascular terrestrial plants, it is greater than 20 (Prahl et al. 1980; Ertel and Hedges 1984; Meyers and Ishiwatari 1995; Lamb et al. 2006; Contreras et al. 2018). On this basis, the C/N ratio is considered to be a representative proxy of the origin of OM deposited in freshwater sediments.

The main aim of the present study was to investigate the major factors influencing the distribution of ^{137}Cs activity concentrations in the bottom sediments of Koronowo Lake 32 years after the Chernobyl nuclear power plant accident. For this purpose, the most critical factors that can

potentially affect the migration and accumulation of ^{137}Cs in lake sediments (grain size, mineralogical composition, and OM content) were investigated. To better track the transport processes occurring in Koronowo Lake, the origin of organic particles in the collected lake sediments was determined based on C/N ratio measurements. For the same purposes, the mineralogical composition of inorganic particles and the concentration of ^{40}K activity in the collected sediment samples were analyzed. Selected parameters of the collected sediment cores were also examined to investigate factors influencing the vertical distribution of ^{137}Cs activity concentrations in the bottom sediments of Koronowo Lake. The obtained data were used to reconstruct changes in sedimentation processes and to assess their potential impact on the delivery and redistribution of radiocesium-bearing particles in this reservoir over time.

2 Materials and methods

2.1 Study area

The study area was located in the main basin of Koronowo Lake (Fig. 1). This lake is an artificial reservoir that was created in 1961. It is situated in the lower part of the Brda River (left tributary of the Vistula River) in the lowland in northern Poland. The surface area, capacity volume level, maximum,

and mean water depth of Koronowo Lake are 1560 ha, 81.0 million m^3, 21.2 m, and 5.7 m, respectively. The catchment area of the studied lake is equal to 4299 km^2 and is mainly covered with agricultural lands and forests (Szatten et al. 2018). The average discharge of the Brda River (the main tributary of Koronowo Lake) in 1962–2015 was approximately 23.7 m^3 s^{-1} (Hydropower Plant Koronowo 2015). The sediment budget in this lake is dominated by suspended sediments, which are delivered mainly by the Brda River. The total load of sediments supplied from the upper basin of the Brda River to Koronowo Lake in 2015 was estimated to be 2439 t, while their outflow from the lake was approx. 1743 t (Szatten et al. 2018).

The main basin of Koronowo Lake is located from Wielonek to the dam in Pieczyska (Fig. 1A). It contains 32.7 million m^3 of water, which constitutes over 1/3 of all water retained in this reservoir. It is the main area for sediment accumulation, especially in the zones near the dam, estuary of inflows, and bays (Szatten et al. 2018). This part of the lake is also characterized by more limnetic conditions with increased biological production in the bays. The main basin of this lake is located in an area formed mainly by glacial outwash sands and gravels (Fig. 1B). In the northern part, there are also humic sands and silts, while in the southern part (near the dam), glacial tills and deluvial sands occur. The northern part of the study area is

Fig. 1 Sampling area **A** (Szatten 2016; modified) and geological setting **B** of Koronowo Lake (Wieczorek and Stoiński 2008; modified)
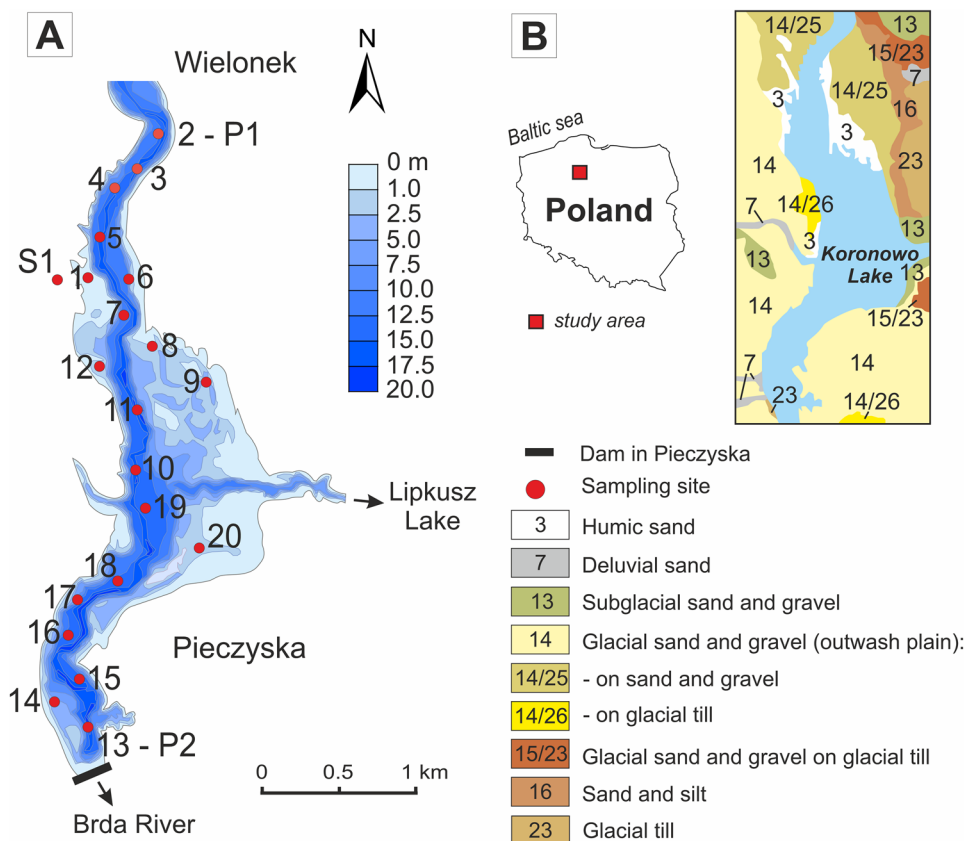
located mainly in an uncultivated area covered with coniferous forest, while in the southern part, there are more buildings, marinas, and recreational areas.

2.2 Sampling and sample treatment

A fieldwork campaign was carried out on the main basin of Koronowo Lake in October 2018 (Fig. 1). One soil profile, 20 surface lake sediment samples, and 2 sediment cores were collected. The soil profile (S1) had a length of 25-cm depth and was divided in the field into 4 sections depending on the lithology (Fig. S1; Supplementary Material). Lake sediments were collected using a Kayak-type gravity corer (55 mm in internal diameter). Surface lake sediments (0–3-cm depth) were collected in 6 transects from the littoral and profundal zones of the lake. Sediment cores were taken from the deepest points of the lake's bottom in the northern part of the main basin (core P1: sampling site 2, lake depth: 9 m, profile length: 32 cm) and in the southern part near the dam (core P2: sampling site 13, lake depth: 15 m, profile length: 27 cm). The sediment cores were divided in the field into 1-cm thick slices. All samples were packed in plastic bags and stored in a refrigerator at 4 °C. Then, all samples were transported to the laboratory, where they were weighed, dried (for 48 h at 60 °C), homogenized, and prepared for the analyses.

2.3 Grain-size and elemental analysis

The grain size distribution of surface lake sediments was measured using sieve analysis (for particles > 1000 μm) and a CILAS 1190 laser particle size analyzer at the Institute of Geology CAS. The instrument was set in wet dispersion mode, providing a range from 0.04 to 1000 μm. The data were obtained after dispersion in KOH, removing carbonates by HCl and removing organic matter by H_2O_2 and HNO_3. The obtained results are reported in three fractions: clay (up to 2 μm), silt (2–63 μm), and sand (63–2000 μm). Surface sediments were classified according to the Shepard sediment classification diagram (Shepard 1954) using the "ggtern" R package (Hamilton and Ferry 2018).

The contents of total organic carbon (TOC) and total nitrogen (TN) were measured in all collected samples using a Vario CUBE elemental analyzer. Sulfanilic acid was used as a standard for analysis. Prior to analysis, carbonates were removed from the samples with 5% hydrochloric acid. Milled and homogenized samples (5–6 mg) were transferred into tin capsules. The uncertainties of the TOC and TN measurements were lower than 0.6% and 0.18%, respectively.

2.4 XRD and SEM−EDS analyses

All surface lake sediment samples and selected samples from sediment cores P1 (at 20-cm depth) and P2 (at 6-cm and 27-cm depth) were examined using X-ray and SEM−EDS methods. Mixtures of powdered samples, the internal standard (10 wt.% ZnO), and 4 ml of methanol were milled in a McCrone micronizing mill for 5 min to obtain homogenous samples with narrow grain-size distributions. Then, the specimens were prepared for X-ray analysis using the side-loading method, which minimizes the preferred orientation (Środoń et al. 2001). The mineral composition of the samples was determined with a Thermo Electron ARL X'TRA diffractometer at Clay Minerals Laboratory in the Institute of Geological Sciences PAS. It is equipped with a 12-position sample holder and a Peltier cooled solid-state detector operating in a Bragg−Brentano geometry using CuKα radiation (40 kV, 30 mA). Diffraction patterns were collected in a 2θ range of 2.5–65° with a step size of 0.02° (5 s/step).

Qualitative and quantitative analyses were performed using Q-min software, which works based on a combination of the mineral intensity factor (MIF) technique and preregistered pure standards collection. Determination of mineral composition was achieved by fitting the measured XRD pattern of the sample with patterns of pure standards (Środoń et al. 2001). During matching, some ranges were excluded from matching, and some were optimized with higher weights. These were the ranges with stable reflections of the internal standard and clay minerals.

The accuracy of the quantitative XRD analysis depends to a large extent on the crystallinity of the selected phases—the higher the crystallinity is, the higher the sensitivity and precision of this method. For example, in the case of phases such as calcite, gypsum, anhydrite, and ankerite/dolomite, their detection is possible in the presence of even below approximately 1%, while for smectitic clay minerals, it is approximately 5%. The precision of the obtained results also depends on the crystallinity of the phases, but generally, it can be assumed to be equal to ± 3–5% of the absolute values (Raven and Self 2017).

The surface lake sediment samples were analyzed using a scanning electron microscope (SEM) FE-SIGMA VP (Carl Zeiss Microscopy GmbH) in conjunction with two energy-dispersive X-ray spectrometers (Quantax XFlash 6|10, Bruker Nano GmbH). The powdered samples were placed on an aluminum mount with conductive carbon tape and coated with a carbon layer (20 nm) with a vacuum coater (Quorum 150 T ES). Analyses were performed with a 60-μm aperture and 20-keV acceleration voltage.

2.5 Gamma spectroscopy

The concentrations of ^{137}Cs and ^{40}K activity in all collected samples were measured using a low background gamma spectrometer (Canberra-Packard) with a Broad Energy Germanium (BE5030) detector (FWHM = 1.28 keV at 661.7 keV for ^{137}Cs and 1.72 keV at 1460.8 keV for ^{40}K). All samples were analyzed in a round polyethylene cup (flat cylinder geometry). The energy calibration was performed using a radioactive standard. The reference material IAEA-SL-2 was used to verify the quality of the measurements. The obtained spectra were analyzed with Genie 2000 software. The average counting time per sample ranged from 24 to 72 h. The counting time and uncertainty of the measurements depended on the minimal detection activity (MDA) and the sample mass (from 2 to 45 g). The uncertainty of the ^{137}Cs and ^{40}K activity concentration measurements ranged from 11 to 39% and from 9 to 44%, respectively. The MDA of ^{137}Cs and ^{40}K varied from 0.34 to 6.8 Bq kg^{-1} and from 4.4 to 81.3 Bq kg^{-1}, respectively. All measured ^{137}Cs and ^{40}K activity concentrations were converted to the first day of sampling (October 24, 2018).

2.6 Data analysis

^{137}Cs, ^{40}K, and TOC and TN spatial distribution maps were generated using the inverse distance weighting (IDW) interpolation method ArcGIS ver. 10.6 (Esri Co., Ltd., Redlands, CA, USA). Statistical analyses were performed using R 4.0.3 (R Core Team 2020). The Shapiro–Wilk test (confidence level 95%) was used to test the normal distribution of the analyzed data. Spearman's rank correlation coefficients were calculated to assess the relationship (p value < 0.05) between measured variables. To conduct a principal component analysis (PCA), the data were centered, scaled, and then tested to examine their suitability using the Kaiser–Meyer–Olkin (KMO) test.

3 Results

3.1 Surface lake sediments

3.1.1 Particle size distribution and organic matter content

The surface lake sediments were classified as fine- (< 63 μm) and coarse-grained (> 63 μm) sediments. According to Shepard's classification diagram, the fine-grained sediments were classified as silt (sample nos. 2–5, 7, 10, 11, 13, 15, 16, and 18–19), whereas the coarse-grained sediments were recognized as sand (sample nos. 6, 8, 9, 14, 17, and 20) and silty sand (sample nos. 1 and 12) (Figs. 2 and 3). The obtained data showed that the grain size of surface lake sediments is
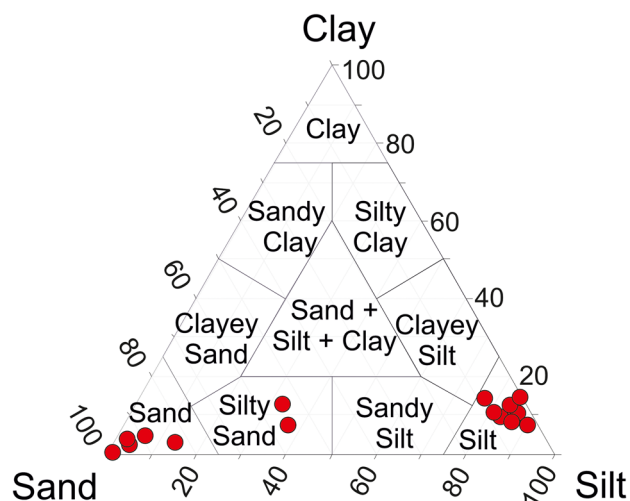
Fig. 2 Shepard's classification diagram of surface (0–3-cm depth) lake sediments in Koronowo Lake

significantly related to the depth of the reservoir (Table 1). Most fine-grained surface lake sediments occur in the "old," pre-reservoir Brda Valley, where the lake is now the deepest (Fig. 1). The sand fraction dominates ($R_s = -0.61$, p value < 0.05) in the littoral zone, whereas the clay ($R_s = 0.49$, p value < 0.05) and silt fractions ($R_s = 0.62$, p value < 0.05) dominate in the profundal zone of the lake (Table 1). The silt fraction prevails in all fine-grained surface lake sediments (Fig. 3A). A relatively high content of clay fraction was also observed in samples collected from the shallower (at approx. 2 m of a depth) part of the lake (sampling sites no. 12 (12.4%) and 1 (8.6%)). The average water content of fine- (arithmetic mean, $n = 12$) and coarse-grained bottom sediments (arithmetic mean, $n = 8$) was 89% and 31%, respectively, whereas the average wet bulk density was 1.08 g cm^{-3} and 1.63 g cm^{-3}, respectively.

The average contents of TOC and TN in fine-grained surface lake sediments (arithmetic mean, $n = 12$) were 17.9% and 2.6%, respectively, while those in coarse-grained surface lake sediments (arithmetic mean, $n = 8$) were 1.3% and 0.3%, respectively. The elevated content of OM (expressed as the content of TOC and TN) was observed mainly in the case of fine-grained bottom sediments deposited in the deepest parts of Koronowo Lake (Figs. 4 and 5). The content of OM in surface lake sediments deposited in the littoral zone was much lower than that in the profundal zone, except for sands collected at sampling sites no. 1 and 17 (in which the content of TOC was up to 3.4% and 5.2%, respectively). The C/N ratio calculated for fine-grained surface lake sediments ranged from 5.4 to 9.3. Due to the results being below the detection limit, it was not possible to calculate the C/N ratio for coarse-grained surface lake sediments, except for samples no. 1 (C/N = 20.9), 14 (C/N = 4.5), and 17 (C/N = 5.5).

Fig. 3 Grain-size distribution **A** and mineralogical composition **B** of surface (0–3-cm depth) lake sediments in Koronowo Lake. Sampling sites are presented in Fig. 1
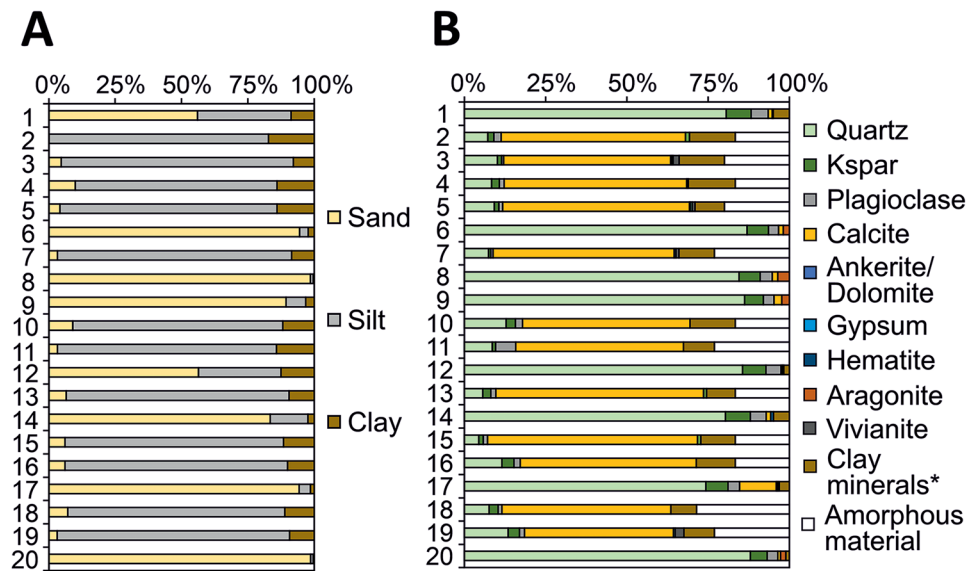
3.1.2 XRD and SEM-SEM analyses

Silts were mainly composed of calcite (up to ~65%), amorphous material (up to ~30%), clay minerals (muscovite, chlorite, kaolinite, smectite group, and illite−smectite) (from ~8 to ~14%), quartz (up to ~13%), and an admixture of plagioclase, potassium feldspar, gypsum, ankerite/dolomite, and vivianite (Fig. 3B). The sands and silty sands were mainly composed of quartz (up to ~88%), calcite (up to ~11%), potassium feldspar (up to ~8%), clay minerals (up to ~5%), plagioclase (up to ~5%), and an admixture of aragonite, gypsum, ankerite/dolomite, and hematite. The highest contents of the kaolinite, muscovite, illite−smectite, and smectite group in silts were approximately 1.6, 3.8, 7.4, and 9.6%, respectively. In the case of sands and silty sands, the muscovite and smectite group were not identified, while the highest concentrations of kaolinite, chlorite, and illite−smectite were approximately 1.3, 0.4, and 4.9%, respectively. The most enriched fine-grained bottom sediments in clay minerals were samples no. 2, 3, and 10. In the case of coarse-grained bottom sediments, the highest content of clay minerals was observed in samples no. 1, 14, and 17. The contents of clay minerals, amorphous material, and calcite in the surface lake sediments of Koronowo Lake are significantly positively correlated with the depth of the lake, the silt and clay fraction contents, and ^{137}Cs and OM contents (Table 1). They are also significantly negatively correlated with the wet bulk density of the collected bottom sediments and the contents of ^{40}K, sand fraction, quartz, potassium feldspar, and plagioclase.

The SEM−EDS analyses showed that the amorphous material was represented mainly by the remains of organic debris composed of amorphous silica and organic material (Fig. 6A–C). Based on the conducted analyses, the presence

of quartz, calcite, potassium feldspar, plagioclase, and clay minerals was confirmed. The presence of authigenic calcite (Fig. 7A) and vivianite (Fig. 7C) was observed in the case of fine-grained surface lake sediments. Additionally, iron oxyhydroxides (Fig. 6D) and framboidal pyrites (Fig. 7D) were also recognized. The presence of monazite, zircon, hematite, and titanium oxides (e.g., samples no. 14, 17) was observed in the case of sands and silty sands (Fig. 7B).

3.1.3 Spatial distribution of ^{137}Cs and ^{40}K activity concentrations

The ^{137}Cs content in the surface lake sediments of Koronowo Lake is characterized by a bimodal distribution, which is related to the elevated content of this radionuclide in fine-grained sediments and the decreased content in coarse-grained bottom sediments (Figs. 4 and 5). The average ^{137}Cs activity concentrations in fine-grained bottom sediments are almost four times higher (17.67 ± 3.96 Bq kg^{-1}; arithmetic mean, $n = 12$) than in coarse-grained bottom sediments (5.08 ± 0.82 Bq kg^{-1}; arithmetic mean, $n = 8$). Relatively high concentrations of ^{137}Cs activity were also measured in sample no. 14 (21.2 ± 2.6 Bq kg^{-1}) and 17 (7.8 ± 1.3 Bq kg^{-1}), which contain significant amounts of sandy fraction (Fig. 3A).

Similar to ^{137}Cs, the content of ^{40}K in the surface lake sediments of Koronowo Lake is also characterized by a bimodal distribution. In the case of fine-grained bottom sediments, the content of ^{40}K is lower (160.2 ± 36.7 Bq kg^{-1}; arithmetic mean, $n = 12$) than in coarse-grained bottom sediments (237.9 ± 22.0 Bq kg^{-1}; arithmetic mean, $n = 8$). The highest concentrations of ^{40}K activity were detected in the surface lake sediments collected from sampling site no. 1

Table 1 Spearman's rank correlation among the measured parameters in surface (0–3-cm depth) lake sediments of Koronowo Lake. Correlation coefficients > 0.4 and with p value ≤ 0.05 are bolded

	137Cs	40K	TN	TOC	Wt	Blk	Depth	Sand	Clay	Silt	Qtz	Kfs	Pg	Cal	Ill-Smc	Smc	Am	Cl
137Cs	**1.00**																	
40K	**−0.46**	**1.00**																
TN	**0.76**	**−0.73**	**1.00**															
TOC	**0.60**	**−0.70**	**0.85**	**1.00**														
Wt	**0.67**	**−0.71**	**0.85**	**0.89**	**1.00**													
Blk	**−0.64**	**0.67**	**−0.84**	**−0.93**	**−0.97**	**1.00**												
Depth	**0.60**	**−0.75**	**0.78**	**0.75**	**0.74**	**−0.73**	**1.00**											
Sand	**−0.55**	**0.54**	**−0.65**	**−0.65**	**−0.65**	**0.71**	**−0.61**	**1.00**										
Clay	0.24	−0.36	**0.48**	**0.66**	**0.66**	**−0.72**	**0.49**	**−0.66**	**1.00**									
Silt	**0.66**	**−0.60**	**0.68**	**0.66**	**0.65**	**−0.69**	**0.62**	**−0.93**	**0.50**	**1.00**								
Qtz	**−0.50**	**0.69**	**−0.74**	**−0.88**	**−0.83**	**0.88**	**−0.77**	**0.75**	**−0.62**	**−0.75**	**1.00**							
Kfs	−0.37	**0.79**	**−0.64**	**−0.71**	**−0.66**	**0.65**	**−0.66**	**0.75**	**−0.51**	**−0.71**	**0.77**	**1.00**						
Pg	**−0.43**	**0.75**	**−0.59**	**−0.51**	**−0.44**	**0.40**	**−0.61**	**0.51**	−0.19	**−0.61**	**0.60**	**0.68**	**1.00**					
Cal	**0.47**	**−0.77**	**0.72**	**0.84**	**0.83**	**−0.84**	**0.73**	**−0.69**	**0.59**	**0.66**	**−0.92**	**−0.78**	**−0.68**	**1.00**				
Ill-smc	**0.58**	−0.28	**0.64**	**0.56**	**0.41**	**−0.46**	**0.55**	**−0.67**	0.37	**0.60**	**−0.53**	**−0.49**	**−0.46**	0.38	**1.00**			
Smc	**0.51**	**−0.54**	**0.57**	**0.73**	**0.78**	**−0.79**	**0.52**	**−0.61**	**0.68**	**0.62**	**−0.75**	**−0.68**	**−0.45**	**0.77**	0.26	**1.00**		
Am	**0.62**	**−0.67**	**0.79**	**0.70**	**0.69**	**−0.68**	**0.68**	**−0.83**	**0.54**	**0.80**	**−0.69**	**−0.81**	**−0.64**	**0.63**	**0.69**	**0.55**	**1.00**	
Cl	**0.57**	**−0.45**	**0.61**	**0.71**	**0.65**	**−0.70**	**0.59**	**−0.80**	**0.66**	**0.74**	**−0.76**	**−0.76**	**−0.54**	**0.69**	**0.71**	**0.81**	**0.72**	**1.00**

137Cs activity concentration (Bq kg$^{−1}$), ^{40}K activity concentration (Bq kg$^{−1}$), *TN* total nitrogen (%), *TOC* total organic carbon (%), *Wt.* water content (%), *Blk.* wet bulk density (g cm$^{−3}$), *Depth* depth of the lake at sampling point (m), *Sand* sand fraction (%), *Clay* clay fraction (%), *Silt* silt fraction (%), *Qtz* quartz (%), *Kfs* potassium feldspar (%), *Pg* plagioclase (%), *Cal* calcium (%), *Ill-Smc* illite–smectite (%); *Smc* smectite group (%), *Am.* amorphous material (%), *Cl.* sum of clay minerals (kaolinite, muscovite, chlorite, illite–smectite, smectite group) (%)

Fig. 4 Spatial distribution of **A** ^{137}Cs and **B** ^{40}K activity concentrations (Bq kg^{-1}), **C** total organic carbon (TOC), and **D** total nitrogen (TN) (%) content in surface (0–3-cm depth) lake sediments of Koronowo Lake
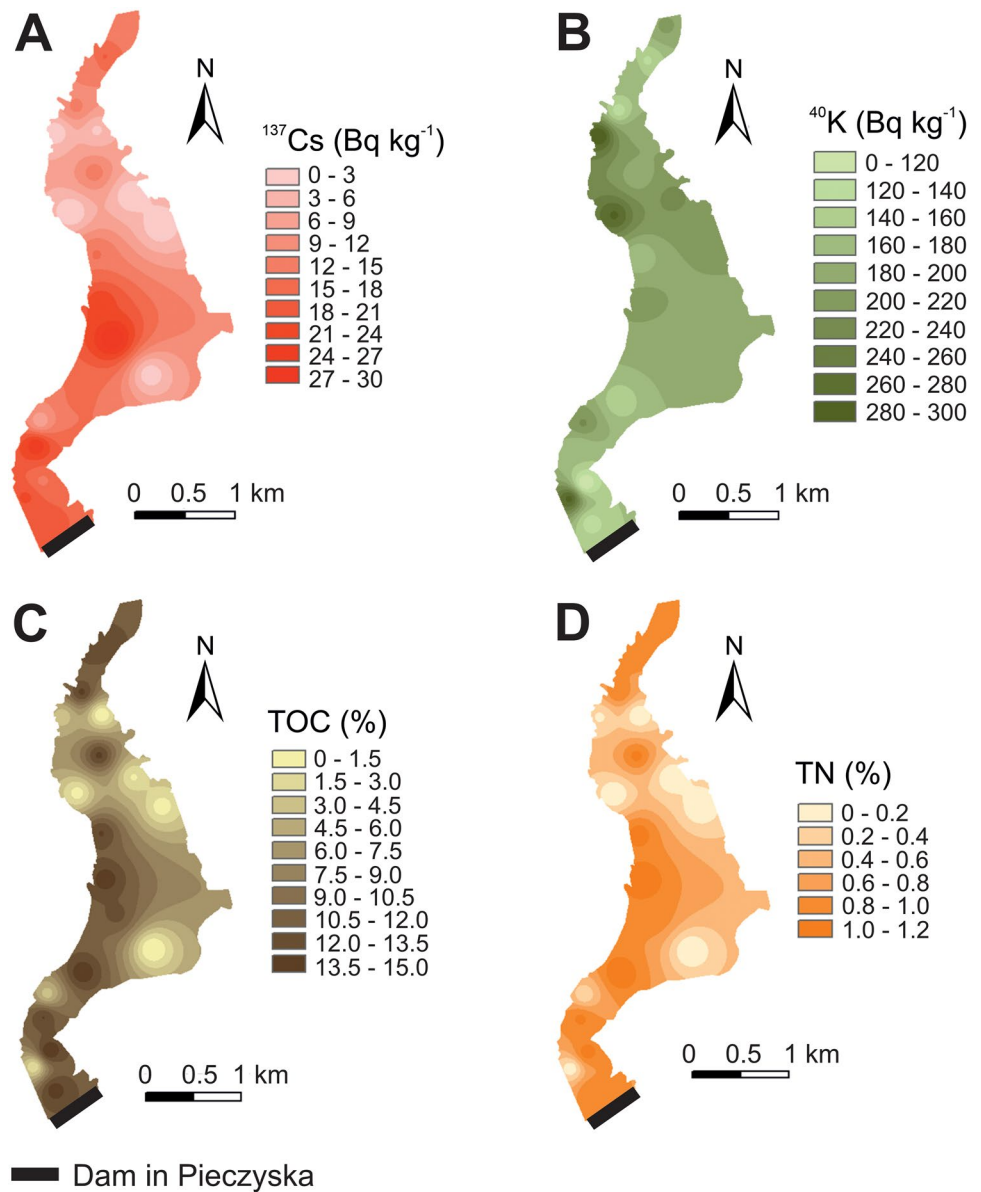
(299.1 ± 26.3 Bq kg^{-1}), 12 (282.1 ± 25.5 Bq kg^{-1}), and 14 (284.48 ± 24.85 Bq kg^{-1}).

The spatial distributions of ^{137}Cs and ^{40}K activity concentrations in the surface lake sediments of Koronowo Lake are presented in Fig. 4. They showed that bottom sediments deposited in the profundal zone of the lake contain more ^{137}Cs than in the littoral zone, which is the opposite in the case of ^{40}K. Apart from the depth of the lake, the ^{137}Cs content is also significantly positively correlated with the silt fraction, amorphous material, clay minerals (especially illite−smectite and smectite group), and organic matter (expressed as TOC and TN) in the surface lake sediments of Koronowo Lake (Table 1; Fig. 8). There is also a significant negative correlation between ^{137}Cs and the sand fraction, quartz content, and wet bulk density of the collected sediment samples. The content of

^{40}K is significantly positively correlated with the wet bulk density of the collected sediment samples and the contents of sand fraction, quartz, potassium feldspar, and plagioclase. There is also a significant negative correlation between the content of ^{40}K and amorphous material, calcite, clay minerals, and OM in these surface lake sediments.

3.1.4 PCA results

The PCA of selected parameters indicates that Axis 1 and Axis 2 explained 78% and 8.6% of the variance of the components, respectively (Fig. 8). The first PCA axis (PC1) was dominated by high positive loading of the depth of the lake and the content of ^{137}Cs, TOC, clay minerals, silt, and clay fraction and by high negative loading of the wet bulk density and the content

Fig. 5 Correlation on the 3D graph between ^{137}Cs activity concentration (Bq kg^{-1}), **A** Clay*—sum of clay minerals (kaolinite, muscovite, chlorite, illite–smectite, and smectite group (%)), Silt—silt fraction (%), and **B** Clay—clay fraction (%). Correlation on the 2D graph between the content of ^{137}Cs (Bq kg^{-1}), **C** Clay* minerals (%), and **D** total organic carbon (TOC) (%) in surface (0–3-cm depth) lake sediments of Koronowo Lake. Sampling sites are presented in Fig. 1
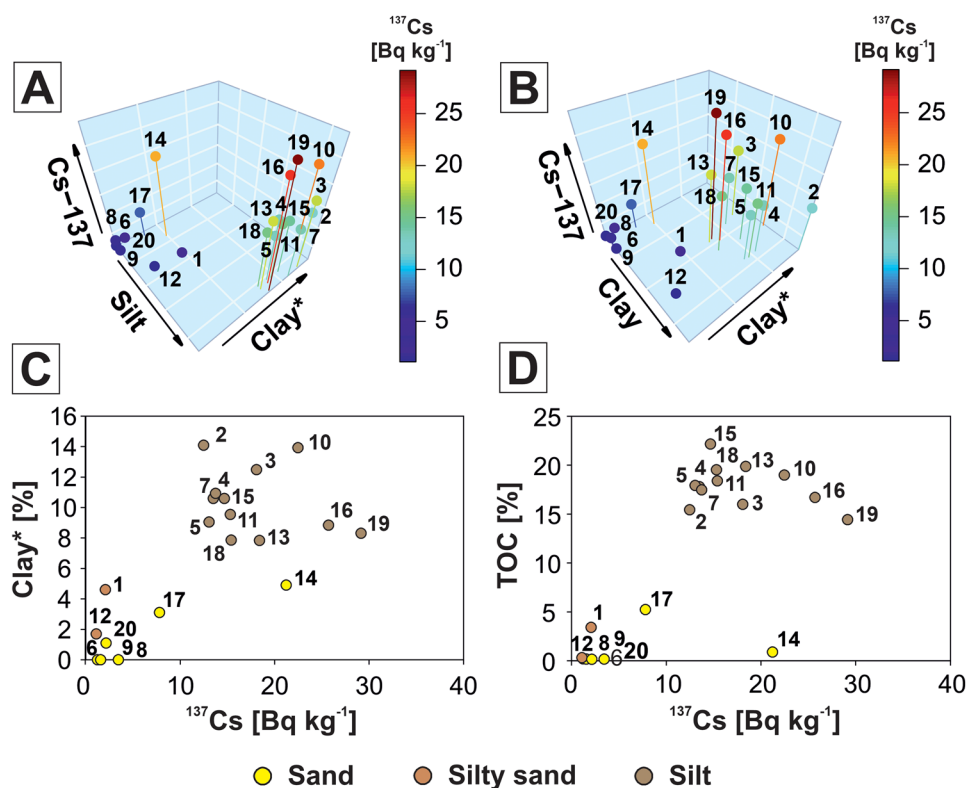
of potassium feldspar and quartz. ^{137}Cs showed high positive loading to the first (PC1) axis ($R^2 = 0.74$, $p < 0.001$). Potassium ^{40}K, instead of ^{137}Cs, had high negative loading to the first (PC1) axis ($R^2 = -0.72$, $p < 0.001$) and high positive loading to the second (PC2) axis ($R^2 = 0.66$, $p < 0.001$).

The PCA biplot shows that the surface lake sediments of Koronowo Lake can be divided into three groups. The first group includes fine-grained sediments (silts) with significantly elevated contents of ^{137}Cs, clay minerals, and OM. The second group is represented by coarse-grained sediments (sands) characterized by higher values of wet bulk density. These sediments are also characterized by elevated contents of ^{40}K, quartz, and potassium feldspar and low contents of ^{137}Cs. The last group is represented by coarse-grained sediments with a higher silt fraction (samples no. 1, 12, and 14). This group is also characterized by low concentrations of ^{137}Cs activity (except for sample no. 14, which contains 21.2 ± 2.6 Bq kg^{-1} of ^{137}Cs) and elevated concentrations of ^{40}K activity.

3.2 Lake sediment columns

3.2.1 Lithology, mineralogical composition, and organic matter content

The lithology of core P1 (sampling site no. 2) was constant along the entire length of the sediment column and was presented by brown silts up to a depth of 29 cm, where the presence of black sand with organic debris was observed (Fig. 9). Similarly, in core P2 (sampling site no. 13), brown silts were also observed with no significant changes in lithology over the entire length of the sediment column. The average wet bulk densities in core P1 (arithmetic mean, $n = 32$) and core P2 (arithmetic mean, $n = 27$) were 1.3 g cm^{-3} and 1.1 g cm^{-3}, respectively. In core P1, the wet bulk density of sediments was variable along the entire length of the sediment column with a slight increase from a depth of 19 cm, while in core P2, it was much more constant with a slight increase from a depth of 25 cm.

The mineralogical composition of lake sediments in the top part (0–3-cm depth) of core P1 was the same as that in the surface sediment sample at sampling site no. 2 (Fig. 3B). At a depth of 20 cm, the mineralogical composition of the collected sediment samples differed significantly from that in the surface layer of the sediment column. A much lower content of calcite (~25%) and amorphous material (~13%), as well as elevated contents of quartz (~18%), potassium feldspar (~5%), gypsum (~4.3%), and plagioclase (~3.4%) with an admixture of anhydrite (~0.8%) and ankerite/dolomite (~0.7%), were observed. Additionally, a significant increase in the content of clay minerals (from ~14 to ~30%) was recognized in this sediment layer, where illite−smectite, smectite group, muscovite/phlogopite, and chlorite were equal to approximately 17%, 5.6%, 5%, and 3%, respectively.
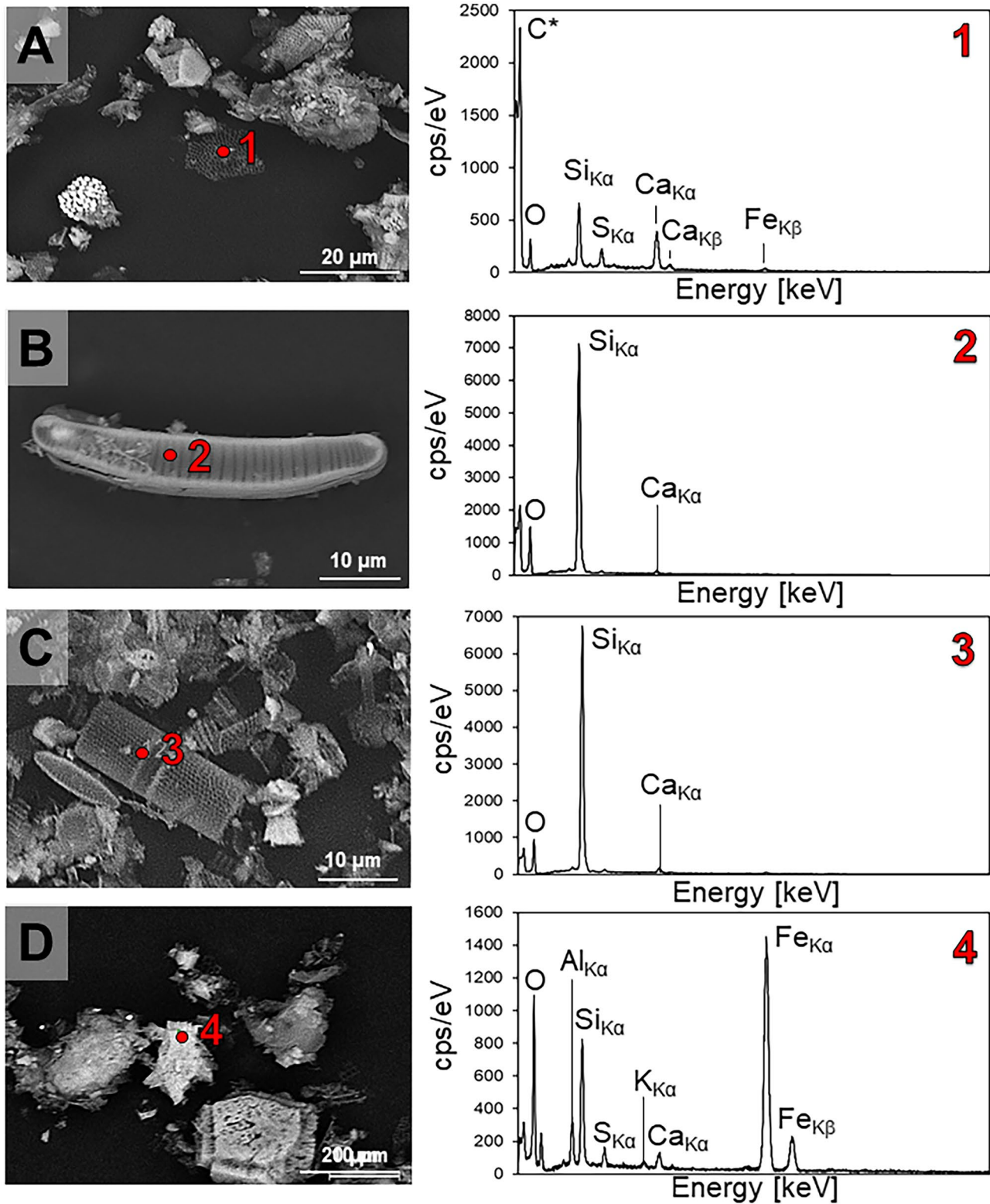
Fig. 6 The SEM–EDS analysis of surface (0–3-cm depth) lake sediments in Koronowo Lake. **A** Organic matter (sample no. 13). **B** Organic debris (diatom *Eunotia* spp.) (sample no. 2). **C** Organic debris (diatom *Aulacoseira* spp.) (sample no. 19). **D** Iron oxyhydroxides (sample no. 3). Sampling sites are presented in Fig. 1
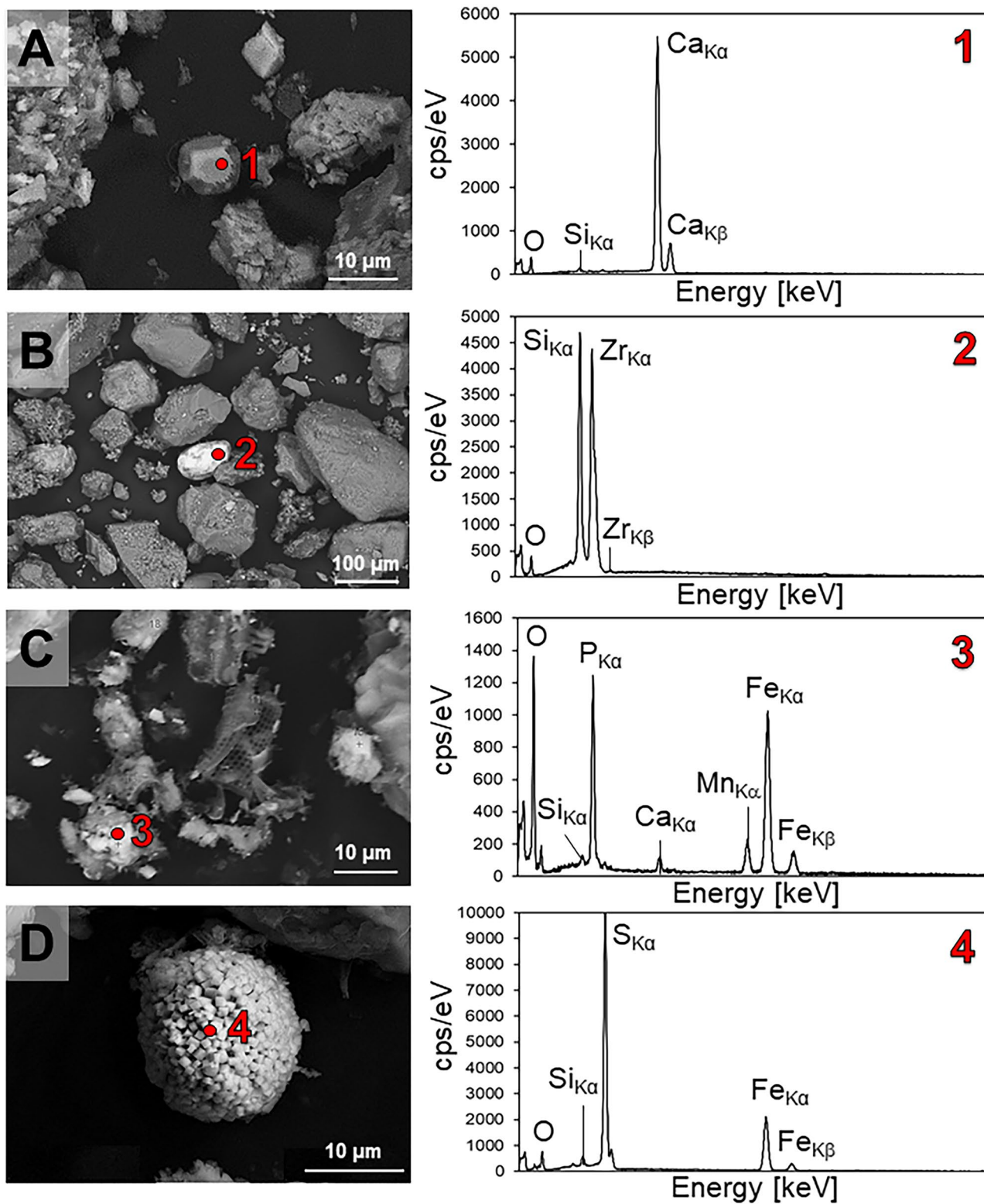
Fig. 7 The SEM–EDS analysis of surface (0–3-cm depth) lake sediments in Koronowo Lake. **A** Authigenic calcite (sample no. 13). **B** Zircon (sample no. 14). **C** Vivianite (sample no. 3). **D** Framboidal pyrite (sample no. 14). Sampling sites are presented in Fig. 1
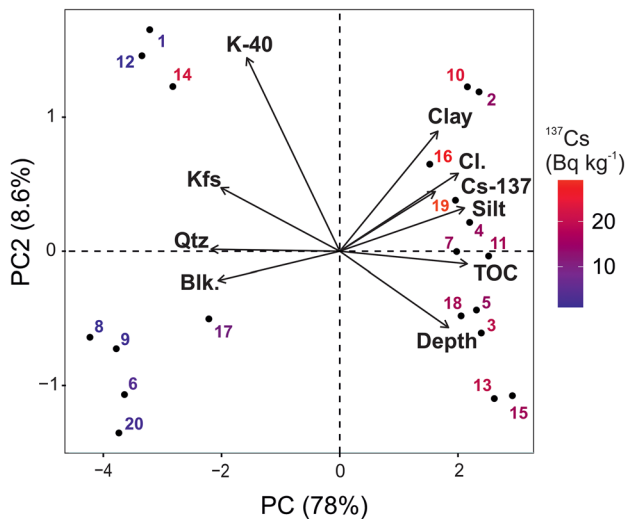
Fig. 8 The PCA biplot based on the selected parameters in surface (0–3-cm depth) lake sediments of Koronowo Lake: *Cs-137*, activity concentration (Bq kg⁻¹); *K-40*, activity concentration (Bg kg⁻¹); *TOC*, total organic carbon (%); *Blk.*, wet bulk density (g cm⁻³); *Depth*, depth of the lake at sampling point (m); *Clay*, clay fraction (%); *Silt*, silt fraction (%); *Qtz*, quartz (%); *Kfs*, potassium feldspar (%); *Cl.*, sum of clay minerals (kaolinite, muscovite, chlorite, illite–smectite, smectite group) (%). Sampling sites are presented in Fig. 1

The mineralogical composition of lake sediments in the surface layer (0–3-cm depth) of core P2 was the same as

that in the surface sediment sample at sampling site no. 13 (Fig. 3B). At a depth of 6 cm in this core, there was not much difference in the mineralogical composition of the collected sediments compared to the surface layer, except for a slightly lower content of potassium feldspar (by 1%), higher content of calcite (by 2%), presence of chlorite (~1.3%), and lack of muscovite. In the bottom part (27-cm depth) of core P2, slightly lower contents of calcite (~38%) and amorphous material (~13%) and higher contents of quartz (~16%), potassium feldspar (~5%), gypsum (~3%), plagioclase (~2.7%), and aragonite (~2.2%) were observed. A significant increase in the content of clay minerals (from ~8 to ~20%), including smectite group (~8.6%), illite−smectite (~8.3%), chlorite (~2.4%), and muscovite (~0.7%), was also recognized in this sediment layer. The SEM−EDS analysis confirmed the presence of such mineral phases as potassium feldspar, plagioclase, calcium carbonates, and clay minerals in the selected sediment samples in both cores. The amorphous material, similar to the case of surface lake sediments, was identified mostly as organic debris (e.g., diatoms). Some amounts of zircon, titanium oxides, monazite, and framboidal pyrite were also identified in the selected sediment samples in both cores.

The average contents of TOC and TN were equal to 9.5% and 1.05% in core P1 (arithmetic mean; $n=30$) and 16.6% and 2.1% in core P2 (arithmetic mean; $n=27$), respectively. The contents

Fig. 9 Lithology and vertical distribution of ¹³⁷Cs and ⁴⁰K activity concentrations (Bq kg⁻¹), content of total organic carbon (TOC), and total nitrogen (TN) (%), and C/N ratio in P1 **A** and P2 **B** cores. Sampling sites are presented in Fig. 1
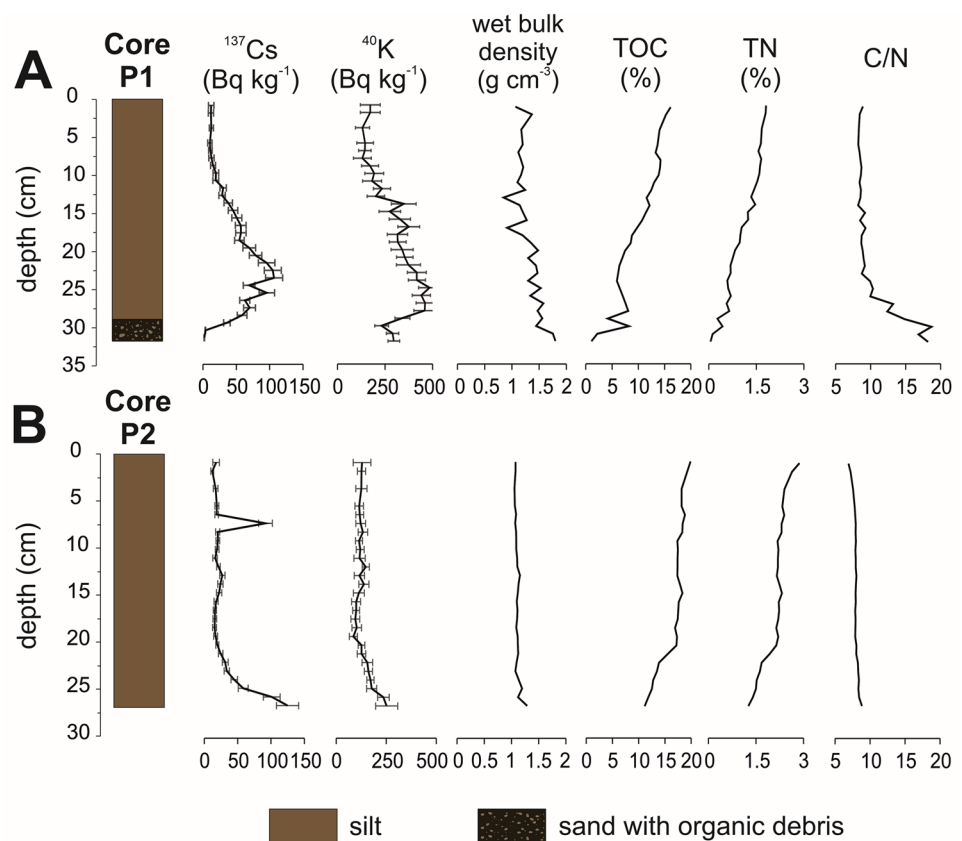
of TOC and TN in core P1 decreased with depth, while core P2 was more constant over the entire length of the sediment column, with a slight decrease from 22 cm depth (Fig. 9). The C/N ratio calculated for lake sediments from the top to a depth of 26 cm of core P1 (C/N ratio ranged from 9.6 to 12.05) indicated the autochthonous origin of deposited OM. At a depth of 30 cm in this core, a significant admixture of terrestrial OM (C/N ratio > 20) was observed (Meyers and Ishiwatari 1993; Lamb et al. 2006; Contreras et al. 2018). The C/N ratio calculated for lake sediments of core P2 also indicated the primary sources of OM (C/N ratio ranged from 8.1 to 10.3) over the entire length of this sediment column.

3.2.2 Vertical distribution of ^{137}Cs and ^{40}K activity concentrations

The vertical distribution of ^{137}Cs and ^{40}K activity concentrations differed significantly between the collected sediment columns (Fig. 9). In core P1 (sampling site. no. 2), an elevated content of ^{137}Cs was observed at depths between 12 and 30 cm in this core. The highest content of ^{137}Cs (106.6 ± 12.8 Bq kg^{-1}) was measured at a depth of 24 cm in this sediment column. A significant decrease in ^{137}Cs content occurred above 30 cm of the core depth, where pre-reservoir sediments were identified. The vertical distribution of ^{137}Cs activity concentrations in core P2 (sampling site no. 13) showed a gradual increase in the content of this radioisotope from a depth of 20 cm (Fig. 9). The highest ^{137}Cs content was observed at the bottom of the core (124.8 ± 16.7 Bq kg^{-1}). A sharp peak in ^{137}Cs content (91.8 ± 10.4 Bq kg^{-1}) was also observed at a depth of 6 cm in this sediment column.

An increase in ^{40}K activity concentration, as in the case of ^{137}Cs, was observed in the sediments located at a depth of approximately 14 to 30 cm in core P1 (Fig. 9). The highest ^{40}K activity concentration (488.2 ± 52.9 Bq kg^{-1}) was measured at a depth of 25 cm in this core. Almost two times lower concentrations of ^{40}K activity were observed in core P2. A gradual increase in the content of ^{40}K was also observed above 20 cm of the core depth. The highest concentration of ^{40}K activity (251.8 ± 55.3 Bq kg^{-1}) was detected, similar to ^{137}Cs, at a depth of 27 cm in this sediment column.

4 Discussion

4.1 Key factors controlling the distribution of ^{137}Cs in bottom sediments of Koronowo Lake

4.1.1 Particle size distribution and transport processes

Grain size is one of the most important factors determining the spatial distribution of ^{137}Cs activity concentrations in the bottom sediments of Koronowo Lake. This is mainly because radiocesium can be easily adsorbed onto fine-sized particles due to their large specific surface area (He and Walling 1996; Fan et al. 2014; Funaki et al. 2019). It is also associated with a higher content of clay minerals (able to bind ^{137}Cs), which are more prevalent in fine-grained sediments (Cremers et al. 1988; Spezzano 2005; Tanaka et al. 2015; Hagiwara et al. 2020). The obtained results showed that fine-grained surface lake sediments of Koronowo Lake contain more ^{137}Cs than coarse-grained surface lake sediments, similar to e.g. the case of the Ogaki Dam Reservoir (Funaki et al. 2019). Moreover, the observed high correlation between the content of ^{137}Cs and silt ($R_s = 0.66$; p value > 0.05) indicated that the silt-sized fraction is a major contributor to the distribution of ^{137}Cs in the studied lake, which was also observed in the case of the Tomioka River (Hagiwara et al. 2020). Tanaka et al. (2015) also noticed that the silt-sized fraction contained a greater amount of ^{137}Cs than the clay-sized fraction, which is supposed to accumulate more radiocesium (Livens and Baxter 1988; Spezzano 2005; Funaki et al. 2019). This phenomenon may be related to the transport of the finest particles by a river in near-permanent suspension (as wash load) and pass through the dam lake without deposition (Tanaka et al. 2015; Sedláček et al. 2022).

The transport processes influencing the sorting of sediment particles may therefore also be responsible for the distribution of ^{137}Cs in the bottom sediments of Koronowo Lake. They may provide, for example, the accumulation of fine-grained particles with ^{137}Cs in the deepest part of the lake (along the course of the river) and near the dam (Figs. 1 and 4A). This is probably caused by the physical transport of smaller radiocesium-bearing particles through the river and its deposition downstream as a result of the decreasing river flow velocity (Carlsson 1978; Spezzano 2005; Tanaka et al. 2015; Hagiwara et al. 2020). The second possible transport mechanism of radiocesium-bearing particles may be horizontal movement, which in a shallow lake (such as Koronowo Lake) may be caused by wind-wave action and river flow (Hilton et al. 1986; Luettich et al. 1990). However, in our case, the horizontal movement might be slightly different than, for example, in a shallow Lake Nishiura (Tsuji et al. 2019). This is because Koronowo Lake is narrower and more elongated, so there may be a gradual movement of sediments with ^{137}Cs from the slopes of the reservoir to the center of the "old Brda valley" and further along the reservoir (Figs. 1 and 4A).

Similar transport processes may also influence the deposition of coarse-grained bottom sediments (characterized by a low content of ^{137}Cs) in the shallower parts of Koronowo Lake (Figs. 1 and 3A). These coarse particles probably originate from the shore of the lake, which is eroded by wind-wave action and/or water-level fluctuations and transported short distances due to their higher settling velocity (Tanaka

et al. 2015; Funaki et al. 2019). Such an origin of these bottom sediments might be evidenced by the presence of allogeneic minerals (such as titanium and zircon), and minerals enriched with potassium ^{40}K (such as potassium feldspar and plagioclase) (Madruga et al. 2014; Hagiwara et al. 2020; Bobos et al. 2021) (Figs. 3B and 7B). This would also explain the heterogeneous spatial distribution of ^{40}K activity concentrations in the surface lake sediments of Koronowo Lake (Fig. 4). In addition, the presence of vascular land plant remains may also indicate the input of terrestrial material into the lake, as indicated by the relatively high C/N ratio (>20) in these bottom sediments (e.g., at sampling site no. 1) (Meyers and Ishiwatari 1995; Lamb et al. 2006; Contreras et al. 2018).

It should also be noted that in some coarse-grained bottom sediment samples (sampling sites no. 14 and 17), a significantly increased content of ^{137}Cs was observed (Figs. 1 and 5). This indicates that the particle size distribution does not simply explain the spatial distribution of ^{137}Cs activity concentrations in the bottom sediments of Koronowo Lake. Tanaka et al. (2015) also emphasized that the distribution of ^{137}Cs could not be simply related to the specific surface area of the particles due to the complicated origin of riverbed sediments. Somboon et al. (2018) found, for example, that the coarser fractions of material deposited in river channels and floodplain zones might contain significant amounts of radiocesium. In our case, this phenomenon may be hypothetically related to the intensified accumulation of radiocesium-bearing particles near the dam due to a decrease in the flow velocity of the stream and limited outflow from the lake.

4.1.2 Mineralogical composition of surface lake sediments

Apart from the particle size distribution, the mineralogical composition has a very significant influence on the distribution of ^{137}Cs in bottom sediments in aquatic ecosystems (Kim et al. 2006; Fan et al. 2014; Mukai et al. 2016; Hagiwara et al. 2020; and others). Many studies have shown that Cs binding is especially strong with micaceous minerals and their weathered minerals, such as illites and vermiculites (Sawhney 1972; Cremers et al. 1988; Cornell 1993; Poinssot et al. 1999; Park et al. 2021). In our case, clay minerals have a dominant effect on the sorption and thus the distribution of ^{137}Cs in the bottom sediments of Koronowo Lake, which may be evidenced by a significant positive correlation between the content of ^{137}Cs and clay minerals ($R_s = 0.6$, p value <0.05) (Table 1; Fig. 8). A similar correlation was observed in samples from various regions around the world (Fan et al. 2014; Tanaka et al. 2015; Mukai et al. 2016; Bobos et al. 2021; etc.). However, it should be noted that there are also areas where bottom sediments with similar clay mineral contents are characterized by different ^{137}Cs activity concentrations, e.g., samples collected at sampling sites no. 1 (2.07 ± 0.42 Bg kg^{-1}) and 14

(21.2 ± 2.6 Bq kg^{-1}) (Figs. 1 and 5). This phenomenon may be hypothetically related to a different source and/or level of supplied ^{137}Cs. Regardless, the tendency for an increase in the concentration of ^{137}Cs activity with the amount of clay minerals in the surface lake sediments of Koronowo Lake is maintained.

An increased content of clay minerals was observed, especially in the case of fine-grained surface lake sediments of Koronowo Lake (Fig. 5). A similar relationship was widely reported by many other researchers (Cremers et al. 1988; Tanaka et al. 2015; Funaki et al. 2019; etc.). Moreover, it was noticed that the correlation between the content of clay minerals and silt fraction ($R_s = 0.74$, p value <0.05) is higher than with the clay fraction ($R_s = 0.66$, p value <0.05) (Table 1). This relationship may be hypothetically associated with the aggregation of clay minerals (e.g., with organic matter) and their deposition in the reservoir, while other clay size particles are transported downstream (De La Rocha et al. 2008; Tanaka et al. 2015; Fujii et al. 2018).

Among all clay minerals identified in the surface lake sediments of Koronowo Lake, the most abundant were clay minerals 2:1, such as the illite–smectite and smectite group. The relationship between the content of ^{137}Cs and the illite–smectite and smectite group was equal to 0.58 and 0.51 (p value <0.05), respectively (Table 1). This significant positive correlation can be related to a good sorption capacity of radiocesium by these minerals (Sawhney 1972; Zachara et al. 2002; Kim et al. 2006; Fan et al. 2014; Tachi et al. 2020a; Park et al. 2021). The slight difference in the value of the correlation coefficient between the illite–smectite and smectite group is related to the higher selectivity of Cs$^+$ by illite (Tamura and Jacobs 1960; Bobos et al. 2021). For other clay minerals, muscovite was identified only in selected samples of fine-grained bottom sediments (sites no. 3, 4, 13, 16, and 19). Although these samples were characterized by increased concentrations of ^{137}Cs activity, no significant correlation was found between the contents of muscovite and ^{137}Cs. Another clay mineral, kaolinite, was identified in small amounts (approximately 1%) and only in several samples. There was also no significant relationship between the content of kaolinite and ^{137}Cs, which may also be explained (apart from its low content) by the fact that 1:1 clay minerals are characterized by low cesium sorption and selectivity (Kim et al. 1996; Park et al. 2021). Other clay minerals, such as chlorite, have been recognized in negligible amounts and therefore do not appear to have a significant effect on ^{137}Cs binding.

Calcium carbonates, such as calcite, were found in significant amounts in fine-grained surface lake sediments characterized by an increased content of ^{137}Cs. This convergence, however, may be accidental and determined by the precipitation of authigenic calcite (Fig. 7A) from the water column in the deep parts of the reservoir, where clay

minerals are dominant (Figs. 1 and 3B). This hypothesis might be supported by Kónya et al. (2005), who showed that calcite practically does not sorb cesium, while dolomite and ankerite show only a slightly greater ability to bind this radionuclide (Kónya et al. 2005). Another calcium carbonate phase, aragonite, was noticed only in coarse-grained surface lake sediments deposited in the coastal zone of the lake. These are likely mollusk shell fragments indicating the probable wave-related bottom erosion in the shallow parts of this reservoir.

Other organic debris (e.g., diatoms) composed of amorphous silica were quite abundant in the bottom sediments collected from the profundal zone of Koronowo Lake (Fig. 6B, C). Despite their high content in the bottom sediments enriched with ^{137}Cs, it is difficult to claim whether their presence influences the fixation of this radioisotope. Belousov et al. (2019) observed that sorption of Cs$^+$ on diatomite is more related to the presence of kaolinite and smectite in the studied samples. This is probably because the physical adsorption of radiocesium on the mineral surface, which occurs in the case of diatomite, is of less importance than the process of chemical sorption (Nenadović et al. 2015). The second amorphous material, identified in the collected sediment samples by XRD and SEM analyses, is composed of iron oxyhydroxides (Fig. 6A). Their presence may have some significance for ^{137}Cs binding, as it has been found that deposition of Fe(OH)$_3$ on the surface of clay minerals leads to an increase in the sorption of radiocesium (Kobets et al. 2014). Among the iron-containing minerals observed in fine-grained bottom sediments of Koronowo Lake, there were also vivianites and framboidal pyrites (Fig. 7C, D). Their presence does not affect the distribution of ^{137}Cs but indicates the presence of anaerobic conditions in the deep parts of the lake (Wilkin et al. 1996; O'Connell et al. 2015).

A significant negative correlation coefficient ($R_s = -0.50$, p value < 0.05) with the content of ^{137}Cs was demonstrated by quartz, which occurs mainly in coarse-grained surface lake sediments of Koronowo Lake (Table 1). This is because the sorption capacity of radiocesium by quartz is negligibly small (Muuri et al. 2016). The plagioclase and potassium feldspar, also common in the collected sands and silty sands, showed an insignificant negative correlation with this radioisotope (Table 1). This indicates that these minerals have little effect on the distribution of ^{137}Cs activity concentrations in the bottom sediments of Koronowo Lake. However, Hagiwara et al. (2020) have shown that feldspars could contribute to ^{137}Cs migration in the Tomioka River basin. It is also worth noting that the contents of plagioclase ($R_s = 0.75$; p value < 0.05) and potassium feldspar ($R_s = 0.79$; p value < 0.05) in the surface lake sediments of Koronowo Lake show a strong positive correlation with ^{40}K content (Table 1; Fig. 8). This may indicate a possible influx of terrestrial material into the lake, which could have been eroded and transported from the shore by wind-wave actions and/or water-level fluctuations. A similar application of ^{40}K analysis was demonstrated by Bobos et al. (2021), who associated an increased content of this radioisotope with the sediments formed because of granite weathering.

4.1.3 Content of organic matter and its origin

The distribution of radiocesium in soils and sediments may be related to the content of OM; however, the mechanism of ^{137}Cs accumulation in OM-rich sediments is still considered to be unclear (e.g., Naulier et al. 2017; Fujii et al. 2018). In the present study, most organic matter (expressed as the content of TOC and TN) accumulated in fine-grained surface lake sediments deposited in the deepest parts of Koronowo Lake (Figs. 1 and 4). This is probably related to the larger surface area of finer particles, which enable adsorption of the monolayer of organic matter (Keil et al. 1994; Kim et al. 2006). Moreover, such an increase in nutrients and OM from the littoral to the profundal zone was recognized as typical in eutrophic lakes in Poland (Tadejewski 1966; Frink 1969).

Along with an increase in the content of OM in collected bottom sediment samples, an increase in the concentration of ^{137}Cs activity was observed (Fig. 5). This relationship may indicate that OM could play an important role as a carrier of radiocesium in the studied lake, although it has a lower affinity than illite (Rigol et al. 2002; Naulier et al. 2017; Fujii et al. 2018). Kim et al. (2007) observed a similar relationship for marine sediment samples collected from the East Sea near Wuljin, where the TOC content showed an even better correlation with ^{137}Cs activity concentrations than other single factors. Although the PCA in our case can also confirm a high correlation between the content of TOC and ^{137}Cs, the content of clay minerals seems to be of greater importance (Fig. 8). On this basis, we can hypothesize that the observed relationship may result from a combination of various factors, i.e., the accumulation of ^{137}Cs with fine-grained inorganic particles in OM-rich sediments (Kim et al. 2007). Fuji et al. (2018) also explained that this phenomenon can be related to the formation of microaggregates with autochthonous OM and minerals by extracellular polymeric substances. This hypothesis can also be considered in our case, as the examples of microaggregates consisting mainly of clay minerals and OM were observed in the collected sediment samples during SEM analysis. Additionally, the C/N ratio calculated for the collected bottom sediments indicated that OM deposited in the profundal zone of Koronowo Lake is of autochthonous origin (consisting of phytoplankton and to a lesser extent zooplankton), while in the littoral zone, it is rather a mixture of primary production and influx of organic particles washed off from the soil around the lake and fragments of terrestrial plants (Lamb et al. 2006).

It should also be noted that the part of the fine-grained bottom sediments of Koronowo Lake with a significantly elevated content of OM was characterized by average concentrations of ^{137}Cs activity (Fig. 5). Bobos et al. (2021) observed that some OM-rich and fine-grained bottom sediments were characterized by a low ^{137}Cs content. They claimed that this phenomenon may be associated with the inefficient immobilization of radiocesium by clay minerals (e.g., illite) in an environment enriched with OM. A similar mechanism cannot be excluded in our case. Another potential cause of this phenomenon may be the release of ^{137}Cs from lake sediments as a result of ion exchange with, e.g., NH_4^+ (e.g., Evans et al. 1983; Hazotte et al. 2016). Kaminski et al. (1994) noticed that such a process may generally occur in OM-rich sediments of eutrophic lakes, of which Koronowo Lake is an example. Moreover, the presence of minerals (e.g., framboidal pyrite and vivianite) indicating the presence of anaerobic conditions (which may lead to the degradation of OM and the appearance of NH_4^+) may additionally support this assumption. However, to confirm this hypothesis, it may be necessary to examine the chemical composition of the pore water for the presence of competing ions with Cs^+.

4.2 Vertical distribution of ^{137}Cs activity concentrations in bottom sediments of Koronowo Lake

The main source of ^{137}Cs accumulated in the bottom sediments of Koronowo Lake was the Chernobyl accident, but the record of ^{137}Cs deposited as a result of nuclear weapons testing cannot be ruled out, since this reservoir was created in 1961 (Ciesla et al. 1994; Evrard et al. 2020). Moreover, the presented research showed that ^{137}Cs is still supplied to Koronowo Lake despite more than 30 years having passed since the Chernobyl nuclear power plant accident. This is evidenced by the presence of this radioisotope in the surface layer of the collected sediment columns (Fig. 9).

Because the emitted cesium radioisotopes were bound to particles shortly after their direct atmospheric deposition, a distinct peak of ^{137}Cs activity concentration can be commonly observed in the vertical profiles of sediment records in the contaminated areas (Appleby 2008; Klaminder et al. 2012; Beresford et al. 2016; Ivanov et al. 2021; and others). However, this is the case when mixing of sediments is negligible and cesium is strongly bound to the sediments (Konoplev et al. 2022). In our case, the Chernobyl-derived peak in both collected sediment cores is difficult to distinguish and cannot be described, for example, by the Gaussian function, as in the case of the Schekino Reservoir (Ivanov et al. 2021). The vertical distributions of ^{137}Cs activity concentrations in the collected sediment cores may be due to chemical processes, such as advection or diffusion of ^{137}Cs through the pore waters, rather than physical

processes, such as sediment mixing by wind-wave action or bioturbation (Robbins et al. 1977; Putyrskaya and Klemt 2007; Klaminder et al. 2012).

The observed shape of the vertical distributions of ^{137}Cs activity concentrations may also be determined by the increased supply of radiocesium to Koronowo Lake along with contaminated particles after the construction of the dam. This hypothesis may be confirmed by the fact that dams significantly affect sedimentation in the river system, converting the reservoirs into major sediment traps (Díaz-Asencio et al. 2017; Funaki et al. 2019). Increased erosion in the catchment area may, in turn, intensify the particle load into the reservoir along with the associated pollutants (Betancourt et al. 2010; Díaz-Asencio et al. 2017). Therefore, the elevated concentrations of ^{137}Cs activity in the sediment profiles could correspond, apart from the direct deposition of radiocesium with atmospheric fallout, to an increased delivery of contaminated particles to Koronowo Lake from its catchment. Subsequently, the amount of supplied ^{137}Cs could have decreased over time as sedimentological conditions stabilized and catchment erosion decreased. This hypothesis can be confirmed by the elevated content of ^{40}K (known as an important indicator of detrital influx) in similar layers of sediment columns as for ^{137}Cs (Somboon et al. 2018; Putyrskaya et al. 2020) (Fig. 9). Similarly, the vertical distribution of the C/N ratio in core P1 showed that the source of OM in these sediment layers was of allochthonous origin and changed over time to primary production. This hypothesis may also be justified by a change in the mineralogical composition of lake sediments in the collected sediment cores, indicating a decrease in the content of deposited quartz and potassium feldspar over time. There is no doubt, however, that additional sediment cores should be collected, and more detailed studies of their mineralogical composition and particle size distribution should be carried out to better support this hypothesis.

The conducted research also showed that the vertical distribution of the analyzed parameters in the collected sediment columns differs significantly from each other (Fig. 9). Although such a small number of collected sediment columns does not allow for the study of changes occurring over time in the entire Koronowo Lake, it is possible to determine the most important differences between the northern and southern parts of this study area. One of them is the higher sedimentation rate in the area near the dam (southern part of the reservoir) than in the northern part of the lake. This undoubtedly influences the observed vertical distribution of ^{137}Cs activity concentration in the collected sediment cores (Fig. 9). A clear boundary is visible between the pre-dam and post-dam sediments in core P1, which makes it possible to calculate the sedimentation rate (0.51 cm y^{-1}) in this part of the lake. Such a boundary has already been associated with reservoir age in other studies and used as an additional time maker to

validate the results of sediment dating with ^{210}Pb or ^{137}Cs (Foster et al. 2011; Waters et al. 2015). No such boundary occurs in core P2, but a significant increase in ^{137}Cs activity concentrations at the bottom of the core can be noticed (Fig. 9). Accordingly, it can be assumed that the Chernobyl-derived peak is probably below a depth of 27 cm in this sediment column. Based on this assumption, it can be concluded that the sedimentation rate in the area near the dam is much higher than that in the northern part of the lake (Fig. 1A). This difference is caused by the preferential particle deposition near the dam due to limited outflow from the reservoir, decreasing river flow, and higher primary production associated with more limnetic conditions in this area (Szatten et al. 2018). Moreover, the sharp increase in the ^{137}Cs content at a depth of 6 cm may be related to mixing of sediments or an accidental influx of contaminated particles from surrounding soils, which are located in a cultivated area. This anomaly may also be related to the increased concentration of ^{137}Cs activity in the coarse-grained surface sediment sample collected at sampling site no. 14 (Figs. 1A and 8). However, to prove this hypothesis, it would be necessary to analyze additional soils and bottom sediment samples from this part of the lake.

5 Conclusions

The obtained results showed that ^{137}Cs is still supplied to the lake, as evidenced by its presence in the collected surface lake sediments. It was observed that the spatial distribution of ^{137}Cs activity concentrations is strongly related to the valley-type bottom morphology of the studied lake. Therefore, the highest content of ^{137}Cs (from 12.5 ± 4.1 to 29.2 ± 4.0 Bq kg^{-1}) was detected in the fine-grained (<63 μm) bottom sediments collected from the deepest part of the lake, reflecting the "old," pre-reservoir course of the Brda River (in the central part of the lake, where more limnetic conditions prevail and close to the dam). It was also noted that the ^{137}Cs activity concentration was more strongly related to the silt fraction (2–63 μm) than to the clay fraction (<2 μm) in the collected surface lake sediments.

The conducted research showed that the most important factor influencing the distribution of ^{137}Cs activity concentrations in the surface lake sediments of Koronowo Lake, apart from the bottom morphology and grain size of sediments, is the content of clay minerals. A significant positive correlation was particularly observed between the content of ^{137}Cs and the illite−smectite and smectite group. A positive significant correlation between the content of ^{137}Cs and organic matter (expressed as the content of TOC and TN) was also determined. Moreover, the OM associated with the elevated content of radiocesium was found to be of autochthonous origin. These results may indicate the probable influence of OM on the distribution of ^{137}Cs in the

bottom sediments of Koronowo Lake. It can be assumed, however, that this dependence may also be the result of the accumulation of radiocesium-bearing particles in lake sediments rich in OM.

The vertical distribution of ^{137}Cs activity concentrations in the collected sediment cores showed that the Chernobyl-derived peak of radiocesium is not simply represented by a distinct peak associated with direct atmospheric deposition. The observed peak shape may be hypothetically related to the intensified delivery of contaminated sediments with ^{137}Cs from the catchment area as a result of its erosion after the construction of the dam. This hypothesis may be evidenced, for example, by an increased content of ^{40}K at similar depths as ^{137}Cs in the collected sediment columns, which may indicate an intensified detrital influx at that time. This may also be confirmed by the increased content of minerals, such as quartz, plagioclase, and potassium feldspar in the deeper parts of the collected sediment columns. However, to better support this hypothesis, additional cores should be collected, and a more detailed mineralogical analysis should be performed.

To summarize, the presented studies indicate the key factors that influence the distribution of ^{137}Cs activity concentrations in lake sediments of valley-type dam lake 32 years after the Chernobyl accident. The obtained results can be used to predict the long-term behavior of ^{137}Cs in the bottom sediments of reservoirs, which may be useful for radiological monitoring in other areas contaminated with cesium radioisotopes. This is particularly important, as it has been shown that dam lakes can accumulate large amounts of contaminated particles, which can pose a potential radiological hazard. The obtained results also showed that ^{137}Cs can be used as a tracer to reconstruct changes in sedimentation conditions over time in such lakes. It can be applicable, for example, in the case of studies concerning the problem of reservoir siltation. Moreover, considering climate change and the growing demand for electricity and drinking water, the presented conclusions may be relevant for the construction of a dam in areas contaminated with ^{137}Cs in the future.

Declarations

Competing interests The authors declare no competing interests.

References

Appleby PG (2008) Three decades of dating recent sediments by fallout radionuclides: a review. Holocene 18(1):83–93. https://doi.org/10.1177/0959683607085598

Ashraf MA, Akib S, Maah MJ, Yusoff I, Balkhair KS (2014) Cesium-137: Radio-chemistry, fate, and transport, remediation, and future concerns. Crit Rev Environ Sci Technol 44:1740–1793. https://doi.org/10.1080/10643389.2013.790753

Belousov P, Semenkova A, Egorova T et al (2019) Cesium sorption and desorption on glauconite, bentonite, zeolite and diatomite. Minerals 9:625. https://doi.org/10.3390/min9100625

Beresford NA, Fesenko S, Konoplev A, Skuterud L, Smith JT, Voigt G (2016) Thirty years after the Chernobyl accident: what lessons have we learnt? J Environ Radioact 157:77–89. https://doi.org/10.1016/j.jenvrad.2016.02.003

Betancourt C, Jorge F, Suárez R, Beutel M, Gebremariam S (2010) Manganese sources and cycling in a tropical eutrophic water supply reservoir, Paso Bonito Reservoir. Cuba Lake Reserv Manag 26:217–226. https://doi.org/10.1080/07438141.2010.519856

Bobos I, Madruga MJ, Reis M, Esteves J, Guimarães V (2021) Clay mineralogy insights and assessment of the natural (^{228}Ra, ^{226}Ra, ^{210}Pb, ^{40}K) and anthropogenic (^{137}Cs) radionuclides dispersion in the estuarine and lagoon systems along the Atlantic coast of Portugal. Catena 206:105532. https://doi.org/10.1016/J.CATENA.2021.105532

Carlsson S (1978) A model for the movement and loss of ^{137}Cs in a small watershed. Health Phys 34:33–37. https://doi.org/10.1097/00004032-197801000-00002

Cieśla W, Malczyk P, Kędzia W, Majle T, Pachocki K (1994) ^{137}Cs i ^{134}Cs w glebach województwa bydgoskiego. Zesz Probl Postępów Nauk Rol 414:11–20

Contreras S, Werne JP, Araneda A, Urrutia R, Conejero CA (2018) Organic matter geochemical signatures (TOC, TN, C/N ratio, δ13C and δ15N) of surface sediment from lakes distributed along a climatological gradient on the western side of the southern Andes. Sci Total Environ 630:878–888. https://doi.org/10.1016/J.SCITOTENV.2018.02.225

Cornell RM (1993) Adsorption of cesium on minerals: a review. J Radioanal Nucl Chem Artic 171:483–500. https://doi.org/10.1007/BF02219872

Cremers A, Elsen A, De Preter P, Maes A (1988) Quantitative analysis of radiocaesium retention in soils. Nat 335:247–249. https://doi.org/10.1038/335247a0

De La Rocha CL, Nowald N, Passow U (2008) Interactions between diatom aggregates, minerals, particulate organic carbon, and dissolved organic matter: further implications for the ballast hypothesis. Global Biogeochem Cy 22(4). https://doi.org/10.1029/2007GB003156

Díaz-Asencio M, Corcho-Alvarado JA, Cartas-Aguila H et al (2017) ^{210}Pb and ^{137}Cs as tracers of recent sedimentary processes in two water reservoirs in Cuba. J Environ Radioact 177:290–304. https://doi.org/10.1016/J.JENVRAD.2017.07.005

Ertel JR, Hedges JI (1984) The lignin component of humic substances: distribution among soil and sedimentary humic, fulvic, and base-insoluble fractions. Geochim Cosmochim Ac 48:2065–2074. https://doi.org/10.1016/0016-7037(84)90387-9

Evans DW, Alberts JJ, Clark RA (1983) Reversible ion-exchange fixation of cesium-137 leading to mobilization from reservoir sediments. Geochim Cosmochim Ac 47:1041–1049. https://doi.org/10.1016/0016-7037(83)90234-X

Evrard O, Chaboche PA, Ramon R, Foucher A, Laceby JP (2020) A global review of sediment source fingerprinting research incorporating fallout radiocesium (^{137}Cs). Geomorphology 362:107103. https://doi.org/10.1016/J.GEOMORPH.2020.107103

Fan Q, Tanaka K, Sakaguchi A, Kondo H, Watanabe N, Takahashi Y (2014). Factors Controlling Radiocesium Distribution in River Sediments: Field and Laboratory Studies after the Fukushima Dai-Ichi Nuclear Power Plant Accident. https://doi.org/10.1016/j.apgeochem.2014.07.012

Foster IDL, Collins AL, Naden PS, Sear DA, Jones JI, Zhang Y (2011) The potential for paleolimnology to determine historic sediment delivery to rivers. J Paleolimnol 45:287–306. https://doi.org/10.1007/S10933-011-9498-9

Frink CR (1969) Chemical and mineralogical characteristics of eutrophic lake sediments. Soil Sci Soc Am J 33:369–372. https://doi.org/10.2136/SSSAJ1969.03615995003300030012X

Fujii M, Ono K, Yoshimura C, Miyamoto M (2018) The role of autochthonous organic matter in radioactive cesium accumulation to riverine fine sediments. Water Res 137:18–27. https://doi.org/10.1016/J.WATRES.2018.02.063

Funaki H, Yoshimura K, Sakuma K, Iri S, Oda Y (2019) Evaluation of particulate ^{137}Cs discharge from a mountainous forested catchment using reservoir sediments and sinking particles. J Environ Radioact 210:105814. https://doi.org/10.1016/J.JENVRAD.2018.09.012

Hagiwara H, Konishi H, Nakanishi T et al (2020) Mineral composition characteristics of radiocesium sorbed and transported sediments within the Tomioka river basin in Fukushima Prefecture. J Environ Radioact 211:106042. https://doi.org/10.1016/j.jenvrad.2019.106042

Hamilton NE, Ferry M (2018) ggtern: ternary diagrams using ggplot2. J Stat Softw Code Snippets 87(3):1–17. https://doi.org/10.18637/jss.v087.c03

Hazotte AA, Peron O, Abdelouas A, Montavon G, Lebeau T (2016) Microbial mobilization of cesium from illite: the role of organic acids and siderophores. Chem Geol 428:8–14. https://doi.org/10.1016/j.chemgeo.2016.02.024

He Q, Walling DE (1996) Interpreting particle size effects in the adsorption of ^{137}Cs and unsupported ^{210}Pb by mineral soils and sediments. J Environ Radioact 30:117–137. https://doi.org/10.1016/0265-931X(96)89275-7

Hilton J, Lishman JP, Allen PK (1986) The dominant processes of sediment distribution and focusing in a small, eutrophic, monomictic lake. Limnol Ocean 31:125–133

Huon S, Hayashi S, Laceby JP, Tsuji H, Onda Y, Evrard O (2018) Source dynamics of radiocesium-contaminated particulate matter deposited in an agricultural water reservoir after the Fukushima nuclear accident. Sci Total Environ 612:1079–1090. https://doi.org/10.1016/J.SCITOTENV.2017.07.205

Hydropower Plant Koronowo (2015) Data set of inflow (outflow) of water to (from) Koronowski Reservoir 1962–2015. Unpublished work

Ivanov MM, Konoplev AV, Walling DE et al (2021) Using reservoir sediment deposits to determine the longer-term fate of chernobyl-derived ^{137}Cs fallout in the fluvial system. Environ Pollut 274. https://doi.org/10.1016/J.ENVPOL.2021.116588

Kaminski S, Richter T, Walser M, Lindner G (1994) Redissolution of cesium radionuclides from sediments of freshwater lakes due to biological degradation of organic matter. Radiochimca Acta 66–67:433–436. https://doi.org/10.1524/ract.1994.6667.special-issue.433

Keil RG, Tsamakis E, Fuh CB, Giddings JC, Hedges JI (1994) Mineralogical and textural controls on the organic composition of coastal marine sediments: hydrodynamic separation using SPLITT-fractionation. Geochim Cosmochim Ac 58:879–893. https://doi.org/10.1016/0016-7037(94)90512-6

Kim Y, Cho S, Kang HD, Kim W et al (2006) Radiocesium reaction with illite and organic matter in marine sediment. Mar Pollut Bull 52:659–665. https://doi.org/10.1016/j.marpolbul.2005.10.017

Kim Y, Kim K, Kang HD et al (2007) The accumulation of radiocesium in coarse marine sediment: effects of mineralogy and organic matter. Mar Pollut Bull 54:1341–1350. https://doi.org/10.1016/J.MARPOLBUL.2007.06.003

Kim Y, Kirkpatrick RJ, Cygan RT (1996) ^{133}Cs NMR study of cesium on the surfaces of kaolinite and illite. Geochim Cosmochim Ac 60:4059–4074. https://doi.org/10.1016/S0016-7037(96)00257-8

Klaminder J, Appleby P, Crook P, Renberg I (2012) Post-deposition diffusion of ^{137}Cs in lake sediment: implications for radiocaesium dating. Sedimentology 59:2259–2267. https://doi.org/10.1111/j.1365-3091.2012.01343.x

Kobets SA, Fedorova VM, Pshinko GN et al (2014) Effect of humic acids and iron hydroxides deposited on the surface of clay minerals on the ^{137}Cs immobilization. Radiochemistry 56:325–331. https://doi.org/10.1134/S1066362214030175

Konoplev AV, Ivanov MM, Golosov VN, Konstantinov EA (2019) Reconstruction of long-term dynamics of Chernobyl-derived ^{137}Cs in the Upa River using bottom sediments in the Scheckino reservoir and semi-empirical modelling. Proc Int Assoc Hydrol Sci 381:95–99. https://doi.org/10.5194/piahs-381-95-2019

Konoplev A, Wakiyama Y, Wada T et al (2022) Reconstruction of time changes in radiocesium concentrations in the river of the Fukushima Dai-ichi NPP contaminated area based on its depth distribution in dam reservoir's bottom sediments. Environ Res 206:112307. https://doi.org/10.1016/J.ENVRES.2021.112307

Kónya J, Nagy NM, Nemes Z (2005) The effect of mineral composition on the sorption of cesium ions on geological formations. J Colloid Interface Sci 290:350–356. https://doi.org/10.1016/j.jcis.2005.04.082

Kurikami H, Kitamura A, Thomas Yokuda S, Onishi Y (2014) Sediment and ^{137}Cs behaviors in the Ogaki Dam Reservoir during a heavy rainfall event. J Environ Radioact 137:10–17. https://doi.org/10.1016/j.jenvrad.2014.06.013

Lamb AL, Wilson GP, Leng MJ (2006) A review of coastal palaeoclimate and relative sea-level reconstructions using δ13C and C/N ratios in organic material. Earth-Science Rev 75:29–57. https://doi.org/10.1016/J.EARSCIREV.2005.10.003

Livens FR, Baxter MS (1988) Particle size and radionuclide levels in some west Cumbrian soils. Sci Total Environ 70:1–17. https://doi.org/10.1016/0048-9697(88)90248-3

Luettich RA, Harleman DRF, Somlycidy L (1990) Dynamic behavior of suspended sediment concentrations in a shallow lake perturbed by episodic wind events. Limnol Ocean 35:1050–1067

Madruga MJ, Silva L, Gomes AR, Libânio A, Reis M (2014) The influence of particle size on radionuclide activity concentrations in Tejo River sediments. J Environ Radioact 132:65–72. https://doi.org/10.1016/J.JENVRAD.2014.01.019

Meyers PA, Ishiwatari R (1993) Lacustrine organic geochemistry-an overview of indicators of organic matter sources and diagenesis in lake sediments. Org Geochem 20:867–900. https://doi.org/10.1016/0146-6380(93)90100-P

Meyers PA, Ishiwatari R (1995) Organic matter accumulation records in lake sediments. Phys Chem Lakes 279–328. https://doi.org/10.1007/978-3-642-85132-2_10

Mouri G (2020) Reproduction of sediment deposition and prediction of ^{137}Cs concentration in the major urban rivers of Tokyo. Sci Rep 10:4–6. https://doi.org/10.1038/s41598-020-65700-y

Mukai H, Hirose A, Motai S et al (2016) Cesium adsorption/desorption behavior of clay minerals considering actual contamination conditions in Fukushima. Sci Rep 6:21543. https://doi.org/10.1038/srep21543

Muuri E, Ikonen J, Matara-aho M et al (2016) Behavior of Cs in Grimsel granodiorite. Sorption on main minerals and crushed rock. Radiochim Acta 104:575–582

Naulier M, Eyrolle-Boyer F, Boyer P et al (2017) Particulate organic matter in rivers of Fukushima: an unexpected carrier phase for radiocesiums. Sci Total Environ 579:1560–1571. https://doi.org/10.1016/j.scitotenv.2016.11.165

Nenadović S, Kljajević L, Marković S et al (2015) Natural diatomite (Rudovci, Serbia) as adsorbent for removal Cs from radioactive waste liquids. Sci Sinter 47:299–309. https://doi.org/10.2298/SOS1503299N

O'Connell DW, Mark Jensen M, Jakobsen R et al (2015) Vivianite formation and its role in phosphorus retention in Lake Ørn, Denmark. Chem Geol 409:42–53. https://doi.org/10.1016/J.CHEMGEO.2015.05.002

Park CW, Kim SM, Kim I et al (2021) Sorption behavior of cesium on silt and clay soil fractions. J Environ Radioact 233:106592. https://doi.org/10.1016/J.JENVRAD.2021.106592

Poinssot C, Baeyens B, Bradbury MH (1999) Experimental and modelling studies of caesium sorption on illite. Geochim Cosmochim Acta 63:3217–3227. https://doi.org/10.1016/S0016-7037(99)00246-X

Prahl FG, Bennett JT, Carpenter R (1980) The early diagenesis of aliphatic hydrocarbons and organic matter in sedimentary particulates from Dabob Bay, Washington. Geochim Cosmochim Ac 44:1967–1976. https://doi.org/10.1016/0016-7037(80)90196-9

Putyrskaya V, Klemt E (2007) Modelling ^{137}Cs migration processes in lake sediments. J Environ Radioact 96:54–62. https://doi.org/10.1016/j.jenvrad.2007.01.017

Putyrskaya V, Klemt E, Röllin S, Corcho-Alvarado JA, Sahli H (2020) Dating of recent sediments from Lago Maggiore and Lago di Lugano (Switzerland/Italy) using ^{137}Cs and ^{210}Pb. J Environ Radioact 212:106135. https://doi.org/10.1016/J.JENVRAD.2019.106135

Raven MD, Self PG (2017) Outcomes of 12 Years of the Reynolds Cup Quantitative Mineral Analysis Round Robin. Clays Clay Miner 65:122–134

R Core Team (2020) R: a language and environment for statistical computing. R Foundation for Statistical Computing, Vienna, Austria

Rigol A, Vidal M, Rauret G (2002) An overview of the effect of organic matter on soil-radiocaesium interaction: implications in root uptake. J Environ Radioact 58:191–216. https://doi.org/10.1016/S0265-931X(01)00066-2

Robbins JA, Krezoski JR, Mozley SC (1977) Radioactivity in sediments of the Great Lakes: post-depositional redistribution by deposit-feeding organisms. Earth Planet Sci Lett 36:325–333. https://doi.org/10.1016/0012-821X(77)90217-5

Sawhney BL (1972) Selective sorption and fixation of cations by clay minerals. A Rev Clays Clay Miner 20:93–100. https://doi.org/10.1346/CCMN.1972.0200208

Sedláček J, Bábek O, Grygar TM et al (2022) A closer look at sedimentation processes in two dam reservoirs. J Hydrol 605:127397. https://doi.org/10.1016/J.JHYDROL.2021.127397

Shepard FP (1954) Nomenclature based on sand-silt-clay ratios. J Sed Pet 24:151–158

Sekudewicz I, Gąsiorowski M (2022) Spatial and vertical distribution of ^{137}Cs activity concentrations in lake sediments of Turawa Lake (Poland). Environ Sci Pollut Res Int. https://doi.org/10.1007/s11356-022-21417-1

Somboon S, Kavasi N, Sahoo SK et al (2018) Radiocesium and ^{40}K distribution of river sediments and floodplain deposits in the Fukushima exclusion zone. J Environ Radioact 195:40–53. https://doi.org/10.1016/j.jenvrad.2018.09.003

Spezzano P (2005) Distribution of pre- and post-Chernobyl radiocaesium with particle size fractions of soils. J Environ Radioact 83:117–127. https://doi.org/10.1016/J.JENVRAD.2005.02.002

Środoń J, Drits VA, McCarty DK, Hsieh JC, Eberl DD (2001) Quantitative X-ray diffraction analysis of clay-bearing rocks from random preparations. Clays Clay Miner 49(6):514–528

Staunton S, Dumat C, Zsolnay A (2002) Possible role of organic matter in radiocaesium adsorption in soils. J Environ Radioact 58:163–173. https://doi.org/10.1016/S0265-931X(01)00064-9

Suga H, Fan Q, Takeichi Y et al (2014) Characterization of particulate matters in the Pripyat River in Chernobyl related to their adsorption of radiocesium with inhibition effect by natural organic matter. Chem Lett 43(7):1128–1130. https://doi.org/10.1246/CL.140222

Szatten D (2016) Proposal of a new hydromorphometric division of Koronowski reservoir (in Polish). Geograph Tour 4:79–84. https://doi.org/10.5281/zenodo.56746

Szatten D, Habel M, Pellegrini L, Maerker M (2018) Assessment of siltation processes of the Koronowski Reservoir in the northern Polish lowland based on bathymetry and empirical formulas. Water 10(11):1681. https://doi.org/10.3390/w10111681

Tachi Y, Sato T, Akagi Y et al (2020a) Key factors controlling radiocesium sorption and fixation in river sediments around the Fukushima Daiichi Nuclear Power Plant. Part 1: insights from sediment properties and radiocesium distributions. Sci Total Environ 724:138098. https://doi.org/10.1016/J.SCITOTENV.2020.138098

Tachi Y, Sato T, Takeda C et al (2020b) Key factors controlling radiocesium sorption and fixation in river sediments around the Fukushima Daiichi Nuclear Power Plant. Part 2: Sorption and fixation behaviors and their relationship to sediment properties. Sci Total Environ 724:138097. https://doi.org/10.1016/J.SCITOTENV.2020.138097

Tadejewski A (1966) Bottom sediments in different limnetic zones of an eutrophic lake. Ekol Pol A 14:1–21

Tamura T, Jacobs DG (1960) Structural implications in cesium sorption. Health Phys 2:391–398. https://doi.org/10.1097/00004032-195910000-00009

Tanaka K, Iwatani H, Sakaguchi A, Fan Q, Takahashi Y (2015) Size-dependent distribution of radiocesium in riverbed sediments and its relevance to the migration of radiocesium in river systems after the Fukushima Daiichi Nuclear Power Plant accident. J Environ Radioact 139:390–397. https://doi.org/10.1016/J.JENVRAD.2014.05.002

Tsuji H, Tanaka A, Komatsu K et al (2019) Vertical/spatial movement and accumulation of ^{137}Cs in a shallow lake in the initial phase after the Fukushima Daiichi nuclear power plant accident. Appl Radiat Isot 147:59–69. https://doi.org/10.1016/J.APRADISO.2019.02.009

Waters MN, Golladay SW, Patrick CH, Smoak JM, Shivers SD (2015) The potential effects of river regulation and watershed land use on sediment characteristics and lake primary producers in a large reservoir. Hydrobiologia 749:15–30. https://doi.org/10.1007/S10750-014-2142-8

Wieczorek D, Stoiński A (2008) Detailed geological map of Poland in scale 1:50 000. Map series: 241 – Gostycyn (N-33-96-D). Polish Geological Institute (PGI). https://bazadata.pgi.gov.pl/data/smgp/arkusze_skany/smgp0241.jpg

Wilkin RT, Barnes HL, Brantley SL (1996) The size distribution of framboidal pyrite in modern sediments: an indicator of redox conditions. Geochim Cosmochim Ac 60:3897–3912. https://doi.org/10.1016/0016-7037(96)00209-8

Zachara JM, Smith S, Liu C et al (2002) Sorption of Cs$^+$ to micaceous subsurface sediments from the Hanford Site, USA. Geochim Cosmochim Acta 66:193–211. https://doi.org/10.1016/S0016-7037(01)00759-1

Zapata F, Nguyen ML (2009) Soil erosion and sedimentation studies using environmental radionuclides, in: Froehlich, K., (Eds.), Environmental radionuclides: tracers and timers of terrestrial processes. Radioactivity in the Environment. Elsevier 16:295–322. https://doi.org/10.1016/S1569-4860(09)01607-6

Publisher's Note Springer Nature remains neutral with regard to jurisdictional claims in published maps and institutional affiliations.

Geochemical behavior of heavy metals and radionuclides in a pit lake affected by acid mine drainage (AMD) in the Muskau Arch (Poland)

Ilona Sekudewicz [a,*], Marcin Syczewski [b], Jan Rohovec [c], Šárka Matoušková [c], Urszula Kowalewska [a], Roberts Blukis [b,d], Walter Geibert [e], Ingrid Stimac [e], Michał Gąsiorowski [a]

[a] Institute of Geological Sciences, Polish Academy of Sciences, 00818 Warszawa, Twarda 51/55, Poland
[b] Helmholtz Centre Potsdam, GFZ German Research Centre for Geosciences, Telegrafenberg, 14473 Potsdam, Germany
[c] Institute of Geology, Czech Academy of Sciences, 16500 Praha, Rozvojová 269, Czech Republic
[d] Leibniz-Institut für Kristallzüchtung, Max-Born-Str. 2, 12489 Berlin, Germany
[e] Alfred Wegener Institute, Helmholtz Centre for Polar and Marine Research, Am Handelshafen 12, 27570 Bremerhaven, Germany

HIGHLIGHTS

- Current and past sedimentation conditions in an acidic pit lake are understood.
- The diatom-inferred former pH change in the lake water may be related to flooding.
- ^{137}Cs and ^{210}Po are chronostratigraphic markers of the depositional event.
- Elevated contents of trace metals and radioisotopes are likely related to flooding.
- The C/N ratio indicates the influx of allochthonous organic matter into the lake.

GRAPHICAL ABSTRACT
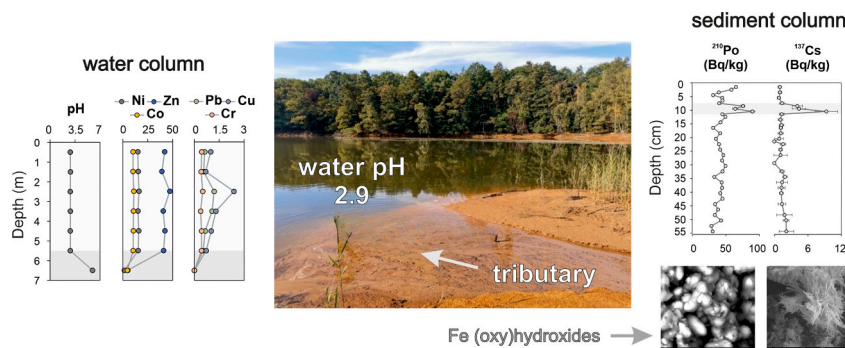
ARTICLE INFO

ABSTRACT

Pit lakes in the 'anthropogenic lake district' in the Muskau Arch (western Poland; central Europe) are strongly affected by acid mine drainage (AMD). The studied acidic pit lake, ŁK-61 (pH <3), is also exposed to floods due to its location in the flood hazard area, which may significantly influence the geochemical behavior of elements. The elemental compositions of water and lake sediment samples were measured with ICP–OES and ICP–MS. The sediment profile was also examined for ^{137}Cs and ^{210}Po activity concentrations using gamma and alpha spectrometry, respectively. Grain size distribution, mineralogical composition, diatoms, and organic matter content in the collected core were also determined. The key factors responsible for the distribution of selected heavy metals (e.g., Cu, Ni, Pb, Zn) and radioisotopes (^{137}Cs and ^{210}Po) in the bottom sediments of Lake ŁK-61 are their coprecipitation/precipitation with Fe and Al secondary minerals and their sorption onto authigenic and allogenic phases. These processes are likely driven by the lake tributary, which is an important source of dissolved elements. The data also showed that the physiochemical parameters of Lake ŁK-61 water changed during an episodic depositional event, i.e., the flood of the Nysa Łużycka River in the summer of 2010. The flood caused an increase in the water pH, as interpreted from the subfossil diatom studies. The down-core profiles of the studied

* Corresponding author.
  E-mail address: i.sekudewicz@twarda.pan.pl (I. Sekudewicz).

heavy metal and radionuclide (HMRs) contents were probably affected by this depositional event, which prevented a detailed age determination of the collected lake sediments with ^{137}Cs and ^{210}Pb dating methods. Geochemical modeling indicates that the flood-related shift in the physicochemical parameters of the lake water could have caused the scavenging of dissolved elements by the precipitation of fresh secondary minerals. Moreover, particles contaminated with HMRs have also possibly been delivered by the river, along with the nutrients (e.g., phosphorus and nitrogen).

1. Introduction

Acid mine drainage (AMD) poses a serious environmental hazard, leading to the degradation of water quality through acidification and the release of toxic elements. Consequently, contaminated water (e.g., lake water) cannot be directly used for drinking or industrial purposes, which can present a significant problem, especially considering challenges related to freshwater procurement (Panagopoulos and Giannika, 2022, 2023). Factors controlling the distribution of heavy metals in natural environments affected by AMD have been widely studied (e.g., Cánovas et al., 2007; Friese, 2004; Hierro et al., 2014; Lee et al., 2002; Torres et al., 2013). However, the geochemical behavior of radioactive isotopes in such ecosystems is still far from being understood (Blasco et al., 2016). Most of the studies regarding radioisotopes in natural ecosystems affected by AMD concern mainly uranium (e.g., Barbero et al., 2014; Hierro et al., 2012; Manjón et al., 2019; Villa et al., 2011; Yamamoto et al., 2010). However, to our knowledge, only a few studies have focused on the distribution of cesium ^{137}Cs or lead ^{210}Pb and polonium ^{210}Po in AMD-affected water reservoirs (Abril et al., 2018; Blasco et al., 2016; Mantero et al., 2020; Thomas et al., 2020, 2022). Nevertheless, understanding the mechanisms responsible for the cycling of these radionuclides in lake ecosystems is crucial because they are useful tools for dating sediments and because they can pose a dangerous threat to biota (Abril et al., 2018; Aközcan et al., 2018; Appleby, 2005; Swarzenski, 2014). In addition, these radioisotopes can be important fingerprints of depositional events, even if they cannot provide an unambiguous, accurate chronology for the sedimentary record (e.g., Abril et al., 2018; Mabit et al., 2014; Zapata and Nguyen, 2009).

Polonium ^{210}Po (half-life = 138.38 days) is a naturally occurring radioactive isotope and it is expected to be in secular equilibrium with its indirect parent isotopes, radium ^{226}Ra (half-life = 1622 years) and so-called 'supported' lead ^{210}Pb (half-life = 22.23 years) in rocks, deep soils and sediments (Appleby, 2005; Appleby and Oldfield, 1978; Swarzenski, 2014; Carvalho et al., 2017). In more recently deposited sediments, ^{210}Po corresponds to a mixture of 'supported' and 'unsupported'/ 'excess' ^{210}Pb, which mainly originates from atmospheric deposition and is considered to be time-dependent. For this reason, a down-core profile of ^{210}Po activity concentrations is supposed to follow an exponential curve (in accordance with the first-order law of radioactive decay), together with excess ^{210}Pb, assuming the constant flux of ^{210}Pb$_{ex}$, undisturbed sedimentation conditions, and lack of post-depositional processes that could cause the redistribution of the deposited ^{210}Pb$_{ex}$ (Appleby, 2005; Appleby et al., 1979; Swarzenski, 2014). Therefore, ^{210}Po is commonly used to indirectly determine ^{210}Pb activity concentrations in sediments, assuming that they are in secular equilibrium (e.g., Matthews et al., 2007; Zaborska et al., 2007).

Radiocesium ^{137}Cs (half-life = 30.07 years) is an anthropogenic radioactive isotope that was released into the natural environment as a result of nuclear weapon tests (1945–1980 with maximum in 1963), and nuclear power plant accidents in Chernobyl (in 1986) and Fukushima (in 2011) (e.g., Appleby, 2008; Norris and Arkin, 1996; Smith and Beresford, 2005). Subsequently, ^{137}Cs was deposited at the bottom of the water reservoirs as a consequence of atmospheric fallout and radiocesium-bearing particle input at a later stage (Ashraf et al., 2014; Smith and Beresford, 2005; Zapata and Nguyen, 2009). As a result, a characteristic peak of the increased concentrations of ^{137}Cs activity can be observed in the sediment profiles, assuming ideal depositional conditions (e.g., Appleby, 2008; Ashraf et al., 2014). Hence, ^{137}Cs is widely regarded as an important chronostratigraphic marker and is commonly used to validate chronologies based on other dating techniques, such as the ^{210}Pb method (Abril et al., 2018; Appleby, 2008; Baskaran et al., 2014; Putyrskaya et al., 2015).

The distribution of heavy metals and radionuclides (HMRs) in AMD-affected pit lakes can be controlled by several factors, including limnological properties, the age of the lake and degree of its neutralization/eutrophication, mineralogical composition of rocks forming the embankments and catchment area, and others (e.g., Blasco et al., 2016; Friese et al., 1998; Gąsiorowski et al., 2021; Geller et al., 2013; Sánchez-España et al., 2008; Schultze, 2013). Moreover, there are many factors that can alter the vertical distributions of the HMR content in the sediment profiles, such as physical mixing caused by wind–wave action and bioturbations, as well as chemical remobilization (e.g., Abril et al., 2018; Appleby, 2005; Baskaran et al., 2014; Klaminder et al., 2012; Putyrskaya et al., 2015). Moreover, some depositional events, such as heavy rainfalls or floods, can also disrupt the processes responsible for the distribution of these elements in the bottom sediments of AMD-affected freshwater ecosystems (e.g., Abril et al., 2018; Cánovas et al., 2007; Guerrero et al., 2021; Herzsprung et al., 2010; Mayes et al., 2021). Such events can cause, for example, a change in the water pH and redox conditions, which are considered the main parameters determining the geochemical behavior of elements in such environments (e.g., Hierro et al., 2014; Shi et al., 2021). An increase in the water pH may lead, for example, to the precipitation of fresh secondary minerals, which can capture and immobilize dissolved solids by coprecipitation/precipitation and sorption processes (e.g., Alpers et al., 1994; Azzali et al., 2014; Hierro et al., 2014). A subsequent decrease in the water pH may cause, in turn, the dissolution of pH-sensitive mineral phases and simultaneous release of immobilized elements (e.g., Mayes et al., 2021; Wisotzky, 1998). Moreover, floods can carry large amounts of dissolved elements and solid particles, which can also significantly affect the distribution of HMRs in the bottom sediments of pit lakes (e.g., Appleby, 2005; Herzsprung et al., 2010; Mayes et al., 2021; Torres et al., 2013; Walling and Quine, 1993). Incoming river waters also likely transport significant amounts of nutrients, such as phosphorus, as observed in the case of Goitsche Lake in Germany (Herzsprung et al., 2010). Nutrient input (e. g., phosphorus and nitrogen) can subsequently affect the growth of microorganisms (e.g., diatoms) and indirectly alter the geochemical behavior of dissolved solids in such ecosystems (e.g., Kleeberg and Grüneberg, 2005; Paulsson and Widerlund, 2021; Schultze, 2013).

The studied Lake ŁK-61 is an acidic pit lake (pH <3) in the Muskau Arch in western Poland (central Europe) that was created as a result of lignite mining (Fig. 1). The lake was studied as part of a regional recognition of the geochemical diversity of water and surface lake sediments (Gąsiorowski et al., 2021). Since it turned out to be quite unique compared to other water reservoirs in the region, we decided to select it for a more detailed study. Lake ŁK-61 is affected by AMD (caused by the oxidation and dissolution of iron sulfides) and may be exposed to depositional events (e.g., floods) due to its location in a flood hazard area (PGW WP, 2021). The main objective of the presented research was to investigate the key processes responsible for the distribution of selected heavy metals (e.g., Cr, Cu, Ni, Pb, Zn) and radionuclides (^{137}Cs and ^{210}Po) in the bottom sediments of Lake ŁK-61. Moreover, the impact of potential depositional events on the geochemical behavior of selected HMRs in the studied lake and on the age determination of deposited lake

sediments using the ^{137}Cs and ^{210}Pb dating methods were also discussed.

2. Materials and methods

2.1. Site description

The study area is located in the Muskau Arch (also known as Łuk Mużakowa and Muskauer Faltenbogen) in the Lubusz Voivodeship (western Poland), near Łęknica (Fig. 1). The Muskau Arch is an arch-shaped glaciotectonic terminal moraine formed during the Last Glacial Period (Bożęcki, 2013; Koźma and Kupetz, 2008). It covers an area of approx. 250 km^2, of which approx. 80 km^2 is located in Poland. Natural resources mined in this area were brown coal (lignite), clays, sand, and gravel (Gruszecki et al., 2006). There are approx. 300–400 lakes, many of which were created as a result of lignite mining from the 19th century to the 1970s (Kupetz, 1997; Koźma and Kupetz, 2008). The exploitation of lignite on the Polish side of the Muskau Arch lasted until 1973, when the 'Babina' mine (located east of Łęknica) was closed. Clay mining in this area continued until the 1990s (Gruszecki et al., 2006). Therefore, the greatest anthropogenic changes in the natural environment can be observed in the area of Łęknica and thereby Lake ŁK-61, which was selected as the study site (Solski et al., 1988).

Lake ŁK-61 (51°31′31.746″N, 14°45′19.824″E), also known as 'Hydro' or 'Staw Południowy' Lake, is located near Łęknica, which is in close proximity to the Polish–German border (Fig. 1). The area of the lake is 2.71 ha, and its maximum depth is 7.5 m. It has one tributary, which is a stream flowing into the lake on its northern side. The regional geology of the study area is characterized by alluvial terrace sands and gravels (Fig. 2) (Bartczak and Gancarz, 1998). To the north of the lake, sands, silts, kaolinite clays, clays, and brown coal were found. ŁK-61 is a pit lake located on the site of an open-pit lignite mine that was operated from 1957 to the 1970s (Koźma, 2009). There were also refractory clay mines on the northern side of the lake, which were closed down in the 1990s (Gruszecki et al., 2006). Currently, the study area is located in a landscape park and is surrounded by deciduous and mixed coniferous forests.

The studied lake is situated a short distance (approx. 200 m) from the Nysa Łużycka River (Lausitzer Neiße), which constitutes the Polish–German border (Fig. 1). It is also located in a flood hazard area, where the probability of flooding is 10 % (once every 10 years) (PGW WP,

2021). The last flood in this area was recorded in the first days of August 2010 (MKOO, 2010). Previously, the highest water level of the Nysa Łużycka River was recorded in 1981 by the stream gauge (Przewóz) located near the study area.

2.2. Sampling and sample preparation

Fieldwork was performed in September 2020 and 2021. The depth of the lake bottom was measured along two transects with a portable echo sounder (Echotest II). Physicochemical parameters of water (temperature, pH, redox potential (Eh), electrical conductivity (EC), and dissolved oxygen (DO)) were measured in situ with a multi-parameter portable meter (Multi 3620 IDS SET G) during sampling in September 2020 (site no. WA) and 2021 (site no. WB). The electrochemical unit was freshly calibrated each time before analysis. The pH electrode was calibrated using calibration buffers (pH 4.0 and 7.0) and the Eh electrode potential was checked using the buffer solutions included in the multimeter set.

Samples from the tributary (site no. T 1-3) and water column (WA) were collected in September 2020 (Fig. 1). Water samples (site no. WA 1-7) were collected every 1 m from the top layer to the bottom of the water column using a vertical sampler with a capacity of 5 L. Each sample was then filtered through cellulose acetate (CA) membrane filters (0.45 μm pore size), preserved with double-distilled HCl (35 %), and stored in 50 mL polyethylene bottles at 4 °C until analysis. The lake sediment column (C1) was collected in September 2020 at the deepest point of the lake using a UWITEC gravity core with a polycarbonate pipe (inner diameter of 90 mm) (Fig. 1). The core (length 55 cm) was divided in the field into 1 cm slices and stored in polyethylene terephthalate (PET) containers at 4 °C. The samples were then transported to the laboratory, dried at 65 °C, ground, and homogenized for further analysis. A portion of each sample (1 g dry mass) was left unground for particle size analysis.

2.3. Tributary and lake water samples

2.3.1. Elemental composition and DOC content

The concentrations of major elements in the water samples were determined with the ICP–OES instrument (Agilent 5100) at the Institute of Geology of the Czech Academy of Sciences (CAS) in Prague. Three
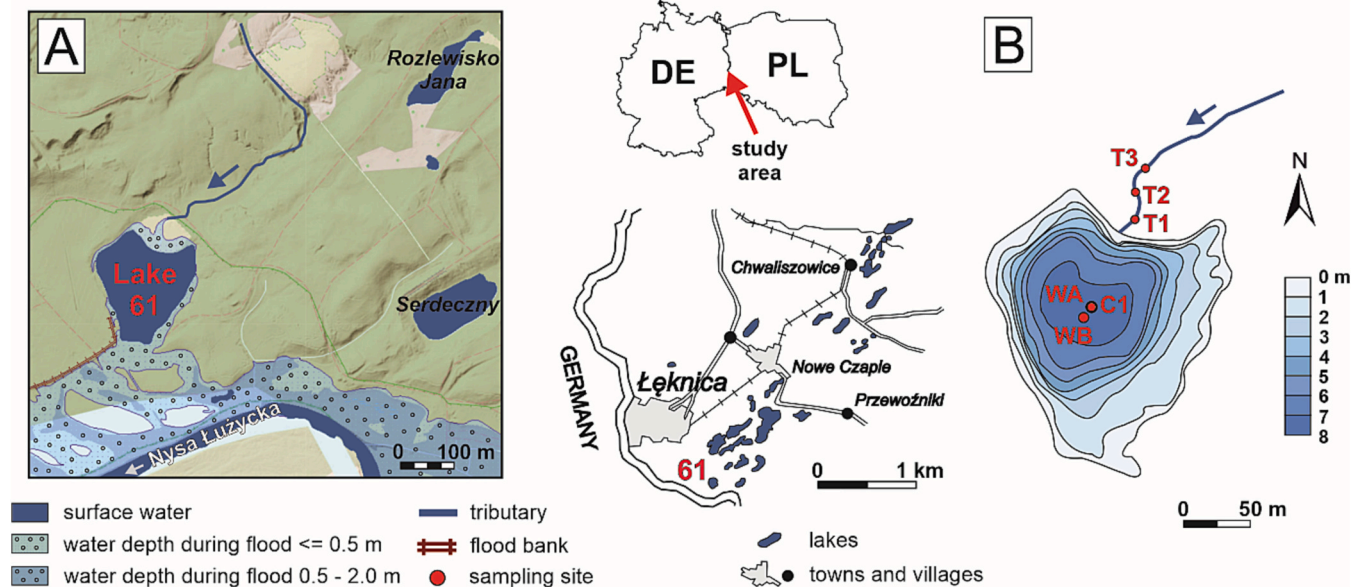

Fig. 1. (A) Sampling site (Sienkiewicz and Gąsiorowski, 2016; modified) with a flood hazard map (MZP) 10 % (once every 10 years) (PGW WP, 2021; modified) and (B) bathymetric map of Lake ŁK-61.
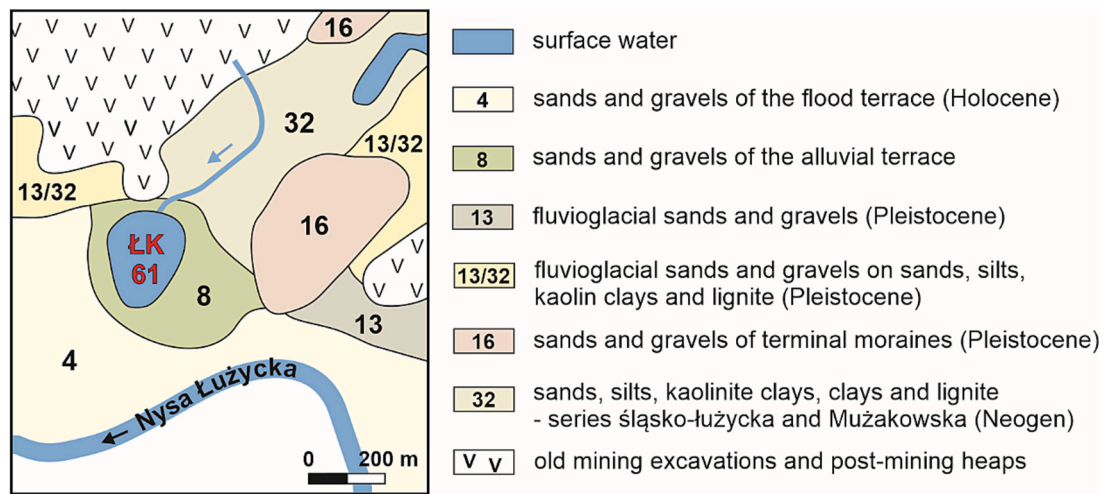
Fig. 2. Geological setting of Lake ŁK-61. The geological data are based on the Detailed Geological Map of Poland in scale 1:50000 (Bartczak and Gancarz, 1998).

replicates of each sample were run. Mixed standards for instrument calibration were prepared from commercially available single-element SRM (Analytika spol. s.r.o.). The QC/QA procedure was based on measurements of the certified reference material (CRM) ERM CA 615 (EC Join Research Center), producing results within the certificate range (Fe, Mn) and with recoveries of 97–102 % (Ca, Mg, K, and Na).

Trace elements in the water samples were quantified using a high-resolution sector-field ICP–MS Element 2 (Thermo Fisher Scientific) at the Institute of Geology CAS. The instrument was tuned using an 'in-house' multielement standard to achieve the highest sensitivity for ^{115}In and ^{238}U, balanced stability, and oxide formation <8 %. Instrumental calibration was performed with a multielement calibration solution prepared from commercially available single-element standards (CPA Chem). The ^{115}In isotope was used as an internal standard to correct the results for instrumental and plasma drift. The QC/QA procedure was based on the analyses of CRM ERM CA 615 (for Cd, Ni, and Pb) and the 'in-house' mixed standard (for other quantified elements). Quantification was performed at low resolution (LR) and medium resolution (MR). All samples were measured in triplicate. The analytical result was accepted when the calculated relative standard deviation (RSD) was <5 %.

Chlorides were quantified using HPLC at the Institute of Geology CAS. Aqueous carbonate/hydrogen carbonate buffer (3.5 mmol L^{-1}) was used as the mobile phase. A Star Ion A300 anion exchange column (Phenomenex) and a CDD-10 A *VP* conductivity detector (Shimadzu) were used for separation and detection. The system was calibrated with a mixed standard solution CRM (Analytika spol. s.r.o.). The QC/QA procedure was based on CRM ERM CA 615 measurements. Two replicates of each measurement were run.

The content of dissolved organic carbon (DOC) was determined by the combustion catalytic infrared method on the Shimadzu TOC-V CPH at the Institute of Geology CAS. A basic standard solution was prepared using oxalic acid dihydrate. As an independent secondary standard, an aqueous solution of potassium hydrogen phthalate (KDP, Shimadzu, in double-distilled water) was inserted after every 5 samples to ensure measurement stability. DOC concentrations in water samples were determined in triplicate, and 2 additional determinations were performed if the RSD was >5 %.

2.4. Lake sediment samples

2.4.1. Grain size and elemental analyses

The lake sediment samples were dispersed in KOH (10 %); then, carbonates were removed by the addition of HCl (35 %), and OM was destroyed with H_2O_2 (32 %) and HNO_3 (65 %) prior to grain size

analysis. The particle size distribution of the selected samples was determined using a laser particle size analyzer (CILAS 1190) at the Institute of Geology CAS. Each sample was sieved to obtain grains <1000 μm. The analyses were performed in wet dispersion mode in the device range from 0.04 to 1000 μm. Classification of lake sediments in terms of particle size was performed using the Shepard sediment classification diagram (Shepard, 1954) and the 'ggtern' R package (Hamilton and Ferry, 2018).

An analysis of total organic carbon (TOC) and total nitrogen (TN) content in the lake sediments was performed using the Vario CUBE elemental analyzer at the Institute of Geological Sciences of the Polish Academy of Sciences (ING PAN) in Warsaw. A small portion (5–6 mg) of each sample was transferred into tin capsules and burned at 1150 °C. Then, CO_2 and N_2 gases were separated in a chromatography column and measured with a thermal conductivity detector. Sulfanilic acid (Sigma Aldrich) was used as the standard to validate the analyses. The measurement uncertainties for TOC and TN were 0.6 % and 0.18 %, respectively.

2.4.2. Alpha and gamma spectrometry

The radiochemical separation of ^{210}Po from the lake sediments was performed according to the modified procedure presented by Flynn (1968). Selected samples (approx. 0.6 g) were spiked with $^{208+209}$Po and digested on a hot plate with HCl (35 %) and HNO_3 (65 %). The organic components were destroyed in the samples by heating with HNO_3 (65 %) and H_2O_2 (32 %) (Jia et al., 2004; Matthews et al., 2007). Finally, polonium isotopes were spontaneously deposited (by an ion exchange reaction) onto silver discs in 0.5 M HCl (Martin and Blanchard, 1969). Sodium citrate and hydroxylamine hydrochloride were added to the solution prior to the deposition process to prevent the deposition of competing ions (e.g., Fe^{3+}) (Flynn, 1968; Jia et al., 2004). The activity concentrations of ^{208}Po, ^{209}Po and ^{210}Po were measured using an Octete (Ortec) alpha spectrometer at the ING PAN in Warsaw. Samples were counted for approx. 72 h. The average (arithmetic mean; $n = 33$) uncertainty of ^{210}Po activity concentration measurements was 1.5 Bq kg^{-1} (3 %). Chemical recovery for $^{208+209}$Po was approx. 60–70 %.

The concentrations of ^{137}Cs and ^{40}K activity in the lake sediments were measured using a low background gamma spectrometer (Canberra-Packard) with a Broad Energy Germanium (BE5030) detector (FWHM = 1.05 keV at 661.7 keV for ^{137}Cs and 1.65 keV at 1460.8 keV for ^{40}K) at the ING PAN in Warsaw. To verify the quality of the measurements, the CRM (IAEA-SL-2) was analyzed. All samples (from 1 to 10 g dry weight) were analyzed in a flat cylinder geometry. Genie 2000 software was used for data acquisition. The sample counting time ranged from 48 to 78 h. All obtained values were recalculated to the sampling date (September

24, 2020). The minimum detectable activity (MDA) values for ^{137}Cs and ^{40}K were 0.7 Bq kg^{-1} and 13.5 Bq kg^{-1}, respectively. The uncertainty of the measurements of ^{137}Cs and ^{40}K activity concentrations varied from 22 to 39 % and from 9 to 23 %, respectively.

2.4.3. ICP–OES analysis

Selected lake sediments were digested in one batch consisting of 17 samples, 4 procedural blanks, and 3 CRM samples. The CRM was marine sediment (NRC-MESS-4). Approx. 75 mg of each sample was transferred into PTFE vials and digested with double-distilled HNO$_3$ (65 %), HCl (32 %), and HF (48 %) using the MARS 6 microwave digestion system (CEM Corporation, USA) at the Alfred Wegener Institute, Helmholtz Centre for Polar and Marine Research in Bremerhaven. The digested samples were evaporated to near dryness using the XVap accessory of the microwave. All samples were then appropriately diluted with double-distilled 1.5 M HNO$_3$ prior to analysis.

The concentrations of selected elements in the prepared samples were measured in triplicate using ICP–OES (iCAP 7000 Series; Thermo Scientific) (Table S2; Supplementary Materials). Single-element standard solutions (Roti®Star, CarlRoth GmbH) were used to perform external calibration for quantitative analysis. Yttrium was added to the samples as an internal standard to correct the results for instrumental drift. CRM was measured every 4–6 samples. Additionally, an 'in-house' mixed standard (prepared from calibration solutions) was analyzed to control the quality of the analyses. RSD for all analyses was <5 % (Table S3; Supplementary Materials). The limit of detection (LOD) and limit of quantification (LOQ) for the measured elements are presented in Table S4 (Supplementary Materials).

2.4.4. Mineralogical analyses

Mineralogical analyses of selected lake sediment samples were conducted at the Helmholtz Centre Potsdam, German Research Centre for Geosciences (GFZ). X-ray diffraction measurements were performed with a STOE STADI P diffractometer with an Ag X-ray source fitted with a curved Ge (111) monochromator and two DECTRIS MYTHEN2 detectors in a flat plate transmission geometry. Diffraction patterns were measured over a range of 0–73° 2Θ (Q = 0–13.3 Å^{-1}) for a duration of 3 h per data point. Rietveld refinements were performed using GSAS-II software (Toby and Von Dreele, 2013). Reference CIF files were obtained from the AMCSD database and were refined for unit cell, grain size, microstrain, and sheet silicates for preferential orientation. The background was approximated using Chebyshev polynomials, and the instrument function was calibrated by empirically fitting the Caglioti function with included asymmetry to an LaB$_6$ standard measured in the same geometry.

Infrared absorption (IR) spectra were measured with a Thermo Fisher Nicolet iS5 FT-IR spectrometer equipped with an iD7 single reflection diamond ATR accessory and KBr optics at the GFZ. For each sample, 32 spectra with a resolution of 4 cm^{-1} were averaged. The spectra shown here are presented without ATR corrections and therefore may not match the exact peak intensity and wavenumber values measured in transmission from other studies. Reference spectra for montmorillonite, kaolinite and ferrihydrite were measured at the GFZ with the same settings as the samples, while the other IR reference spectra were obtained from the RRUFF database.

A scanning electron microscope (SEM) FEI Quanta 3D FEG Dual Beam coupled with energy dispersive spectroscopy (EDS) EDAX Octane elect plus was used to analyze selected lake sediments at the GFZ. Analyses were performed at 20 kV and 4 nA. Before measurements, samples were placed on 10 mm aluminum pin stubs and coated with 20 nm of C using a vacuum coater (LEICA EM ACE600).

2.4.5. Diatom analysis and DI–pH modeling

For diatom analysis, 55 samples were collected, one per centimeter of core. Slides were prepared according to the standard method described by Battarbee (1986). OM was removed by adding H$_2$O$_2$ (30 %). The sediments were then washed three times with distilled water and diluted to 20–100 mL. Permanent slides were mounted with Naphrax (R.I. = 1.75). An Olympus BX40 light microscope with a × 100 oil immersion objective was used to identify and count diatom valves. Diatom identification was based on Krammer and Lange-Bertalot (1986, 1988, 1991a, 1991b), Lange-Bertalot and Metzeltin (1996), Krammer (2000) and Lange-Bertalot et al. (2017). The reconstruction of the lake water pH (DI–pH) was performed using C2 software version 1.8 (Juggins, 2001) with the pH training datasets created for post-mining lakes in the Muskau Arch (Sienkiewicz and Gąsiorowski, 2017). The best squared correlation between inferred and observed values (R2) and the lowest root mean squared error for the training set (apparent RMSE) of the pH model were obtained using the weighted averaging method with a reduced weight of species with a high pH tolerance, together with inverse deshrinking (WATOL_Inv).

2.5. Data analysis and geochemical modeling

Statistical analyses were conducted using R version 4.0.4 (R Core Team, 2021). The Shapiro–Wilk test was used to assess the normality distribution of the data. Most of the data were non-normally distributed; therefore, Spearman's rank correlation coefficients (p value <0.05) were calculated to determine the relationship between selected variables with the R package 'Hmisc' (Frank and Harrell, 2023). Geochemical modeling was performed using Gechemist's WorkBench® software (Bethke, 1996). The database used in this study was a modified GWB's thermo-minteq database.

3. Results

3.1. Elemental composition of tributary and lake water

The physicochemical parameters and elemental composition of the tributary and lake water are presented in Table 1 and Table S1 (Supplementary Materials), respectively. Physicochemical parameters measured in the upper layer of the water column in September 2020 and 2021 did not differ significantly (Table 1). These values were also relatively similar to those measured in the tributary (T 1–3) (Table 1; Table S1). The obtained results showed that ŁK-61 is a stratified lake with a chemocline occurring between depths of 5.5 and 6.5 m in the water column (Fig. 3). The surface layer (epilimnion) of the water column was characterized by low pH (pH = 2.9) and high mineralization values (EC >1900 μS cm^{-1}). In the bottom zone (hypolimnion), the content of DO (<2 mg L^{-1}) decreased significantly, while the values of pH (>5), EC (>2700 μS cm^{-1}), and DOC (>32 mg L^{-1}) increased. An increase in the concentration of Fe, S, K, and Na, as well as a decrease in the concentration of Al, Ca, Mg, Mn, and Si in the hypolimnion of Lake ŁK-61 was also observed (Fig. 3; Table S1).

3.2. Lake sediments

3.2.1. Organic matter content and grain size distribution

The vertical distribution of TOC content was rather constant along the entire length of the collected sediment column (Fig. 4). The highest TOC content (>5 %) was found at depths of 20–21 cm and 41 cm in the core. The TN content was below the detection limit in most of the collected lake sediments, with the exception of samples located at depths of 1–3 cm and 7–10 cm in the core (Fig. 4). The contents of TN in these samples ranged from 0.19 to 0.3 %. Only for these samples was it possible to calculate the C/N ratio, which ranged from 18 to 26. The highest C/N ratio was determined for the sample collected from a depth of 8 cm in the sediment column (C/N = 26).

The wet bulk density of lake sediments varied along the entire length of the core (Fig. 4). The highest values of the wet bulk density (above 1.7 g cm^{-3}) were observed in the case of samples collected at depths of 6, 18, 21, 27–28, 32, and 42 cm in the core. Based on Sheppard's

Table 1

Physicochemical parameters of tributary (T) and lake water (WA and WB) of Lake ŁK-61. Sampling sites are shown in Fig. 1.

Sample name	Bożęcki (2013)			Water column							Tributary			Water column		
				WA1	WA2	WA3	WA4	WA5	WA6	WA7	T1	T2	T3	WB1	WB2	WB3
Sampling date	09/2009	08/2010	09/2010				09/2020					09/2020			09/2021	
Depth (m)		surface		0.5	1.5	2.5	3.5	4.5	5.5	6.5		surface		0.5	6.5	7.5
Temperature (°C)	16.3	20.3	16.7	19.3	18.5	18.3	18.2	18.2	17.7	14.7	18.7	14.0	14.4	19.6	13.7	12.5
pH	2.9	5.3	3.9	2.85	2.88	2.86	2.87	2.86	2.86	5.98	2.80	3.09	3.14	2.9	3.2	6.5
Eh (mV)	765	555	666	540	541	543	544	544	540	−22	532	449	432	541	410	−105
Conductivity (μS cm^{-1})	1856	268	593	1964	1975	1995	1989	2001	2001	2780	1964	1892	1849	1908	2100	2330
Dissolved oxygen (mg L^{-1})	n.d.	n.d.	n.d.	9.25	9.33	9.38	9.41	9.33	9.21	1.60	9.13	8.78	8.70	9.00	4.35	1.83

n.d. – not detected.
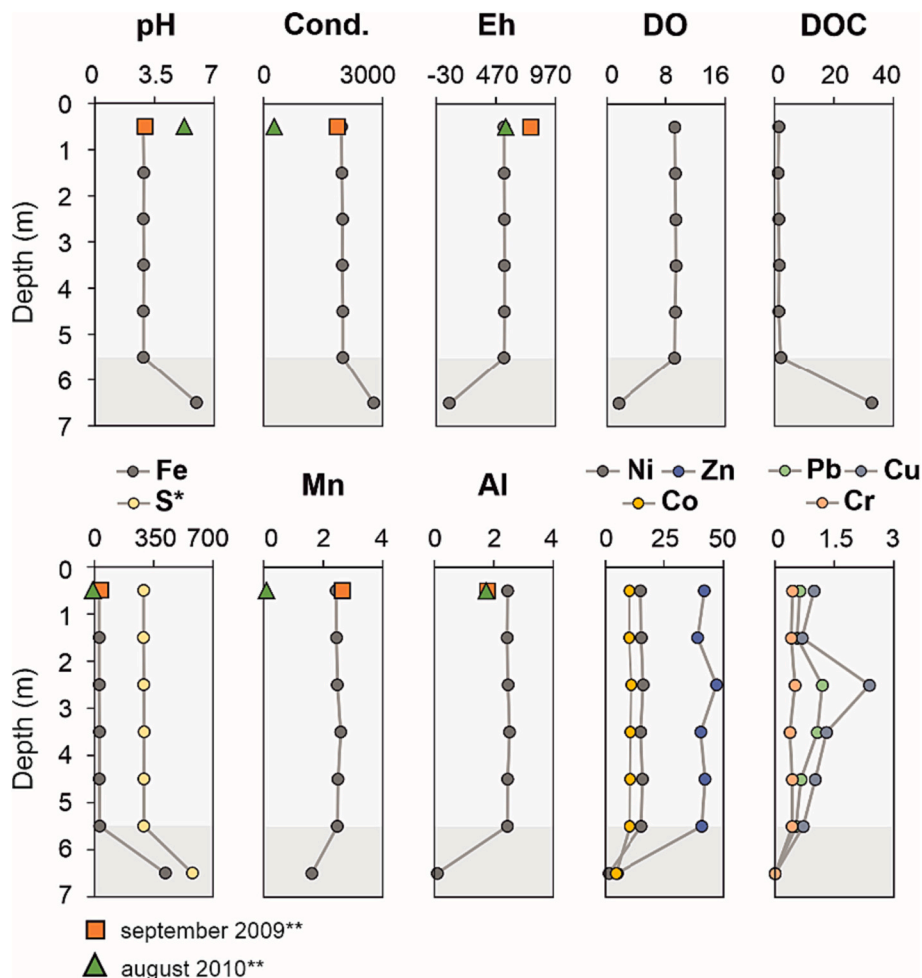
Fig. 3. Vertical distribution of selected physicochemical parameters (pH, Cond. – conductivity (μS cm^{-1}), Eh (mV)), and concentrations of DO (dissolved oxygen), DOC (dissolved organic carbon), Fe, S, Mn, Al (mg L^{-1}) and Ni, Zn, Co, Pb, Cu, Cr (μg L^{-1}) in the water column of Lake ŁK-61. * – data not presented for S from Bożęcki (2013); ** – values reported by Bożęcki (2013).

classification diagram, lake sediment samples were classified as clayey silt and silty clay (Shepard, 1954). The highest clay fraction content (>50 %) was found in the samples collected from depths of 13–18 and 38 cm in the core (Fig. 4). The increased silt fraction content (>60 %) was detected in the samples located at depths of 1, 7, 22, 28, and 40–42 cm. The highest silt fraction content was measured in a sample from a depth of 7 cm (68 %). A significant increase in the sand fraction content was observed in samples collected from depths of 40 cm (2.9 %) and 54 cm (2.8 %) in the sediment column.

3.2.2. Radionuclide distribution

The down-core profile of ^{210}Po activity concentrations was irregular and did not follow a theoretical trend of the vertical distribution of ^{210}Pb$_{ex}$ (assuming a secular equilibrium between these isotopes), which decays exponentially with time, according to the law of radioactive decay (Appleby, 2005; Swarzenski, 2014). Elevated ^{210}Po activity concentrations were detected in samples collected at depths of <3 and 7–11 cm (Fig. 4). The maximum concentration of ^{210}Po activity was registered at a depth of 10 cm in the core (90 ± 3 Bq kg^{-1}). A moderate positive correlation was observed between the concentrations of ^{210}Po activity and the contents of Mn ($R_s = 0.53$), P ($R_s = 0.56$), Sr ($R_s = 0.50$), Zn (R_s
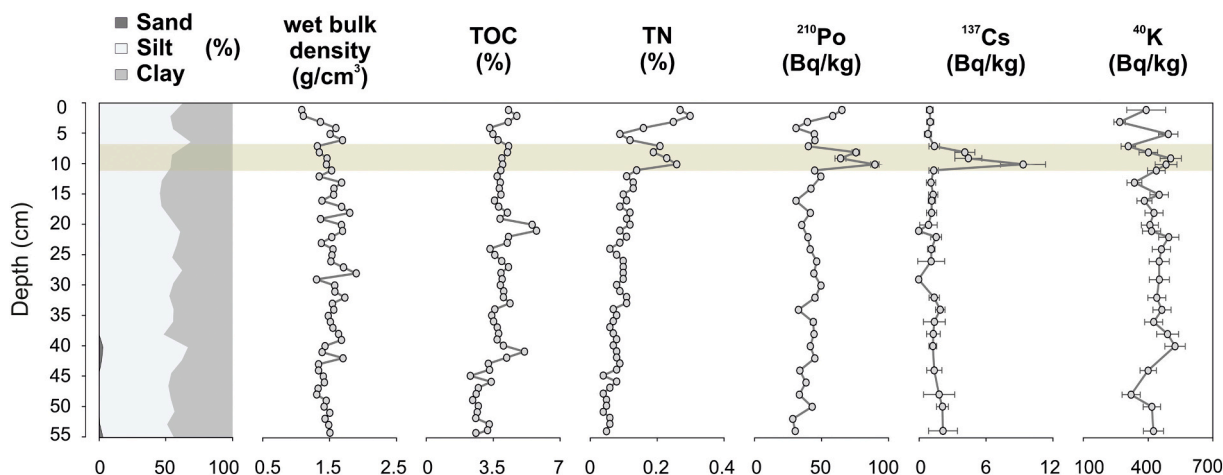
Fig. 4. Down-core profiles of sand, silt, and clay fractions content, wet bulk density, and the concentration of total organic carbon (TOC), total nitrogen (TN), and ^{137}Cs, [210]Po, [40]K activity in Lake ŁK-61. The shaded area represents the probable record of a flood event.

= 0.52), and TN (R_s = 0.52) (Table S5; Supplementary Materials).

The vertical distribution of ^{137}Cs activity concentrations in the collected sediment column was irregular, mostly in its upper part (Fig. 4). In a significant number of samples, the concentration of ^{137}Cs activity was below the detection limit. Elevated concentrations of ^{137}Cs activity were measured in samples located at depths of 7–11 cm in the sediment profile (up to 9 ± 2 Bq kg^{−1}), similar to the case of [210]Po. A slight increase in the ^{137}Cs activity concentration was also noted at depths of 34 cm (1.9 ± 0.4 Bq kg^{−1}) and > 50 cm (2.1 ± 0.5 Bq kg^{−1}). A moderate positive correlation was found between the contents of ^{137}Cs and Mg (R_s = 0.75), Ni (R_s = 0.80), Pb (R_s = 0.74), and Sr (R_s = 0.76) (Table S5; Supplementary Materials).

The vertical distribution of [40]K activity concentrations in the collected core showed a pattern similar to total K, but different than those of [210]Po and [137]Cs (Fig. 4). An increase in [40]K activity concentration was recorded in samples collected at depths of 5, 9–10, 22, 38–40, and > 50 cm. A strong positive correlation between the [40]K activity concentration and the contents of Ba (R_s = 0.92), K (R_s = 0.94), Na (R_s = 0.89), and a moderate positive correlation with Cu (R_s = 0.71) were found (Table S5). Moreover, a strong negative correlation was found between the contents of [40]K and Fe (R_s = −0.84).

3.2.3. Elemental composition

The elemental composition of selected lake sediments is presented in Fig. 5 and Table S2 (Supplementary Materials). The down-core profiles of selected element concentrations were normalized to Al, considering the dominance of alumina-silicate minerals in the catchment area (Loring, 1991). In the upper part of the sediment column, the vertical distribution of almost all elements was significantly disturbed (Fig. 5). The concentrations of most elements (e.g., Na, Mg, P, Cu, Ni, Pb, Zn) notably increased between core depths of 7 and 12 cm. A slightly different vertical distribution, in comparison to the abovementioned elements, was observed for Ca and Mn, where the concentrations of these elements were elevated in samples collected at depths of 1, 3, 7–10, and 16 cm in the core. The Ca content was strongly positively correlated with Mn (R_s = 0.85), P (R_s = 0.73), and TN (R_s = 0.81). The Fe concentration was significantly increased in the upper part of the sediment profile (up to a depth of 3 cm) and at depths of 7, 16–20, and 45 cm. Similarly, the S content was elevated at the top (2–3 cm depth) of the core and slightly elevated at a depth of 7 cm. The contents of Al, Ti, and K were slightly increased in the samples located at depths of 5 cm and > 25 cm in the core.

3.2.4. Mineralogical composition

Quantitative mineralogical analyses using Rietveld refinement were
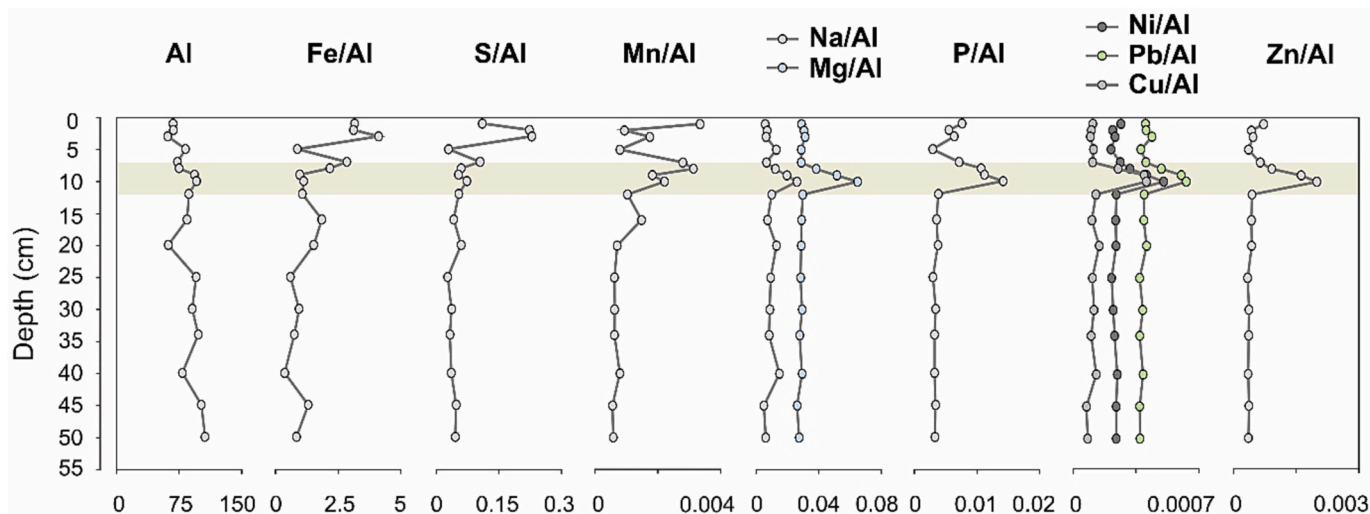
Fig. 5. Vertical distribution of Al content (g kg^{−1}) and normalized concentration profiles of selected elements in the core of Lake ŁK-61. The shaded area represents the probable record of a flood event.

conducted only for selected lake sediments of Lake ŁK-61. Due to the very fine-grained or amorphous nature of a significant fraction of the samples, Rietveld refinement could not be performed to a very high quality and accuracy. XRD analyses showed that the crystalline fraction of the tested samples consists mostly of quartz, kaolinite, and phyllosilicate minerals (possibly muscovite, illite, or smectite group) (Fig. 6). IR analyses showed that the selected lake sediments did not differ significantly from each other (Fig. 7, A). Significant amounts of ferrihydrite and some carbonates were present in the studied samples (e.g., in a sample collected from a depth of 10 cm in the core); however, these could not be reliably quantified from the IR data (Fig. 7, B). However, the amount of ferrihydrite was similar in all lake sediment samples. Qualitatively, the samples displayed very strong fluorescence in Cu-XRD (which is why the analysis was performed using Ag-XRD), indicating a high Fe content. Since no significant crystalline Fe phases could be detected (only very minor amounts of magnetite were found), with the possible exception of sheet silicates, together with the IR data, it can be concluded that ferrihydrite is the major Fe phase in these samples. Small amounts of orthoclase, montmorillonite, vermiculite, magnetite, and dolomite were also detected.

SEM–EDS analyses confirm the XRD results. However, it should be noted that SEM analyses were performed on a slightly wider range of samples. The main minerals found were quartz, kaolinite, and other phyllosilicate minerals. Fe (oxy)hydroxides were present in all samples. However, it seems that their amounts increased as the core depth increased. They generally formed small aggregates with kaolinite and other phyllosilicates, the size of which is up to several hundred microns

(Fig. 8). Fe phases had a similar EDS signal in all studied samples, except for lake sediments collected from depths of 9 and 50 cm in the core, whose chemical composition may correspond to schwertmannite (Fig. 8, C; D). Unfortunately, the rest of the Fe (oxy)hydroxides present in the examined lake sediments could not be distinguished by EDS but rather by observing their morphology. On this basis, it can be assumed that samples collected from depths of 9 and 50 cm in the core may contain two different Fe mineral phases (Fig. 9). We assume that one of these phases represents ferrihydrite; however, its identification was not possible with EDS. Chemical analyses also showed that Fe was adsorbed onto clay minerals. Generally, the Fe content in these mineral phases was approx. a few wt%. Chemical analyses also showed that some elements, such as Ca, Al, Si, P, and Ti, were adsorbed onto Fe (oxy)hydroxides. SEM–EDS studies also revealed the occurrence of accessory minerals, such as Ti oxides, zircon, monazite, and small grains of gold, in all investigated samples.

3.2.5. Diatom analysis

A total of 60 diatom taxa belonging to 35 genera were identified. >300 valves could be identified in only four samples (core depth 1, 8, 9, and 10 cm). In the remaining samples, the frequency of diatoms was not sufficiently high to perform statistical calculations. Samples with a low diatom content were similar to each other. Benthic taxa prevailed in the assemblage. Between 10 and 55 cm, the abundance of diatoms was very low, and the number of valves did not exceed 100 (statistically insignificant). In three subsequent samples (8–10 cm), the number of diatoms increased significantly (over 300 valves, 45 to 50 taxa per sample).
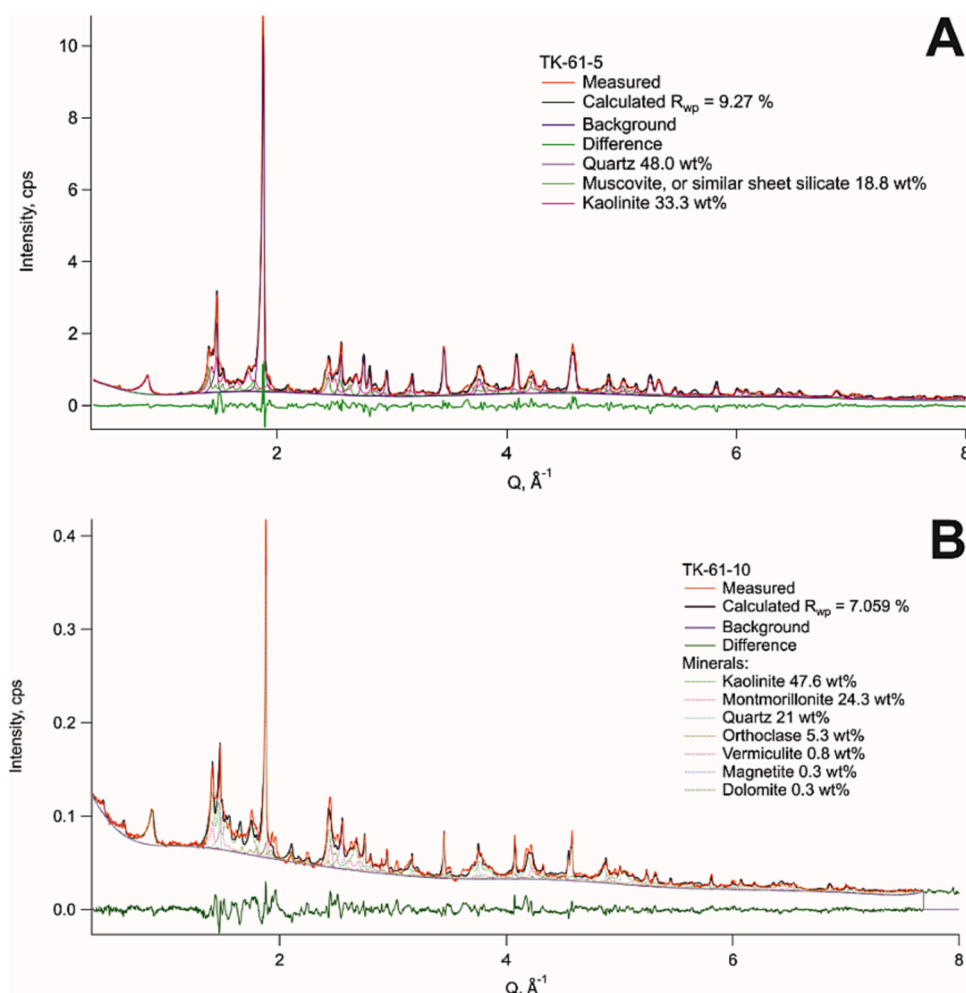
Fig. 6. XRD spectra from selected samples of lake sediments collected at depths of (A) 5 cm and (B) 10 cm in the core of Lake ŁK-61.
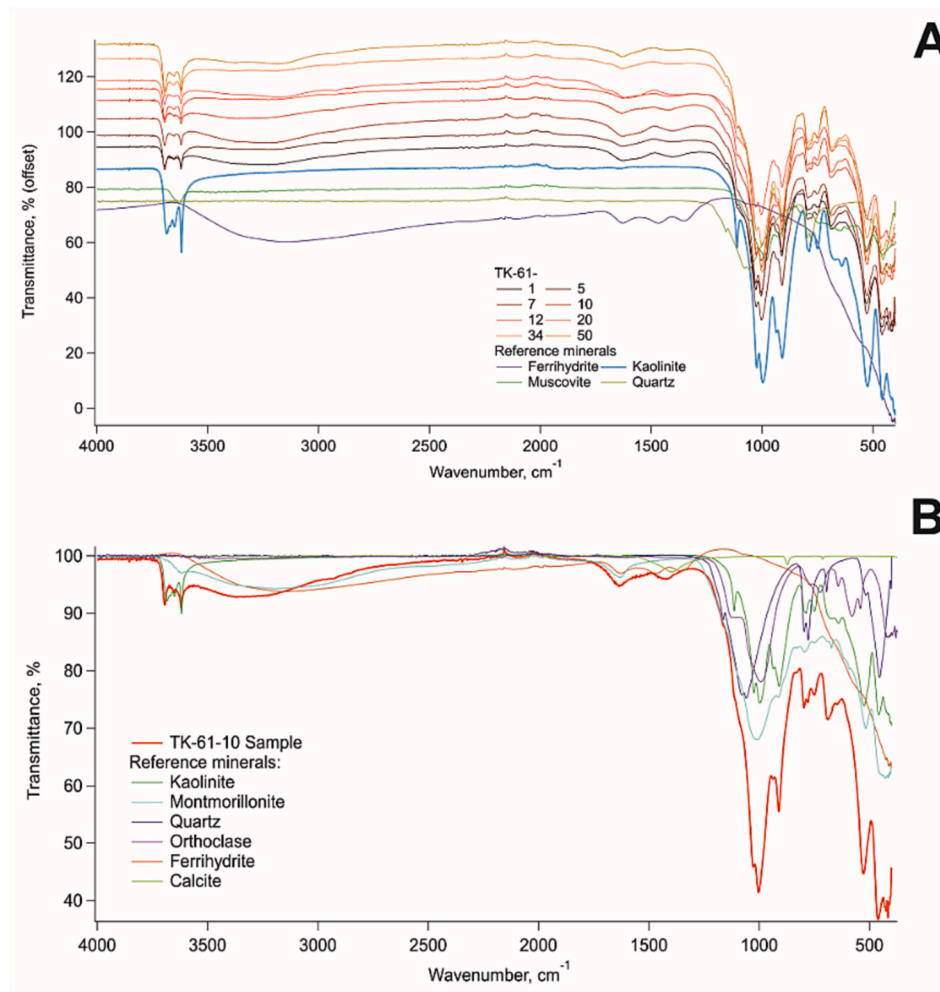
Fig. 7. IR spectra from selected samples of lake sediments collected at (A) different depths and at a depth of (B) 10 cm in the core of Lake ŁK-61.

Moreover, planktonic species appeared in relevant frequency with a simultaneous decline of benthic taxa. A renewed increase in diatom content was observed in the first surface sample, but with less species diversity (only 11 taxa). This sample contained the same dominant taxa as in the low–diatom samples.

3.2.6. DI–pH and geochemical modeling

The reconstruction of the past water pH was based on diatoms from only four samples (core depth 1, 8, 9, and 10 cm) where the frequency of valves was statistically significant (>300). The root-mean square error for the training set (RMSE) was 0.49, and the coefficient of correlation ($R2$) was 0.94. The fluctuations in the water pH in Lake ŁK-61 were as follows: 3.19 (1 cm), 7.02 (8 cm), 7.13 (9 cm), and 6.99 (10 cm). Changes in the DI–pH values were large and amounted to 3.94 pH units. In the modern calibration dataset, the occurrence of fossil diatoms ranged from 89.6 to 100 %. According to the modern analog technique (MAT analysis), the minimum DC values were as follows: 45.9 (1 cm), 133.2 (8 cm), 122.4 (9 cm) and 128.3 (10 cm). The threshold above which fossil taxa had no close analogs in the training set was 72.5. It appears that samples 8, 9 and 10 should be treated with caution.

The results of geochemical modeling based on the elemental composition of the lake water collected from depths of 0.5 and 6.5 m in the water column of Lake ŁK-61 are presented in Tables S6 and S7 (Supplementary Materials), respectively. In addition, the results of geochemical modeling based on the data provided by Bożęcki (2013) for the surface water of Lake ŁK-61 collected in August 2010 are presented in Table S8 (Supplementary Materials).

4. Discussion

4.1. Geochemical characteristics of Lake ŁK-61

Lake ŁK-61 was classified into the group of the youngest pit lakes in the so-called 'anthropogenic lake district' in the Muskau Arch in western Poland, and it is characterized by the lowest water pH values and the highest EC and water hardness values (Oszkinis-Golon et al., 2021; Pukacz et al., 2018). The relatively high content of total dissolved solids (TDS >1960 mg L^{-1}) reflected in the elevated EC values of the lake water can be explained by high solubility of solids in an acidic environment (e.g., Sánchez-España et al., 2008; Friese et al., 1998; Schultze et al., 2010; Stumm and Morgan, 1996). Moreover, the negative correlation between the water pH and the sum of ions may be related to the degree and extent of mass input and pyrite dissolution in the study area (Friese et al., 1998). Similar features, such as a low water pH and increased content of dissolved elements (e.g., Ca, Fe, Mg, Mn, and S), were also recorded in nearby pit lakes (Pukacz et al., 2018). The observed similarities are likely related to the common origin of these lakes, i.e., the exploitation of the same lignite seam (Koźma, 2009). The lower contents of Fe and Al in the lake water are characteristic features of Lake ŁK-61 and are probably related to the differences in the bedrock geology in this area (Bartczak and Gancarz, 1998; Lutyńska and Labus, 2015).

An important source of dissolved elements and possibly solid particles in Lake ŁK-61 is its tributary, which is indicated by the similarity in the elemental composition of the lake inflow and the epilimnion (Table
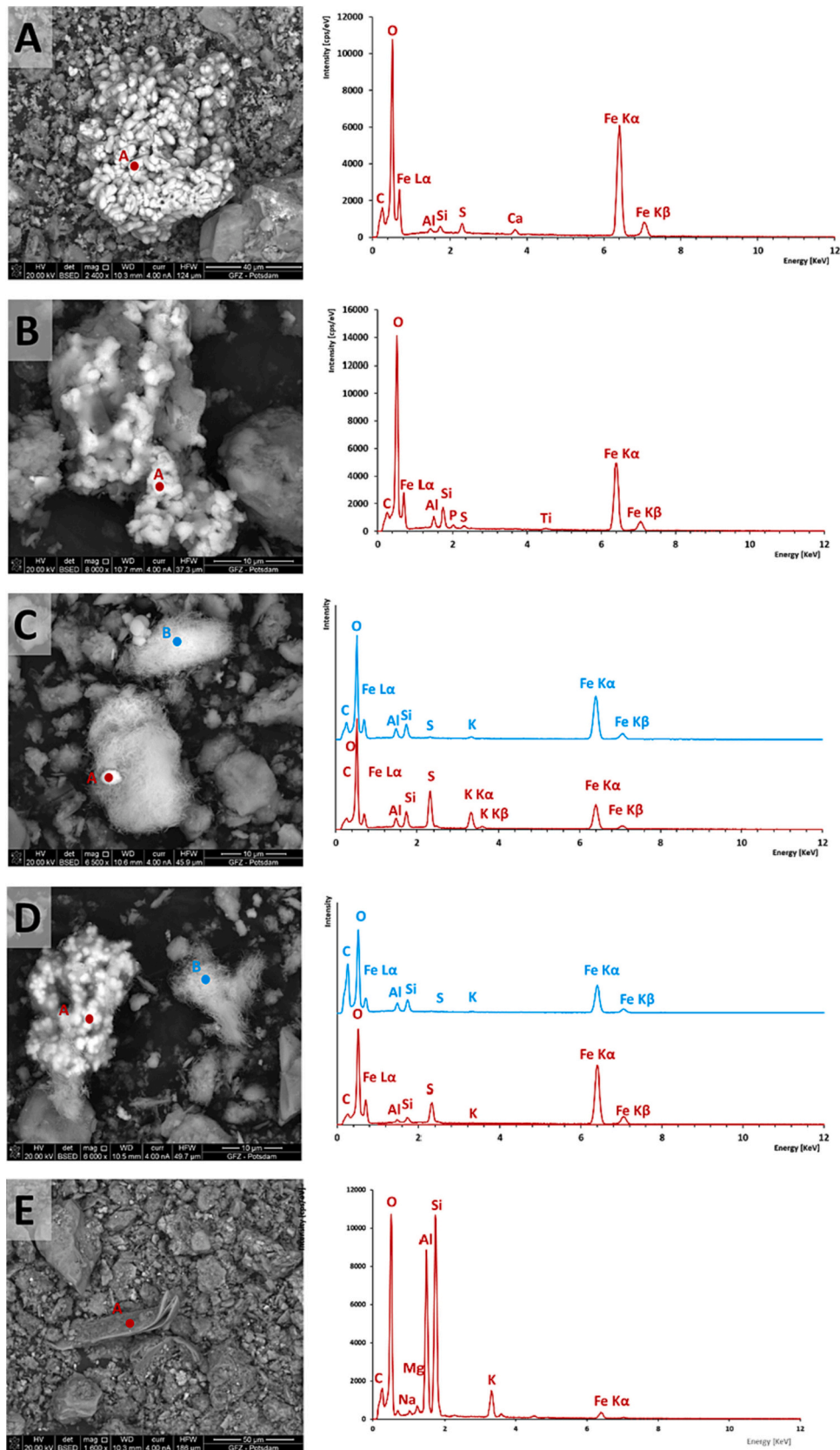
Fig. 8. Chemical composition of minerals found at depths of (A) 5 cm, (B) 7 cm, (C) 9 cm, (D) 50 cm, and (E) 34 cm in the collected core of Lake ŁK-61.
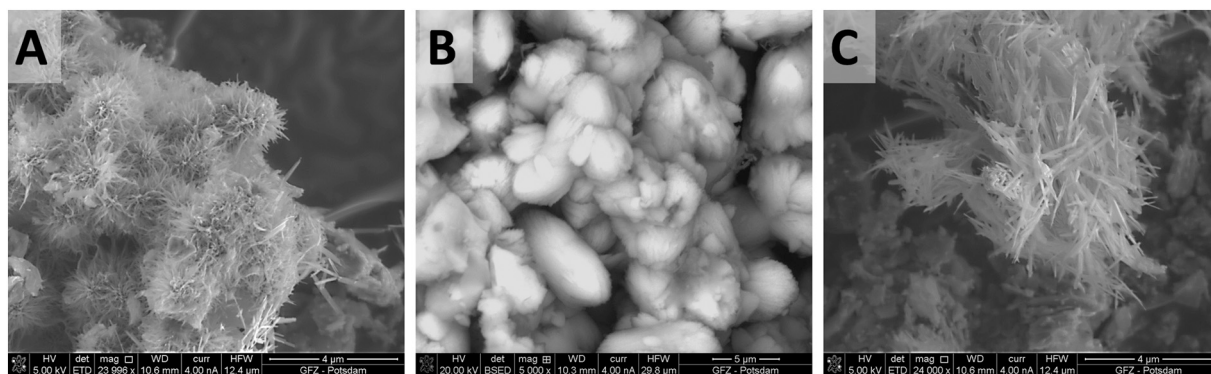
Fig. 9. Different types of (A, B) iron (oxy)hydroxides and (C) schwertmannite found at depths of (A) 50 cm, (B) 7 cm, and (C) 9 cm in the collected core of Lake ŁK-61.

S1). The elemental composition of the Lake ŁK-61 water is dominated by S and Ca, which has also been observed in some pit lakes in the Lusatian lignite district in Germany (Friese et al., 1998). Other dominant elements are Fe and Mg, but they are present in lower concentrations compared to Ca and S (Table S1). The increased contents of Fe and S are likely the result of pyrite oxidation in this area (Geller et al., 2013; Labus and Skoczyńska-Gajda, 2013). Elevated concentrations of Ca and Mg can, therefore, be a consequence of acidity buffering caused by this process (dissolution of carbonates, silicates, etc.), weathering of rocks forming embankments and mining areas, and the influx of dissolved solids carried from the catchment area (e.g., Schultze et al., 2010; Wisotzky, 1998). The observed increase in the content of dissolved heavy metals (e.g., Co, Ni, Zn) in the Lake ŁK-61 water is likely also the result of pyrite decomposition and subsequent acid leaching of the associated rocks (Fig. 3; Table S1) (Wisotzky, 1998). However, it should be noted that the observed heavy metal contents are not as high as, for example, those in some pit lakes of the Iberian Pyrite Belt in Spain due to different primary sulfide mineralization (Sánchez-España et al., 2008).

The available literature data show that, apart from episodic events, the physicochemical parameters and elemental composition of the water in Lake ŁK-61 have not changed significantly over the years (Bożęcki, 2013; Gąsiorowski et al., 2021; Lutyńska and Labus, 2015; Oszkinis-Golon et al., 2021; Pukacz et al., 2018). This indicates that the neutralization process in Lake ŁK-61 is very slow, which is considered typical for pit lakes with extremely acidic water (pH <3) (Sienkiewicz and Gasiorowski, 2016). To our knowledge, one of the significant changes in the geochemical characteristics of the Lake ŁK-61 ('Hydro' in Bożęcki (2013)) water was observed in the summer of 2010 (Bożęcki, 2013). The recorded changes were most likely caused by the flood on the Nysa Łużycka River at the beginning of August 2010 (MKOO, 2010). At that time, a significant increase in the water pH (up to 5.3) and a decrease in the water conductivity (EC = 268 μS cm^{-1}) were registered (Fig. 3; Table 1; S1) (Bożęcki, 2013). Moreover, a decrease in the concentration of Ca, Fe, Mg, Mn, Na, Cl$^-$, NO$_2^-$, and SO$_4^{2-}$, as well as an increase in the concentration of NO$_3^-$ and PO$_4^{3-}$, was also observed (Fig. 3; Table S1).

4.2. Major elements and trace metals in the water column

The conducted research showed that ŁK-61 is a stratified lake, which has been also described by Gąsiorowski et al. (2021). A similar development of stratification in the water column was observed in other pit lakes in this area (e.g., Lutyńska and Labus, 2015), as well as in Germany (e.g., Schultze et al., 2010), the Czech Republic (e.g., Hrdinka et al., 2013), and Spain (e.g., Sánchez-España et al., 2008). The stratification of the water column in Lake ŁK-61 is relatively similar to that observed, for example, in the Cueva de la Mora, Filón Centro (Tharsis), and Herrerías pit lakes in Spain, characterized by oxygenated mixolimnion and

anaerobic monimolimnion with an increased water pH and TDS content (Sánchez-España et al., 2009). The vertical distribution of selected elements in the water column showed similar patterns, as in other acidic pit lakes, where the concentration of dissolved elements, such as Fe, increases in the bottom zone (Fig. 3; Table S1) (e.g., Friese et al., 1998; Ramstedt et al., 2003; Sánchez-España et al., 2009). This phenomenon is likely related to the limited supply of oxygen to the hypolimnion, which causes some substances (e.g., ferrous iron, sulfide, DOC) to be in a chemically reduced form (Boehrer et al., 2017). Moreover, it can also be explained by the reductive dissolution of Fe secondary minerals, which leads to the release of Fe^{2+} and SO$_4^{2-}$ and an increase in the water pH (>5) (e.g., Sánchez-España et al., 2009). The development of reducing conditions responsible for these processes can also be related to oxygen consumption as a result of the decomposition of OM (Boehrer and Schultze, 2008; Davison, 1993; Ramstedt et al., 2003; Stumm and Morgan, 1996).

The K content also increases in the hypolimnion of Lake ŁK-61, which hypothetically can be caused by the reductive dissolution of sulfate minerals (e.g., K-jarosite) (Dutrizac, 2008; Hrdinka et al., 2013). On the other hand, this hypothesis is questionable in our case because the water pH of the epilimnion (pH = 2.85) is higher than that at which jarosite commonly precipitates (pH <2.5) (Paikaray, 2020). Moreover, geochemical modeling indicated that the Lake ŁK-61 water is unsaturated with respect to the jarosite under prevailing conditions. Another reason for the increase in K concentration downward through the water column is the decomposition of aluminosilicates (e.g., potassium feldspar), which can be components of the rocks forming the embankments and catchment area of Lake ŁK-61 (Bożęcki, 2013; Lutyńska and Labus, 2015).

The vertical distribution of Mn content in the water column does not follow the same trend as in the case of Fe and S, although reductive dissolution of Mn-bearing minerals has also been observed in pit lakes (Fig. 3) (Davison, 1993; Friese et al., 1998; Sánchez-España et al., 2009; Schultze et al., 2017). Moreover, other elements that could have been incorporated into the structure/adsorbed onto the surface of the Mn and Fe precipitates were also expected to be released to the aqueous phase as a result of the decomposition of these minerals under anoxic conditions (Hrdinka et al., 2013; Sánchez-España et al., 2009; Shi et al., 2021; Torres et al., 2013). Such an increase in the contents of Fe and Mn downward through the water column, together with Ca, K, Na, and Mg, was recorded, for example, in Udden pit lake in northern Sweden (Ramstedt et al., 2003). However, in our case, an opposite trend was observed in the vertical distribution of concentrations of some major elements (e.g., Al, Ca, Mg, Mn, Si) and heavy metals (e.g., Co, Cu, Ni, Pb, Zn) (Fig. 3; Table S1). This phenomenon can be hypothetically explained by the sorption of these elements, among others, by more thermodynamically stable Fe secondary minerals (such as hematite and goethite), whose precipitation from the water phase was suggested by geochemical

modeling (Table S6, S7) (Shi et al., 2021).

Other mechanisms responsible for the retention of particular elements in the hypolimnion of Lake ŁK-61 may be their coprecipitation/precipitation and adsorption onto Al secondary minerals (e.g., kaolinite), the formation of which was indicated by geochemical modeling (Table S7) (Nordstrom and Ball, 1986; Sánchez-España et al., 2006, 2016; Schultze, 2013). This hypothesis can be supported by a significant decrease in the Al concentration in this part of the water column (Fig. 3; Table S1). Such a phenomenon was observed, for example, in pit lake Cueva de la Mora in Spain, where the precipitation of Al oxyhydroxysulfates (e.g., alunite) according to the depth of the water column was associated with simultaneous adsorption/coprecipitation of Cu (Sánchez-España et al., 2009). The decrease in the content of the abovementioned elements in the bottom zone (pH >6) of Lake ŁK-61 can also be linked to their uptake by allochthonous minerals, such as clay minerals, which predominated in the examined samples (Fig. 6). An increase in water pH may additionally enhance the removal of metal ions, e.g., by kaolinite clay, which shows better sorption properties at higher pH values (Jiang et al., 2010).

It is also possible that the precipitation of metal sulfides has led to a decrease in the trace metal contents across an oxic–anoxic interface, as was noticed, for example, in the Sancho Reservoir in Spain (Friese et al., 1998; Ramstedt et al., 2003; Schultze et al., 2017; Torres et al., 2013). On the other hand, this hypothesis is questionable in our case because the mineralogical analysis did not reveal the presence of metal sulfides in the examined lake sediment samples (except for framboidal pyrite). Vink et al. (2010) suggested that DOC may provide bonding sites for metals released by the reductive dissolution of secondary minerals when sulfides have not yet been formed (Davis, 1984; Christensen et al., 1999; Eyrolle and Benaim, 1999). This explanation may theoretically apply to our case, as the DOC content in the hypolimnion of Lake ŁK-61 increases significantly to 32.7 mg L^{-1} (Fig. 3).

4.3. Major elements and trace metals in lake sediments

The results also showed that Lake ŁK-61 is characterized by acidic water (pH <3) and sediments with a pH close to neutral, as inferred from the water pH (pH >6) measured in the hypolimnion (the pore water pH was not measured) (Fig. 3; Table 1). Friese et al. (1998) suggested that the increase in alkalinity in these types of lakes is related to the reduction of sulfates and degradation of OM. Compared to a lake of this type, such as ML-Halbendorf in Lusatia, Lake ŁK-61 is characterized by bottom sediments with a relatively similar content of Fe and particular trace metals, such as Cu, Ni, and Zn (Table S2) (Friese et al., 1998). The difference can be seen mainly in the concentrations of Al and Mn, which in our case were much higher than those in the lake sediments of ML-Halbendorf. Moreover, the Fe content in the surface layer of the collected core (213 g kg^{-1}) was found to be relatively similar to that measured in Waldsee Lake (269 g kg^{-1}) in Lusatia, which is also a pit lake characterized by a hypolimnion with a water pH of approx. 6 and prevailing anaerobic conditions (Friese, 2004). Compared to the elemental composition of the bottom sediments of other pit lakes in the Muskau Arch in Poland, the surface lake sediments of Lake ŁK-61 contain higher amounts of Al and Fe and lower amounts of Ca, Mn and P (Gąsiorowski et al., 2021). On the other hand, pit lakes located in close proximity to the studied lake (sites 57–62; according to Gąsiorowski et al. (2021)) are characterized by lake sediments with slightly higher contents of Fe and, in some cases, Mn, which likely indicate differences in the bedrock geology and degree of pyrite dissolution.

The elevated content of Fe in the bottom sediments of Lake ŁK-61 is related to the high abundance of Fe secondary minerals, such as ferrihydrite (Figs. 7, 8). Other Fe precipitates, such as poorly crystallized schwertmannite, were found in samples collected from deeper layers in the sediment column (e.g., at depths of 9 and 50 cm) (Fig. 8, C; D). We suspect that the precipitation of this mineral has been related to the changes in the physicochemical properties of the lake water in Lake ŁK-

61, which was discussed in more detail in Section 4.5. Geochemical modeling also indicates the precipitation of other Fe mineral phases, such as goethite and hematite, but we were unable to confirm these models based on mineralogical analyses (Tables S6, S7).

The Al content in the surface layer of the collected sediment column (67.7 g kg^{-1}) was only slightly lower than that measured in the surface lake sediments (99.3 g kg^{-1}) of Lake ŁK-41 (water pH = 7.4) in the Muskau Arch (Poland), which is a pit lake created as a result of clay mining (Gąsiorowski et al., 2021; Sienkiewicz and Gąsiorowski, 2018). This phenomenon can be related to the presence of large amounts of clay minerals (e.g., kaolinite), which are likely transported to Lake ŁK-61 from nearby deposits of kaolinite clays (Figs. 6, 7) (Koźma, 2009; Gruszecki et al., 2006). The presence of numerous Al-bearing minerals can also be related to the physical disaggregation of pit walls and embankments (Sánchez-España et al., 2008). We also suspect that some Al secondary minerals (e.g., kaolinite) precipitated directly from the water column, as indicated by geochemical modeling (Table S7) (see Section 4.2). It should be highlighted, however, that the distinction between authigenic and allogenic kaolinite in the collected samples was difficult, as also noted by Sánchez-España et al. (2016). Titanium, another dominant element (arithmetic mean = 6.5 g kg^{-1}) in the collected lake sediments, seems to be associated with Al (R_s = 0.86) (Table S5). This relationship can be explained by the fact that kaolinite clays occurring in this region are relatively rich in TiO_2 (approx. 1.7 wt%) (Gruszecki et al., 2006). Most likely for this reason, accessory minerals containing Ti, such as titanium oxides, were found in the examined lake sediments during SEM–EDS analyses.

The next most abundant element in the bottom sediments of Lake ŁK-61 was K (arithmetic mean = 14.5 g kg^{-1}). Such a high content of K can be explained by the presence of significant amounts of K-bearing minerals (e.g., orthoclase and muscovite), as confirmed by mineralogical analyses (Figs. 6, 7). These minerals may come from the eroded pit walls, embankments, and the catchment area of Lake ŁK-61. This hypothesis is supported by a significant positive correlation between the contents of K and ^{40}K (R_s = 0.94), which can be used as an indicator of the input of allochthonous minerals, such as potassium feldspars, phyllosilicates, etc. (Bobos et al., 2021; Madruga et al., 2014; Somboon et al., 2018). Based on SEM–EDS analysis, it was also observed that some amounts of K and other major elements, such as Ca, Na, Mg, Ba, Sr, and P, are adsorbed on the surfaces of clay minerals and Fe phases. Moreover, only a few minerals containing other major elements, such as Ca (e.g., gypsum) and Ba (e.g., barite), were found in the examined samples during SEM–EDS analyses. This phenomenon can be explained by the fact that the presence of particular major elements (such as Ca) in the form of authigenic chemical precipitates is rather unlikely at a water pH <3 (Sánchez-España et al., 2008).

Heavy metals (such as Cr, Cu, Ni, Pb, Zn) are most likely associated with Fe and Al precipitates in the bottom sediments of Lake ŁK-61 through precipitation/coprecipitation processes (Cánovas et al., 2007; Hierro et al., 2014; Shi et al., 2021) (see Section 4.2.). Some trace metals are also likely adsorbed onto the surface of Fe (oxy)hydroxides, characterized by good retention capacity due to their large surface areas and high reactivity (Acero et al., 2006; Makvandi et al., 2021; Rose and Bianchi-Mosquera, 1993; Zhu et al., 2012). Similarly, these elements can also be immobilized by allochthonous Al-bearing minerals (e.g., clay minerals) because of their high sorption capacity (e.g., Carrero et al., 2015; Durrant et al., 2018; Jiang et al., 2010). It should be noted, however, that we cannot fully confirm this hypothesis by mineralogical analyses, as the concentrations of trace metals were below the detection limit of the techniques used (e.g., SEM–EDS). The mechanisms controlling the vertical distribution of the concentrations of the studied heavy metals in the collected sediment profile are discussed in more detail in Section 4.5.

4.4. Distribution of radionuclides in lake sediments

^{210}Po and its progenitor ^{210}Pb are likely immobilized in the bottom sediments of Lake ŁK-61 by allochthonous minerals (e.g., clay minerals), as well as by Fe and Al precipitates (Carvalho et al., 2017; Cook et al., 2018; Ram et al., 2021; Shi et al., 2021). ^{210}Po can also be associated with Mn-bearing minerals, as indicated by a moderate positive correlation between the concentrations of Mn and ^{210}Po activity ($R_s = 0.53$) in the collected samples (Table S5) (Benoit and Hemond, 1990; Carvalho et al., 2017; Yang et al., 2013). It is also worth noting that ^{210}Po shows a moderate positive correlation with TN ($R_s = 0.53$) and P ($R_s = 0.53$), which may indicate its relationship with delivered nutrients (Table S5). The presence of the studied radioisotopes may also be related to sulfates (e.g., anglesite, barite, celestine, gypsum), which are good hosts for ^{226}Ra, and indirectly also for its daughter radioisotopes, including ^{210}Pb and ^{210}Po (Cook et al., 2018). On the other hand, this hypothesis is doubtful in our case since only a few barite and gypsum crystals were found in the examined samples during SEM–EDS analyses. It is also unlikely that these radionuclides were captured by sulfides, since the presence of these minerals (except for framboidal pyrite) in the collected lake sediments was not confirmed by mineralogical analyses (Carvalho et al., 2017; Ram et al., 2019).

The down-core profile of ^{210}Po activity concentrations was significantly disturbed and did not follow the exponential curve, as can be theoretically expected in undisturbed sediment profiles, according to the law of radioactive decay (Fig. 4) (e.g., Appleby, 2005; Swarzenski, 2014). Therefore, calculating the detailed age of the collected lake sediments (assuming equilibrium with ^{210}Pb) was impossible using the ^{210}Pb dating technique. Similar disturbances in the vertical distribution of ^{210}Po activity concentrations were observed, for example, in the cores collected from lakes affected by increased S and N inputs – Mały Staw (pH = 6.2) and Wielki Staw (pH = 5.2) in the Sudety Mountains in Poland (Sienkiewicz et al., 2006). In these cases, landslips, sediment slumps, and avalanches were suggested as possible causes of these disturbances. Another example is pit lake TR-33 (pH = 6.5) in the Muskau Arch in Poland, where the down-core profile of ^{210}Pb activity concentrations was altered by horizons of interbedded clay (Sienkiewicz and Gasiorowski, 2016). We suspect that in our case this phenomenon may be linked to another depositional event, such as a flood (see Section 4.5).

Radiocesium in the bottom sediments of Lake ŁK-61 can originate from its direct atmospheric deposition after the Chernobyl accident, as well as from the subsequent wash off of solids and OM from the surrounding areas, which could have incorporated ^{137}Cs during its initial deposition (e.g., Ashraf et al., 2014; Beresford et al., 2016; Naulier et al., 2017). The concentrations of ^{137}Cs activity in the surface lake sediments (1.0 ± 0.3 Bq kg^{-1}) of Lake ŁK-61 are much lower compared to, for example, Turawa Dam Lake (southwestern Poland), where the highest content of ^{137}Cs in the surface lake sediments was 103 ± 12 Bq kg^{-1} (Sekudewicz and Gąsiorowski, 2022). This difference is related to the fact that the average value of ^{137}Cs deposition in the soils (0.39 ± 0.10 kBq m^2) of the Lubuskie Voivodship (where Lake ŁK-61 is located) is one of the lowest compared to other provinces of Poland (Isajenko et al., 2022). For comparison, the maximum concentration of ^{137}Cs activity (9.4 ± 2.0 Bq kg^{-1}) measured in the collected core was slightly lower than those found in other pit lakes in the Muskau Arch in Poland, e.g., in Lake TR-17 (16.2 ± 3.4 Bq kg^{-1}; water pH = 5.2) and Lake ŁK-46 (20.9 ± 3.6 Bq kg^{-1}; water pH = 3.6) (unpublished data; sites according to Gąsiorowski et al. (2021)).

Most likely, ^{137}Cs in the bottom sediments of Lake ŁK-61 is immobilized by clay minerals (e.g., smectite group), whose presence in the examined samples was confirmed by mineralogical analyses (Figs. 6, 7) (Park et al., 2021; Walling and Quine, 1993; Zapata and Nguyen, 2009). This is due to the high affinity of Cs$^+$ for the 2:1 clays, i.e., illite and smectite group (Cornell, 1993; Durrant et al., 2018; Mukai et al., 2016; Park et al., 2019; Sawhney, 1972). Moreover, ^{137}Cs can be associated with 1:1 layered clays, such as kaolinite, which was relatively common

in the collected lake sediments (Fig. 6). However, it should be noted that sorption onto kaolinite is much less efficient than that onto 2:1 layered clays due to its lower cation exchange capacity (CEC) and absence of frayed edge sites (FES) (Durrant et al., 2018). Moreover, the uptake of ^{137}Cs by clay minerals may be limited in the studied lake, as competition between Cs$^+$ and H$^+$ ions may occur at low pH (<4) (Belousov et al., 2019; Fuller et al., 2014). On the other hand, Fuller et al. (2014) suggested that this may be significant in the case of high concentrations of ^{137}Cs (allowing for FES saturation). We also assume that the precipitation of Fe (oxy)hydroxides or other secondary minerals in Lake ŁK-61 has a rather insignificant effect on ^{137}Cs retention since its coprecipitation is rather negligible (Lieser and Steinkopff, 1989). Moreover, ^{137}Cs adsorption onto Fe or Al precipitates is rather unlikely because the presence of other monovalent cations (e.g., K$^+$, Na$^+$) can practically eliminate Cs$^+$ adsorption (McKinley et al., 2001).

The increased ^{137}Cs activity concentrations at depths of 7–11 cm in the collected core are hardly linked to its direct atmospheric deposition after the Chernobyl accident. This is because the peak of ^{137}Cs content coincides with elevated concentrations of elements of different origins (e.g., Cu, Ni, Pb, Na, Mg, Sr) (Figs. 4, 5) (Appleby, 2008; Ashraf et al., 2014; Beresford et al., 2016; Smith and Beresford, 2005). We assume that the strong positive correlation between the contents of ^{137}Cs and Ni ($R_s = 0.80$), and Pb ($R_s = 0.74$) indicates their common origin but an origin that is different from the direct Chernobyl fallout (Table S5). Consequently, ^{137}Cs hardly provides reliable geochronological dating; nevertheless, it might serve as a chronostratigraphic marker that is likely related to the 2010 flood (see Section 4.5). We also suspect that a slight increase in the concentration of ^{137}Cs activity in the bottom part of the core (depth > 50 cm) may hypothetically correspond to 1986 (Fig. 4). Unfortunately, the limitations of the sampling method preclude the investigation of the deeper sediment deposits.

4.5. The potential impact of flooding on the distribution of selected heavy metals and radionuclides in lake sediments

As already mentioned, the vertical distributions of HMRs content were significantly disturbed in the upper part of the collected sediment profile (Figs. 4, 5). We suspect that an increase in the concentrations of some elements, such as Ca, Mn, Fe, and S, in the top part (depth of 0–3 cm) of the core is related to the presence of Fe and Mn mineral phases and carbonates that have not yet been dissolved under reducing conditions (see Section 4.2.). On the other hand, an almost threefold increase (compared to the average) in the contents of some major elements (e.g., Na, N, Mg, P), heavy metals (e.g., Cu, Ni, Pb, Zn), and radionuclides (^{137}Cs and ^{210}Po) between depths of 7 and 12 cm in the sediment column of Lake ŁK-61 cannot be explained in this way (Figs. 4, 5). Similar increases in the contents of Ni and Zn were observed, for example, in the sediment profile (4–7 cm depth) of ML-F Lake in Lusatia, where it was linked to the change from aerobic to anaerobic conditions and precipitation of metal sulfides (Friese et al., 1998). In our case, however, such an explanation is doubtful because the mineralogical analyses did not show the presence of metal sulfides (except for framboidal pyrite) in the examined samples (see Section 4.2.). Moreover, the observed down-core profiles of HMRs content do not seem to be significantly related to the cycling of Fe and S, as no significant or moderate negative correlation was found between the concentrations of these particular elements (Table S5).

The most likely scenario explaining such vertical distributions of the HMRs content in the collected core is a past change in the physico-chemical parameters of Lake ŁK-61 water. This is indicated by the diatom-inferred pH model, which shows pH values ~7 ± 0.5 at depths of 8–10 cm in the core. We assume that this change was caused by the flood of the Nysa Łużycka River in the summer of 2010 (MKOO, 2010). This assumption can be confirmed by the recorded shift in the water pH (from 2.9 to 5.3) at that time by Bożęcki (2013) (Fig. 3; Table 1). Moreover, the author also observed a decrease in the concentration of, e.g., Fe, Mn, Ca,

Na, SO_4^{2-}, and Cl^-, and an increase in the concentration of, e.g., NO_3^- and PO_4^{3-}, in the lake water during that period (Table S1). We suspect that the decrease in the concentration of the abovementioned elements at that time was caused by the 'dilution effect', as well as by coprecipitation/precipitation and adsorption of dissolved solids onto newly formed precipitates. A similar phenomenon was observed, for example, in the Rio Tinto River in Spain, where water oversaturated in kaolinite was found only when the pH increased (~5) during high floods (Cánovas et al., 2007). In our case, this hypothesis may be supported by geochemical modeling performed on the basis of data presented by Bożęcki (2013) and by mineralogical analyses of selected lake sediments (Fig. 8, C; Table S8). We suspect that as a result of these processes, a certain amount of HMRs have been retained and buried in the bottom sediments of the studied lake, forming an enriched sediment layer (Figs. 4, 5).

The flood could have carried uncontaminated particles, which (as fresh sorption sites) possibly captured dissolved elements, as observed, for example, in the Coledale Beck catchment in the UK (Mayes et al., 2021). Moreover, the possible concurrent influx of buffering sedimentary material (e.g., calcite) could have caused the lower acidity of the lake water, as observed by Bożęcki (2013) at that time (Table 1) (Herzsprung et al., 2010). An increase in the water pH likely enhanced the sorption of pollutants onto supplied detrital material to Lake ŁK-61, such as kaolinite, which showed better sorption properties at higher pH values (Jiang et al., 2010). The increase in the HMRs content in the upper part (depths of 7–12 cm) of the core can also be explained by the input of dissolved and suspended matter contaminated with heavy metals, as was observed, for example, in Goitsche Lake in Germany (Herzsprung et al., 2010). The influx of detrital material to Lake ŁK-61 during the flood can be evidenced by an increased ^{137}Cs activity concentrations (which can be used as an important indicator of soil erosion and its redistribution) in this sediment layer (Fig. 4) (Walling and Quine, 1993; Zapata and Nguyen, 2009). Moreover, an increase in the C/N ratio (>20) in samples collected from depths of 7–10 cm in the core also indicates the influx of allochthonous OM (e.g., vascular land plants) into the studied lake (Meyers and Ishiwatari, 1995). Hence, it can be assumed that the source of contamination could have also been the supplied OM, which possibly contained certain amounts of previously incorporated HMRs, considering their bioavailability (Ashraf et al., 2014; Carvalho et al., 2017; Yang et al., 2013). We also suspect that the Nysa Łużycka River has supplied some amounts of ^{210}Po and presumably ^{210}Pb to the studied lake, as it was found that the annual surface flow for ^{210}Po is relatively high (245 kBq year^{-1}) in this river (Skwarzec et al., 2012). Moreover, a moderate positive correlation between the concentrations of ^{210}Po activity and the contents of other elements, such as Mn, P, N, Sr, and Zn, indicates their similar origin (Table S5).

We also suspect that the fertilizers were also delivered into Lake ŁK-61 during the flood, as interpreted from the recorded increase in the concentrations of NO_3^- and PO_4^{3-} in the lake water in the summer of 2010 (Table S1) (Bożęcki, 2013). This past phenomenon could be reflected in the currently observed elevated TN and P content in the upper part (depths of 7–12 cm) of the core (Figs. 4, 5). A moderate positive correlation between the contents of ^{210}Po and P ($R_s = 0.56$) may confirm this hypothesis because phosphate fertilizers are known to be the main anthropogenic source of ^{210}Pb and ^{210}Po (Barbero et al., 2014; Carvalho et al., 2017). We also assume that the increase in the water pH and the supply of nutrients have increased the primary productivity and algal species diversity (as observed from the subfossil diatom studies), which could have played an important role in the scavenging and thus immobilization of HMRs in the bottom sediments of Lake ŁK-61 (Kleeberg and Grüneberg, 2005; Paulsson and Widerlund, 2021; Schultze, 2013).

5. Conclusions

The main processes controlling the distribution of selected heavy metals (e.g., Cu, Ni, Pb, Zn) and radionuclides (^{137}Cs and ^{210}Po) in acidic pit lake ŁK-61 in the Muskau Arch in Poland are: 1) mineral dissolution, 2) coprecipitation/precipitation with Fe and Al secondary minerals, and 3) sorption processes with authigenic and allogenic phases.

The mineralogical analyses and geochemical modeling indicated that Fe secondary minerals (e.g., ferrihydrite) precipitate in the epilimnion (pH <3), while Al-bearing minerals (e.g., kaolinite) can also be formed under reducing conditions in the hypolimnion (pH >5) of Lake ŁK-61. We assume that Fe and Al precipitates incorporate/capture some of the studied major elements (e.g., Al, Ca, Mg, Mn, Si) and heavy metals (e.g., Co, Ni, Pb, Zn), causing a significant decrease in these element concentrations in the hypolimnion. The simultaneous increase in the contents of other elements in this part of the water column, such as Fe and S, probably results from the reductive dissolution of some of the Fe (oxy) hydroxides. We suspect that DOM together with bacteria affects the geochemical behavior of these elements in the water column; however, the real nature of this process should be tested in the future by complementary methods.

The geochemical behavior of the studied elements in the Lake ŁK-61 water is significantly affected by its tributary, which is an important source of dissolved elements and solid particles, as evidenced by comparative studies of the elemental composition of the water samples collected from the lake inflow and the epilimnion. An input of detrital material from the catchment area may also importantly influence the distribution of HMRs in the lake sediments, as they may constitute fresh sorption sites for dissolved solids and/or be a source of pollutants. The influx of allochthonous particles into the studied lake is confirmed by analysis of the mineralogical composition of the selected lake sediments, which showed the presence of allogenic phases (e.g., quartz, clay minerals, Ti oxides, zircons).

The vertical distributions of HMRs content in the upper part of the sediment profile attest that sedimentation conditions in Lake ŁK-61 were significantly disturbed in the past, which prevented the detailed age calculation of the lake sediments by the ^{137}Cs and ^{210}Pb dating methods. The observed disturbances, which are particularly visible between depths of 7 and 12 cm in the core, were characterized by elevated contents of selected major elements (e.g., Ca, Mg, Mn, P, N), heavy metals (e.g., Cu, Ni, Pb, Zn), and radioisotopes (^{137}Cs and ^{210}Po). Such element enrichments are interpreted to be linked with the flood in August 2010, which caused an increase in the water pH as reconstructed from the diatom-inferred pH proxy. Hence, ^{137}Cs- and ^{210}Po-enriched layers in the collected sediment profile may be associated with this episodic event and therefore serve as important chronostratigraphic markers. We assume that the recorded pH increase in the lake water initiated the precipitation of fresh secondary minerals, as supported by geochemical modeling and mineralogical analyses. The newly formed mineral phases likely captured dissolved solids, which were subsequently buried in the bottom sediments. It cannot be disregarded that particles contaminated with HMRs were also delivered to Lake ŁK-61 from the catchment area. We also suspect that nutrients delivered by the flood, such as P and N, significantly increased primary production and algal growth and consequently affected HMRs cycling in the studied reservoir.

The presented findings may be helpful in establishing the depositional chronology of sediments in reservoirs affected by mining activities and in identifying records of past depositional events, such as floods. The obtained results may also be useful in predicting the geochemical behavior of HMRs in pit lakes located in flood-risk areas in general and contribute to AMD-affected lake treatment management strategies. Moreover, because the studied heavy metals and radionuclides are toxic pollutants that pose a serious threat to living organisms, our study enhances environmental monitoring methods in areas affected by AMD and bring new approaches to environmental protection. This is particularly important considering that heavy rainfalls and floods, which affects the distribution of HMRs in water reservoirs, are predicted to occur more frequently as the climate change progresses.

CRediT authorship contribution statement

I. Sekudewicz: Conceptualization, Sample collection, Formal analysis, Investigation, *V*isualization, Writing – original draft, Writing – review & editing. M. Syczewski: Formal analysis, Investigation, *V*isualization. J. Rohovec: Investigation. Š. Matoušková: Investigation. U. Kowalewska: Formal analysis, Investigation. R. Blukis: Formal analysis, Investigation. W. Geibert: Investigation. I. Stimac: Investigation. M. Gąsiorowski: Sample collection, Supervision.

Declaration of competing interest

The authors declare that they have no known competing financial interests or personal relationships that could have appeared to influence the work reported in this paper.

Data availability

Data will be made available on request.

Appendix A. Supplementary data

Supplementary data to this article can be found online at https://doi.org/10.1016/j.scitotenv.2023.168245.

References

Abril, J.M., San Miguel, E.G., Ruiz-Canovas, C., Casas-Ruiz, M., Bolívar, J.P., 2018. From floodplain to aquatic sediments: Radiogeochronological fingerprints in a sediment core from the mining impacted Sancho reservoir (SW Spain). Sci. Total Environ. 631–632, 866–878. https://doi.org/10.1016/j.scitotenv.2018.03.114.

Acero, P., Ayora, C., Torrentó, C., Nieto, J.M., 2006. The behavior of trace elements during schwertmannite precipitation and subsequent transformation into goethite and jarosite. Geochim. Cosmochim. Acta 70, 4130–4139. https://doi.org/10.1016/j.gca.2006.06.1367.

Aközcan, S., Külahcı, F., Mercan, Y., 2018. A suggestion to radiological hazards characterization of ^{226}Ra, ^{232}Th, ^{40}K and ^{137}Cs: spatial distribution modelling. J. Hazard. Mater. 353, 476–489. https://doi.org/10.1016/j.jhazmat.2018.04.042.

Alpers, C.N., Blowes, D., Nordstrom, D.K., Jambor, J.L., 1994. Secondary minerals and acid mine-water chemistry. Mineral. Assoc. Canada Short Course 247–270.

Appleby, P.G., 2005. Chronostratigraphic techniques in recent sediments. In: Tracking Environmental Change Using Lake Sediments. Kluwer Academic Publishers, pp. 171–203. https://doi.org/10.1007/0-306-47669-x_9.

Appleby, P.G., 2008. Three decades of dating recent sediments by fallout radionuclides: a review. Holocene. https://doi.org/10.1177/0959683607085598.

Appleby, P.G., Oldfield, F., 1978. The calculation of lead-210 dates assuming a constant rate supply of unsupported ^{210}Pb to the sediment. Catena 5, 1–8.

Appleby, P.G., Oldfield, F., Thompson, R., Huttunen, P., Tolonen, K., 1979. ^{210}Pb dating of annually laminated lake sediments from Finland. Nature. https://doi.org/10.1038/280053a0.

Ashraf, M.A., Akib, S., Maah, M.J., Yusoff, I., Balkhair, K.S., 2014. Cesium-137: radiochemistry, fate, and transport, remediation, and future concerns. Crit. Rev. Environ. Sci. Technol. 44, 1740–1793. https://doi.org/10.1080/10643389.2013.790753.

Azzali, E., Marescotti, P., Frau, F., Dinelli, E., Carbone, C., Capitani, G., Lucchetti, G., 2014. Mineralogical and chemical variations of ochreous precipitates from acid sulphate waters (asw) at the Roşia Montană gold mine (Romania). Environ. Earth Sci. 72, 3567–3584. https://doi.org/10.1007/S12665-014-3264-Z/FIGURES/9.

Barbero, L., Gázquez, M.J., Bolívar, J.P., Casas-Ruiz, M., Hierro, A., Baskaran, M., Ketterer, M.E., 2014. Mobility of Po and U-isotopes under acid mine drainage conditions: an experimental approach with samples from Río Tinto area (SW Spain). J. Environ. Radioact. 138, 384–389. https://doi.org/10.1016/j.jenvrad.2013.11.004.

Bartczak, E., Gancarz, A., 1998. Szczegółowa Mapa Geologiczna Polski 1:50 000, sheet 645 – Łęknica (M-33-18-A), 646 – Trzebiel (M-33-18-B). Polish Geological Institute (PIG). https://baza.pgi.gov.pl/.

Baskaran, M., Nix, J., Kuyper, C., Karunakara, N., 2014. Problems with the dating of sediment core using excess ^{210}Pb in a freshwater system impacted by large scale watershed changes. J. Environ. Radioact. 138, 355–363. https://doi.org/10.1016/j.jenvrad.2014.07.006.

Battarbee, R.W., 1986. Diatom analysis. In: Berglund, B.E. (Ed.), Handbook of Holocene Palaeoecology and Palaeohydrology. John Willey and Sons, pp. 527–570.

Belousov, P., Semenkova, A., Egorova, T., Romanchuk, A., Zakusin, S., Dorzhieva, O., Tyupina, E., Izosimova, Y., Tolpeshta, I., Chernov, M., Krupskaya, V., 2019. Cesium sorption and desorption on glauconite, bentonite, zeolite, and diatomite. Minerals 9, 1–16. https://doi.org/10.3390/min9100625.

Benoit, G., Hemond, H.F., 1990. ^{210}Po and ^{210}Pb remobilization from lake sediments in relation to iron and manganese cycling. Environ. Sci. Technol. 24, 1224–1234. https://doi.org/10.1021/es00078a010.

Beresford, N.A., Fesenko, S., Konoplev, A., Skuterud, L., Smith, J.T., Voigt, G., 2016. Thirty years after the Chernobyl accident: what lessons have we learnt? J. Environ. Radioact. 157, 77–89. https://doi.org/10.1016/j.jenvrad.2016.02.003.

Bethke, C.M., 1996. Geochemical Reaction Modeling. Oxford University Press. https://doi.org/10.1093/oso/9780195094756.001.0001.

Blasco, M., Gázquez, M.J., Pérez-Moreno, S.M., Grande, J.A., Valente, T., Santisteban, M., de la Torre, M.L., Bolívar, J.P., 2016. Polonium behaviour in reservoirs potentially affected by acid mine drainage (AMD) in the Iberian Pyrite Belt (SW of Spain). J. Environ. Radioact. 152, 60–69. https://doi.org/10.1016/j.jenvrad.2015.11.008.

Bobos, I., Madruga, M.J., Reis, M., Esteves, J., Guimarães, V., 2021. Clay mineralogy insights and assessment of the natural (^{228}Ra, ^{226}Ra, ^{210}Pb, ^{40}K) and anthropogenic (^{137}Cs) radionuclides dispersion in the estuarine and lagoon systems along the Atlantic coast of Portugal. Catena 206, 105532. https://doi.org/10.1016/J.CATENA.2021.105532.

Boehrer, B., Schultze, M., 2008. Stratification of lakes. Rev. Geophys. 46, RG2005 https://doi.org/10.1029/2006RG000210.

Boehrer, B., von Rohden, C., Schultze, M., 2017. Physical features of meromictic lakes: stratification and circulation. In: Gulati, R., Zadereev, E., Degermendzhi, A. (Eds.), Ecology of Meromictic Lakes, Ecological Studies, 228. Springer, Cham, pp. 15–34. https://doi.org/10.1007/978-3-319-49143-1_2.

Bożęcki, P., 2013. Studium osadów tworzących się w obszarze eksploatacji węgla brunatnego w rejonie Łęknicy (Łuk Mużakowa) (in Polish). Akademia Górniczo-Hutnicza im. Stanisława Staszica, Kraków.

Cánovas, C.R., Olías, M., Nieto, J.M., Sarmiento, A.M., Cerón, J.C., 2007. Hydrogeochemical characteristics of the Tinto and Odiel Rivers (SW Spain). Factors controlling metal contents. Sci. Total Environ. 373, 363–382. https://doi.org/10.1016/J.SCITOTENV.2006.11.022.

Carrero, S., Pérez-López, R., Fernandez-Martinez, A., Cruz-Hernández, P., Ayora, C., Poulain, A., 2015. The potential role of aluminium hydroxysulphates in the removal of contaminants in acid mine drainage. Chem. Geol. 417, 414–423. https://doi.org/10.1016/j.chemgeo.2015.10.020.

Carvalho, F., Fernandes, S., Fesenko, S., Holm, E., Howard, B., Martin, P., Phaneuf, M., Porcellid, D., Prohl, G., Twining, J., 2017. The Environmental Behaviour of Polonium. In: Technical Reports Series No. 484. International Atomic Energy Agency, Vienna.

Christensen, J.B., Botma, J.J., Christensen, T.H., 1999. Complexation of cu and Pb by DOM in polluted groundwater: a comparison of experimental data and predictions by computer speciation models (WHAM and MINTEQA2). Water Res. 15, 3231–3238.

Cook, N., Ehrig, K., Rollog, M., Ciobanu, C., Lane, D., Schmandt, D., Owen, N., Hamilton, T., Grano, S., 2018. ^{210}Pb and ^{210}Po in geological and related anthropogenic materials: implications for their mineralogical distribution in base metal ores. Minerals 8, 211. https://doi.org/10.3390/min8050211.

Cornell, R.M., 1993. Adsorption of cesium on minerals: a review. J. Radioanal. Nucl. Chem. Artic. https://doi.org/10.1007/BF02219872.

Davis, J.A., 1984. Complexation of trace metals by adsorbed natural organic matter. Geochim. Cosmochim. Acta 48, 679–691.

Davison, W., 1993. Iron and manganese in lakes. Earth Sci Rev. 34, 119–163. https://doi.org/10.1016/0012-8252(93)90029-7.

Durrant, C.B., Begg, J.D., Kersting, A.B., Zavarin, M., 2018. Cesium sorption reversibility and kinetics on illite, montmorillonite, and kaolinite. Sci. Total Environ. 610–611, 511–520. https://doi.org/10.1016/j.scitotenv.2017.08.122.

Dutrizac, J.E., 2008. Factors affecting the precipitation of potassium jarosite in sulfate and chloride media. Metall. Mater. Trans. B Process Metall. Mater. Process. Sci. 39, 771–783. https://doi.org/10.1007/S11663-008-9198-7/FIGURES/22.

Eyrolle, F., Benaim, J.Y., 1999. Metal available sites on colloidal organic compounds in surface waters. Water Res. 4, 995–1004.

Flynn, W.W., 1968. The determination of low levels of polonium-210 in environmental materials. Anal. Chim. Acta 43, 221–227. https://doi.org/10.1016/S0003-2670(00)89210-7.

Frank, M., Harrell, E., 2023. Package "Hmisc" Title Harrell Miscellaneous.

Friese, K., 2004. Depth distribution of heavy metals in lake sediments from lignite mine pit lakes of Lusatia (Germany). Stud. Quat. 21, 197–205.

Friese, K., Hupfer, M., Schultze, M., 1998. Chemical characteristics of water and sediment in acid mining lakes of the Lusatian Lignite District. In: Geller, W., Klapper, H., Salomons, W. (Eds.), Acidic Mining Lakes, Environmental Science. Springer, Berlin, Heidelberg, pp. 25–45. https://doi.org/10.1007/978-3-642-71954-7_3.

Fuller, A.J., Shaw, S., Peacock, C.L., Trivedi, D., Small, J.S., Abrahamsen, L.G., Burke, I.T., 2014. Ionic strength and pH dependent multi-site sorption of Cs onto a micaceous aquifer sediment. Appl. Geochem. 40, 32–42. https://doi.org/10.1016/j.apgeochem.2013.10.017.

Gąsiorowski, M., Stiensa, J., Sienkiewicz, E., Sekudewicz, I., 2021. Geochemical variability of surface sediment in post-mining lakes located in the Muskau arch (Poland) and its relation to water chemistry. Water Air Soil Pollut. 232, 1–12. https://doi.org/10.1007/s11270-021-05057-8.

Geller, W., Schultze, M., Kleinmann, R., Wolkersdorfer, C., 2013. Acidic pit lakes: The legacy of coal and metal surface mines. In: Environ. Sci. Eng. (Subseries Environ. Sci.). Springer Berlin, Heidelberg.

Gruszecki, J., Dobek, P., Pasieczna, A., Tomassi-Morawiec, H., 2006. Objaśnienia do Mapy Geośrodowiskowej Polski 1:50 000. Arkusz Łęknica (645) i Trzebiel (646) (in Polish). Polish Geological Institute (PIG). http://bazadata.pgi.gov.pl/data/mgsp/txt/mgsp0646.pdf.

Guerrero, J.L., Gutiérrez-Álvarez, I., Hierro, A., Pérez-Moreno, S.M., Olías, M., Bolívar, J.P., 2021. Seasonal evolution of natural radionuclides in two rivers affected by acid mine drainage and phosphogypsum pollution. Catena 197, 104978. https://doi.org/10.1016/J.CATENA.2020.104978.

Hamilton, N.E., Ferry, M., 2018. ggtern: ternary diagrams using ggplot2. J. Stat. Softw. Code Snippets 87 (3), 1–17. https://doi.org/10.18637/jss.v087.c03.

Herzsprung, P., Schultze, M., Hupfer, M., Boehrer, B., Tümpling, W.v., Duffek, A., Van der Veen, A., Friese, K., 2010. Flood effects on phosphorus immobilisation in a river water filled pit lake-case study Lake Goitsche (Germany). Limnologica 40, 182–190. https://doi.org/10.1016/J.LIMNO.2009.11.007.

Hierro, A., Bolivar, J.P., Vaca, F., Borrego, J., 2012. Behavior of natural radionuclides in surficial sediments from an estuary impacted by acid mine discharge and industrial effluents in Southwest Spain. J. Environ. Radioact. 110, 13–23. https://doi.org/10.1016/j.jenvrad.2012.01.005.

Hierro, A., Olías, M., Ketterer, M.E., Vaca, F., Borrego, J., Cánovas, C.R., Bolivar, J.P., 2014. Geochemical behavior of metals and metalloids in an estuary affected by acid mine drainage (AMD). Environ. Sci. Pollut. Res. 21, 2611–2627. https://doi.org/10.1007/S11356-013-2189-5/FIGURES/7.

Hrdinka, T., Šobr, M., Fott, J., Nedbalová, L., 2013. The unique environment of the most acidified permanently meromictic lake in the Czech Republic. Limnologica 43, 417–426. https://doi.org/10.1016/J.LIMNO.2013.01.005.

Isajenko, K., Piotrowska, B., Stawarz, O., Wojtkowski, K., 2022. Monitoring promieniowania jonizującego realizowany w ramach państwowego monitoringu środowiska w latach 2020–2022. Zadanie 3: Monitoring stężenia cezu-137 w glebie (in Polish). Centralne Laboratorium Ochrony Radiologicznej, Warszawa.

Jia, G., Torri, G., Petruzzi, M., 2004. Distribution coefficients of polonium between 5% TOPO in toluene and aqueous hydrochloric and nitric acids. Appl. Radiat. Isot. 61, 279–282. https://doi.org/10.1016/j.apradiso.2004.03.021.

Jiang, M. Qin, Jin, X. Ying, Lu, X.Q., Chen, Z. Liang, 2010. Adsorption of Pb(II), Cd(II), Ni (II) and Cu(II) onto natural kaolinite clay. Desalination 252, 33–39. https://doi.org/10.1016/J.DESAL.2009.11.005.

Juggins, S., 2001. Software for Ecological and Palaeoecological Data Analysis and Visualization. User Guide Version 1.5, 1–73.

Klaminder, J., Appleby, P., Crook, P., Renberg, I., 2012. Post-deposition diffusion of ^{137}Cs in lake sediment: implications for radiocaesium dating. Sedimentology 59, 2259–2267. https://doi.org/10.1111/j.1365-3091.2012.01343.x.

Kleeberg, A., Grüneberg, B., 2005. Phosphorus mobility in sediments of acid mining lakes, Lusatia, Germany. Ecol. Eng. 24, 89–100. https://doi.org/10.1016/J.ECOLENG.2004.12.010.

Koźma, J., 2009. Rezerwat geologiczno-krajobrazowy Kopalnia Babina w Łęknicy. In: Kupetz, A., Kupetz, M. (Eds.), Der Muskauer Faltenbogen. Wyd. Verlag Dr Freidrich Pfeilt.

Koźma, J., Kupetz, M., 2008. The transboundary Geopark Muskau arch (Geopark Łuk Mużakowa, Geopark Muskauer Faltenbogen). Prz. Geol. 56, 692–698.

Krammer, K., 2000. Diatoms of Europe. Vol. 1: The Genus Pinnularia. A.R.G. Gantner Verlag, Kommanditgesellschaft, Königstein, pp. 1–703.

Krammer, K., Lange-Bertalot, H., 1986. Süßwasserflora von Mitteleuropa. Bacillariophyceae. I. Teil: Naviculaceae. Gustav Fisher Verlag, Stuttgart.

Krammer, K., Lange-Bertalot, H., 1988. Süßwasserflora von Mitteleuropa. Bacillariophyceae. 2. Teil: Bacillariaceae, Epithemiaceae, Surirellaceae. Gustav Fisher Verlag, Stuttgart.

Krammer, K., Lange-Bertalot, H., 1991a. Süßwasserflora von Mitteleuropa. Bacillariophyceae. 3. Teil: Centrales, Fragilariaceae, Eunotiaceae. Gustav Fisher Verlag, Stuttgart.

Krammer, K., Lange-Bertalot, H., 1991b. Süßwasserflora von Mitteleuropa. Bacillariophyceae. 4. Teil: Achnanthaceae, Kritische Ergänzungen zu Navicula (Lineolatae) und Gomphonema, Gesamtliteraturverzeichnis Teil 1–4. Gustav Fisher Verlag, Stuttgart.

Kupetz, M., 1997. Geologischer Bau und Genese der Stauchendmoräne Muskauer Faltenbogen. Brandenburgische Geowiss. Beitr. 4, 2.

Labus, K.M., Skoczyńska-Gajda, S., 2013. Origin of sulfates in the post-mining lakes in the eastern part of Muskau Arch (Polish-German borderland). Geol. Q. 57, 561–566. https://doi.org/10.7306/GQ.1110.

Lange-Bertalot, H., Metzeltin, D., 1996. Indicators of oligotrophy. 800 taxa representative of three ecologically distinct lake types: carbonate buffered, oligodystrophic, weakly buffered soft water. In: Lange-Bertalot, H. (Ed.), Iconographia Diatomologica, Annotated Diatom Micrographs 2. Koeltz Scientic Books, Köningstein.

Lange-Bertalot, H., Hofmann, G., Werum, M., Cantonati, M., 2017. Freshwater Benthic Diatoms of Central Europe: Over 800 Common Species Used in Ecological Assessment. English Edition With Updated Taxonomy and added Species. Koeltz Botanical Books, Schmitten-Oberreifenberg, p. 942.

Lee, G., Bigham, J.M., Faure, G., 2002. Removal of trace metals by coprecipitation with Fe, Al and Mn from natural waters contaminated with acid mine drainage in the Ducktown Mining District, Tennessee. Appl. Geochem. 17, 569–581. https://doi.org/10.1016/S0883-2927(01)00125-1.

Lieser, K.H., Steinkopff, T.H., 1989. Chemistry of radioactive cesium in the hydrosphere and in the geosphere. Radiochim. Acta 46, 39–48. https://doi.org/10.1524/RACT.1989.46.1.39.

Loring, D.H., 1991. Normalization of heavy-metal data from estuarine and coastal sediments. ICES J. Mar. Sci. 48, 101–115. https://doi.org/10.1093/ICESJMS/48.1.101.

Lutyńska, S., Labus, K., 2015. Identification of processes controlling chemical composition of pit lakes waters located in the eastern part of Muskau Arch (Polish-German borderland). Arch. Environ. Prot. 41, 60–69. https://doi.org/10.1515/aep-2015-0031.

Mabit, L., Benmansour, M., Abril, J.M., Walling, D.E., Meusburger, K., Iurian, A.R., Bernard, C., Tarján, S., Owens, P.N., Blake, W.H., Alewell, C., 2014. Fallout ^{210}Pb as a soil and sediment tracer in catchment sediment budget investigations: a review. Earth-Science Rev. 138, 335–351. https://doi.org/10.1016/j.earscirev.2014.06.007.

Madruga, M.J., Silva, L., Gomes, A.R., Libânio, A., Reis, M., 2014. The influence of particle size on radionuclide activity concentrations in Tejo River sediments. J. Environ. Radioact. 132, 65–72. https://doi.org/10.1016/J.JENVRAD.2014.01.019.

Makvandi, S., Huang, X., Beaudoin, G., Quirt, D., Ledru, P., Fayek, M., 2021. Trace element signatures in hematite and goethite associated with the Kiggavik–Andrew Lake structural trend U deposits (Nunavut, Canada). Mineral. Deposita 56, 509–535. https://doi.org/10.1007/S00126-020-00980-Y/FIGURES/13.

Manjón, G., Mantero, J., Vioque, I., Galván, J., Díaz-Francés, I., García-Tenorio, R., 2019. Some naturally occurring radionuclides (NORM) in a river affected by acid mining drainages. Chemosphere 223, 536–543. https://doi.org/10.1016/j.chemosphere.2019.02.059.

Mantero, J., Thomas, R., Holm, E., Rääf, C., Vioque, I., Ruiz-Canovas, C., García-Tenorio, R., Forssell-Aronsson, E., Isaksson, M., 2020. Pit lakes from southern Sweden: natural radioactivity and elementary characterization. Sci. Rep. 10, 1–17. https://doi.org/10.1038/s41598-020-70521-0.

Martin, A., Blanchard, R.L., 1969. The thermal volatilisation of caesium-137, polonium-210 and lead-210 from in vivo labelled samples. Analyst 94, 441–446. https://doi.org/10.1039/AN9699400441.

Matthews, K.M., Kim, C.K., Martin, P., 2007. Determination of ^{210}Po in environmental materials: a review of analytical methodology. Appl. Radiat. Isot. 65, 267–279. https://doi.org/10.1016/J.APRADISO.2006.09.005.

Mayes, W.M., Perks, M.T., Large, A.R.G., Davis, J.E., Gandy, C.J., Orme, P.A.H., Jarvis, A.P., 2021. Effect of an extreme flood event on solute transport and resilience of a mine water treatment system in a mineralised catchment. Sci. Total Environ. 750 https://doi.org/10.1016/J.SCITOTENV.2020.141693.

McKinley, J.P., Zeissler, C.J., Zachara, J.M., Jeffrey Serne, R., Lindstrom, R.M., Schaef, H.T., Orr, R.D., 2001. Distribution and retention of ^{137}Cs in sediments at the Hanford site, Washington. Environ. Sci. Technol. 35, 3433–3441.

Meyers, P.A., Ishiwatari, R., 1995. Organic matter accumulation records in lake sediments. Phys. Chem. Lakes 279–328. https://doi.org/10.1007/978-3-642-85132-2_10.

MKOO, 2010. MKOO (Międzynarodowa Komisja Ochrony Odry przed Zanieczyszczeniem) - Wezbranie w zlewni Nysy Łużyckiej 7–10 sierpnia 2010 r (in Polish) Wrocław, Drezno, Praga. http://www.mkoo.pl/download.php?fid=4043&lang=PL.

Mukai, H., Hirose, A., Motai, S., Kikuchi, R., Tanoi, K., Nakanishi, T.M., Yaita, T., Kogure, T., 2016. Cesium Adsorption/desorption Behavior of Clay Minerals Considering Actual Contamination Conditions in Fukushima. https://doi.org/10.1038/srep21543.

Naulier, M., Eyrolle-Boyer, F., Boyer, P., Métivier, J.M., Onda, Y., 2017. Particulate organic matter in rivers of Fukushima: an unexpected carrier phase for radiocesiums. Sci. Total Environ. 579, 1560–1571. https://doi.org/10.1016/j.scitotenv.2016.11.165.

Nordstrom, D.K., Ball, J.W., 1986. The geochemical behavior of aluminum in acidified surface waters. Science 232, 54–56. https://doi.org/10.1126/SCIENCE.232.4746.54.

Norris, R.S., Arkin, W.M., 1996. Known nuclear tests worldwide, 1945-1995. In: NRDC Nuclear Notebook, The Bulletin of the Atomic Scientists, May/June, pp. 61–63.

Oszkinis-Golon, M., Frankowski, M., Pukacz, A., 2021. Macrophyte diversity as a response to extreme conditions in the post-mining lakes of the muskau arch (West Poland). Water (Switzerland) 13, 2909. https://doi.org/10.3390/W13202909/S1.

Paikaray, S., 2020. Environmental stability of schwertmannite: a review. Mine Water Environ. 403 (40), 570–586. https://doi.org/10.1007/S10230-020-00734-2, 2020.

Panagopoulos, A., Giannika, V., 2022. Decarbonized and circular brine management/ valorization for water & valuable resource recovery via minimal/zero liquid discharge (MLD/ZLD) strategies. J. Environ. Manag. 324 https://doi.org/10.1016/J.JENVMAN.2022.116239.

Panagopoulos, A., Giannika, V., 2023. Study on the water resources and the opportunities for sustainable desalination & minimal/zero liquid discharge (MLD/ ZLD) practices in Greece (eastern Mediterranean). Sustain. Water Resour. Manag. 9 https://doi.org/10.1007/S40899-023-00884-5.

Park, C.W., Kim, S.M., Kim, I., Yoon, I.H., Hwang, J., Kim, J.H., Yang, H.M., Seo, B.K., 2021. Sorption behavior of cesium on silt and clay soil fractions. J. Environ. Radioact. 233, 106592 https://doi.org/10.1016/J.JENVRAD.2021.106592.

Park, S.M., Alessi, D.S., Baek, K., 2019. Selective adsorption and irreversible fixation behavior of cesium onto 2:1 layered clay mineral: a mini review. J. Hazard. Mater. 369, 569–576. https://doi.org/10.1016/J.JHAZMAT.2019.02.061.

Paulsson, O., Widerlund, A., 2021. Algal nutrient limitation and metal uptake experiment in the Åkerberg pit lake, northern Sweden. Appl. Geochem. 125 https://doi.org/10.1016/J.APGEOCHEM.2020.104829.

PGW WP, 2021. PGW WP (Państwowe Gospodarstwo Wodne Wody Polskie) – MZP (Mapy zagrożenia powodziowego). https://wody.isok.gov.pl/imap_kzgw/?gpmap=gpMZP. (Accessed 18 April 2023).

Pukacz, A., Oszkinis-Golon, M., Frankowski, M., 2018. The physico-chemical diversity of pit lakes of the Muskau arch (Western Poland) in the context of their evolution and genesis. Limnol. Rev. 18, 115–126. https://doi.org/10.2478/limre-2018-0013.

Putyrskaya, V., Klemt, E., Röllin, S., Astner, M., Sahli, H., 2015. Dating of sediments from four Swiss prealpine lakes with ^{210}Pb determined by gamma-spectrometry: progress and problems. J. Environ. Radioact. 145, 78–94. https://doi.org/10.1016/j.jenvrad.2015.03.028.

R Core Team, 2021. R: A Language and Environment for Statistical Computing. R Foundation for Statistical Computing, Vienna, Austria (R version 4.0.4).

Ram, R., Vaughan, J., Etschmann, B., Brugger, J., 2019. The aqueous chemistry of polonium (Po) in environmental and anthropogenic processes. J. Hazard. Mater. 380, 120725 https://doi.org/10.1016/j.jhazmat.2019.06.002.

Ram, R., Kalnins, C., Pownceby, M.I., Ehrig, K., Etschmann, B., Spooner, N., Brugger, J., 2021. Selective radionuclide co-sorption onto natural minerals in environmental and anthropogenic conditions. J. Hazard. Mater. 409 https://doi.org/10.1016/j.jhazmat.2020.124989.

Ramstedt, M., Carlsson, E., Lövgren, L., 2003. Aqueous geochemistry in the Udden pit lake, northern Sweden. Appl. Geochem. 18, 97–108. https://doi.org/10.1016/S0883-2927(02)00068-9.

Rose, A.W., Bianchi-Mosquera, G.C., 1993. Adsorption of Cu, Pb, Zn, Co, Ni, and Ag on goethite and hematite; a control on metal mobilization from red beds into stratiform copper deposits. Econ. Geol. 88, 1226–1236. https://doi.org/10.2113/GSECONGEO.88.5.1226.

Sánchez-España, J., López Pamo, E., Santofimia Pastor, E., Reyes Andrés, J., Martín Rubí, J.A., 2006. The removal of dissolved metals by hydroxysulphate precipitates during oxidation and neutralization of acid mine waters, Iberian pyrite belt. Aquat. Geochem. 12, 269–298. https://doi.org/10.1007/S10498-005-6246-7/METRICS.

Sánchez-España, J., Pamo, E.L., Pastor, E.S., Ercilla, M.D., 2008. The acidic mine pit lakes of the Iberian Pyrite Belt: an approach to their physical limnology and hydrogeochemistry. Appl. Geochem. 23, 1260–1287. https://doi.org/10.1016/j.apgeochem.2007.12.036.

Sánchez-España, J., Yusta, I., Burgos, W.D., 2016. Geochemistry of dissolved aluminum at low pH: Hydrobasaluminite formation and interaction with trace metals, silica and microbial cells under anoxic conditions. Chem. Geol. 441, 124–137. https://doi.org/10.1016/J.CHEMGEO.2016.08.004.

Sánchez-España, J.S., Pamo, E.L., Diez, M., Santofimia, E., 2009. Physico-chemical gradients and meromictic stratification in Cueva de la Mora and other acidic pit lakes of the Iberian Pyrite Belt. Mine Water Environ. 28, 15–29. https://doi.org/10.1007/S10230-008-0059-Z/FIGURES/12.

Sawhney, B.L., 1972. Selective sorption and fixation of cations by clay minerals. A review. Clay Clay Miner. 20, 93–100. https://doi.org/10.1346/CCMN.1972.0200208.

Schultze, M., 2013. Limnology of pit lakes. In: Geller, W., Schultze, M., Kleinmann, R., Wolkersdorfer, C. (Eds.), Acidic Pit Lakes. Springer Berlin, Heidelberg, pp. 23–224. https://doi.org/10.1007/978-3-642-29384-9_3. Environ. Sci. Eng.

Schultze, M., Pokrandt, K.H., Hille, W., 2010. Pit lakes of the Central German lignite mining district: creation, morphometry and water quality aspects. Limnologica 40, 148–155. https://doi.org/10.1016/j.limno.2009.11.006.

Schultze, M., Boehrer, B., Wendt-Potthoff, K., Katsev, S., Brown, E.T., 2017. Chemical setting and biogeochemical reactions in meromictic lakes. In: Gulati, R., Zadereev, E., Degermendzhi, A. (Eds.), Ecology of Meromictic Lakes, Ecological Studies, 228. Springer, Cham, pp. 35–59. https://doi.org/10.1007/978-3-319-49143-1_3.

Sekudewicz, I., Gąsiorowski, M., 2022. Spatial and vertical distribution of ^{137}Cs activity concentrations in Lake sediments of Turawa Lake (Poland). Environ. Sci. Pollut. Res. Int. 29 https://doi.org/10.1007/S11356-022-21417-1.

Shepard, F.P., 1954. Nomenclature based on sand-silt-clay ratios. J. Sediment. Res. 24, 151–158. https://doi.org/10.1306/D4269774-2B26-11D7-8648000102C1865D.

Shi, M., Min, X., Ke, Y., Lin, Z., Yang, Z., Wang, S., Peng, N., Yan, X., Luo, S., Wu, J., Wei, Y., 2021. Recent progress in understanding the mechanism of heavy metals retention by iron (oxyhydr)oxides. Sci. Total Environ. 752 https://doi.org/10.1016/J.SCITOTENV.2020.141930.

Sienkiewicz, E., Gasiorowski, M., 2016. The evolution of a mining lake - from acidity to natural neutralization. Sci. Total Environ. 557–558, 343–354. https://doi.org/10.1016/j.scitotenv.2016.03.088.

Sienkiewicz, E., Gąsiorowski, M., 2017. The diatom-inferred pH reconstructions for a naturally neutralized pit lake in south-west Poland using the mining and the combine pH training sets. Sci. Total Environ. 605 – 606, 75–87. https://doi.org/10.1016/j.scitotenv.2017.06.171.

Sienkiewicz, E., Gąsiorowski, M., 2018. The influence of acid mine drainage on the phytoand zooplankton communities in a clay pit lake in the ŁUK Muzakowa Geopark (western Poland). Fundam. Appl. Limnol. 191, 143–154. https://doi.org/10.1127/FAL/2018/1079.

Sienkiewicz, E., Gasiorowski, M., Hercman, H., 2006. Is acid rain impacting the Sudetic lakes? Sci. Total Environ. 369, 139–149. https://doi.org/10.1016/J.SCITOTENV.2006.05.001.

Skwarzec, B., Strumińska-Parulska, D.I., Boryło, A., Kabat, K., 2012. Polonium, uranium and plutonium radionuclides in aquatic and land ecosystem of Poland. J. Environ. Sci. Heal. - Part A Toxic/Hazard. Subst. Environ. Eng. 47, 479–496. https://doi.org/10.1080/10934529.2012.646153.

Smith, J.T., Beresford, N.A., 2005. Radioactive fallout and environmental transfers. In: Smith, J.T., Beresford, N.A. (Eds.), Chernobyl — Catastrophe and Consequences. Springer Berlin, Heidelberg, pp. 35–80. https://doi.org/10.1007/3-540-28079-0_2.

Solski, A., Jędrczak, A., Matejczuk, A., 1988. Skład chemiczny wód zbiorników pojezierza antropogenicznego w rejonie Tuplice-Łęknica (in Polish). Zeszyty Naukowe Uniwersytetu Zielonogórskiego 84, 65–76.

Somboon, S., Kavasi, N., Sahoo, S.K., Inoue, K., Arae, H., Tsuruoka, H., Shimizu, M., Fukushi, M., 2018. Radiocesium and ^{40}K distribution of river sediments and floodplain deposits in the Fukushima exclusion zone. J. Environ. Radioact. 195, 40–53. https://doi.org/10.1016/j.jenvrad.2018.09.003.

Stumm, W., Morgan, J.J., 1996. Aquatic Chemistry. John Wiley & Sons, New York.

Swarzenski, P.W., 2014. ^{210}Pb dating. In: Encyclopedia of Scientific Dating Methods. Springer, Netherlands, Dordrecht, pp. 1–11. https://doi.org/10.1007/978-94-007-6326-5_236-1.

Thomas, R., Mantero, J., Pérez-Moreno, S.M., Ruiz-Canovas, C., Vioque, I., Isaksson, M., Forssell-Aronsson, E., Holm, E., García-Tenorio, R., 2020. ^{226}Ra, ^{210}Po and lead isotopes in a pit lake water profile in Sweden. J. Environ. Radioact. 223–224 https://doi.org/10.1016/J.JENVRAD.2020.106384.

Thomas, R.I., Mantero, J.I., Ruiz Cá Novas, C.I., Holm, E., García-Tenorio, R., Forssell-AronssonID, E., IsakssonID, M., 2022. Natural Radioactivity and Element Characterization in Pit Lakes in Northern Sweden. https://doi.org/10.1371/journal.pone.0266002.

Toby, B.H., Von Dreele, R.B., 2013. GSAS-II: the genesis of a modern open-source all purpose crystallography software package. J. Appl. Crystallogr. 46, 544–549. https://doi.org/10.1107/S0021889813003531.

Torres, E., Ayora, C., Canovas, C.R., García-Robledo, E., Galván, L., Sarmiento, A.M., 2013. Metal cycling during sediment early diagenesis in a water reservoir affected by acid mine drainage. Sci. Total Environ. 416–429 https://doi.org/10.1016/j.scitotenv.2013.05.014.

Villa, M., Manjón, G., Hurtado, S., García-Tenorio, R., 2011. Uranium pollution in an estuary affected by pyrite acid mine drainage and releases of naturally occurring radioactive materials. Mar. Pollut. Bull. 62, 1521–1529. https://doi.org/10.1016/j.marpolbul.2011.04.003.

Vink, J.P.M., Harmsen, J., Rijnaarts, H., 2010. Delayed immobilization of heavy metals in soils and sediments under reducing and anaerobic conditions; consequences for flooding and storage. J. Soils Sediments 10, 1633–1645. https://doi.org/10.1007/S11368-010-0296-1/FIGURES/4.

Walling, D.E., Quine, T.A., 1993. Use of Caesium-137 as a Tracer of Erosion and Sedimentation: Handbook for the Application of the Caesium-137 Technique. UK Overseas Dev. Adm. Res. Scheme R 4579.

Wisotzky, F., 1998. Chemical reactions in aquifers influenced by sulfide oxidation and in sulfide oxidation zones. In: Geller, W., Klapper, H., Salomons, W. (Eds.), Acidic Mining Lakes. Environmental Science. Springer, Berlin, Heidelberg. https://doi.org/10.1007/978-3-642-71954-7_11.

Yamamoto, M., Sakaguchi, A., Kofuji, H., 2010. Uranium in acidic mine drainage at the former Ogoya mine in Ishikawa prefecture of Japan. J. Radioanal. Nucl. Chem. 283, 699–705. https://doi.org/10.1007/s10967-009-0400-4.

Yang, W., Guo, L., Chuang, C.Y., Schumann, D., Ayranov, M., Santschi, P.H., 2013. Adsorption characteristics of ^{210}Pb, ^{210}Po and ^{7}Be onto micro-particle surfaces and the effects of macromolecular organic compounds. Geochim. Cosmochim. Acta 107, 47–64. https://doi.org/10.1016/j.gca.2012.12.039.

Zaborska, A., Carroll, J.L., Papucci, C., Pempkowiak, J., 2007. Intercomparison of alpha and gamma spectrometry techniques used in ^{210}Pb geochronology. J. Environ. Radioact. 93, 38–50. https://doi.org/10.1016/J.JENVRAD.2006.11.007.

Zapata, F., Nguyen, M.L., 2009. Chapter 7 soil erosion and sedimentation studies using environmental radionuclides. Radioact. Environ. 16, 295–322. https://doi.org/10.1016/S1569-4860(09)01607-6.

Zhu, J., Huang, Q., Pigna, M., Violante, A., 2012. Competitive sorption of Cu and Cr on goethite and goethite–bacteria complex. Chem. Eng. J. 179, 26–32. https://doi.org/10.1016/J.CEJ.2011.07.011.

Supplementary Materials

Geochemical behavior of heavy metals and radionuclides
in a pit lake affected by acid mine drainage (AMD)
in the Muskau Arch (Poland)

Ilona Sekudewicz[1], Marcin Syczewski[2]; Jan Rohovec[3], Šárka Matoušková[3],

Urszula Kowalewska[1], Roberts Blukis[2,4], Walter Geibert[5],

Ingrid Stimac[5], Michał Gąsiorowski[1]

[1]Institute of Geological Sciences, Polish Academy of Sciences, 00818 Warszawa, Twarda 51/55, Poland

[2]Helmholtz Centre Potsdam, GFZ German Research Centre for Geosciences, Telegrafenberg, 14473 Potsdam, Germany

[3]Institute of Geology, Czech Academy of Sciences, 16500 Praha, Rozvojová 269, Czech Republic

[4]Leibniz-Institut für Kristallzüchtung, Max-Born-Str. 2, 12489 Berlin, Germany

[5]Alfred Wegener Institute, Helmholtz Centre for Polar and Marine Research, Am Handelshafen 12, 27570 Bremerhaven, Germany

Corresponding author: Ilona Sekudewicz; i.sekudewicz@twarda.pan.pl

ORCID number of corresponding author: 0000-0003-4525-8200

1. **Results**

   1.1. Tributary and lake water

Table S1 Elemental composition of samples collected from the tributary (T) and water column (WA) of Lake ŁK-61.

Sampling sites are shown in Fig. 1.

	Bożęcki (2013)			Water column							Tributary		
Sample name				WA1	WA2	WA3	WA4	WA5	WA6	WA7	T1	T2	T3
Sampling date	09/2009	08/2010	09/2010				09/2020					09/2020	
Depth (m)		surface		0.5	1.5	2.5	3.5	4.5	5.5	6.5		surface	
DOC (mg/L)	n.d.	n.d.	n.d.	1.5	1.3	1.5	1.6	1.5	2.2	32.7	1.3	3.2	3.0
Cl$^-$ (mg/L)	18.4	15.5	15.5	2.4	2.1	2.1	2.4	2.2	2.2	6.5	n.d.	n.d.	n.d.
NO$_3^-$ (mg/L)	0.7	1.6	2.2	n.d.	n.d.	n.d.	n.d.	n.d.	n.d.	n.d.	n.d.	n.d.	n.d.
SO$_4^{2-}$ (mg/L)	990.0	406.0	204.0	n.d.	n.d.	n.d.	n.d.	n.d.	n.d.	n.d.	n.d.	n.d.	n.d.
Al (mg/L)	1.8	1.7	1.7	2.5	2.5	2.5	2.5	2.5	2.5	< d.l.	2.5	3.0	2.8
Ca (mg/L)	298.6	249.0	127.7	253.5	254.5	256.8	268.0	259.1	257.3	188.5	259.5	283.0	286.7
Fe (mg/L)	19.7	4.0	0.8	29.7	29.8	30.0	31.0	30.3	32.9	419.4	33.4	28.8	37.1
K (mg/L)	5.8	5.4	5.5	9.1	9.0	9.0	9.4	9.2	9.2	22.0	9.2	9.1	10.1
Mg (mg/L)	30.6	34.3	24.0	37.8	38.0	38.3	39.8	38.6	38.4	32.0	38.7	41.6	41.9
Mn (mg/L)	2.7	0.0	1.1	2.4	2.5	2.5	2.6	2.5	2.5	1.6	2.5	2.8	2.8
Na (mg/L)	8.6	6.9	6.8	8.5	8.2	8.3	8.6	8.4	8.4	8.9	8.5	8.4	8.5
S (mg/L)	n.d.	n.d.	n.d.	291.1	290.6	292.1	293.7	292.8	291.7	578.1	288.7	307.8	309.9
Si (mg/L)	n.d.	n.d.	n.d.	20.1	20.0	20.5	20.7	20.4	20.1	8.9	20.4	23.3	23.6
Li (µg/L)	n.d.	n.d.	n.d.	79.5	80.0	79.0	87.0	80.4	79.7	39.3	77.8	83.8	95.4
Rb (µg/L)	n.d.	n.d.	n.d.	49.9	50.8	51.2	50.3	51.0	50.7	68.1	50.1	53.5	56.6
Cs (µg/L)	n.d.	n.d.	n.d.	0.2	0.2	0.2	0.2	0.2	0.2	0.2	0.2	0.3	0.3
Pb (µg/L)	n.d.	n.d.	n.d.	0.6	0.6	1.2	1.1	0.7	0.5	0.0	0.6	0.4	0.3
Cr (µg/L)	n.d.	n.d.	n.d.	0.4	0.4	0.5	0.4	0.4	0.4	< d.l.	0.5	0.3	0.3
Co (µg/L)	n.d.	n.d.	n.d.	10.2	10.2	11.0	10.7	10.5	10.4	4.5	10.3	9.2	9.9
Ni (µg/L)	n.d.	n.d.	n.d.	15.0	15.4	16.2	15.2	15.9	15.4	1.5	15.1	14.7	15.2
Cu (µg/L)	n.d.	n.d.	n.d.	1.0	0.7	2.4	1.3	1.0	0.7	< d.l.	0.7	0.9	1.0
Zn (µg/L)	n.d.	n.d.	n.d.	41.9	39.1	47.1	40.4	42.2	40.9	4.9	41.3	38.3	40.0

d.l. – detection limit
n.d. – not detected

1.2. Lake sediments

Table S2 Elemental composition (mg kg^{-1}) of selected samples from the core of Lake ŁK-61 and certified reference material (NRC-MESS-4) measured by ICP-OES. Sampling site is shown in Fig. 1.

Sample depth (cm)	Al	Ca	Ba	Cr	Cu	Fe	K	Li	La	Mg	Mn	Na	Ni	P	Pb	S	Sr	Ti	Zn
1	67691	2769	241.0	62.2	7.1	213128	10193	31.6	24.4	1792	226.6	409.7	17.7	514.6	26.9	7435	77.5	5065	49.2
2	68311	1512	253.3	60.1	6.6	212118	10854	32.1	23.6	1898	63.9	494.5	14.7	374.4	27.4	15223	64.4	5208	29.8
3	61359	2389	253.5	54.1	5.6	252160	9713	28.8	21.4	1743	106.8	407.1	14.0	389.7	26.6	14010	71.6	4695	29.2
5	82753	982	352.3	80.3	9.0	72228	17102	40.4	29.7	2171	65.2	1022.7	17.1	240.6	30.8	2408	69.0	6926	30.1
7	73011	2668	258.6	65.4	7.6	207419	11165	33.8	26.2	1919	204.3	494.8	18.8	521.4	29.2	7643	79.5	5396	47.1
8	75114	2885	289.1	77.9	18.4	162288	12719	39.5	32.3	2606	235.5	891.4	23.4	798.7	36.5	4482	85.2	5585	69.4
9	93412	2024	403.1	105.8	36.5	90122	17104	53.6	41.2	4317	170.2	1711.8	37.7	1042.6	55.7	4936	90.8	6117	151.9
10	95927	2429	407.7	115.5	38.6	107345	17026	61.2	45.0	5546	212.1	2291.1	47.8	1356.8	59.8	7019	97.3	5575	191.8
12	86735	1417	349.3	83.6	10.6	92354	15753	43.0	34.0	2351	89.5	848.5	20.4	331.5	33.9	4668	78.3	7100	38.9
16	84464	1754	288.0	78.8	8.4	155901	13462	41.0	31.5	2233	124.8	623.3	19.6	298.6	32.8	3518	69.6	6734	36.7
20	61975	1089	286.1	62.4	8.7	94397	13792	30.3	27.9	1630	43.6	769.2	14.5	233.2	25.0	3691	58.7	5172	27.3
25	95390	790	363.7	94.4	9.8	56338	17421	47.3	35.6	2472	58.8	875.4	20.0	281.9	34.8	2600	73.9	8024	33.0
30	90777	793	340.6	90.1	10.1	85081	15843	47.5	34.1	2431	56.4	794.2	19.8	307.6	34.7	3317	75.6	7503	34.1
34	97963	771	353.7	96.4	9.4	73104	16608	47.2	37.0	2489	60.4	812.8	22.1	315.0	35.8	3206	75.9	8053	36.2
40	78930	769	381.9	86.7	9.8	28799	18003	40.3	34.6	2112	62.3	1115.4	19.0	254.3	30.3	2834	73.0	7078	28.3
45	101647	812	320.4	97.8	7.1	132579	13901	44.3	37.6	2436	56.4	551.1	23.9	343.7	37.1	4839	76.3	8034	38.1
50	105960	826	339.9	102.6	8.1	88609	16139	49.5	39.0	2665	61.1	682.4	24.9	347.3	38.9	4805	78.4	8328	38.3
NRC-MESS-4*	73446	13425	898.8	91.8	30.3	38800	23447	60.9	35.0	14960	287.4	12264.6	44.0	989.1	27.4	1263	125006	3617	145.1

* the reported values are the average concentration (arithmetic mean; n = 3)

Table S3 Relative standard deviation (%) of the analysis of selected lake sediments of Lake ŁK-61 and certified reference material (NR-MESS-4) performed using ICP-OES. Sampling site is shown in Fig. 1.

Sample depth (cm)	Al	Ca	Ba	Cr	Cu	Fe	K	Li	La	Mg	Mn	Na	Ni	P	Pb	S	Sr	Ti	Zn
1	0.82	1.12	0.86	2.01	1.10	0.34	0.80	0.33	2.09	1.67	0.74	0.81	1.51	1.83	1.07	0.83	0.96	0.93	0.84
2	0.78	0.18	0.93	1.19	3.42	0.33	0.61	0.19	0.42	0.45	1.23	1.22	1.26	0.70	0.44	0.29	0.78	1.01	0.33
3	0.89	0.83	0.71	0.09	4.23	0.35	0.50	0.13	0.09	0.40	0.63	2.16	0.94	1.09	2.81	0.42	1.09	0.74	0.77
5	0.95	0.97	1.02	0.20	0.37	0.35	0.97	0.33	1.93	0.23	2.06	2.03	1.34	0.62	0.67	1.31	1.17	1.04	0.96
7	0.11	0.76	0.16	0.83	2.23	0.45	0.72	0.20	0.99	0.59	0.66	1.98	0.49	1.05	1.02	0.91	0.24	0.13	0.70
8	0.14	0.12	0.13	0.34	0.82	0.23	0.80	0.51	0.66	0.26	0.28	1.92	0.15	0.18	0.68	0.44	0.10	0.13	0.21
9	1.97	0.61	1.72	1.07	1.14	0.17	0.20	0.65	1.61	0.83	1.79	1.01	0.67	0.76	0.95	1.85	1.87	1.82	0.82
10	0.92	0.48	0.53	1.30	0.97	0.27	0.99	0.45	0.28	1.01	0.89	0.58	0.72	0.72	0.46	0.51	0.71	0.59	0.44
12	0.14	0.30	0.38	0.24	0.70	0.17	0.68	0.43	1.59	0.26	0.53	1.43	1.00	0.59	1.54	0.77	0.26	0.30	0.52
16	0.19	0.61	0.38	0.76	1.89	0.28	0.62	0.56	1.70	0.43	0.62	0.78	0.58	0.51	0.70	0.37	0.32	0.25	0.42
20	0.31	0.38	0.03	0.29	3.12	0.31	0.63	0.28	1.80	0.36	1.25	1.77	1.85	0.55	2.60	1.57	0.11	0.14	0.93
25	0.02	0.17	0.22	0.45	2.99	0.49	0.66	0.05	0.91	0.67	0.52	0.40	0.61	0.92	1.04	2.41	0.08	0.12	0.15
30	0.46	0.95	0.15	0.80	2.85	2.09	0.31	0.34	1.04	0.52	0.40	0.73	0.92	1.24	1.24	2.75	0.22	0.09	0.94
34	0.33	0.67	0.15	0.56	2.75	0.25	0.66	0.48	0.87	0.43	0.88	0.83	0.61	0.61	1.05	0.56	0.35	0.18	0.82
40	0.14	0.25	0.36	0.34	1.23	0.42	1.11	0.40	0.45	0.12	1.14	1.37	0.99	0.77	0.49	1.93	0.27	0.30	0.41
45	0.49	0.74	0.59	0.14	4.47	0.08	0.74	0.26	2.23	0.33	1.08	2.17	0.57	0.87	1.69	0.84	0.69	0.67	0.84
50	0.23	1.01	0.12	1.14	0.58	3.17	0.60	0.16	0.87	1.20	0.53	1.35	1.33	1.89	1.63	0.43	0.27	0.02	1.20
NRC-MESS-4*	0.29	0.46	0.27	0.45	0.66	1.57	0.72	0.38	0.81	0.27	0.39	0.72	0.34	0.68	1.14	2.34	0.29	0.24	0.38

* the reported values are the average (arithmetic mean; n = 3)

Table S4 Limit of detection (LOD) and limit of quantification (LOQ) for major and minor elements (mg L^{-1}) measured in selected lake sediments of Lake ŁK-61 using ICP-OES. Sampling site is shown in Fig. 1.

	Al	Ca	Ba	Cr	Cu	Fe	K	Li	La	Mg	Mn	Na	Ni	P	Pb	S	Sr	Ti	Zn
LOD	9.6	0.09	0.16	0.01	0.01	5.4	2.6	0.01	0.01	5.14	0.66	2.02	0.01	0.2	0.01	0.26	0.03	0.55	0.02
LOQ	45.8	4.82	0.77	0.07	0.04	25.4	12.5	0.03	0.02	24.5	3.1	9.6	0.06	1.0	0.02	1.2	0.15	2.6	0.07

Table S5 Spearman's rank correlation coefficients among selected parameters of the sediment profile collected from Lake ŁK-61 (p-value <0.05).

	Al	Ca	Ba	Cr	Cu	Fe	K	Li	Mg	Mn	Na	Ni	P	Pb	S	Sr	Ti	Zn	b.d.	TOC	TN	^{137}Cs	^{40}K	^{210}Po
Al	1.00																							
Ca		1.00																						
Ba	0.67		1.00																					
Cr	0.93		0.84	1.00																				
Cu			0.79	0.60	1.00																			
Fe	-0.55	0.80	-0.79	-0.62	-0.53	1.00																		
K	0.63	-0.63	0.94	0.77	0.65	-0.92	1.00																	
Li	0.91		0.78	0.95	0.62	-0.56	0.70	1.00																
Mg	0.84		0.71	0.87	0.67		0.57	0.89	1.00															
Mn		0.85				0.53				1.00														
Na			0.90	0.64	0.91	-0.69	0.83	0.60	0.63		1.00													
Ni	0.84		0.64	0.88	0.62		0.49	0.86	0.95		0.55	1.00												
P		0.73				0.59				0.72			1.00											
Pb	0.88		0.68	0.90	0.60		0.54	0.90	0.99		0.58	0.97		1.00										
S		0.67	-0.53			0.84	-0.67				-0.54			0.76	1.00									
Sr				0.53	0.49		0.52		0.69		0.53		0.78	0.77	0.69	1.00								
Ti	0.86	-0.74	0.56	0.72		-0.72	0.63	0.69	0.60	-0.52		0.58		0.62		-0.59	1.00							
Zn		0.58							0.63	0.67		0.71	0.78	0.63		0.91		1.00						
b.d.		-0.63	0.60	0.50		-0.74	0.67			-0.63	0.52			-0.53		-0.67			1.00					
TOC	-0.81	0.50	-0.65			0.52	-0.50	-0.65	-0.57			-0.53		-0.61		0.50	-0.84			1.00				
TN	-0.63	0.81	-0.51			0.70	-0.53			0.66				0.58		0.68	-0.89	-0.49		0.74	1.00			
^{137}Cs				0.60						0.75		0.80	0.63	0.74		0.76		0.64				1.00		
^{40}K		-0.51	0.92	0.64	0.71	-0.84	0.94	0.58			0.89					-0.56				0.60			1.00	
^{210}Po										0.53			0.56			0.50		0.52			0.52			1.00

Al – aluminum, Ca – calcium, Ba – barium, Cr – chromium, Cu – copper, Fe – iron, K – potassium, Li – lithium, La – lanthanum, Mg – magnesium, Mn – manganese, Na – sodium, Ni – nickel, P – phosphorus, Pb – lead, S – sulfur, Sr – strontium, Ti – titanium, Zn – zinc (mg kg^{-1}), TOC – total organic carbon (%), TN – total nitrogen (%), ^{137}Cs – activity concentration (Bq kg^{-1}), ^{40}K – activity concentration (Bq kg^{-1})

Table S6. Mineral saturation index at a depth of 0.5 m of the water column in Lake ŁK-61.

Mineral saturation states	Log Q/K
Hematite	3.2218 s/sat
$Fe(OH)_{2.7}Cl_3$	2.0364 s/sat
Goethite	0.4242 s/sat

s/sat - saturation index exceeded

Table S7. Mineral saturation index at a depth of 6.5 m of the water column in Lake ŁK-61.

Mineral saturation states	Log Q/K
$Al_4(OH)_{10}SO_4$	11.8837 s/sat
Alunite	10.3118 s/sat
Kaolinite	8.2104 s/sat
Imogolite	6.3912 s/sat
Halloysite	5.8609 s/sat
Diaspore	4.7993 s/sat
Hematite	4.1779 s/sat
Gibbsite (C)	3.9200 s/sat
$Al(OH)_3$ (Soil)	3.3700 s/sat
Al_2O_3	3.3633 s/sat
Boehmite	3.0025 s/sat
Goethite	0.9134 s/sat
$AlOH_SO_4$	0.8588 s/sat
$Al(OH)_3$ (am)	0.8224 s/sat
Lepidocrocite	0.4132 s/sat

s/sat - saturation index exceeded

Table S8. Mineral saturation index in the surface layer of the water column of Lake ŁK-61 in August 2010, based on literature data (Bożęcki, 2013).

Mineral saturation states	Log Q/K
Schwertmannite	32.7406 s/sat
Hematite	14.8319 s/sat
$Fe(OH)_{2.7}Cl_3$	7.3098s /sat
Alunite	6.7468 s/sat
Goethite	6.2269s /sat
K-Jarosite	5.9864 s/sat
$Al_4(OH)_{10}SO_4$	5.6884 s/sat
Lepidocrocite	5.5168 s/sat
Kaolinite	5.4243 s/sat
Ferrihydrite (aged)	4.1977 s/sat
Imogolite	3.5366s /sat
Ferrihydrite	3.4060 s/sat
Diaspore	3.2804 s/sat
Halloysite	3.1906 s/sat
Gibbsite (C)	2.4079 s/sat
$Al(OH)_3$ (Soil)	1.8579 s/sat
Boehmite	1.5343 s/sat
Na-Jarosite	0.5614 s/sat
Al_2O_3	0.5072 s/sat
$AlOHSO_4$	0.2911 s/sat

s/sat - saturation index exceeded

References:

Bożęcki, P., 2013. Studium osadów tworzących się w obszarze eksploatacji węgla brunatnego w rejonie Łęknicy (Łuk Mużakowa) (in Polish). Akademia Górniczo- Hutnicza im. Stanisława Staszica, Kraków.